TRANSPORTATION RESEARCH
RECORD

No. 1458

Materials
and Construction

Concrete Research

A peer-reviewed publication of the Transportation Research Board

TRANSPORTATION RESEARCH BOARD
NATIONAL RESEARCH COUNCIL

NATIONAL ACADEMY PRESS
WASHINGTON, D.C. 1994

Transportation Research Record 1458
ISSN 0361-1981
ISBN 0-309-06065-6
Price: $30.00

Subscriber Category
IIIB materials and construction

Printed in the United States of America

Sponsorship of Transportation Research Record 1458

GROUP 2—DESIGN AND CONSTRUCTION OF TRANSPORTATION FACILITIES
Chairman: Charles T. Edson, Greenman Pederson, Inc.

Concrete Section
Chairman: Thomas J. Pasko, Jr., Federal Highway Administration

Committee on Performance of Concrete
Chairman: Donald J. Janssen, University of Washington
M. Arockiasamy, Philip D. Cady, William P. Chamberlin, Glenn William De Puy, Philip H. DeCabooter, John W. Figg, Kenneth C. Hover, Joseph F. Lamond, James W. Mack, Richard C. Meininger, Roger P. Northwood, John T. Paxton, Steven A. Ragan, V. Ramakrishnan, John Ryell, David Stark, Joyce M. Susa, Richard Edwin Weyers

Committee on Mechanical Properties of Concrete
Chairman: Michael M. Sprinkel, Virginia Department of Transportation
Archie F. Carter, Jr., Robert J. Girard, W. Charles Greer, Jr., James D. Grove, Lloyd E. Hackman, Lawrence I. Knab, Louis A. Kuhlmann, Joseph F. Lamond, Colin Lobo, V. M. Malhotra, Edward G. Nawy, Steven A. Ragan, V. Ramakrishnan, Masood Rasoulian, Gary L. Robson, M. Reza Salami, Charles F. Scholer, Raymond J. Schutz, S. P. Shah, James M. Shilstone, Sr., Parviz Soroushian, D. Gerry Walters, Dan G. Zollinger

Committee on Chemical Additions and Admixtures for Concrete
Chairman: V. Ramakrishnan, South Dakota School of Mines
Bernard C. Brown, John W. Bugler, Ramon L. Carrasquillo, Henry H. Duval, Jr., Richard D. Gaynor, Robert Douglas Hooton, Kenneth C. Hover, Daniel P. Johnston, Kamal Henri Khayat, Torbjorn Larsen, Mosongo Moukwa, H. Celik Ozyildirim, Michael F. Pistilli, Jere Rose, Maris A. Sermolins, A. Haleem Tahir, Samuel S. Tyson, Suneel N. Vanikar, Thomas G. Weil, David Whiting

Transportation Research Board Staff
Robert E. Spicher, Director, Technical Activities
Frederick D. Hejl, Engineer of Materials and Construction
Nancy A. Ackerman, Director, Reports and Editorial Services
Marianna Rigamer, Oversight Editor

Sponsorship is indicated by a footnote at the end of each paper. The organizational units, officers, and members are as of December 31, 1993.

Transportation Research Record 1458

Contents

Foreword

The papers in this volume deal with various facets of concrete technology. They should be of interest to state and local construction, design, materials, and research engineers as well as contractors and material producers.

The first four papers discuss concrete performance from the perspectives of design, specifications, and testing. Wahhab and Asi report on a study to determine the optimum mix design proportions for roller compacted concrete for locally available materials by varying the water-to-cement ratio, coarse-to-fine aggregate ratio, and total aggregate-to-cement ratio. Armaghani and Bloomquist present accomplishments of a major research program underway in Florida to develop a durability specification and rating system for concrete mixtures and structures. Kalinski et al. discuss a study in which the spectral-analysis-of-surface-waves method was used to nondestructively delineate cracking in a damaged concrete that was not visibly detectable. Oren et al. report on a study to evaluate the potential of image analysis for characterizing air voids in portland cement concrete, voids and constituents of asphalt concrete, and aggregate gradation in asphalt concrete. Mather provides a discussion on the paper.

Khazanovich presents a new approach for determining the effects that concrete creep has on deflection and stress distributions in reinforced concrete bridges during construction. He claims the proposed method is simple to implement and, at the same time, offers very high accuracy. Salami et al. discuss an application of genetic algorithms to the system optimization of failure, constitutive modeling and strengths of concrete, and other geological materials. They note that genetic algorithm is capable of optimizing the system parameters quickly and accurately. Ramakrishnan and Yalamanchi present the results of an experimental investigation to determine the influence of specimen size, fiber type, and fiber content on the flexural behavior of steel fiber reinforced concrete. Ramakrishnan et al. present the results of an experimental evaluation of the physical and elastic properties of monofilament polypropylene fiber reinforced concretes. They report a significant increase in impact strength, an increase in the toughness, and a positive improvement in the fatigue resistance with the addition of fibers. Zellers and Ramakrishnan present a comparative evaluation of physical properties for plain concrete and concrete reinforced with collated fibrillated polypropylene fibers. They report a slight increase in the flexural strength as the fiber content was increased. They also report that the addition of fibers produced less than five percent difference in the static modulus, compressive strength, and pulse velocity.

The following three papers address the use and management of by-products in cementitious systems. MacKay and Emery present case histories documenting the use of various combinatioins of cements, fly ash, and by-product kiln dusts to stabilize/solidify a wide range of contaminated materials. The stabilization processes developed enabled the treated materials to satisfy environmental and engineering requirements. Salt et al. discuss the use of portland cement to solidify/stabilize contaminated spent blasting abrasives and produce a usable construction material. The research resulted in the production of concrete blocks that were used as filler material in dolphins around bridge piers. Soroushian et al. report on an experimental program substituting lightweight aggregate with recycled plastics in lightweight concrete. They noted that plastics enhanced the toughness characteristics, shrinkage cracking, and impact resistance and produced desirable permeability characteristics and acceptable compressive strength-to-unit weight ratios.

The following three papers discuss the curing of concrete containing admixtures. Okamoto and Whiting report on the use of maturity and pulse velocity techniques to predict strength gain of rapid concrete pavement repairs during the curing period. Khayat and Lessard discuss an investigation to determine the influence of early heat curing on the properties of air-entrained, high-strength concrete. They report that this concrete can secure high early strength without early heat curing. Thomas and Matthews summarize the findings of a 5-year laboratory investigation on the effect of curing on the durability of fly ash concrete. They report that, although all concretes required adequate curing to achieve their potential properties, concretes containing fly ash were more sensitive to poor curing.

Kakodkar et al. present the results of a study to determine the influence of five different Class C fly ashes on inhibiting the expansion of concrete due to alkali-silica reaction. The test results had shown that some Class C fly ashes, at adequate replacement levels, were effective in reducing the expansions

to negligible levels even in highly reactive sands. Ramakrishnan et al. present the results of an extensive study to determine the influence of natural pozzolans in reducing the deleterious expansion of concrete due to alkali-silica reaction. The test results showed that all the natural pozzolans used in the study, except one, were very effective in reducing the expansions due to alkali-silica reaction. Johnston discusses a modified interpretation of the ASTM P214 test results for determining potential reactivity of sands used for concrete in South Dakota.

Optimization of Roller-Compacted Concrete for Local Application

H.I. AL-ABDUL WAHHAB AND I.M. ASI

Recently constructed asphalt pavements in Saudi Arabia are experiencing a high level of wheel track rutting, which is mainly attributed to the high ambient pavement temperature, the high volume of loaded trucks, and the viscoelastic behavior of the asphalt pavement. One proposed solution is to use reinforced concrete rigid pavement. Because of corrosion of the reinforcement bars, a common problem in Saudi Arabia, it is better to use roller-compacted concrete (RCC) pavements. A comprehensive and rational design of RCC mixes, such as conventional concrete, is extremely complex, because it is influenced by numerous factors that depend on the sources of materials and their properties; methods of preparation, placement, compaction, and curing; and, most important, prevailing environmental conditions. Incorporation of all these factors into RCC mix design not only requires the arduous selection of appropriate proportions of the ingredients, but also inaccuracies occur in the required properties of RCC that are usually rectified by trial-and-error procedures. Effects of variation of the water to cement ratio, coarse-to-fine aggregate ratio, and total aggregate to cement ratio, on rollability, density, and strength of RCC are investigated for three compactive efforts. The main objective is to find optimum mix design proportions for locally available materials by varying the mentioned variables and to develop a model to predict the flexural strength of local mixes.

The increase in the number of heavily loaded trucks using the Saudi Arabian road network, and the country's high ambient temperatures, have resulted in wheel path rutting. One proposed solution to this problem is to use rigid pavement. However, because of humidity levels and high water-table levels (especially in the coastal areas of Saudi Arabia) and an environment that causes corrosion of reinforcement bars and dowels, roller-compacted concrete pavement (RCCP) may be an option. RCCP is a mixture of aggregates, binder, and a small amount of water, which forms a zero-slump portland cement concrete that is spread and compacted, first with an asphalt paver and then with a vibratory roller, to obtain satisfactory results. The resulting pavement is of higher strength and load-carrying capability than conventional concrete pavement. Traditional RCCP is like a central-mixed cement-treated base (CTB) or soil cement. Some major differences that exist between them are (*1,2*)

- Compressive and flexural strengths of RCCP are higher than CTB, because of the greater content of portland cement (usually 12 to 14 percent cement for RCCP and 6 to 8 percent cement for CTB.
- RCCP does not need a protective wearing surface whereas CTB needs to be covered.
- A true paver or laydown machine normally is used for placing and finishing RCCP.
- RCCP is designed to resist abrasion from traffic, to remain durable under severe weather exposure, and to have a satisfactory surface finish and straight-edge tolerance for the traffic served.

Civil Engineering Department, King Fahd University of Petroleum and Minerals, Dhahran 31261, Saudi Arabia.

The first highly publicized RCCP was built in Canada by the British Columbia Forest Products Company on Vancouver Island at Caycuse Dry Log Sort in summer 1975. Because of the ease and simplicity of construction, and that it's possible to save one-third or more of the cost of conventional concrete pavement construction (*3*), this new technology is catching on so fast that, to date, several RCCPs have been built in other parts of Canada, the United States, Spain, Sweden, and Australia (*4–7*).

Some advantages of RCCP are its high flexural strength (25 percent higher than CTB) and its high resistance to abrasion and fuel and hydraulic spills. Tires turning in hot weather have no effect on it, and it is less affected by summer temperature. Finally, it has the advantage of reduced construction time and cost (*1–6*). However, because RCCP technology is in its infancy, standard procedures for proportioning and fabricating samples are virtually nonexistent. Commonly used procedures are based on an arbitrary selection of mix parameters. Batches are prepared using trial-and-error procedures, and adjusted to achieve the required density, rollability, and strength. Some samples have been fabricated by consolidating them on vibrating tables (*2*) and by using a modified proctor (*8*) and a Kango hammer (*5*).

This study applied factorial experiment design, which facilitates analysis of the combined effects of two or more variables and their interactions in terms of density, rollability, and strength—with a view to optimizing mix designs. Samples were fabricated using a California kneading compactor.

MATERIALS

The three main ingredients of RCCP are aggregate, portland cement, and water. The selected materials are described in the following sections.

Aggregate

Composition and variation of the aggregate is an important component of all concretes, particularly of roller-compacted concrete (RCC). Several concrete properties, such as density and surface texture, are affected by parameters such as the coarse-to-fine aggregate ratio and the coarse-to-total-aggregate ratio. If the aggregates are well proportioned, a high density and impermeable RCC is formed. RCC has a low water content and therefore is likely to segregate. To avoid segregation, maximum aggregate size should not exceed 22 mm ⅞ in.) (*9*) and should contain a high proportion of fines. However, if the pavement is to be laid in lifts, the base lift could have an aggregate size of up to 37.5 mm (1.5 in.). At least 66 percent of the aggregate should be crushed stone (*6*). Aggregate gradations used in Canada and Spain are indicated in Figure 1. The Canadian limits appear to have a wider band, although

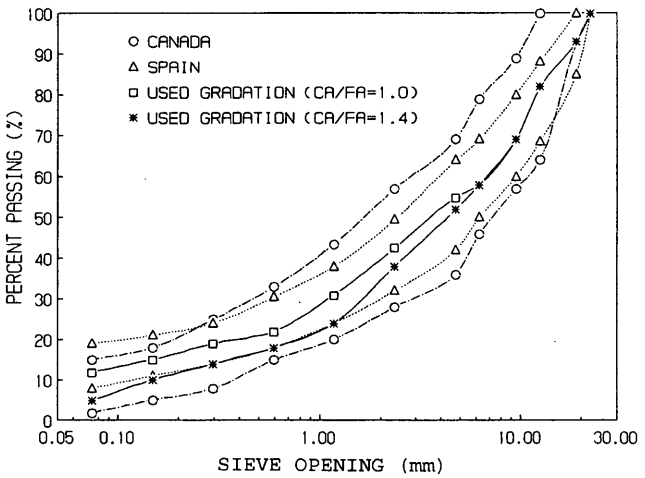

FIGURE 1 Aggregate gradations used in Canada and Spain.

they appear to have common limits, ranging from .075 to 19 mm (.003 to 0.75 in.). All gradations were chosen to minimize segregation in the mix.

In this research, coarse and fine aggregates were collected from local areas. Coarse aggregate was collected from the Al-Summan area near Riyadh. The area is potentially a large source of aggregate. The aggregate (limestone) is excavated and crushed into various sizes to have angular shape and rough texture. The fine aggregate was natural sand and was collected near Dhahran. The two aggregates were proportioned to form two gradation envelopes with different coarse-to-fine aggregate (CA/FA) ratios (Figure 1). Those gradations were chosen to fall within the specified limits shown in Figure 1 and contain enough fines to prevent segregation. The aggregate was subjected to a series of quality tests in accord with ASTM standard specifications for concrete aggregate ASTM C33. Test results and ASTM limits are presented in Table 1. Results indicate that the selected aggregate satisfies ASTM requirements.

Cement Content

Cementitious content by weight of aggregate should be between 12 and 14 percent (*2*). It may be made up of portland cement and additives such as fly ash. Because wear resistance is not a factor in the bottom lift of a multiple-lift construction, a reduction of cement content from 6 to 8 percent by weight of aggregate is recommended (*7*). In cases where sulphate exposure is not a problem, any available portland cement, (with the exception of Type III portland cement) or a combination of portland cement and pozzolan, or blended hydraulic cement with pozzolan, can be used. If sulphate exposure is a problem, Type II, Type V, or a moderate sulphate-resistant blended hydraulic cement should be used (*2*). Because sulphate attack is a major problem affecting concrete durability in the coastal areas of Saudi Arabia, ASTM Type V cement was used in all the mixes.

Water Content

Water content is proportioned in such a way that the resulting RCC has zero-slump and maximum density under compaction. The

TABLE 1 Summary of Test Results on Aggregates

Aggregate Type	Property	Test Results		ASTM Limit
Coarse	Grading	3/4" maximum size grading specified in literature		-
	Specific gravity	Bulk specific gravity oven dry basis	= 2.613	-
		Bulk specific gravity (SSD) basis	= 2.646	-
		Apparent specific gravity	= 2.702	-
	Absorption	24-hour	= 1.26%	-
	Abrasion loss	23.25%		40%
	Presence of clay lumps and friable particles	0.74%		3% to 10%
	Soundness	0.58%		12%
Fine	Grading	Fine modulus = 1.46		2.3-3.1
	Specific gravity	Bulk specific gravity oven dry basis	= 2.614	-
		Bulk specific gravity (SSD) basis	= 2.634	-
		Apparent specific gravity	= 2.667	-
	Absorption	24-hour	= 0.77%	-
	Presence of clay lumps and friable particles	#8 = 0.45%	#16 = 0.18%	3%
	Soundness	1.38%		10%

method outlined in ASTM D558 (ASTM 1988h) treats RCC as soil cement instead of concrete and thus establishes a relationship between moisture and density for an applied compactive effort. Abrams and Jacksha (*10*) have suggested a water cement (W/C) ratio in the range of 0.3 to 0.4. Results of initial mix trials indicate that this range is too narrow for local aggregates. The W/C ratio range was therefore adjusted to a range of 0.3 to 0.5. In this research, potable water available from a laboratory faucet was used in all stages of testing, preparation, and curing of the concrete.

EXPERIMENTAL PROGRAM

RCC for pavements must attain a consistency similar to soil cement yet still possess some features of conventional concrete, such as strength and durability. In the design of a mix, particular attention should be given to the three most important factors controlling the quality of concrete: W/C ratio, CA/FA ratio, and total aggregate to cement ratio (TA/C).

To achieve the appropriate mix design for rollability, density, and strength (comprehensive and flexural), trials usually have to be conducted that are not only laborious but also time-consuming. One objective of this study is to investigate several mix proportions in terms of rollability, strength, and density, for three different compactive efforts.

To test for the different variables, five levels of W/C (0.3 to 0.5), four levels of TA/C (5.4 to 7.0), and two levels of CA/FA (1.0 and 1.4) were chosen, as shown in Table 2. By using these levels, a factorial experiment was designed to explore the effect of the factors on rollability, density, and flexural strength of RCC and the interactions among the factors.

Typical RCC mix proportions for four countries are shown in Table 3. The rationale behind a country's selected the mix proportions relates to a mix's strength and serviceability, the availability of constituent materials, and cost.

A Hobart electrically operated, laboratory mechanical mixer with a capacity of 0.012 m^3 (732 $in.^3$) was used to mix the ingredients for RCC. Mixing was done in batches; water was the last ingredient added. The water and other ingredients were mixed vigorously for 3 min to reduce the chance of segregation.

The Ronny Anderson method (*5*) was used to measure rollability (the ability to roll or compact the zero-slump concrete with reasonable effort while maintaining its homogeneity without segregation). In the Ronny Anderson method, 2.5 kg (5.5 lb) of RCC is placed into a cylindrical form. A 13.3-kg (20.3-lb) weight is lifted into place, and a vibrating table is run for 20 sec. The rate at which the weight sinks (the rate of compaction) may be used as a measure of rollability.

Currently there are no standard procedures for making test specimens. The authors decided to use a California kneading compactor to compact the test specimens because it is the best means of simulating construction compaction (similar to ASTM D3202-83 setup). The kneading compactor was calibrated to find a suitable foot pressure for achieving the highest density with minimal degradation. This pressure was found to be 1551 kPa (225 psi).

The RCC from each mix was cast into three 400 × 100 × 100-mm (16 × 4 × 4 in.) beams using a single layer; the beams were then subjected to three chosen compactive efforts corresponding to 50, 100, and 150 tamps, respectively, at a foot pressure of 1551 kPa (225 psi). Initial consolidation was achieved by subjecting the sample to a static load of 621 kPa (90 psi) before it was transferred to the compactor. Applying static load not only constitutes initial compaction but is also a means of obtaining a relatively flat finished beam surface.

The specimens were covered with wet burlap for 24 hr and cured for 28 days in a curing tank filled with water, per ASTM Standard C192.

RESULTS

Within the range of W/C ratios, all samples were within an acceptable range of rollability. Figures 2 to 7 show the effects of varying W/C, C, CA/FA, and number of tamps, on flexural strength and mix density. Results indicate that for the W/C ratio used, the 28-day flexural strength improves by increasing the W/C ratio to a maximum value, then it starts decreasing. This finding is attributed to the fact that, in the early stages, cement mortar acts as a filler material, filling the voids between the aggregates until all voids are filled. The same is true for density. The maximum flexural strength was 6.7 MPa (971.5 psi), corresponding to a W/C ratio of 0.45 and a CA/FA

TABLE 2 Schematic Representation of the Experimental Design

Levels of A (CA/FA)	Levels of C (TA/C)	Levels of B (W/C)				
		.3	.35	.4	.45	.50
1.4	7.0	$a_1b_1c_1$*	$a_1b_2c_1$	$a_1b_3c_1$	$a_1b_4c_1$	$a_1b_5c_1$
	6.4	$a_1b_1c_2$	$a_1b_2c_2$	$a_1b_3c_2$	$a_1b_4c_2$	$a_1b_5c_2$
	5.8	$a_1b_1c_3$	$a_1b_2c_3$	$a_1b_3c_3$	$a_1b_4c_3$	$a_1b_5c_3$
	5.4	$a_1b_1c_4$	$a_1b_2c_4$	$a_1b_3c_4$	$a_1b_4c_4$	$a_1b_5c_4$
1.0	7.0	$a_2b_1c_1$	$a_2b_2c_1$	$a_2b_3c_1$	$a_2b_4c_1$	$a_2b_5c_1$
	6.4	$a_2b_1c_2$	$a_2b_2c_2$	$a_2b_3c_2$	$a_2b_4c_2$	$a_2b_5c_2$
	5.8	$a_2b_1c_3$	$a_2b_2c_3$	$a_2b_3c_3$	$a_2b_4c_3$	$a_2b_5c_3$
	5.4	$a_2b_1c_4$	$a_2b_2c_4$	$a_2b_3c_4$	$a_2b_4c_4$	$a_2b_5c_4$

*Three samples were fabricated and tested for each cell.

TABLE 3 Typical Mix Proportions for Four Countries

CANADA		
Aggregate	3480 lb/yd³	CA/FA = 1.86
Portland Cement Type I	448 lb/yd³	TA/C = 6.5
Fly Ash	90 lb/yd³	W/C = 0.35
Water	188 lb/yd³	
Average Compressive Strength = 4570 psi (31.5 MPa) at 28 days		
SPAIN		
Gravel 10 to 30 mm	390 lb/yd³	CA/FA = 1.38
Gravel 0 to 10 mm	2750 lb/yd³	
Sand 0 to 5 mm	400 lb/yd³	TA/C = 8.05
ASTM Class C Fly Ash	150 lb/yd³	
Category P-450 Cement	290 lb/yd³	W/C = 0.42
Water	185 lb/yd³	
Average Compressive Strength = 2850-3560 psi (20-25 MPa) at 28 days		
SWEDEN		
Gravel 16-30 mm	573 lb/yd³	CA/FA = 1.5
Gravel 0-16 mm	2076 lb/yd³	
Sand 0- 5 mm	691 lb/yd³	TA/C = 5.26
Cement	635 lb/yd³	
Water	219 lb/yd³	W/C = 0.34
Average Compressive Strength = 5800 psi (40 MPa) after 28 days		
U.S.A. [Portland Airport]		
Gravel	1550 lb/yd³	CA/FA = 1.17
Sand	1700 lb/yd³	
Cement Type I	488 lb/yd³	TA/C = 5.35
Pozzolan (Class F)	119 lb/yd³	
Water	260 lb/yd³	W/C = 0.43
Average Flexural Strength = 710 psi at 28 days		
U.S.A. [Multnomah County Rd.]		
Aggregate	3309 lb/yd³	CA/FA = 0.75
Cement-Pozzolan Type I P	550 lb/yd³	TA/C = 6.02
Water	242 lb/yd³	W/C = 0.44
Average Flexural Strength = 600 psi (4.1 MPa) at 28 days		

1 kg/m³ = 1.868 lb/yd³ TA/C = Total Aggregate to Cement ratio
CA/FA = Coarse to Fine Aggregate ratio W/C = Water to Cement ratio

ratio of 1.4, for a mixture of 15 percent cement with 150 tamps. Flexural strength of normal concrete prepared using the same aggregate gradation at an optimum W/C ratio generates a value of 4.2 MPa (612.0 psi). That indicates an increase of about 37 percent in the flexural strength of RCC above that of normal concrete.

The total aggregate cement (TA/C) ratios used in the mixes were 5.4, 5.8, 6.4, and 7.0. For all W/C ratios, an increase in the total aggregate resulted in a decrease in strength. At lower TA/C ratios, the volume of the cement paste is greater, and it plays a greater role in improving strength. On the other hand, increasing the CA/FA ratio increases gaps between the aggregate, allowing the cement to coat the aggregate effectively. That resulted in the mixes' increased flexural strength.

To check that the studied variables (TA/C, CA/FA, and W/C) significantly affect flexural strength and density, an analysis of variance was performed on all test results. Analysis of variance determined that the source of variation due to TA/C, CA/FA, and W/C is highly significant when compared with values of F (variance ratios) at a 95 percent probability level (0.05 significance level). That finding indicates the underlying influence of such variables on the strength and density of RCC.

Statistical methods were used to fit a model between the obtained flexural strength of the RCC mixes and the applied variables (CA/FA, TA/C, W/C, and number of tamps). Figures 2 to 4 indicate that the relation between flexural strength and W/C ratio has the shape of a sine function, but for the other variables the relation is linear. The resulting model is

$$\text{Flexural strength} = 7.44 - 1.18\,(\text{TA/C}) + 1.81 \sin\left[\left(\frac{\text{W/C} - .3}{.15}\right) * \frac{\pi}{2}\right] + 1.94\,(\text{CA/FA}) + 0.0059\,(\text{no. of tamps}) \quad (1)$$

The model has a coefficient of determination of 95.6 percent.

A stepwise selection analysis indicates that the important variables affecting flexural strength are TA/C, W/C, CA/FA, and the

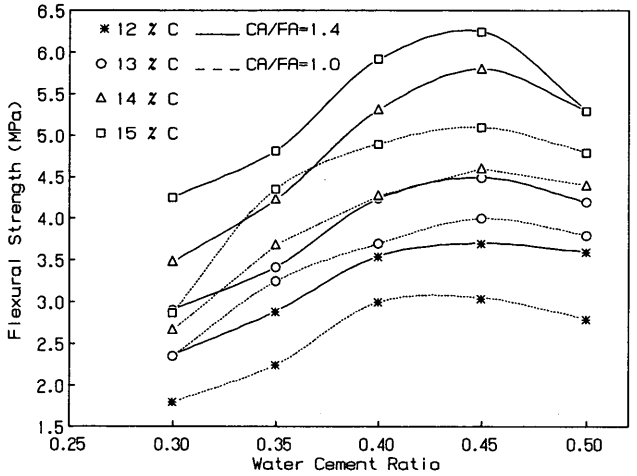

FIGURE 2 Relation between W/C ratio and flexural strength for a compaction effort of 50 tamps.

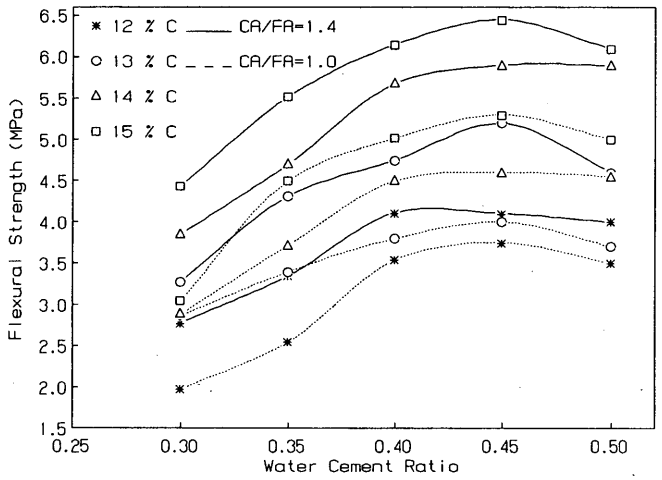

FIGURE 3 Relation between W/C ratio and flexural strength for a compaction effort of 100 tamps.

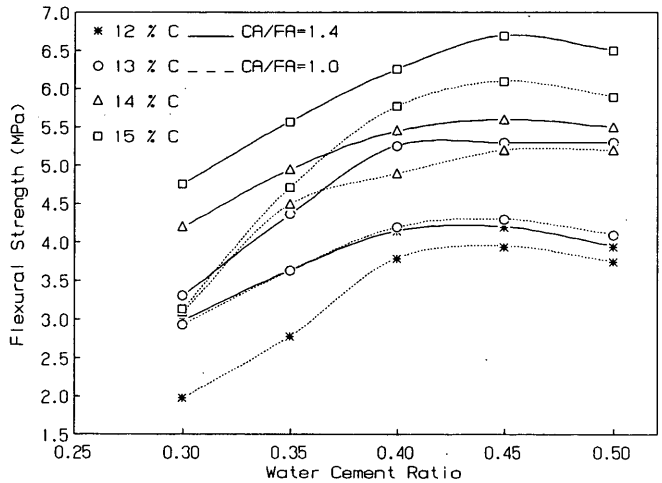

FIGURE 4 Relation between W/C ratio and flexural strength for a compaction effort of 150 tamps

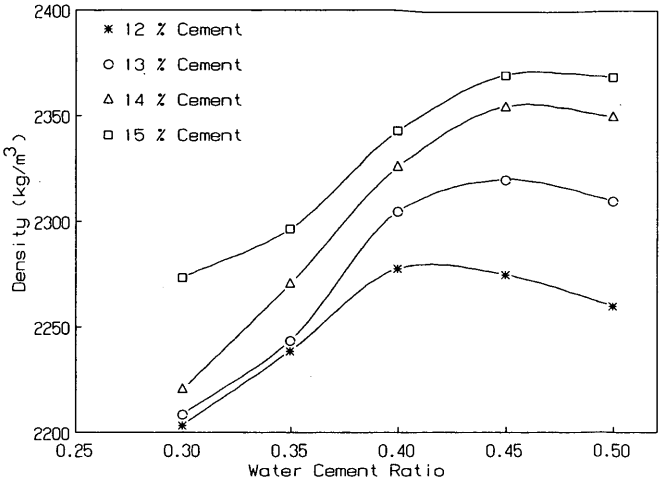

FIGURE 5 Relation between W/C ratio and density for a compaction effort of 50 tamps.

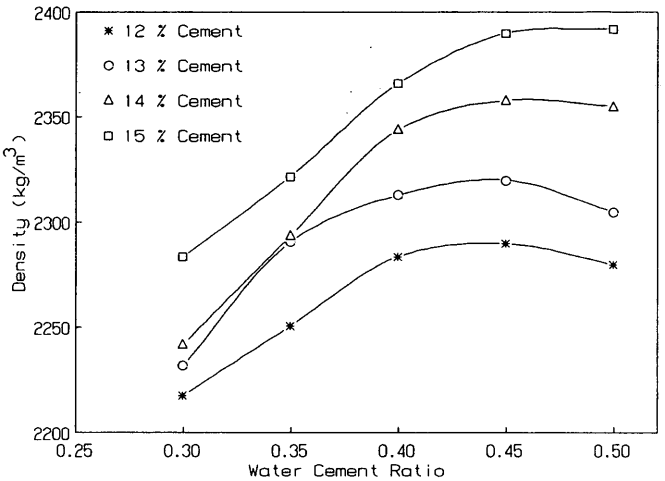

FIGURE 6 Relation between W/C ratio and density for a compaction effort of 100 tamps.

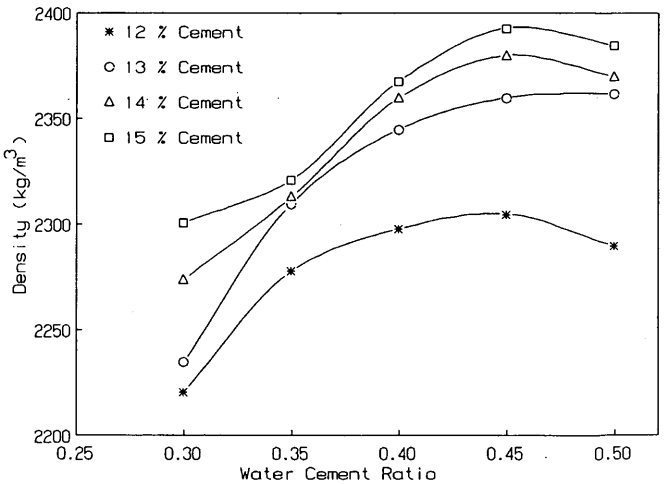

FIGURE 7 Relation between W/C ratio and density for a compaction effort of 150 tamps.

TABLE 4 Fitted Model Statistics

Stepwise Selection				
Selection: Forward	Maximum steps: 500		F-to-enter: 4.00	
Control: Manual	Step: 4		F-to-remove: 4.00	
R-squared: .95785	Adjusted: .95638	MSE: 0.0531012	d.f.: 115	

Variables in Model	Coeff.	F-Remove	Variables Not in Model	P. Corr.	F-Enter
1. TA/C	-1.18228	1160.8486			
2. W/C	1.81215	980.7224			
3. CA/FA	1.93613	338.8497			
4. TAMPS	0.00593	132.6122			

Model Fitting Results

Independent variable	coefficient	std. error	t-value	sig. level
CONSTANT	7.438022	0.256845	28.9592	0.0000
TA/C	-1.182281	0.0347	-34.0712	0.0000
W/C	1.812152	0.057866	31.3165	0.0000
CA/FA	1.936132	0.10518	18.4079	0.0000
TAMPS	0.005934	0.000515	11.5157	0.0000

R-SQ. (ADJ.) = 0.9564 SE = 0.230437 MAE = 0.185586 DurbWat = 1.297
Previously: 0.0000 0.000000 0.000000 0.000
120 observations fitted, forecast(s) computed for 0 missing val. of dep. var.

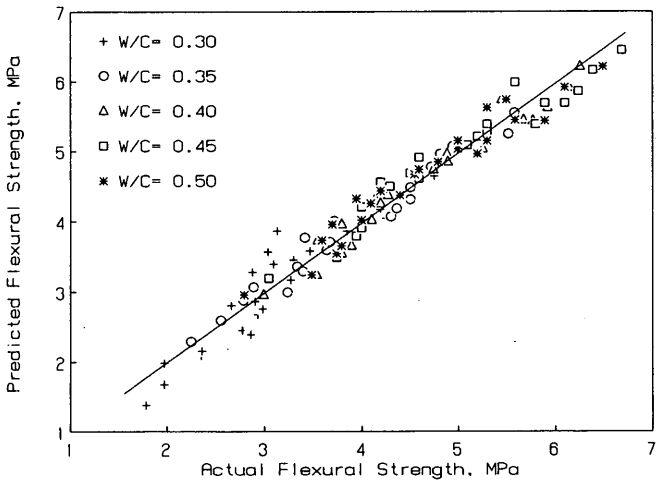

FIGURE 8 Comparison between predicted and actual flexural strength.

number of tamps, respectively. Stepwise analysis and model fitting results are shown in Table 4. The model is applicable to local materials and can be used for the ranges of all variables indicated in Table 2. Figure 8 shows the relation between measured flexural strength and the model predicted values and indicates that the predicted values are close to the measured ones.

CONCLUSIONS

- Chosen local aggregates meeting the requirements of ASTM C33 can be used for fabrication of quality RCCP.
- For the local aggregates, a W/C ratio ranging from 0.3 to 0.5 produces mixes with acceptable rollability.
- Because of its lower water content, the flexural strength RCC is about 37 percent higher than the flexural strength of normal concrete.
- Statistical analyses reveal that the effects of TA/C and CA/FA ratios on flexural strength and density are highly significant for all W/C ratios studied.
- Gain in strength between 100 and 150 tamps is not so significant to justify the effort.
- The model is descriptive of the strength data developed for these particular aggregates within the range of the experimental variables.

ACKNOWLEDGEMENT

The authors thank the Ministry of Communications and the King Fahd University of Petroleum and Minerals for providing valuable support.

REFERENCES

1. Al-Otaibi, M. H., A. M. Samad, S. A. Shihata, and F. F. Wafa. Roller Compacted Concrete Pavement; Materials Characterization. *Proc., 3rd Saudi Engineering Conference,* Vol. 1, Riyadh, Saudi Arabia, Nov. 1991, pp. 95–102.
2. Pittman, D. W., and S. A. Ragan. *A Guide for Design and Construction of Roller-Compacted Concrete Pavements.* Final Report prepared for US Army Corps of Engineers, Washington, D.C., Nov. 1986.
3. Pittman, D. W. Construction of Roller-Compacted Concrete Pavements. In *Transportation Research Record 1062,* TRB, National Research Council, Washington, D.C., 1986, pp. 13–19.
4. Abrams, J. M., J. L. Jacksha, R. L. Norton, and D. J. Irvine. Roller-Compacted Concrete Pavement at Portland International Airport. In

Transportation Research Record 1062, TRB, National Research Council, Washington, D.C., 1986, pp. 20–24.
5. Anderson, R. Swedish Experiences with RCC. *Concrete International: Design and Construction,* Vol. 9, No. 2, Feb. 1987, pp. 18–24.
6. Jofre, C., A. Josa, and F. Molina. The Paving of Low-Volume Roads in Spain with Roller-Compacted Concrete. In *Transportation Research Record 1106,* TRB, National Research Council, Washington, D.C., 1987, pp. 301–308.
7. Piggot, R. W. Roller-Compacted Concrete for Heavy-Duty Pavements: Past Performance, Recent Projects, and Recommended Construction Methods. In *Transportation Research Record 1062,* TRB, National Research Council, Washington, D.C., 1986, pp. 7–12.
8. Logie, C. V., and J. E. Oliverson. Burlington Northern Railroad Intermodal Hub Facility. *Concrete International: Design and Construction,* Vol. 9, No. 2, Feb. 1987, pp. 37–41.
9. Piggot, R. W., and O. O. Naas. Roller-Compacted Concrete Pavements in British Columbia, Canada. *Proc., Symposium on Roller Compacted Concrete, ASCE,* Denver, Colorado, May 1–2, 1985, pp. 31–47.
10. Abrams, J. M. and J. L. Jacksha. An Airport Apron and a Country Road. *Concrete International: Design and Construction,* Vol. 9, No. 2, Feb. 1987, pp. 30–36.

Publication of this paper sponsored by Committee on Performance of Concrete.

Development of Concrete Durability Specification and Ratings in Florida

JAMSHID M. ARMAGHANI AND DAVID G. BLOOMQUIST

A major research program is underway in Florida to develop a durability specification and rating system for concrete mixtures and structures. As part of the program, field and laboratory water-permeability tests have been developed and are being used with the AASHTO T277 rapid chloride permeability test to predict concrete durability. Presented are the scope and accomplishments to date, including descriptions and applications of the laboratory and field permeability tests, and the development of a permeability classification system on the basis of water permeability results. The durability specification and rating system should result in significant long-term improvement of concrete structures in aggressive environments. Other benefits include effective concrete quality control, efficient use of bridge maintenance funds, and substantial reduction in the cost of bridge rehabilitation.

Durability plays an important role in determining the long-term performance of concrete bridges in aggressive environments. Poor concrete durability can result in premature deterioration of bridges and other structures, resulting in substantial repair costs. Sea water can cause corrosion of the reinforcing steel and damage to the bridge substructure, and, in cold climates, deicing salts contribute to steel corrosion and deterioration of the bridge superstructure. Millions of dollars are spent annually to repair bridges. In the Florida Keys, for example, the cost of repairing corrosion-related damage on a 10-year-old bridge was approximately 25 percent of the original construction cost.

Despite its significant impact, concrete durability has not been emphasized in most specifications. Compressive strength traditionally has been considered as the only criterion on which concrete quality is assessed. Most material engineers design concrete mixtures on the basis of target strength, and they tacitly assume that this strength will ensure high durability. Results from a study in Florida (*1*) indicated that concrete mixtures of equal strength yielded variable levels of permeability (a property closely related to concrete durability). Tests also revealed that high strength did not automatically produce high durability, (i.e., compressive strengths of 45 to 50 MPa may not produce consistently low permeability values). Only at compressive strengths of at least 55 MPa (8,000 psi) would the concrete develop low permeability and corresponding high durability.

Designing mixtures for 55 MPa (or greater) may require a high cement content, an option that may not be favored in certain situations. In warm environments with mass concrete elements, for example, high cement content produces excessive heat and can cause high thermal volume change. That problem often results in macro or micro cracking, which obviously offsets any improvement in durability.

J. Armaghani, Florida Department of Transportation, 2006 N.E. Waldo Road, Gainesville, Fla. 32609. D. Bloomquist, Civil Engineering Department, University of Florida, 345 Weil Hall, Gainesville, Fla. 32611.

Another option is to engineer concrete mixtures with moderate strengths and low permeability. In such mixtures, the cement is partially replaced by pozzolans, such as fly ash, blast furnace slag, and microsilica. The mixtures require low water-to-cement (W/C) ratios and the use of ordinary and high-range water reducers to achieve desired workability. The key to developing durable mixtures and ensuring their in-service quality is to establish ratings and specifications for durability in terms of strength and permeability. To achieve this objective, development of standardized permeability tests is necessary.

In 1989, the Florida Department of Transportation (FDOT) embarked on a long-term, multiphase research program to develop a durability specification and rating system for concrete mixtures and structures. This paper presents an overview of the FDOT research program and describes the laboratory and field tests developed to measure permeability. It also includes a tentative permeability classification system that has been derived from water permeability test results. Anticipated benefits from ongoing research are also cited.

FDOT RESEARCH PROGRAM

The study has two primary goals: (a) develop a durability specification for concrete mixtures in terms of strength and permeability, and (b) devise standard durability ratings for concrete structures. A number of tasks were formulated to accomplish these goals.

The first task involved developing equipment and procedures for testing concrete permeability, in the laboratory and the field. Water permeability tests were designed to provide predictive estimation of concrete durability. The task was completed, and the resulting new field and laboratory equipment were used to complete subsequent tasks.

Figure 1 shows a flow chart of the major components of the program. A wide range of concrete mixtures and structures were tested and the results compiled in a large data base. From the data base, permeability classifications were developed and durability classes established for concrete mixtures and structures. Finally, tentative durability specifications and rating standards for concrete were developed and are being implemented.

PERMEABILITY TESTS

Research was directed toward developing equipment and procedures for measuring water permeability, in the laboratory and field. This portion of the research was a cooperative effort between FDOT and the University of Florida. The rapid chloride permeability test (RCPT) was used in the testing program.

As the laboratory water permeability test (LPT) and the apparatus for the RCPT were set up in the FDOT research laboratory, a

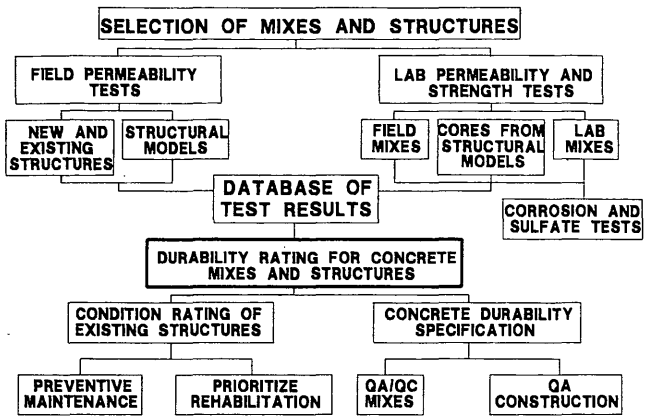

FIGURE 1 Flow chart of main tasks of the research program.

field permeability test (FPT) was used to measure the permeability of various in-place structural elements of bridges around the state.

LPT

The LPT used for this study is a water permeability test developed at the University of Florida (*2*). Figure 2 shows the test apparatus. The test specimen is a 50-mm (2-in.) thick slice of concrete cut from a 100-mm (4-in.) diameter cylinder or core. The specimen's perimeter is coated with a 25-mm (1-in.) thick epoxy layer, then sealed in a permeameter cell and connected to a manometer tube, as shown in Figure 2. The test begins by injecting water into the manometer tube and reservoir of the permeameter cell. Then 0.69 MPa (100 psi) of pressure is applied to the top of the manometer tube to force water into the specimen. The 0.69 MPa pressure was chosen sufficiently high to simulate a constant head flow test and at the same reduce potential injury to operators.

The amount of water flowing into the specimen is monitored via the manometer tube until a steady-state flow is reached. Experience has demonstrated that steady-state flow is reached after 14 to 21 days. The test is continued for an additional 7 days, during which time the flow of water is recorded at 24 hr intervals.

To obtain the coefficient of permeability, the amount of water, Q, is plotted versus time, after steady-state flow is achieved. Then, by regression, the best fit linear curve and its slope is established for the data points. Finally, Darcy's law is used to determine the water permeability.

Because the permeability of concrete decreases as it is curing, it has been common practice to test the permeability at 28 and 91 days. At each time, two replicate samples are tested and the average of the two is calculated. The test is normally completed between 28 and 31 days. Efforts are underway to reduce testing time by using nitrogen as the fluid.

RCPT

RCPT is the AASHTO T277 and ASTM C 1202-91 test procedure for rapid determination of concrete resistance to the penetration of chloride ions. Various components of the test apparatus are shown in Figure 3. A 50-mm (2-in.) thick specimen is cut from a 100-mm (4-in.) diameter cylinder or core. The specimen is coated on its perimeter with a thin layer of epoxy, then placed and sealed between two acrylic cells. The amount of electric charge that passes through

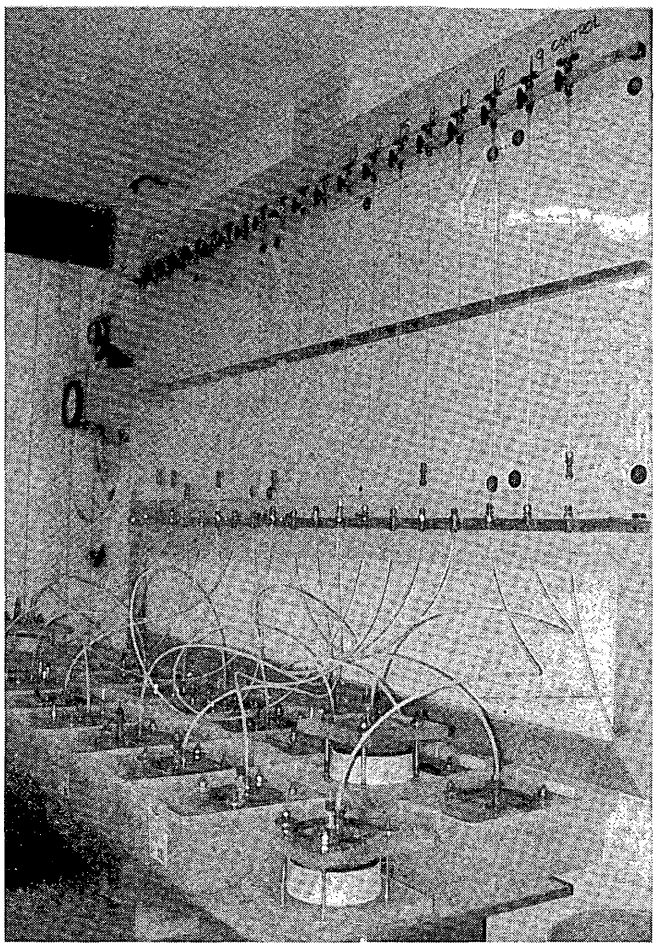

FIGURE 2 Laboratory water-permeability test system.

the sample indicates the sample's chloride permeability. Permeability classification is determined by comparing the sample's coulomb value to those of the classification chart in AASHTO/ASTM standards.

FPT

The FPT, also developed at the University of Florida (*3*), was designed to measure the permeability of in-place structural elements. Several modifications to the equipment were made by FDOT to simplify the test procedure and to reduce the test's duration. Figure 4 shows various components of the apparatus. The control panel and manometer loop for monitoring water flow are housed inside an aluminum case. A pressure-regulated nitrogen supply, air compressor, and hand-held pump provide pressure and vacuum at various stages of the test. The system also uses a drill and coring machine with a 22-mm (7/8-in.) diameter core bit to drill test holes in the member. An array of testing probes is used to force water into the member. Figure 5 shows several of the probes with different test-regions lengths. The area to be tested is sealed off by means of neoprene "packers," cylindrical shaped pieces that, when compressed, expand to seal and isolate the test region. The packers expand as the knurled knobs at the top end of the probe are tightened.

To run a test, a 150-mm (6-in.)-deep hole is drilled in the concrete. The probe is inserted and sealed by the rubber packers' ex-

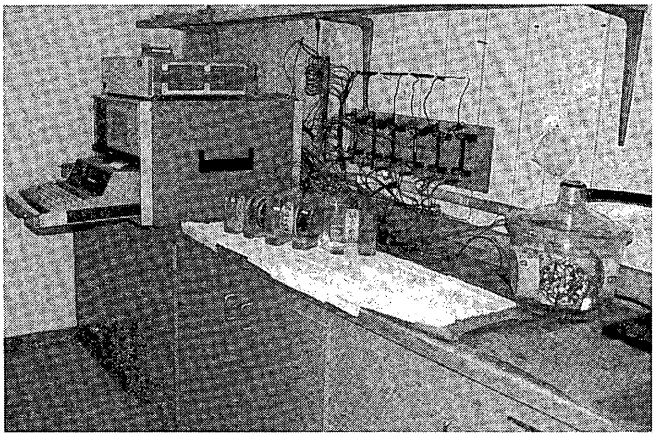

FIGURE 3 Chloride permeability test apparatus.

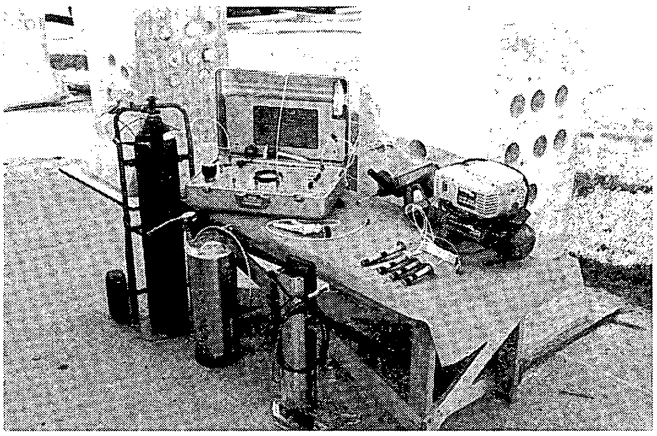

FIGURE 4 Components of field permeability test (FPT) apparatus.

pansion against the hole wall. Depth of the test region inside the concrete is adjustable, ranging from 32 to 89 mm (1.25 to 3.5 in.)

The concrete area around the probe is saturated for at least 1 hr before starting. The test begins by removing air from the system, then water under pressure is injected through holes in the probe and forced into the concrete. The pressure applied to the water may range from 0.69 to 2.1 MPa (100 to 300 psi), depending on the concrete's strength and permeability. Water flow is monitored on the manometer loop at equal time intervals ranging from 5 to 30 min. The test normally is completed in 2 to 3 hrs., depending on how rapidly a steady-state flow condition is reached. The flow rate is measured and applied to a permeability formula (commonly referred to as the Packer/Lugeon equation) to compute the permeability coefficient, k, of the concrete. The equation is given as

$$k = \frac{q}{2\pi L h} \sinh^{-1} \frac{L}{2r}$$

where

q = constant rate of flow into the concrete,
L = length of the test section,
h = differential head, and
r = radius of the hole.

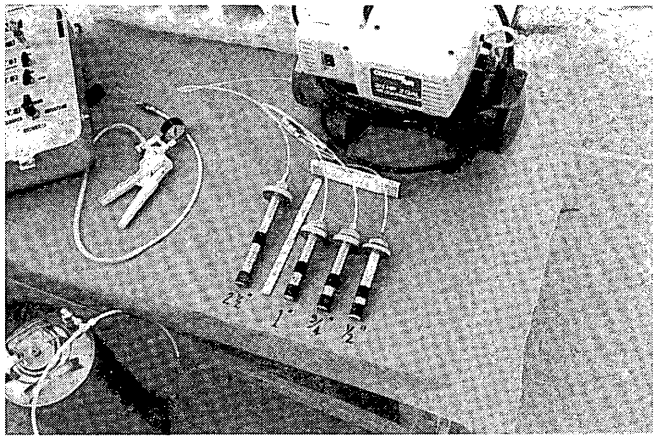

FIGURE 5 Field permeability test probes.

Note that the actual flow pattern into the surrounding concrete is not known but is modeled as a sphere emanating from the probe center, with ellipsoid-shaped equipotential surfaces.

DETAILS OF TESTING PROGRAM

Laboratory Sampling and Testing

A wide range of concrete mixtures produced in laboratory and field environments is being tested. More than 100 laboratory-produced mixtures have been batched and tested since 1989. These concrete mixtures have W/C ratios ranging from 0.25 to 0.45 and cementitious contents ranging from 335 to 580 kg/m^3 (564 to 977 lb/yd^3). Fly ash, microsilica, and slag were included as part of the cementitious material added to concrete mixtures. The fly ash contents ranged between 10 and 50 percent, whereas microsilica contents ranged between 5 and 15 percent. Slag was incorporated at a rate of 50 percent cement replacement. Various types of aggregates were used in the concrete mixtures, including crushed limestone, granite, and river gravel. ASTM Type II cement was used in all but a few mixtures. In every mixture, 222 cc/45 kg of cement (7.5 fl. oz/100 lb cement) of Type D (ASTM C 494) water reducer admixture was used to achieve a target slump of 50 to 100 mm (2 to 4 in.). In addition, Type F (ASTM C 494) high range water reducer was used in several mixtures to supplement the ordinary water reducer to achieve the target slump.

Concrete samples from each mixture were tested for various properties including, compressive, tensile, and flexural strengths; elastic properties; water and chloride permeability; and corrosion and sulfate resistance. The material properties, mixture designs, and results of strength, permeability, and corrosion resistance of 22 of the mixtures evaluated to date are detailed elsewhere (*1*). Design variables for these mixtures included W/C ratio, cement content, and the incorporation of variable rates of fly ash and silica fume as cement replacement.

Results of compressive strength and chloride permeability tests for the 22 mixtures are correlated and presented in Figure 6 (*1*). Concrete mixtures that fall within the same compressive strength range are grouped together. Chloride permeability test results for individual mixtures and the different permeability classes are shown on the vertical axis of Figure 6. The correlation between both test

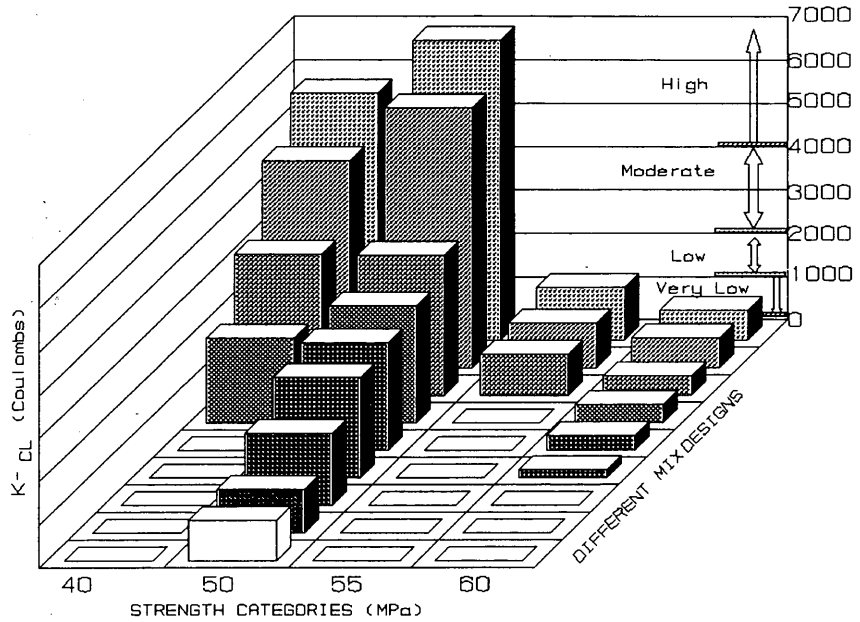

FIGURE 6 Correlation between compressive strength and chloride permeability (K-CL).

results suggests that concrete mixtures in the same strength category do not necessarily fall in the same permeability classification. That finding further demonstrates the need to perform both compressive strength and permeability tests to arrive at a better assessment of concrete durability.

Field Sampling and Testing

The field testing program involves obtaining core samples and testing elements of bridges representing different age groups, including those under construction. It also involves obtaining core samples and testing large, 0.75-m × 0.75-m × 1.50-m (2.5 × 2.5 ft 5 ft) models of columns. The models were cast and cured in two locations outside the laboratory and at bridge construction sites.

Models outside the laboratory were cast with laboratory concrete mixtures that have a proven record of high durability. Figure 7 shows six column models, each representing two concrete mixtures cast outside the laboratory. Each model was cored at several locations; the cores then were tested for laboratory water permeability, chloride permeability, and compressive strength. Field permeability tests were also performed on the column models. Figure 8 shows a previously cored model being presaturated at several points in preparation for field permeability testing. Test results from the models were used to establish correlation between the three permeability tests, and between the permeability and strength of concrete.

Models in the field were cast with the same concrete that was delivered to the construction site and were subjected to the same environmental conditions as the actual structure. Test results obtained from these models should represent properties of concrete within the structure. Figure 9 shows a field model being tested with the FPT apparatus.

Figure 10 shows FPT apparatus testing of a newly placed bridge pile. The tests were performed to evaluate the quality of the bridge pile after construction. Each structural element or model is tested at 2 or 3 locations. Cores also are obtained from the structure for subsequent laboratory testing of permeability and compressive strength. Test results from the actual elements are compared with those obtained from the field models to determine how they compare. Additional specimens are extracted from bridges of various age groups to determine the chloride content and to detect carbonation. Finally, a thorough condition evaluation (and corrosion detection) is conducted.

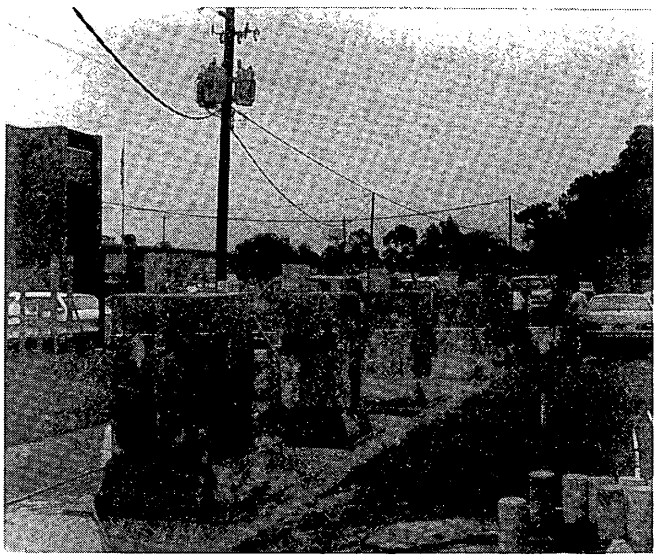

FIGURE 7 Column models cast outside the laboratory.

Whereas this aspect of the research program was time-consuming, labor intensive, and required close coordination with field engineers and contractors, conducting such field tests on actual structural elements and models is essential to developing a durability specification and rating system that is practical to implement.

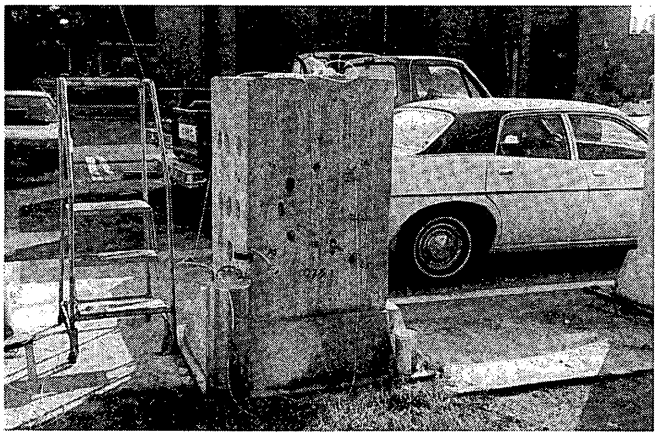

FIGURE 8 Field permeability testing of a column model.

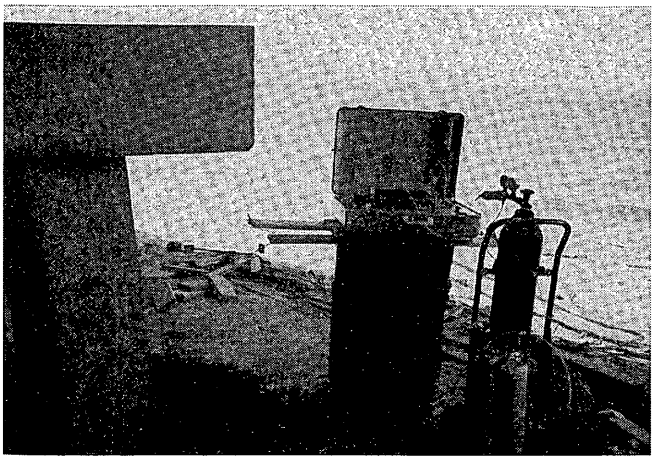

FIGURE 10 Field permeability testing of a bridge pile.

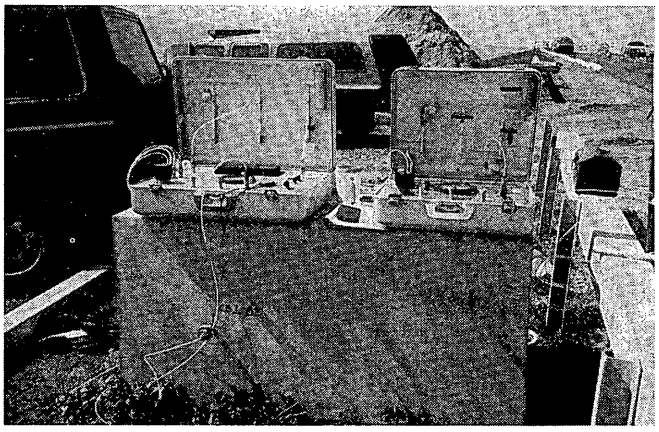

FIGURE 9 Field permeability testing of a field model.

DURABILITY RATINGS AND SPECIFICATIONS

Data Base of Test Results

As part of the testing program, a data base computer program, FLAGCONS (*4*), was developed to manage the laboratory test data. The program was upgraded to handle the field permeability data as well. It provides averages and standard deviations for groups of test results, maintains testing and batching schedules, and flags days on which conflicts exist between sample testing and concrete batching. It has simplified storage, processing, and analysis of the massive amount of data generated by ongoing research.

Correlation of Test Results

From the data base, various correlations between test results are performed. The main correlation established to date is the one among laboratory, field and chloride permeability test data (*1,5*). Table 1 shows the tentative permeability classifications for concrete, the different classifications are basically the same as those listed in AASHTO T277, with the exception of one class termed "very high." The range of chloride permeability values follows AASHTO/ASTM criteria. Ranges for laboratory water permeability (K-water) and field water permeability (K-field) were derived from the data base of more than 100 test results. The data base represents all field and laboratory tests obtained thus far, including test results from research and field models, as well as from old and new structures.

The range of water permeability (laboratory and field) for each classification was established by using a series of steps. First, each concrete mixture prepared in the laboratory or field was sampled for three different permeability tests. Also, where possible, cores were obtained from models and actual elements for laboratory testing of chloride and water permeability. In addition, field permeability tests were performed on the same models and elements. Second, the results for the three tests were tabulated and grouped according to chloride permeability classifications. Finally, ranges for laboratory and field water-permeability values for each permeability class were determined from the data groups corresponding to each chloride permeability classification.

The difference between laboratory and field values is likely because of the test setup (i.e., size of test area) and assumptions made in the field permeability equation derivation. Another difference, that the permeability in the horizontal direction (field) is not the same as the vertical (lab) direction, is possibly due to placement effects. Efforts are underway to develop correlations between permeability and other tests, such as corrosion resistance, sulfate resistance, and chloride content. In addition, results of the condition surveys and corrosion evaluation of existing bridges will be compared with results of concrete permeability and strengths tests on the same bridges.

Durability Rating System for Existing Structures

From the correlation between the condition of the bridges versus concrete permeability and strength, a durability rating system will be developed for in-service structures. The rating values will form a standard by which the condition of bridges can be inferred. The classification could range from very poor to excellent, depending on the rating value assigned. On the basis of this classification, a priority list of deteriorated bridges can be created, resulting in a more accurate assessment of necessary rehabilitation funds. Durability

TABLE 1 Permeability Classification

Concrete Permeability Classification	Permeability Range		
	K-Chloride [a] Coulomb	K-Water (Lab) [b] cm/s (10^{-12})	K-Field [b] cm/s (10^{-12})
Negligible	< 100	< 0.25	< 25
Very Low	100 - 1000	0.25 - 2.5	25 - 150
Low	1000 - 2000	2.5 - 25	150 - 750
Moderate	2000 - 4000	25 - 250	750 - 1500
High	> 4000	250 - 2500	1500 - 5000
Very High	N/A	> 2500	> 5000

1 cm = 0.39 in
[a] According to AASHTO T277 & ASTM C1202
[b] Derived From FDOT Data Base

ratings would also allow identification of those bridges that are in the early stages of deterioration. In these cases, less costly preventive maintenance might be initiated to halt further deterioration. Early prevention tends to reduce the potential for more costly rehabilitation in the future and ensures longer service life. Implementation of a durability rating system would allow better management and substantial cost savings of bridge maintenance programs.

Durability Specification for Concrete Mixtures

After analyzing various correlations between test results, different classes of durability can be established for concrete mixtures as well. The classes would have requirements for both strength and permeability and range from high to very low. Specification requirements would then be developed for concrete in different environments. For example, requirements for high durable concrete would be adopted in the design of mixtures for severely aggressive environments, such as sea water. Specifications provide guidance for material selection and mixture proportioning. Laboratory permeability and strength tests would be performed on concrete mixtures to ensure compliance with the specification requirements. During construction, quality, in terms of strength and durability, would be verified and samples of concrete prepared and tested for strength and permeability. The quality of the as-built structure is evaluated by performing field permeability tests on the structural elements and models. Results of strength and durability tests are compared with the standard ratings for high-durable structures, providing the project engineer with an excellent tool for quality assurance of the final product. The permeability tests are particularly valuable in settling disputes between owners and contractors over different interpretations of quality construction. In cases where the FPT was used, FDOT engineers were able to make a more accurate assessment of quality and thereby arrive at rational decisions regarding concrete acceptance.

SUMMARY

This paper presents the findings to date of an extensive research program to develop a durability specification and rating system for concrete. A major product of this research is the development of tentative permeability classifications on the basis of laboratory and field water-permeability.

Significant benefits are expected from this research, including accurate evaluation and classification of durability for concrete mixtures and structures, effective management of bridge rehabilitation and maintenance programs, and efficient use of bridge maintenance funds through savings in bridge rehabilitation costs.

The rating system described allows a material engineer to design mixtures that produce concrete with optimum strength and high durability. A project engineer can use FPT and standard durability ratings for quality assurance of newly constructed structures. A maintenance engineer and consultant can test the permeability of a structure and use the test results to evaluate present conditions and predict a structure's future performance.

ACKNOWLEDGEMENT

The authors thank Mike Bergin, David Romano, Armon Lowery, and Diep Tu for their significant contribution to this research project.

REFERENCES

1. Armaghani, J., T. Larsen, and D. Romano. Aspects of Concrete Strength and Durability. In *Transportation Research Record No. 1335,* TRB, National Research Council, Washington, D.C., 1992, pp. 63–69.
2. Soongswang, P., M. Tia, D. Bloomquist, C. Meletiou, and L. Sessions. An Efficient Test Setup for Determining the Water-Permeability of Concrete. In *Transportation Research Record No. 1204,* TRB, National Research Council, Washington D.C., 1988, pp. 77–82.
3. Meletiou, C., M. Tia, and D. Bloomquist. Development of a Field Permeability Apparatus and Method for Concrete. *ACI Materials Journal,* Jan/Feb. 1992, pp. 83–89.
4. Adegodegoke, O., and J. Armaghani. Software for Managing Concrete Test Data. *Proc., 9th ASCE National Conference on Microcomputers in Civil Engineering,* Orlando, Fla., Oct. 30–31 1991, pp. 237–241.
5. Armaghani, J., D. Romano, M. Bergin, and J. Moxley. High Performance Concrete in Florida Bridges. *Proc., ACI Symposium on High Performance Concrete in Severe Environments.* ACI Convention, Nov. 1993.

Publication of this paper sponsored by Committee on Performance of Concrete.

Nondestructive Identification of Internally Damaged Areas of Concrete Beam Using the Spectral Analysis of Surface Waves Method

M. E. KALINSKI, K. H. STOKOE II, J. O. JIRSA, AND J. M. ROESSET

An unidentified vehicle struck the bottom of a railroad overpass in Austin, Texas, and severely damaged one of the concrete beams in the overpass structure. The damaged beam was removed and taken intact to the University of Texas at Austin where the spectral analysis of surface waves (SASW) method was used to delineate nondestructively the damaged zones. SASW measurements performed on the overpass beam revealed a significant velocity contrast between damaged and undamaged zones. Damaged zones exhibited velocities ranging from 4,000 to 6,900 ft/sec (1,200 to 2,100 m/sec), depending on the extent of cracking. Velocities of undamaged zones ranged from 7,100 to 9,000 ft/sec (2,150 to 2,750 m/sec), with most values around 7,800 ft/sec (2,400 m/sec). The measurements were consistent with visual inspection of the beam. More important, the measurements indicated the presence of cracking that was not visually detectable.

A prestressed concrete beam in service on a railroad overpass bridge in Austin, Texas, was struck and severely damaged by an unidentified vehicle. The vehicle struck the side of the beam about 3 in. (8 cm) from its base. The beam was subsequently removed and taken intact to the University of Texas at Austin where researchers began testing the beam. The beam is 40-ft (12.2-m) long and constructed with concrete, possessing a reported 28-day compressive strength of 6,400 psi (44.1 MPa). Approximate dimensions of the beam are given in Figure 1. The inset in Figure 1 shows the location of the beam in the overpass structure and the impact area.

The objective of the work presented in this paper was to evaluate, nondestructively and noninvasively, the integrity (damaged versus undamaged zones) of the damaged overpass beam. This work represents an initial step in a comprehensive study of the load-carrying capacity of the beam, first in its damaged state and then after repair with an epoxy grout. Integrity testing of the damaged beam was conducted by applying the spectral analysis of surface waves (SASW) method. The SASW method measures surface wave velocities, which can be related to the properties of the material being tested. The main benefit of the SASW method is that information about interior profiles in beams can be obtained by making nondestructive measurements on only one side of the beam. Other nondestructive techniques from which comparable profiles can be developed, such as tomographic imaging with sonic waves, require access to both sides of the beam.

In this paper, a brief overview of the SASW method and its applications to this particular study are outlined. SASW results from the beam are then presented and compared with cracking patterns observed on the beam. Finally, the capabilities and limitations of the SASW method to detect cracks in structural concrete elements are discussed.

Department of Civil Engineering, University of Texas at Austin, Austin, Tex. 78712.

OVERVIEW OF SASW METHOD

Surface wave velocity measurements are one means of nondestructively obtaining information about the geometry and in-place elastic moduli of layered systems, such as geotechnical profiles and pavement systems (*1–3*). The SASW method provides a convenient approach to the measurement and analysis of surface wave velocities (*4–8*). When modulus varies with depth in a layered system, surface waves with different wavelengths travel at different velocities and are said to be dispersive. It is this dispersive characteristic that is measured in SASW testing.

Surface Wave Dispersion

How surface wave dispersion is measured in SASW testing is best explained by the example shown in Figure 2(a). Surface waves with frequencies f_1 and f_2 are seen to propagate through two different layered systems. The first system is a uniform half-space of intact concrete. The second system has a layer of intact concrete over damaged concrete. Relative vertical particle motion is shown as a function of depth for each surface wave. The motion represents the zone stressed (sampled) by each surface wave. The high-frequency wave, f_1, represents a short-wavelength wave and travels through shallow material. The velocity of the short-wavelength wave is a function of the near-surface elastic moduli, which, for the case shown, is 5,650 ksi (38.9 GPa) for both profiles. However, the lower-frequency wave, f_2, has a longer wavelength and travels through deeper material. Its velocity depends on the moduli of the near surface and deeper materials. Figure 2(b) shows the dispersion curves, plots of surface wave velocity versus wavelength, for each of the two systems in Figure 2(a) and illustrates how a dispersion curve can reveal the presence of a low-modulus layer beneath a high-modulus layer.

Measurement of Surface Wave Dispersion

SASW testing is performed with an energy source, two or more receivers, and recording instrumentation. The source and receivers are placed on the surface of a layered system along an array axis as

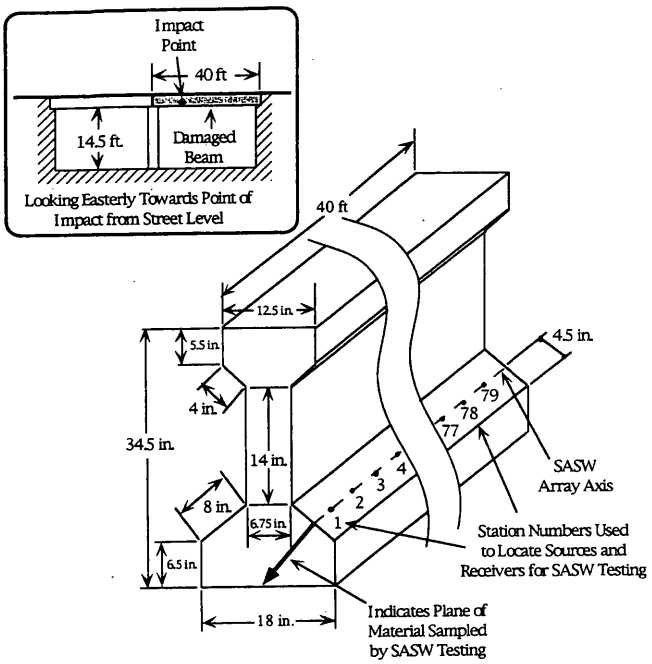

FIGURE 1 Approximate dimensions of prestressed concrete beam and locations where SASW testing was performed.

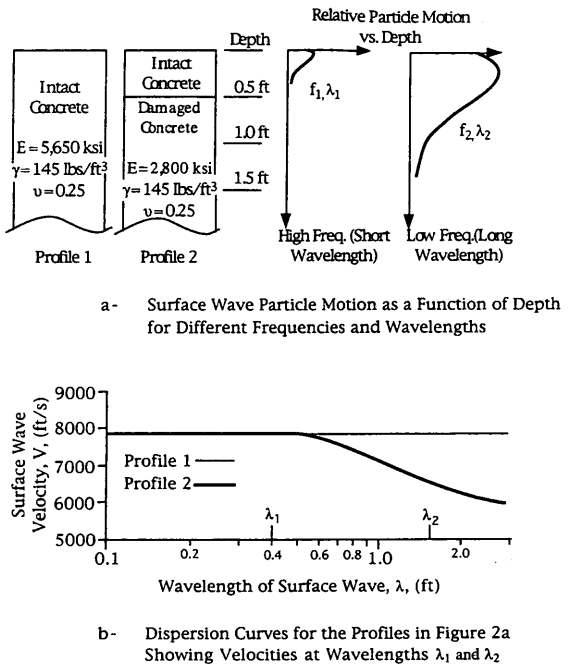

FIGURE 2 Effect of modulus variations on dispersion curve measured by the SASW method for two-layered systems.

shown in Figure 3. The source is used to impart energy to the surface vertically. Vertical motion at the two receiver locations is recorded in the time domain as transducer voltage, as shown in Figure 4(a). An exponential window typically is applied to the time records to attenuate later-arriving reflected energy relative to the direct arrival surface wave energy as shown in Figure 4(b) (*9*). The two windowed time-domain records, $x(t)$ and $y(t)$, are then converted to complex numbers, $X(f)$ and $Y(f)$, in the frequency domain using Fourier analysis. The cross power spectrum, $G(f)$, is defined as

$$G(f) = X(f)Y*(f) \tag{1}$$

where $Y*(f)$ is the complex conjugate of $Y(f)$. The phase of the cross power spectrum, $\Phi(f)$, is the phase difference between $X(f)$ and $Y(f)$ and is expressed as a function of frequency as follows:

$$\Phi(f) = \tan^{-1}\left\{\frac{Tm\,[G(f)]}{\mathrm{Re}\,[G(f)]}\right\} \tag{2}$$

The phase difference physically represents the number of cycles of a given frequency between two receiver locations as the waveform passes from one receiver to another. Relative, or "wrapped," phase differences fall between π and $-\pi$ radians as the phase values repeat themselves every 2π radians. The absolute number of cycles between receivers is determined by unwrapping the phase spectrum. Examples of wrapped and unwrapped phase spectra are shown in Figure 5(a). Once the phase spectrum is unwrapped, surface wave velocity, $V(f)$, can be calculated as a function of frequency as follows:

$$V(f) = \frac{2\pi \mathbf{R} f}{\Phi(f)} \tag{3}$$

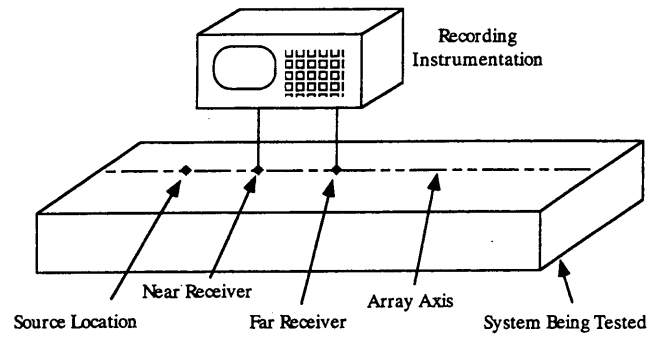

FIGURE 3 Typical SASW data acquisition setup.

where **R** is the receiver spacing, and $\Phi(f)$ is expressed in radians. Because velocity is the product of wavelength and frequency, the wavelength 1 associated with each frequency is simply

$$\lambda = \frac{2\pi \mathbf{R}}{\Phi(f)} \tag{4}$$

A dispersion curve of wave velocity versus wavelength is then constructed from all available frequencies using Equations 3 and 4. Development of a dispersion curve is the end-product of the physical measurement. Analytical modeling of the dispersion curve is performed subsequently to construct stiffness profiles (*10,11*).

Given a distance R between SASW array elements, velocities of wavelengths greater than $2R$ should not be considered valid because of near-field effects (*8,12*). For data acquisition on concrete or other

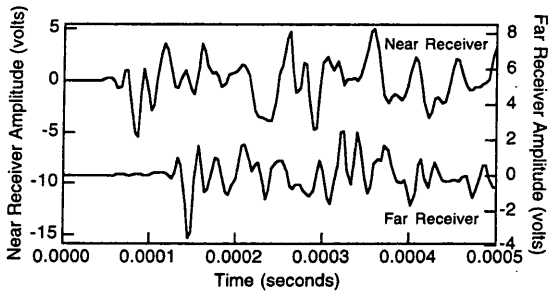

a- Unwindowed Time Records

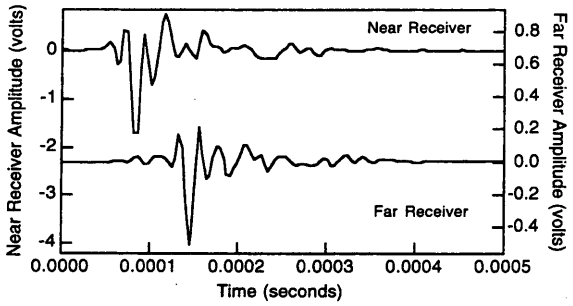

b- Windowed Time Records

FIGURE 4 Windowed and unwindowed time records recorded for SASW array 10–11.

systems possessing a finite thickness, the maximum recordable wavelength is constrained further by the thickness of the concrete. Velocity information for wavelengths greater than the thickness of the concrete is not valid because of interference from the other side of the concrete member.

APPLICATION OF SASW METHOD

Whereas the SASW method historically has been applied to describe layered systems, such as soil profiles and pavement systems, recent efforts have been made to apply the SASW method to the identification of cracking in concrete structural elements. Experimental and analytical work on rock, cracked concrete blocks, and prototype concrete structural elements has indicated that surface wave velocities decrease at all wavelengths when an open crack exists between the SASW receivers (*12,13*). In some cases, surface wave velocities measured in damaged concrete decreased without the presence of visible cracking between the receivers. This illustrates the potential of the SASW method to detect damage that is otherwise visually undetectable. However, surface wave velocities did not decrease when the receivers and the cracks were on opposite sides of the specimen and the crack depth was less than half of the specimen thickness. Surface wave velocities also have been observed to decrease in intact specimens at wavelengths greater than the thickness of the specimen because of interference from the other side of the specimen (*12,14*).

The damaged railroad overpass beam described in this paper provided an excellent opportunity to extend previous observations on cracked rock and concrete to an actual field-damaged specimen. SASW tests were performed on the side of the overpass beam that was struck. Source and receiver locations were designated as stations along an array axis, as shown in Figure 1. Stations were spaced 6 in. (15.2 cm) apart and were numbered 1 to 79. Figure 1 also shows the material being sampled beneath the array axis, as represented by the line extending from the array axis into the concrete along a plane perpendicular to the surface of the concrete beam.

SASW data were recorded using each pair of adjacent station locations as receiver locations. Dispersion curves were then determined for each of the receiver pairs. The dispersion curves were used to construct a mosaic of wave velocity versus depth into the beam by plotting dispersion curves along the length of the beam midway between the receiver locations used to determine each particular dispersion curve. For example, for the dispersion curve determined with the source at Station 9, a near receiver at Station 10 and a far receiver at Station 11, the dispersion curve was plotted at Station 10.5. To plot wave velocity versus depth, dispersion curves were smoothed and velocities were reported at 0.1-ft (0.03-m) wavelength intervals from 0.1 to 1.0 ft (0.03 to 0.3 m). Thus, a grid of velocity versus depth data was posted at 6-in. (15.2-cm) intervals along the beam and generated at 0.1-ft (3-cm) wavelength intervals into the beam. In this case, wavelength was approximated as depth into the beam.

Finally, velocity profiles at all mid-stations (such as Station 10.5 noted above) were contoured and compared with visual cracking

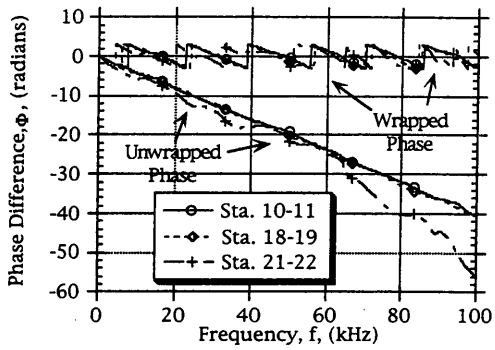

a- Cross Power Spectra

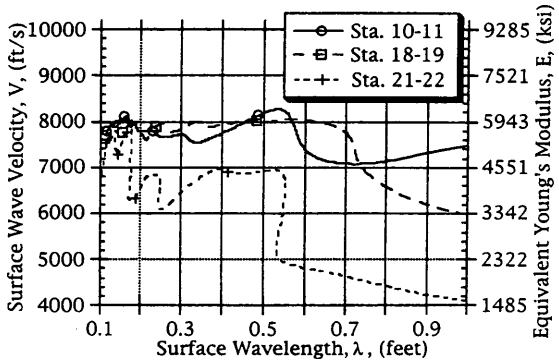

b- Dispersion Curves

FIGURE 5 Cross power spectra and dispersion curves for SASW Arrays 10–11, 18–19, and 21–22.

patterns to evaluate the ability of the method to identify and delineate cracked zones. Interpretations were made of the internal cracking pattern in the beam from observations made on all sides of the beam. The observations could be interpolated into the beam and cross-sections of the beam could be sketched showing the interpreted areas of internal damage at various positions. By comparing these cross-sections with the velocity profile, the SASW method was evaluated as a potential means of nondestructively identifying internal damage within the beam.

Note that the surface wave velocity of a given wavelength is not the velocity of the material at the depth equal to the wavelength. The velocity of a given wavelength depends on the velocity of all the material between the surface and about one wavelength in depth. Forward modeling or inversion is required to convert a dispersion curve into a profile of shear wave velocity or elastic modulus versus depth (*10*). However, previous experience indicates that dispersion curves can yield qualitative information about the internal condition of concrete, so dispersion curves were considered adequate to describe the concrete for this study.

RESULTS

Figure 6 shows each side of the beam, illustrating the observed cracking and the station locations used in SASW testing. Severely damaged and spalled zones are indicated by stippling, and the area of the impact is indicated with a large black dot. Three major systems of cracks existed in the beam. The first system is a group of concentric cracks on the impacted side of the beam. These cracks appear to be a direct result of the impact. The second system is a large cuspate delamination-type feature that expresses itself on the nonimpacted and bottom sides. The feature is concave toward the nonimpacted and bottom sides. The damage is characterized by a

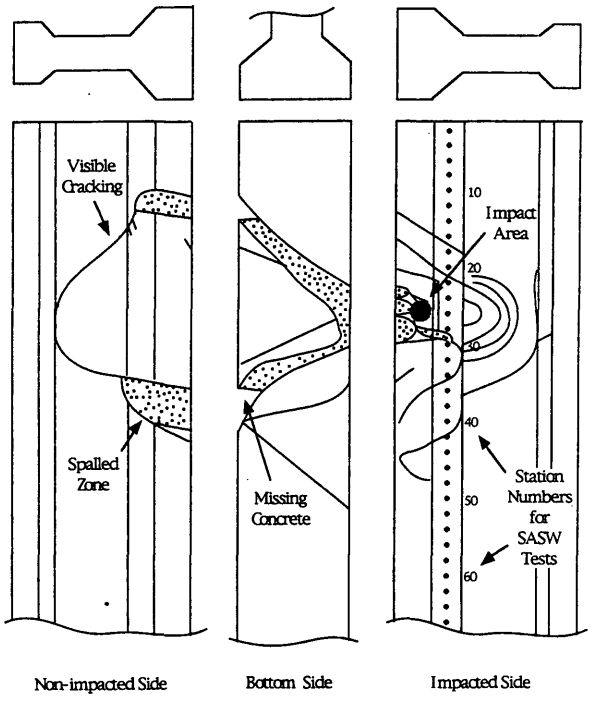

FIGURE 6 Visible cracking and spalling observed on each side of the overpass beam.

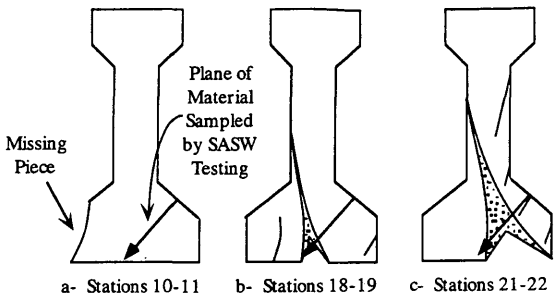

FIGURE 7 Cross sections along the beam showing interpreted areas of internal damage.

thick zone of highly fractured and spalling concrete where the zone intersects the surface of the beam. The feature appears to be a result of beam bending upon impact. It also appears to have permanently separated the cuspate section of concrete relative to the rest of the beam as a result of inelastic deformation of the prestressing tendons. The third system is cracking on the other side of the diaphragm from the impact area. The beam was attached to five other beams in the overpass structure, with a diaphragm near the center of each beam (between Stations 35 and 40 used in the SASW tests). When the impact occurred, the diaphragm acted as a reaction point on the beam and caused the beam to bulge outward. Cracks associated with the mechanism are not as well defined as the other two systems of cracks, but they seem to be present on the bottom and impact sides.

The first step to evaluating the success of the SASW method was to interpret the internal damage by observing cracking on the exterior of the beam. Cross-sections revealing the beam's internal damage were made at discrete intervals along the beam. Examples of these cross-sections are shown in Figure 7 for cross-sections between Stations 10 and 11, 18 and 19, and 21 and 22. These three cross-sections represent zones with varying degrees of visible damage on the side of the beam being tested. The cuspate damage system could be interpreted with relative confidence because it expressed itself on more than one side of the beam, but the other two systems only expressed themselves on one side of the beam, but the other two systems only expressed themselves on one side of the beam, so interpretations concerning them are not as reliable. Finally, SASW data were recorded for comparison with the cross sections.

Figure 4 shows a pair of unwindowed and windowed time records for SASW data recorded with Stations 10 and 11 as receiver locations. The records represent typical data obtained from an undamaged zone and show the attenuation of later-arriving energy relative to direct surface wave arrivals through the use of windowing.

Figure 5(a) shows the wrapped and unwrapped phase plots of the cross power spectra for data recorded between Stations 10 and 11, 18 and 19, and 21 and 22. Figure 5(b) shows the resulting dispersion curves calculated from these three phase spectra. The dispersion curves also indicate values for the equivalent Young's moduli. The equivalent moduli are based on assumptions of a concrete unit weight of 145 lb/ft^3 (2 330 kg/m^3), a Poisson's ratio of 0.25, and a reasonable thickness of similar material. The approximate relationship between surface wave velocity, V, and equivalent Young's Modulus, E, can then be given as follows (*15*):

$$E \cong 13.37\, V^2 \tag{5}$$

where V is in ft/sec, and E is in lb/ft^2.

The reasonably linear nature of the spectra in Figure 5(b) from the Station 10–11 array indicates a relatively uniform velocity within the concrete. Variations in velocity normally would express themselves as changes in slope of the unwrapped cross power spectra. However, the unwrapped phase is quite linear [Figure 5(a)]. The corresponding dispersion curve exhibits a relatively constant velocity as a function of wavelength varying from about 7,100 ft/sec (2150 m/sec) to about 8,200 ft/sec (2500 m/sec). Comparison of the dispersion curve with the cross section in Figure 6(a) shows that although some damage exists on the other side of the beam, it is not directly beneath the array; therefore, it does not affect the observed surface wave velocities. The dispersion curve indicates that intact, high-quality concrete along the plane tested in good agreement with what was predicted [Figure 7(a)].

Figures 7(b) and 7(c) indicate deep and shallow damage at arrays 18–19 and 21–22, respectively. Figure 5(a) displays an increase in the phase spectra slope for array 21–22, which is indicative of a velocity decrease. Dispersion curves in Figure 5(b) show the velocity decrease as a function of wavelength for both the 18–19 and 21–22 stations. The velocity decrease occurs at longer wavelengths with the deep damage for Array 18–19 but affects shorter wavelengths when the damage is closer to the surface for Array 21–22. Again, the SASW dispersion curves are in good agreement with the predicted cross sections.

Data from Figure 5(b) were posted with velocity data from the rest of the beam on the velocity contour plot shown in Figure 8. Trends present on the contour plot indicate how the SASW method is able to delineate damage within the beam through variations in surface wave velocity. The velocity decrease between Stations 17 and 22 corresponds to a transition zone between undamaged and damaged concrete. The low velocity zone between Stations 22 and 33 corresponds to the severely damaged portion of the beam. An increase in velocity between Stations 33 and 37 indicates another transition zone between damaged and undamaged concrete. Velocities measured beyond Station 37 return to those of undamaged concrete. However, another anomalous zone exists between Stations 45 and 49, where little or no damage is visible. In general, surface wave velocities in undamaged portions of the beam ranged between 7,100 and 9,000 ft/sec (2150 to 2750 m/sec), but were concentrated around 7,800 ft/sec (2400 m/sec). Surface wave velocities in damaged zones ranged from 4,000 to 6,900 ft/sec (1200 to 2100 m/sec).

Surface wave measurements made between Stations 17 and 22 indicate how the SASW method may be used to identify damage that is visually undetectable on the surface being tested. All wavelengths in the undamaged zone at Station 17 possessed intact concrete velocities, as shown in Figure 8, but velocities decreased as stations approached the damaged zone. The longer-wavelength velocities were the only ones to decrease initially; however, all wavelengths were affected once the stations were within the damaged zone at Station 22. Previous observations of other specimens may explain the wavelength dependence (*12,14*). Observation of concrete specimens with finite thickness reveal that velocities decrease when wavelengths exceed the concrete thickness because of interference from the concrete-air interface on the opposite side of the specimen. A large crack existed within the concrete member between Stations 17 and 22, as indicated on the cross sections in Figure 7(b) and 7(c). The crack was roughly parallel to the surface being tested, but dipped from Station 22 to 17. The crack may have acted as a concrete-air interface and caused the velocities of the wavelengths greater than its depth to decrease. The crack expressed itself on the bottom and nonimpacted side of the beam, but was visually undetectable between Stations 17 and 22 on the surface being tested.

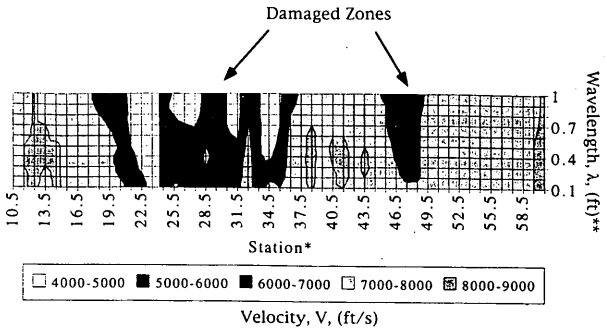

Note: *Velocities plotted midway between receiver stations; hence for Array 10-11, data is plotted at station 10.5.
**Wavelength is empirically related to depth into concrete beam.

FIGURE 8 Contoured surface wave velocity data from SASW testing of overpass beam.

Given a situation in which the bottom and nonimpacted sides of the beam are not accessible for visual inspection, SASW testing could be used as an indicator of otherwise invisible damage within the beam. The depth to the crack also could be estimated as the point on the dispersion curve where the velocities of increasing wavelengths begin to decrease.

Surface wave measurements taken between Stations 33 and 37 also demonstrate the potential of the SASW method to delineate internal damage. The transition zone between damaged and undamaged concrete is indicated by an increase in surface wave velocity from Stations 33 to 37. A crack crosses the array axis in the "undamaged" zone at Station 42, but the crack is apparently not significant enough to decrease surface wave velocity. The crack may be superficial enough not to affect surface wave propagation, or it may possess acoustic "bridges" of undamaged material that allow the surface wave energy to cross. At any rate, there seems to be a threshold crack area below which surface wave velocities are not affected. Future work to compare SASW-detectable cracking with strength-reducing cracking should address the significance of this finding by determining how much of the strength-reducing damage SASW testing can detect.

Measurements taken between Stations 45 and 49 demonstrated the potential of the SASW method to delineate internal damage. The surface wave velocities measured in this interval appear to indicate internal damage caused by bulging of the beam when it was struck. This damage is suggested by the presence of cracking near Stations 45 through 49, but the SASW velocity information delineates specific zones of damage. The velocity decrease with increasing wavelength may indicate damaged concrete overlain by undamaged concrete, but it also may indicate an internal delamination-type crack parallel to the surface being tested. This crack could be acting as a free surface that decreases the longer-wavelength velocities similar to the Station 17–22 interval. In either case, the surface wave velocity decrease in the Station 45–49 interval indicates internal damage within the beam that may not have been predicted solely on the basis of visual inspection.

CONCLUSIONS

The results of this study demonstrate the qualitative ability of the SASW method to confirm and delineate internal cracking within a

damaged concrete structural element. Surface wave velocities in the undamaged portions of the overpass beam used in this study ranged between 7,100 and 9,000 ft/sec (2150 and 2750 m/sec), but were concentrated around 7,800 ft/sec (2400 m/sec). Surface wave velocities in damaged zones ranged from 4,000 to 6,900 ft/sec (1200 to 2100 m/sec). These slow velocity zones indicated internal damage between Stations 18 and 37 and again between Stations 45 and 49. The velocity contrasts along the beam corresponded well with the external cracking present on the beam and fairly well with the internal damage estimated on the cross sections. Visual inspection of the cross-sections alone supported only a crude interpretation of the internal damage. However, surface wave velocity information provided by the SASW method suggests that SASW testing can be used to confirm and delineate the internal damage initially predicted upon visual inspection. As importantly, this testing could be used to determine whether damaged zones had been repaired adequately by epoxy grouting for instance, once a repair operation is complete. A poor grout job presumably would leave voids in the concrete that could be identified by SASW testing as slow-velocity zones.

Note, however, that a velocity decrease at a given wavelength does not necessarily mean the concrete is damaged at depths greater than that wavelength. The behavior of a surface wave with a given wavelength is dominated by the material between the surface and a depth equal to about one-third of the wavelength. That holds for all surface waves, regardless of the crack geometry.

Forward modeling or inversion is the process that uses dispersion curve data to create a profile of shear wave velocity or modulus versus depth. Inversion theory for layered systems generally is based on assumptions of a continuous system possessing vertical stiffness gradients. However, a system such as cracked concrete is more complex. Cracks act as discontinuities between pieces of concrete that otherwise would be relatively homogeneous and isotropic. Future work should be aimed at understanding the more complicated systems and the mechanisms that cause surface wave velocities to decrease, before an appropriate inversion method can be developed.

Even with the quantification of surface wave data through accurate inversion, the SASW method will have limitations. Cracks resealed by an applied force, such as a bending force or a prestressed tendon, cannot be detected (*14*). Cracks existing on the opposite side of a concrete specimen from the SASW array are undetectable if they are less than half the thickness of the specimen. However, such cracks would be detected if other sides of the beam were accessible for SASW testing. This could greatly increase the volume of data to be manipulated. Further work needs to be aimed at streamlining data acquisition and processing methods to manage efficiently the larger volumes of data.

ACKNOWLEDGMENTS

The authors thank Riyad Aboutaha, Rob Zobel, and the other researchers and staff at Ferguson Structural Engineering Laboratory of the University of Texas at Austin. Their cooperation in allowing collection of data on their specimens is greatly appreciated. The authors also thank the Texas Department of Transportation for providing support for two projects under the technical guidance of Jeff Jackson and Robert Cochrane. Finally, support from the National Science Foundation is greatly appreciated.

REFERENCES

1. Ballard, R. F., Jr. *Determination of Soil Shear Moduli at Depth by In Situ Vibratory Techniques.* Miscellaneous Paper No. 4-691, U.S. Army Corps of Engineers Waterways Experiment Station, Vicksburg, Miss., 1964.
2. Heukelom, W., and C. R. Foster. Dynamic Testing of Pavements. *Proc., ASCE Journal of Soil Mechanics and Foundations Division,* Vol. 86, No. SM1, Part 1, Feb., 1960.
3. Richart, F. E., Jr., J. R. Hall, Jr., and R. D. Woods. *Vibrations of Soils and Foundations.* Prentice Hall, Englewood Cliffs, N.J., 1970.
4. Stokoe, K. H., II, G. J. Rix, and S. Nazarian. In Situ Seismic Testing with Surface Waves. *Proc., 12th International Conference on Soil Mechanics and Foundation Engineering,* Rio de Janeiro. Brazil, 1989.
5. Stokoe, K. H., II, S. Nazarian, G. J. Rix, I. Sanchez-Salinero, J. C. Sheu, and Y. J. Mok. In Situ Seismic Testing of Hard-to-Sample Soils by Surface Wave Method. *Proc., 40th Geotechnical Engineering Conference,* University of Minnesota at Minneapolis, 1992.
6. Nazarian, S., K. H. Stokoe, II, R. C. Briggs, and R. Rogers. Determination of Pavement Layer Thicknesses and Moduli by SASW Method. In *Transportation Research Record No. 1196,* TRB, National Research Council, Washington, D. C., 1988, pp. 133–150.
7. Nazarian, S. *In Situ Determination of Elastic Moduli of Soil Deposits and Pavement Systems by Spectral-Analysis-of-Surface-Waves Method.* Ph.D. dissertation. University of Texas at Austin, 1984.
8. Sanchez-Salinero, I. *Analytical Investigation of Seismic Methods Used for Engineering Applications.* Ph.D. dissertation. University of Texas at Austin, 1987.
9. Bay, J. A., and K. H. Stokoe II. Field Determination of Stiffness and Integrity of PCC Slabs Using the SASW Method. *Proc., Conference on Nondestructive Evaluation of Civil Structures and Materials,* University of Colorado at Boulder, 1990.
10. Roesset, J. M., D. W. Chang, and K. H. Stokoe II. Comparison of 2-D and 3-D Models for Analysis of Surface Wave Tests. *Proc., 5th International Conference on Soil Dynamics and Earthquake Engineering,* Karlsruhe, Germany, 1991, pp. 11–26.
11. Foinquinos Mera, R. *Analytical Study and Inversion for the Spectral Analysis of Surface Waves Method.* M. S. thesis. University of Texas at Austin, 1991.
12. Bowen, B. R. *Damage Detection in Concrete Elements with Surface Wave Measurements.* Ph.D. dissertation. University of Texas at Austin, 1992.
13. Madianos, M. *Field and Laboratory Investigation* of *Rock Masses Using Surface Wave Seismic Testing (SASW).* M. S. thesis. University of Texas at Austin, 1991.
14. Kalinski, M. E. Measurements of Internally Cracked Concrete Structural Elements by the SASW Method. M. S. thesis. University of Texas at Austin. (n.d.)
15. Achenbach, J. *Wave Propagation in Elastic Solids.* Elsevier Publishing Company, New York, 1973.

Publication of this paper sponsored by Committee on Performance of Concrete.

Image Analysis of Portland Cement Concrete and Asphalt Concrete Pavements Using Scanning Electron Microscope Images

GLENN M. OREN, VERNON J. MARKS, AND WENDELL G. DUBBERKE

The major objective of this study was to evaluate the potential of image analysis for characterizing air voids in portland cement concrete (PCC), voids and constituents of asphalt concrete (AC), and aggregate gradation in AC. Images for analysis were obtained from a scanning electron microscope (SEM). Sample preparation techniques are presented that enhance signal differences so that backscattered electron (BSE) imaging, which is sensitive to atomic number changes, can be effectively employed. Work with PCC and AC pavement core samples has demonstrated that the low vacuum scanning electron microscope is better suited to doing rapid analyses. The conventional high vacuum SEM can be used for AC and PCC analyses, but some distortion within the sample matrix will occur. Images with improved resolution can be obtained from SEM BSE micrographs. In a BSE image, voids filled with barium sulfate/resin yield excellent contrast in both PCC and AC. There is a good correlation between percent of air by image analysis and linear traverse.

Determining air content and air void parameters in hardened PCC using the linear traverse or point count methods is tedious and time-consuming. Using digital image analysis to measure air voids is of much interest but the need to obtain sufficient contrast between voids and the surrounding matrix presents a serious obstacle. Although image analyzers typically are capable of differentiating at least 256 levels of gray, serious problems can result from uneven illumination, brightness fall-off of the camera lens system, or differential shadowing within voids viewed via a light microscope-based system. This paper describes two techniques developed by the authors to enhance the contrast of images obtained from the scanning electron microscope (SEM). A brief description of the instrumentation and techniques used is included.

IMAGE ANALYSIS

A thorough explanation of image analysis is beyond the scope or intent of this paper. Those interested in further information may find it elsewhere (*1–3*).

However, for those unfamiliar with image analysis, a definition of what it is, how it works, and what results can be expected may be useful. For the purposes of this paper, an image analyzer is a computer-based system capable of measuring the size, shape, and spatial relationship of voids. Images analyzed in this study were obtained from an SEM.

Computers work with numbers, not images; thus the images obtained from the microscope must first be converted into numbers, that is, digitized. If an image is considered simply a large array of dots (pixels), with each pixel having a value assigned to it representing its brightness or gray level, then each pixel point can be thought of as having three attributes; one number defines brightness, and two other numbers define location, i.e., x and y coordinates. Typical image analysis systems use a numerical scale for levels of gray that ranges from 0 (pure black) to 255 (pure white).

Because the major concern is to distinguish air voids from surrounding matrix, an image may be simplified so that all pixels above a threshold value are presented as pure white and all pixels below the threshold are presented as pure black. Once such a binary image is obtained, a series of mathematical operations can be applied to the stored image to calculate, for instance, the percentage of air void area, by simply summing the number of pure white (or pure black) pixels. More complex operations can be used to determine void sizes, perimeters, edge-to-edge mean free path, for example, on the basis of gray level and spatial location. The key is to ensure sufficient contrast between air voids and matrix, that is, the aggregate and paste.

BSE IMAGING

A particularly useful method of imaging in the SEM uses backscattered electrons (BSE). In the BSE mode, signal intensity is dependent upon the mean atomic number of the specimen at the point of excitation. The strong dependency (Figure 1) has been used successfully to differentiate hydration states of cement pastes (*4*). However, BSE imaging is not capable of differentiating air voids, because the resulting gray level values are not unique.

HEAVY GOLD SPUTTERING

To accentuate differences between the aggregate/paste matrix and air voids, the authors hypothesized that an extremely thick coating of gold would provide a high-intensity signal from the matrix, whereas signals from voids would undergo more scattering and deflection with a resulting loss in signal intensity. Those familiar with electron microscopy may recognize that a sputtered gold coating 20 to 30 nm thick, is often used on specimens to provide a con-

G. Oren, Iowa State University, 251B Bessey Hall, Ames, Iowa 50011. V. Marks and W. Dubberke, Iowa Department of Transportation, Office of Materials, 800 Lincoln Way, Ames, Iowa 50010.

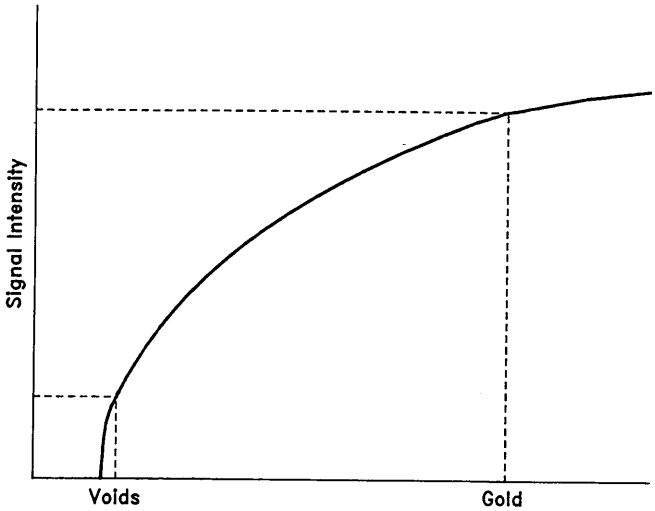

FIGURE 1 Relationship between atomic number and signal intensity.

ductive pathway and to eliminate "charging." To enhance signal contrast, a coating thickness in the range of 200–300 nm is necessary (Figure 2).

DISADVANTAGES OF SEM AND SPUTTERING TECHNIQUE

The purpose of this work was to develop a method to perform rapid analysis over the entire surface of 10-cm diameter portland cement concrete (PCC) cores. Although signal differences provided by the gold sputtering technique proved satisfactory, several problems became apparent during subsequent analyses. A short discussion of these difficulties follows, because they set the stage for the development of a second technique.

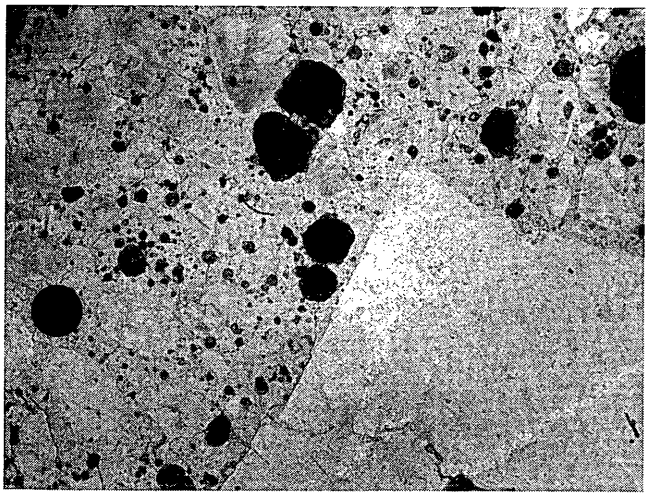

FIGURE 2 BSE image of heavy gold sputter coated PCC core.

Two potential problems arose that were related to the high vacuum requirement of the conventional SEM. First, prepumping of large samples (10-cm diameter cores, 5-mm thick) was necessary to prevent a shutdown of the SEM from excessive outgassing. The required amount of prepumping varied from several hours to overnight, depending on the condition of the PCC, detracting, of course, from the usefulness and speed of the method.

Second, microcracking occurred on the sample surface because of the excessive vacuum applied to the samples. Although microcracks can be eliminated easily by image processing techniques, it is diagnostically useful to know whether microcracking has occurred before a sample is subjected to a vacuum.

In addition, several other limitations are imposed by the conventional SEM. Standard high vacuum SEMs typically have a fairly restricted range of stage movement in the X and Y direction of a sample surface. To adequately sample across the specimen plane of a 100-mm × 100-mm × 5-mm sample is beyond the capability of most conventional systems, and novel approaches to repositioning a sample while it is under high vacuum must be devised.

Finally, the minimum magnification of conventional SEMs is typically 10×, yet it is desirable to image at magnifications of 1× or 2× to cover a larger field of view, especially for characterizing large, entrapped air voids. With some instruments, it is possible to achieve 2× magnification by fully tilting the stage so that it is out of the viewing area (as much as possible) and placing the specimen well below the normal viewing plane. This method, however, eliminates the possibility of moving a sample and reduces signal intensity. Note that the extent to which a sample can be lowered beyond the normal position is also contingent on the amount of residual free play in the particular instrument's coarse focus control knob.

LOW VACUUM SEM

Because of limitations imposed by the high-vacuum SEM, subsequent efforts considered the potential of a newer low-vacuum SEM (LVSEM). The LVSEM system is capable of operating at near atmospheric pressure. The technique of gold sputter coating then becomes the limiting time factor, because several hours of prepumping are required to obtain sufficient vacuum for sputtering. For this reason, a second technique was devised for use with the LVSEM.

BARIUM SULFATE WITH RESIN TREATMENT

Barium sulfate paste ($BaSO_4$ suspended in water) is used routinely in medicine as a contrast agent for X-ray examinations. Similarly, $BaSO_4$ can be used to fill the voids in a polished concrete specimen to yield high-contrast BSE images with the SEM. The paste exhibits excessive drying shrinkage, especially in large or deep voids. That problem can be eliminated by mixing $BaSO_4$ powder with an acrylic resin, such as LR White, a low viscosity embedding resin used for electron microscopy, in a ratio of approximately 20 g $BaSO_4$ to 5 g LR White. After thorough mixing, one drop of accelerator is added to the paste which is then stirred quickly until completely mixed. The paste is spread onto the core and worked in with a flat-edged blade held at a 45-degree angle. Excess paste can be removed easily with glassine paper.

The paste is allowed to cure for 15 min. A few final strokes across a 1200 grit paper (dry) followed by wiping with a soft, lint-free cloth are all that is necessary to prepare the surface for the LVSEM.

A micrograph of a $BaSO_4$ resin treated core prepared by the procedure described is shown in Figure 3. Note that to obtain the level of contrast exhibited in the micrograph, minimal effort is required in optimization of SEM controls. A low- to mid-range setting of contrast control, moderate beam current, and very little time and effort are required to obtain satisfactory results.

EXPERIMENTAL ANALYSIS

A JEOL 840A high vacuum SEM operated at 25 kev in the BSE mode was used for this study. A magnification of 20× yielded images covering an area of 0.187 cm^2. Ten images were acquired randomly for each sample, providing a total analysis area of 1.87 cm^2. Although the sampling scheme required only about 15 min for image digitization and subsequent analysis of all 10 frames, the actual number of voids analyzed far exceeded the number obtained using the linear traverse system. The latter operated over a 241-cm (95-in.) traverse (Figure 4) and required about 7 hr.

Further work is necessary to evaluate optimum magnification and the number and location of areas to be analyzed. It appears likely that a combination of analyses would be needed to accurately characterize any given core. For example, a 1× magnification may serve to characterize the entire entrapped air void system, yet such a low magnification cannot detect small entrained voids. Conversely, higher magnifications (100×–400×), as are required to elucidate entrained voids, are not useful for characterizing the entrapped air void system.

In addition, at issue is whether it is to necessary to include large aggregate in an analysis scheme. Efficiency and accuracy in characterizing an air void system are increased if large aggregate is excluded from the area analyzed. Some coarse aggregate contains large air voids that inadvertently may be included by some operators. Using low magnification, may be possible to analyze the large aggregate fraction in a similar way to, or in conjunction with, the entrapped air void system.

A possibility may be to use compositional imaging. For example, characteristic X-rays detected by an energy dispersive spectrometer could be used to map elementally a sample with elemental concentration scaled to intensity of a unique color (*5,6*). The resulting images could then be analyzed for feature sizes by image analysis. Success of this method depends on the development of a vastly improved X-ray collection device, because high quality compositional images currently require up to 20 hr of collection time per image.

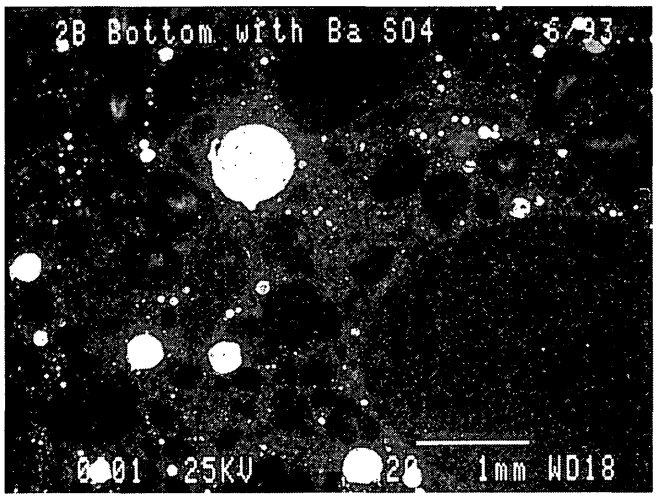

FIGURE 3 $BaSO_4$ with resin-treated PCC core, 14.8× magnification.

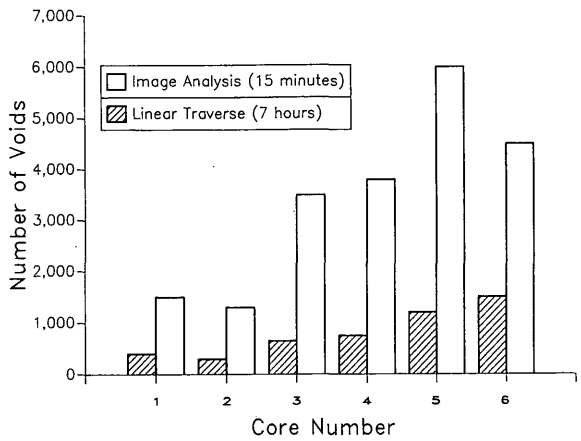

FIGURE 4 Number of voids detected by each method.

COMPARISON OF PCC VOID DETERMINATIONS

Most work to date was conducted with a conventional SEM. Comparative results of percent air (on the same surface) are encouraging; they indicate there is a strong correlation ($R^2 = 0.92$) between linear traverse and SEM-based image analysis (Figure 5). Cores for Figure 5 are from Iowa DOT samples, and the linear traverse results are from Iowa DOT and an outside testing laboratory. Linear traverse data were obtained as described in ASTM C457 and were based on a 95-in. traverse.

The American Concrete Institute *Guide to Durable Concrete* recommends parameters for freeze-thaw resistant concrete. With current linear traverse air content data, the air content should be 6.0 ± 1.5 percent, a specific surface (surface area of the air voids)

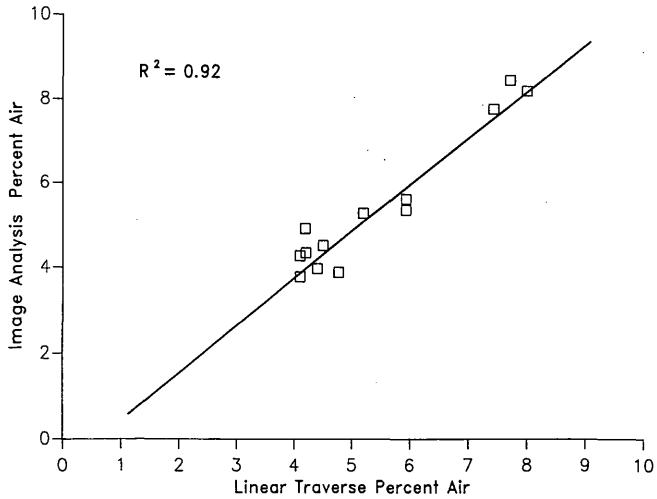

FIGURE 5 Percent air; linear traverse versus image analysis.

TABLE 1 Core Air Content Data

Core No.	Air Content		Specific Surface				Spacing Factor			
	Linear Traverse	Image Analysis	Linear Traverse		Image Analysis		Linear Traverse		Image Analysis	
			mm^2/mm^3	in^2/in^3	mm^2/mm^3	in^2/in^3	mm	in	mm	in
1	4.77	3.88	13	339.	29	725.	0.33	0.013	0.15	0.006
2	4.19	4.91	11	275.	37	945.	0.41	0.016	0.13	0.005
3	5.93	5.35	21	544.	53	1348.	0.20	0.008	0.08	0.003
4	5.93	5.61	24	611.	45	1146.	0.18	0.007	0.10	0.004
5	7.72	8.45	30	751.	43	1099.	0.15	0.006	0.10	0.004
6	7.43	7.76	36	902.	60	1534.	0.13	0.005	0.08	0.003
7	4.50	4.51	31	791.	36	907.	0.13	0.005	0.13	0.005
8	4.10	3.78	21	526.	43	1098.	0.20	0.008	0.10	0.004
9	4.10	4.27	13	336.	27	697.	0.33	0.013	0.15	0.006
10	5.20	5.27	18	469.	23	573.	0.23	0.009	0.20	0.008
11	4.40	3.97	22	559.	34	867.	0.20	0.008	0.13	0.005
12	4.20	4.34	--	----	--	----	----	----	----	----
13	8.00	8.19	--	----	--	----	----	----	----	----

of greater than 24 mm^2/mm^3 (600 $in.^2/in.^3$) and a spacing factor (average maximum distance from any point in cement paste to the edge of the nearest void) of 0.2 mm (0.008 in.) or less.

The specific surface was determined by both linear traverse and image analysis (Table 1). There was a poor correlation ($R^2 = 0.40$) between linear traverse specific surface and image-analysis specific surface (Figure 6). Image analysis resulted in higher specific surface values as compared with linear traverse (Figure 7). The spacing factor by image analysis was consistently lower than linear traverse (Figure 8). A comparison of the bubble size distribution obtained by

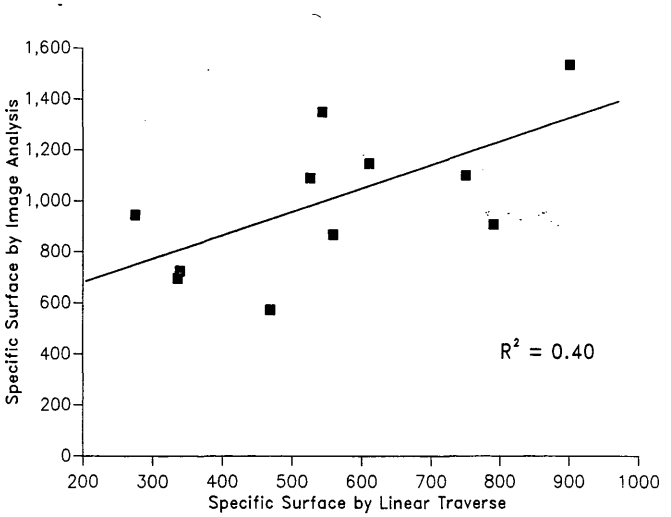

FIGURE 6 Specific surface; linear traverse versus image analysis.

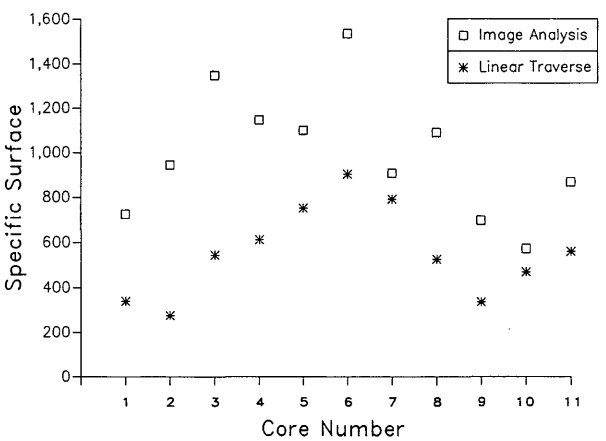

FIGURE 7 Specific surface values.

the linear traverse and that obtained by image analysis would clarify the reason for the two methods' differences in specific surface. As shown in Figure 4, image analysis detected more voids than linear traverse. Perhaps image analysis detected substantially more very small voids. Unfortunately, the linear traverse systems employed in this study were not configured to provide information on bubble size.

One rudimentary way to evaluate the image analysis bubble-size distribution is to compare the data from the bubble-size distribution of published data (*7,8*) for a concrete of similar water-cement ratio and air content (Figure 9). Results of such a comparison indicate that image analysis yields similar results in terms of bubble size distribution. Again, however, the specific surface area reported in the

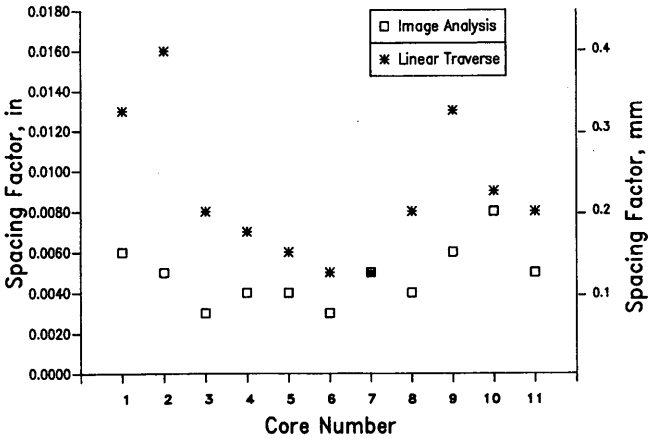

FIGURE 8 Spacing factor.

literature is less than that obtained by image analysis and, in fact, also is less than that determined by calculating average chord length using the published bubble-size distribution. Powers (*8*) notes, "The number of bubbles calculated from the specific surface diameter is considerably smaller than that calculated from size distribution. . . ." Ideally, it would be helpful to analyze hundreds of cores by each method; however, obtaining quality linear traverse results has proven difficult.

ADVANTAGES OF SEM IMAGE ANALYSIS

Analysis performed on SEM images offers much potential for understanding air-void distribution in concrete. Unquestionably, the speed at which a computer can classify and size objects is superior to manual methods. Many thousands of voids can be analyzed more accurately, providing more information to the investigator in less time. Data can be acquired regarding other measurements, such as shape and chemistry.

The chief drawback to image analysis, however, continues to be the difficulty of achieving adequate contrast to allow successful automated differentiation of one object from another. To an image analyzer, all voids must be within a given range of gray values, and these gray values must be unique to voids. An image analyzer cannot reason that a bright area within a void is part of the void. Image analysis systems lack the human brain's superb ability to interpret many such details. Light microscope-based analysis systems have inherent difficulties that make it difficult to properly manage light intensities to the extent required by an image analyzer. By using BSE imaging, the pitfalls associated with attempting to establish distinct gray-level differences on the basis of varying intensities of reflected light are avoided. Contrast, or gray-level distinction, is achieved by evaluating differences in atomic number. An atomic number difference of 1 can result in significant contrast differences for sensitive, backscattered systems.

Consider then, the signal difference between a calcium-rich concrete environment (calcium has an atomic number of 20) and a barium-rich material (barium has an atomic number of 56). Tremendous differences in contrast can be achieved by using a high atomic number material such as the $BaSO_4$ resin. The heightened difference in the signal results in significantly better images. BSE imaging yields far better resolution of voids' boundaries.

The newer LVSEM, with its ability to operate in a low-vacuum environment, is obviously the instrument of choice; although the conventional high-vacuum SEM will work, it may require prepumping of samples. Several benefits are derived from using the LVSEM, and they warrant further discussion. Adequate characterization of samples requires analysis of a number of cores, therefore minimizing specimen preparation and analysis time per sample is important. The LVSEM not only virtually eliminates pumpdown time, it significantly shortens specimen preparation, because $BaSO_4$ resin treatment takes only minutes.

Second, modifying an LVSEM to achieve lower magnification is much simpler. The specimen stage can be removed easily, as it is attached to the roll-out door (Hitachi instruments). The entire door and stage assembly can be removed and replaced with a fabricated plate. Further, because a high vacuum is not necessary, the replacement door is easy and inexpensive to construct. In this manner, the column is unobstructed, and a sample can be lowered farther down the column without difficulty.

Image analysis presents another way of observing air voids, because area fractions of the specimen can be analyzed versus lineal fractions as provided by the linear traverse. The linear traverse is a one-dimensional approximation of void content, whereas image analysis is a two-dimensional estimate. By observing the image, one can determine whether the void distribution is uniform.

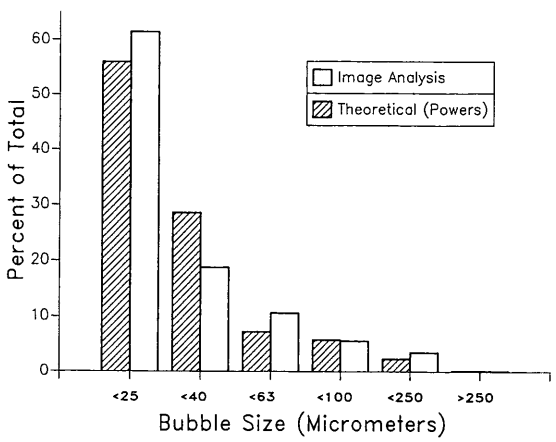

FIGURE 9 Void size distribution; theoretical versus measured.

ANALYSIS OF ASPHALT CONCRETE

Adaptation of the described instrumentation to the characterization of asphalt concrete (AC) appears realistic. Using BSE imaging at 2× magnification, AC cores exhibit significant differences in contrast between the large aggregate and the asphalt matrix in uncoated cores (Figure 10). Another advantage of BSE imaging is the ability to easily detect even dark-colored aggregate as atomic number, not color, and provide signal intensity.

Analysis of a void system can be achieved by either heavy gold sputtering or filling the voids with $BaSO_4$ in resin. Each of these techniques, however, has limitations for AC.

LIMITATIONS OF HEAVY GOLD SPUTTERING ON AC

The application of a heavy gold layer on the core surface provides the necessary contrast between voids and the surrounding matrix

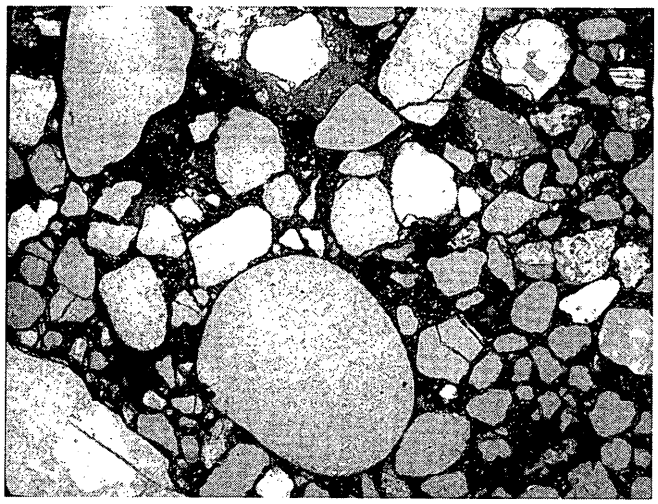

FIGURE 10 BSE image of uncoated AC core.

but eliminates differentiation between the asphalt matrix and aggregate, as both are heavily coated with gold. Thus, to provide a measure of void area, aggregate, and asphalt, it is necessary to perform the analysis in two steps, namely, (*a*) analyze aggregate versus void and asphalt, (*b*) apply gold sputtering and analyze to delineate voids from aggregate and asphalt.

LIMITATIONS OF $BaSO_4$ RESIN TREATMENT

Implementation of the $BaSO_4$ treatment appears to be a more logical approach, because atomic number differences between AC, aggregate, and $BaSO_4$-filled voids would be significant and would permit a three gray-level analysis scheme. Unfortunately, the action of solvents used in the LR White resin are too disruptive to the asphalt matrix. Barium clearly becomes part of the AC matrix. Water miscible resins have been used successfully, but further research is needed. The AC will appear nearly black in the SEM image and allow determination of the AC content without extraction, using toxic solvents.

INSTRUMENTAL LIMITATIONS FOR AC ANALYSIS

The high vacuum requirement of the conventional SEM can be detrimental to AC surfaces. Mild distortion of the matrix is apparent at vacuums of 1×10^{-6} torr, although no damage is apparent at approximate vacuums of 1×10^{-3} torr. The latter figure, 1×10^{-3} torr, was observed in samples viewed with a conventional SEM operating in a "poor" vacuum state. The instrument of choice for AC analysis is obviously the LVSEM.

CONCLUSIONS

The following conclusions are supported by the SEM image-analysis research:

- Improved image resolution can be obtained from SEM BSE images.
- Gold sputter coating yields excellent contrast of voids in a BSE image for PCC or AC samples.
- Barium sulfate resin–filled voids yield an excellent BSE contrast of voids; voids were distinguishable from asphalt cement and aggregate in an AC sample as they were generally in a PCC sample.
- Image analysis of SEM images detects significantly more voids than does linear traverse.
- There is a good correlation between percent of air by image analysis and linear traverse.
- There is a poor correlation between specific surface by image analysis and linear traverse.
- Image analysis using SEM images consistently yields a greater specific surface and a lower spacing factor than linear traverse because it detects more voids.

REFERENCES

1. Gonzales, R. C., and P. A. Wintz. *Digital Image Processing.* 2nd ed. Addison-Wesley, Reading, Mass., 1987.
2. Pratt, W. K. *Digital Image Processing.* 2nd ed. John Wiley and Sons. New York, 1991.
3. Rosenfeld, A., and A. Kak. *Digital Picture Processing.* 2nd ed. Academic Press, New York, 1982.
4. Kjellsen, K. O., R. J. Detwiler, and O. E. Gjorv. Backscattered Electron Imaging of Cement Pastes Hydrated at Different Temperatures. *Cement and Concrete Research.* Vol. 20, 1990, pp. 308–311.
5. Newbury, D. E., C. E. Fiori, R. B. Marinenko, R. L. Mykelbust, C. R. Swyt, and D. S. Bright. Compositional Mapping with the Electron Probe Microanalyzer; Part I. *Anal. Chem.* Vol. 62, 1990, pp. 1159A–1166A.
6. Newbury, D. E., C. E. Fiori, R. B. Marinenko, R. L. Mykelbust, C. R. Swyt, and D. S. Bright. Compositional Mapping with the Electron Probe Microanalyzer; Part II. *Anal. Chem.* Vol. 62, 1990, pp. 1245A–1254A.
7. Backstrom, J. E., R. W. Burrows, R. C. Mielenz, and V. E. Wolkodoff. Origin, Evolution, and Effects of the Air Void System in Concrete (Part III), Influence of Water-Cement Ratio and Compaction. *Proc., American Concrete Institute,* Vol. 55, 1958, pp. 359–375.
8. Powers, T. C. *The Properties of Fresh Concrete.* John Wiley and Sons. New York, 1968.

DISCUSSION

BRYANT MATHER
Director, Structures Laboratory,
U.S. Army Engineer Waterways Experiment Station,
Vicksburg, Miss. 39180–6199.

One of the things the workers on concrete microstructure need is a guide to the use of image analysis. The authors have provided good material for that purpose. I trust their research gets studied by the ASTM Committee on Petrography of Concrete as material for revision of ASTM standard C 457 on the Microscopical Determination of Parameters of the Air-Void System in Hardened Concrete.

The reason some people who look at the surface of a random plane through concrete see more and smaller sections of air voids has to do with the quality of preparation of such surfaces for examination (*1*; discussion). If preparation of the surface leaves roughness that cannot be distinguished from small air-void sections, those sections will not be detected. Yet the authors do not discuss how their image analysis procedure detects such small sections when linear traverse fails to do so, even though no different degree of surface preparation was involved.

Remember that there are no very small air bubbles. There are, however, very small air-void sections on surfaces when the plane of

the surface intersects a void near the point of tangency of the surface and the void. Such small sections are very shallow when the void is in the removed concrete and, in comparison, very deep when the void is mostly below the surface. The former are very hard to detect; the latter are often artificially enlarged in surface preparation—more so the weaker the paste and the larger the void. Procedures for calculating air-void parameters from air-void section data were given elsewhere (*1–4*).

The authors do not compare any of their results from tests of hardened concrete with actual values of air content of unhardened concrete. There has been much discussion of why values for air content of hardened concrete do not agree with those of unhardened concrete. Presumably logical reasons were adduced for why the air content of hardened concrete should be lower than that of fresh concrete or why that of hardened should be higher than that of fresh concrete. My view is that if one has a properly adjusted apparatus and uses it in accordance with ASTM C 231, allows the concrete sample so tested to harden in the bowl of the pressure meter, and then takes appropriate samples of the concrete for test by ASTM C 457, either point count or linear traverse, all three will agree. They will agree, that is, so long as things that look like air-void sections on the surface, but are not, are not counted as air voids. The pseudo air-void sections that I am most aware of are cenospheres from fly ash and fallen out spherical sand grains cut below their equatorial plane when the surface to be examined was "facing up" as the concrete hardened. In that case, there is a lack of bond at the underside of a sand grain from bleeding. If one does not fill the holes on the surface and looks at it carefully he or she can tell a bleed-water lined void as under a sand grain or one lined by glass from one lined by the "soap" film surrounding an entrained-air void. In the case of cenospheres, giving the prepared surface a light acid etch will cause a collar of glass to be revealed at the edges of cenospheres. Part of the variation between image-analysis results and linear-traverse results found by the authors may be attributable to discriminating observations made by an operator, which the image analyzer cannot make because the holes (air voids and others) are filled before examination.

Advice given by Walker (*5*) regarding air voids in hardened concrete merits careful study. In her discussion of image analysis she comments

> . . . systems that require filling the voids (thus hiding their interior surface) cannot be used to make certain distinctions possible by a human operator, can often mentally reconstruct what the surface if this or that flaw had not occurred. The human operator can judge if a void observed is an air void, a fly ash cenosphere, or the hole left where a small round grain of sand has fallen out.

In her discussion of fly ash (*6*), she wrote

> The walls of the cenospheres are frequently thin enough and the cenospheres large enough to be mistaken for entrained air voids. To detect and distinguish from air voids, etch, rinse, blot, and examine with the stereomicroscope. The glass walls can be seen with low-angle illumination projecting above the paste.

I invited my colleague, G. Sam Wong, to comment on the foregoing discussion. He added the following (personal communication):

> I agree with your comments and to take it even further concerning the differentiating of material such as cenospheres, there is also the differentiation of paste from aggregates. This is easily done by the petrographer using a microscope; this is not done so easily using image analysis. Chemistry is often not useful since most elements that are common in portland cement are also common in aggregates. Color often is not useful since the color of aggregate may have similar qualities as that of portland cement paste. They did not show how they distinguish paste from aggregate. It is easy with asphalt if you do not use a black aggregate. The voids filled with some sort of enhancing substance has been used successfully and it suffers the same sort of programs using light microscopy for image analysis as that in the SEM.
>
> On page 8 they mention the examination of 10 random images of 0.187 cm^2. I calculate this to make an area which would be 4.3 mm on a side. Sand begins at 4.75 mm, which would mean that if they took a representative sample and they have 75 percent aggregate in the concrete then 75 percent of the sections examined would have nothing but aggregate in them and that would include the fine aggregate. It would be impossible to see a single coarse aggregate particle. I believe that it is only by good fortune that the figure 5 information is like it is. Total area with paste and voids that would be available for examination would be 25 percent of 1.87 cm^2 or 0.4675 cm^2.

REFERENCES

1. Powers, T. C. The Air Requirement of Frost-Resistant Concrete. *HRB Proc.*, Vol. 29, 1949, pp. 184–202. Discussion by T. F. Willis, pp. 203–211.
2. Lord, G. W., and T. F. Willis. Calculation of Air Bubble Size Distribution from Results of Rosiwal Traverse of Aerated Concrete. *ASTM Bulletin*, No. 177, 1951, pp. 56–61. Discussion by Robert E. Philleo, *ASTM Bulletin*, No. 179, 1952, pp. 73–74.
3. Willis, T. F. Discussion, Linear Traverse Technique for Measurement of Air in Hardened Concrete *ACI Journal Proc.*, Part 2, Vol. 47, 1951, pp. 124-1–124-2.
4. Willis, T. F. Measuring Air in Hardened Concrete. *ACI Journal Proc.*, Vol. 48, 1952, pp. 901–903.
5. Walker, H. N. *Petrographic Methods of Examining Hardened Concrete: A Petrographic Manual.* Report FHWA/VA-R14, Virginia Transportation Research Council, Charlottesville, Va., 1992.
6. Walker, H. N. *Bias of Air-Void System Data from Fly Ash Concretes.* Report VHTRC 84–R6. Virginia Transportation Research Council, Charlottesville, Va., 1952.

AUTHORS' CLOSURE

Image analysis performed on SEM images detects more small air voids than does linear traverse performed via light microscopy. Unfortunately, the linear traverse systems used in this study did not provide individual measurements on air-void sizes, so direct comparison of size distributions was not possible. However, we do know that the average chord lengths provided by linear traverse were larger than that obtained from image analysis of SEM images.

Powers (*8*) offers one clue for that difference in a discussion of the linear traverse, in which he states, ". . . accuracy is limited by the resolving power of the microscope." A typical light microscope has a resolving power (the ability to differentiate two objects as being separate entities) of about 2,500 angstroms. A modem SEM typically has a resolution better than 35 angstroms, which represents a very significant improvement above the light microscope's ability to resolve small objects.

Further, the SEM is noted for its increased depth of focus, which makes it much easier for an operator to view the magnified specimen clearly. Light microscopes require constant focusing because of the poor depth of focus; that, combined with their much poorer resolution, serves to render even the most dedicated operator eye weary in a short period of time. Analyzing a linear traverse via the light microscope is indeed a time-consuming and monotonous task, subjecting an operator to continual eye strain, and boredom can have very serious consequences.

Two points Walker makes regarding the identification of plucked sand grains, fly ash cenospheres, and surface flaws bear discussion.

First, I agree that filling of the voids can obscure fly ash cenospheres and plucked sand grains. In fact, before filling voids with $BaSO_4$, we always make a cursory examination of cores with the SEM. A few minutes' examination gives one a clear picture (much more than viewing them with a light microscope) and can be extremely useful for resolving poor sample preparation or the distribution of small and large aggregate and air voids, generally. In fact, during one particular analysis, we were able to determine quickly the presence of numerous cenospheres that, upon subsequent examination using the light microscope, were seen only with much difficulty. The difference in the two imaging systems' ability to identify minute structures is dramatic. Again, the resolving power and depth of focus of the SEM is unquestionably far superior to the light microscope; it serves to greatly aid an investigator's efforts and provides an improved method for differentiating minute structures.

Second, I am less concerned about a few random sand grains plucked from a sample than I am about the total number of voids measured. A case in point is illustrated in Figure 4. A 7-hr linear traverse detected and measured approximately 1,200 air voids; whereas, with the image analyzer, a 7-hr analysis would have measured approximately 168,000 voids on the same sample. The dramatic speed provided by the image analyzer means that one can analyze many more cores instead of relying on the questionable practice of analyzing only a few.

Assuming one does not intend to fill the voids, the gold-coating technique is the method of choice. Figure 2 indicates that, even with a heavy gold-coating, one can still differentiate fine and large aggregate and, thus, presumably cenospheres. If in fact there is a question regarding cenospheres, the energy dispersive spectrometer (attendant on most SEM'S) can provide the conclusive chemical analysis within seconds. The interactive software on image analysis systems can be used to quickly subtract the voids from analysis—as well as from dislodged sand particles. The chief drawback to interactive image processing, however, is that it requires an operator's interpretation, which dramatically increases analysis time.

It has nearly been 50 years since the linear traverse came into use; it needs to be replaced with a more efficient method. Although many questions remain regarding image analysis, it has tremendous potential. To adequately characterize the air content in a road, one has to measure a very large number of voids. Linear traverse does not allow one to do that economically; it is that simple.

Just as simply, we need to be able to measure voids long before the road has been finished, because once the road has been built void content is somewhat of a moot point. I question whether we should relegate highly trained petrographers to task of sitting before a light microscope hour after hour to perform simple duties.

With respect to using color for analysis, electron microscopes "see" shades of gray only, so color is not an issue. In truth, color is not a very useful characteristic for distinguishing voids; the use of BSE offers much more potential. As the number of BSE is related to atomic number, tremendous signal differences can be achieved between the hydrocarbon asphalt cement and aggregate, regardless of color. BSE imaging (See Figure 10) is straightforward and produces outstanding images. BSE analysis can be performed with very little effort to determine in-place gradation of aggregate. In terms of concrete, published research demonstrates the ability to quantitatively determine W/C ratios and hydration states of paste using the electron microscope in the BSE mode. A challenge for earlier investigators was to successfully differentiate air voids; this paper demonstrates two methods for doing that.

In addition, there are BSE systems that reportedly are capable of measuring .1 differences in atomic number. Although we have not used a sensitive BSE detector, it would be interesting to view concrete and asphalt with such a system.

I too was initially surprised with the high correlation between linear traverse and image analysis in terms of percent of air. I had expected correlation to be very poor considering the extremely low number of voids measure by the linear traverse in combination with human error. However, percent air is dominated by the larger bubbles that the linear traverse can resolve, and percent air is a fairly crude measure. The last reason is justification for calculating either specific surface or the spacing factor; unfortunately, even these measures fall short because they rely on average chord length and really do not consider large discrepancies—beyond which basic equation to use. One must calculate the average chord length as accurately as possible; if one cannot resolve smaller voids, one cannot measure them.

With respect to area analysis, I am not sure whether Mather means to discredit its use or only challenge our not collecting a sufficient number of frames. If we are willing to accept lineal analysis (or point count), we must accept area analysis because the stereological development of the two methods relates to the assumption that $Vv = AA = LL$.

Regarding the number of frames collected for our comparisons, I agree that more area is desirable; even 50 or 100 frames (total analysis times of approximately 1 or 2 hr respectively) may be warranted if one wants to thoroughly characterize a core. A good statistician, however, would recommend reducing the area scanned on one core and greatly increasing the number of cores analyzed. In future, one might wish to forget about measuring the large aggregate and collecting information from the paste fraction only. If interested in air content one might not want to waste time analyzing large aggregate. Also, it may be better to obtain only five frames of data on 10 cores, instead of 50 frames of data from only one core. However, from just five frames, one can get a reasonable estimate of what is happening on any particular core. If results indicate a possible problem, then more extended analysis is warranted; otherwise it is better to move on to another sampling location. Statistically, the analysis of one core, whether by image analysis or linear traverse, is of little use. I believe that what we will see in the future is a totally new way of measuring things, accompanied by a different set of measurements. One could argue the virtues of linear traverse or image analysis until blue in the face. What we really need to concern ourselves with is how to assess the quality of the roads as we build them, not after we build them. We cannot do that with linear traverse.

The contents of this report reflect the views of the author and do not necessarily reflect the official views of ISU and the Iowa Department of Transportation. This report does not constitute any standard, specification, or regulation.

Publication of this paper sponsored by Committee on Mechanical Properties of Concrete.

Prediction of Creep Effect in Segmental Concrete Bridge Construction

LEV KHAZANOVICH

Presented is a theoretically sound and practical approach for determining concrete creep effects on deflection and stress distributions in reinforced concrete bridges subject to structural system changes during construction. An approximate solution adopted by the American Concrete Institute (ACI) sometimes produces a significant error and considers only one structural system change. An exact solution would require calculation of an integral relaxation function. A simplified and accurate solution for determining concrete creep effects for any number of structural system changes is described. The proposed method is as simple to implement as the ACI method and is highly accurate.

Construction of reinforced concrete bridges presents the problem of structures with a variable structural system. Although it is well known that creep and imposed displacements can cause redistribution of the stresses and bending moments in structures, the significance of structural system changes on the long-term stress distribution in concrete structures is not well documented. Introduction of delayed restraints and the special characteristics of concrete as an aging viscoelastic material allow increased deflection under constant loading and, as a result, lead to redistribution of stresses. The effect was first considered in the design of the bridges over the Neva in (then) Leningrad, USSR (*1*) and the Vltava in Hlanda, Czech Republic (*2*).

In general, the problem requires the solution of a system of integral-type equations. A numerical solution may be obtained with a step-by-step method, taking into account particular sequences of construction. In that manner, a continuous beam built span by span has been analyzed in a work by Bažant and Ony (*3*).

In the case of homogeneous structures (i.e., structures in which the material properties are the same at all points), the exact solution in closed form was obtained by Kharlab (*1*) and independently (in less advanced form) by Dezi et al. (*4*). However, the solution requires calculation of an integral relaxation function. A simplified solution by the Age-Adjusted Effective Modulus Method (AEMM) was obtained by Bažant and Najjar (*2*), Bažant (*5*), and Kristtek and Bažant (*6*). The solution was adopted by American Concrete Institute (ACI) as a recommendation (*7*). In most cases, the method gives a good approximation, although sometimes its error is significant. Moreover, the ACI recommendation considers only the case of one structural system change.

The aim of this paper is to develop a simplified but accurate solution for any number of structural system changes by combining Kharlab's exact solution and Bažant's simplified solution.

CREEP OF CONCRETE

Different approaches to describing the constitutive relationship of concrete considering creep exist: models derived by ACI (*7*), by Bažant and Panula (*8*), and by Bažant and Prasannan (*9*), among others.

In the present study, a linear creep law is assumed. The assumption is acceptable for stresses less than 0.4 of the standard cylinder compressive strength. The relation between stress σ and strain ϵ may be written in the Stieltjes integral form, as follows:

$$\epsilon(t) - \epsilon_0(t) = \int_{t_0}^{t} J(t, \tau) d\sigma(\tau) \tag{1}$$

where

t_0 = age when the stress and deformation first appear;
$\epsilon_0(t)$ = stress-independent inelastic strain, such as shrinkage strain or thermal dilatation; and
$J(t, \tau)$ = creep compliance, [i.e., strain at time t (including elastic strain) caused by a unit constant stress acting since time τ].

In terms of the creep coefficient $\phi(t, \tau)$, creep compliance is defined as

$$J(t, \tau) = \frac{1 + \phi(t, \tau)}{E(\tau)} \tag{2}$$

where $E(\tau)$ is the instantaneous elastic modulus.

In general, a universally acceptable model does not exist. In this investigation, however, the ACI model has been chosen as the most widely used one. According to the ACI recommendation (*7*)

$$\phi(t, \tau) = \phi_u(\tau) f(t - \tau) \tag{3}$$

where

$$f(t - \tau) = \frac{(t - \tau)^{0.6}}{10 + (1 - \tau)^{0.6}} \tag{4}$$

$$\phi_u(\tau) = \phi(\infty, 7)\, 1.25\, \tau^{-0.118} \tag{5}$$

$$E(\tau) = E(28) \sqrt{\frac{\tau}{4 + 0.85\, \tau}} \tag{6}$$

where t, τ are given in days.

STRUCTURES SUBJECTED TO ONE STRUCTURAL SYSTEM CHANGE

A statically determinate or indeterminate homogeneous system V_0 is loaded by its constant dead load at age t_0. At time t_1, the system V_0 is changed to system $V_{(1)}$ by means of introducing a redundant

ERES Consultants, Inc., 505 West University Avenue, Champaign, Ill. 61820.

rigid restraint without any sudden change of stresses. Following Kharlab (*1*), consider system V_1, which has the same configuration at time t_0 as system $V_{(1)}$ and has elastic modulus $E(t_0)$. Then, force variables (stresses, bending moments), $Y(t, x)$, and deformation variables (strains, deflections), $W(t, x)$, at time t and location x can be represented in terms of the corresponding elastic force variables, $Y_0^{el}(x)$ and $Y_1^{el}(x)$, and elastic deformation variables, $W_0^{el}(x)$ and $W_1^{el}(x)$, as follows:

$$Y(t, x) = Y_0^{el}(x)\,[1 - \zeta(t, t_0, t_1)] + Y_1^{el}(x)\,\zeta(t, t_0, t_1) \tag{7}$$

$$W(t, x) = W_0^{el}(x)[1 + \phi(t_1, t_0)] + W_1^{el}(x)\,[\phi(t, t_0) - \phi(t_1, t_0)] \tag{8}$$

$$\zeta(t, t_0, t_1) = \int_{t_1}^{t} R(t, \tau)\, dJ(t, t_0) \tag{9}$$

where $R(t, \tau)$ is the relaxation function, which is defined as the stress at age t caused by unit constant strain introduced at age τ.

Integral relaxation function, $\zeta\ (t, t_0, t_1)$, may be calculated numerically with high accuracy in a step-by-step manner (*4*), although such a process may at times be tedious. The simplified solution obtained using the AEMM (*2,5,6*) has the following form:

$$Y(t, x) = Y_0^{el}(x)\,[1 - r(t, t_0, t_1)] + Y_1^{el}(x)\,r(t, t_0, t_1) \tag{10}$$

$$W(t, x) = W_0^{el}(x)\,[1 + \phi(t_1, t_0)] + W_1^{el,1}(x)\,[\phi(t, t_0) - \phi(t_1, t_0)] \tag{11}$$

$$r(t, t_0, t_1) = \frac{\phi(t, t_0) - \phi(t_1, t_0)}{1 + \chi(t, t_1)\,\phi(t, t_1)} \tag{12}$$

where $W_1^{el}(x)$ is the elastic deformation variable in the elastic system V_1 based on elastic modulus $E(t_1)$, and $\chi(t, t_1)$ is the aging coefficient (*2,5,7*).

Comparison of the exact and simplified solutions for the force variable (Equations 7 and 10, respectively) shows that $r(t, t_0, t_1)$ can be considered as an approximation of the integral relaxation function $\zeta\ (t, t_0, t_1)$. The approximation is good enough if $t_0 \approx t_1$ or $t_0 \ll t_1$. Nevertheless, sometimes the error from that approximation is significant. The AEMM can be improved by introducing a delayed coefficient $\alpha(t_1, t_0)$ and recasting the solution for the force variables in the form

$$Y(t, x) = Y_0^{el}(x)\,[1 - \gamma(t, t_0, t_1)] + Y_1^{el}(x)\,\gamma(t, t_0, t_1) \tag{13}$$

where

$$\gamma(t, t_0, t_1) = \frac{\phi(t, t_0) - \phi(t_1, t_0)}{1 + \alpha(t_1, t_0)\,\chi(t, t_1)\,\phi(t, t_1)} \tag{14}$$

Values of coefficient $\alpha(t_1, t_0)$ have been obtained and are represented in Table 1. For interpolation in the table, it is better to assume linear dependence on log t_0 and log $(t_1 - t_0)$. For the sake of those who may be interested in a long-term solution only, values of $\gamma(t, t_0, t_1)$ have also been computed for $t - t_1 = 10^4$ days, and are presented in Table 2.

Comparison of the exact and simplified solutions for the deformation variable (Equations 8 and 11, respectively) shows that a discrepancy arises only in the determination of elastic variables; the exact solution requires calculation of them based on modulus $E(t_0)$, but the approximate solution requires use of modulus $E(t_1)$. Therefore, using the exact solution is not more complicated than the approximate one and, as a result, it is preferable.

NUMERICAL EXAMPLE

As an example, consider a pair of two simply supported beams, which are made continuous over the middle support after they have

TABLE 1 Delayed Coefficient $\alpha\ (t_1, t_0)$

$t_1 - t_0$ days	$\phi(\infty, 7)$	t_0 days			
		10^1	10^2	10^3	10^4
0	0.5	1.0	1.0	1.0	1.0
0	1.5	1.0	1.0	1.0	1.0
0	2.5	1.0	1.0	1.0	1.0
0	3.5	1.0	1.0	1.0	1.0
10	0.5	0.551	0.949	0.989	0.997
10	1.5	0.765	0.954	0.988	0.998
10	2.5	0.791	0.953	0.989	0.998
10	3.5	0.798	0.952	0.988	0.997
10^2	0.5	0.229	0.871	0.963	0.990
10^2	1.5	0.578	0.892	0.962	0.990
10^2	2.5	0.641	0.893	0.962	0.990
10^2	3.5	0.668	0.892	0.961	0.989
$\geqslant 10^3$	0.5	0.073	0.804	0.924	0.968
$\geqslant 10^3$	1.5	0.520	0.856	0.925	0.968
$\geqslant 10^3$	2.5	0.608	0.865	0.924	0.968
$\geqslant 10^3$	3.5	0.645	0.868	0.923	0.967

TABLE 2 Long-Term Values of Function $\gamma(t, t_0, t_1)(t - t_1 = 10^4$ days)

t_1-t_0 days	f(∞, 7)	t_0 days			
		10^1	10^2	10^3	10^4
10	0.5	0.282	0.190	0.149	0.119
10	1.5	0.550	0.383	0.317	0.267
10	2.5	0.675	0.479	0.408	0.356
10	3.5	0.745	0.536	0.465	0.414
10^2	0.5	0.155	0.101	0.077	0.061
10^2	1.5	0.320	0.209	0.166	0.138
10^2	2.5	0.405	0.266	0.215	0.184
10^2	3.5	0.457	0.301	0.246	0.215
≥ 10^3	0.5	0.047	0.030	0.023	0.018
≥ 10^3	1.5	0.102	0.066	0.050	0.040
≥ 10^3	2.5	0.133	0.086	0.066	0.054
≥ 10^3	3.5	0.153	0.099	0.076	0.063

already started carrying their own weight [Figure 1 (a) and (b)]. The spans are assumed to start carrying their dead load of 17.7 N/cm (10 lb/in.) at age t_0 = 28 days. At 60 days, the beams are joined monolithically above the middle support. The second moment of area of each beam is assumed to be 0.0405 m^4 (5 ft^4). Furthermore, $E(28)$ = 27.9 MPa (4 Mpsi), and ϕ (∞, 7) = 2.5.

To evaluate the bending moment in the beam above the middle support at 100 days, it is necessary to find the following parameters:

- Bending moments in the corresponding elastic systems.
- Aging coefficient, χ(100, 60); and
- Delay coefficient, α(60, 28).

Elastic bending moment above the inner support in the system without a joint above this support is $M_0^{el} = 0.\ N - m$.

Elastic bending moment at the same location in the system with a joint is M_1^{el} = 113.9 kN-m (84,400 ft-lb).

According to ACI recommendations (*7*)

χ(20, 10) = 0.774 χ(110, 100) = 0.804

χ(110, 10) = 0.842 χ(200, 100) = 0.935

From linear interpolation, χ(100, 60) = 0.874.

Similarly, from Table 1

α(20, 10) = 0.764 α(110, 100) = 0.952

α(110, 10) = 0.641 α(200, 100) = 0.888

and from linear interpolation α(60, 28) = 0.799

Substitution of these values into Equation 13 gives γ(100, 28, 60) = 0.155.

Finally, from Equation 14, the magnitude of the bending moment in the beam above the middle support at age 100 days is M(100) = 0 (1−0.155) + 113.9 (0.155) = 17.7 kN-m (13080 ft-lb).

For determination of long-term bending moment at the same location, one can use Table 2

γ(20, 10) = 0.675 γ(110, 100) = 0.479

γ(110, 10) = 0.405 γ(200, 100) = 0.266

From interpolation, γ = 0.464; as a result, M(10060) = 52.9 kN-m (39160 ft-lb).

Figure 1 (c) presents the bending moment distribution at t = 60, 100, and 10,060 days. Table 3 shows a comparison of these results (proposed method) with the corresponding AEMM and exact solutions. One may conclude that the proposed method is as simple to implement as the AEMM at the same time it is highly accurate.

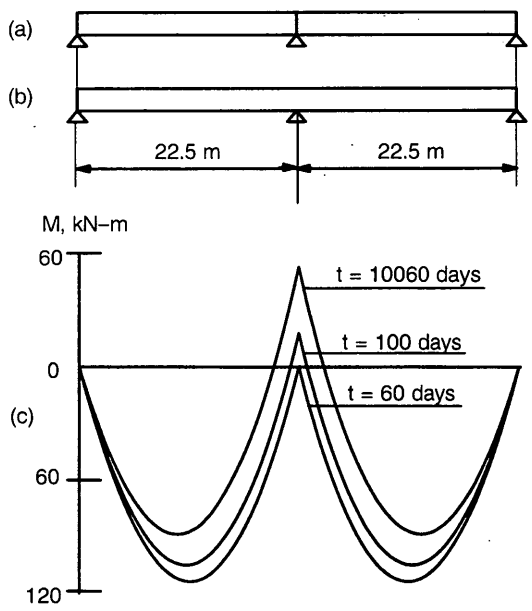

FIGURE 1 (a) Initial structural system; (b) structural system at 60 days; (c) bending moment distributions at 60, 100, and 10,060 days.

TABLE 3 Comparison of Exact and Simplified Methods

t, days	Bending moment over inner support (kN-m)		
	Exact solution	Proposed Method	AEMM
60	0	0	0
100	17.7	17.7	16.1
10060	50.9	52.9	46.3

STRUCTURES WITH DELAYED RESTRAINTS INTRODUCED AT DIFFERENT SUCCESSIVE TIMES

For structures with delayed restraints introduced at different successive times, use of Kharlab's principle of independent restraint actions (*1*) is justified. It states that if the principle of superposition is satisfied, then the $(i + 1)$th delayed restraint acts on system $V_{(i)}$ as if it were its first and only restraint, (i.e., as if it were not introduced onto system $V_{(i)}$, which is subjected to i delayed restraints, but onto system V_i, for which all restraints were initial, and onto which no new restraints would be introduced subsequently. Application of this principle to the case of constant loads and discrete structural changes leads to the following expression for any force variables $Y_j(x, t)$ and deformation variables $W_j(x, t)$ in a system $V_{(j)}$ with j delayed restraints, in terms of the corresponding force and deformation variables, $Y_i^{el}(x)$ and $W_i^{el}(x)$, in the elastic system V_i based on elastic modulus $E(t_0)$

$$Y_j(t, x) = Y_0^{el}(x)\,[1 - \zeta(t, t_0, t_1)] + \sum_{i=1}^{j-1} [Y_i^{el}(x)\,[\zeta(t, t_0, t_i) - \zeta(t, t_0, t_{i+1})] + Y_j^{el}(x)\,\zeta(t, t_0, t_j) \quad (15)$$

$$W_j(t,x) = W_0^{el}(x)\,[1 + \phi(t_1, t_0)] + \sum_{i=1}^{j-1} [W_i^{el}(x)\,[\phi(t_{i+1}, t_0) - \phi(t_i, t_0)] + W_j^{el}[\phi(t, t_0) - \phi(t_j, t_0)] \quad (16)$$

$$\zeta(t, t_0, t_j) = \int_{t_j}^{t} R(t, \tau)\, dJ(t, t_0) \quad (17)$$

where t_i is the time when the restraint was introduced.

In a manner similar to the case involving one delayed restraint, the integral relaxation functions $\zeta(t, t_0, t_i)$ may be replaced by functions $\gamma(t, t_0, t_1)$. Therefore, a simplified solution for the force variables under multiple delayed restraints may be presented in the form

$$Y_j(t, x) = Y_0^{el}(x)\,[1 - \gamma(t, t_0, t_1)] + \sum_{i=1}^{j-1} [Y_i^{el}(x)\,\{\gamma(t, t_0, t_i) - \gamma(t, t_0, t_{i+1})\}] + Y_j^{el}(x)\,\gamma(t, t_0, t_j) \quad (18)$$

For the deformation variables, as in the case with one delayed restraint, the exact solution is recommended.

CONCLUSIONS

The study highlights an important consideration for time-dependent analysis of structures with a variable structural system. Concrete bridges are one example of structures subjected to repeated structural changes. The specific objective was to develop a simple but accurate method for evaluating stress and displacement redistribution in homogeneous structures.

The product of this study is a method obtained by modifying the AEMM method. It requires evaluation of one additional coefficient, the values of which are tabulated.

The proposed method was compared with the AEMM method and Kharlab's exact solution. It was found that the proposed method is as simple to implement as the AEMM and that it is highly accurate.

REFERENCES

1. Kharlab, V. D. *A Problem in Linear Mechanics of Visco-Elastic Body: Concerning Equilibrium of a System with Increasing Number of Restraints.* Dissertation (in Russian). Leningrad, USSR, 1963.
2. Bažant, Z. P., and L. L. Najjar. Comparison of Approximate Linear Methods for Concrete Creep. *Journal of the Structural Engineering Division,* Vol. 113, No. 3, ASCE, 1973, pp. 1851–1874.
3. Bažant, Z. P., and J. S. Ony. Creep in Continuous Beam Built Span-by-Span. *Journal of the Structural Engineering,* Vol. 109, No. 7, ASCE, 1983, pp. 1648–1688.
4. Dezi, L., G. Menditto, and A. M. Tarantino. Homogeneous Structures Subjected to Repeated Structural System Changes. *Journal of Engineering Mechanics,* Vol. 116, No. 8, ASCE, 1990, pp. 1723–1732.
5. Bažant, Z. P. Prediction of Creep, Shrinkage and Temperature Effect in Concrete Structures. *American Concrete Institute Journal,* Vol. 19, 1972, pp. 212–217.
6. Kristtek, V., and Z. P. Bažant. Shear Lag Effect and Uncertainty in Concrete Box Girder Creep. *Journal of the Structural Engineering,* Vol. 113, No. 3, ASCE, 1987, pp. 557–574.
7. *Prediction of Creep, Shrinkage and Temperature Effect in Concrete Structures. Design for Effect of Creep, Shrinkage and Temperature,* No. 76, American Concrete Institute, Detroit, Mich., 1982, pp. 193–300.
8. Bažant, Z. P., and L. Panula. Practical Prediction of Creep and Shrinkage of Concrete. *Materials and Structures,* Parts I and II, Vol. 11, No. 65, 1978, pp. 307–328; Parts III and IV, Vol. 11, No. 66, 1979, pp. 415–434; Parts V and VI, Vol. 12, No. 69, 1979, pp. 169–183.
9. Bažant, Z. P., and S. Prasannan. Solidification Theory for Concrete Creep. *Journal of Engineering Mechanics,* Part I and II, Vol. 115, ASCE, 1989, pp. 1691–1725.

Publication of this paper sponsored by Committee on Mechanical Properties of Concrete.

System Optimization of Failure, Constitutive Modeling, and Strengths of Concrete and Other Geological Materials Using Genetic Algorithm

M. REZA SALAMI, ABDOLLAH HOMAIFAR, AND SHILONG ZHAO

An application of genetic algorithms (GAs) to the system optimization of failure, constitutive modeling, and strengths of concrete and other geological materials is presented. GA is a relatively new, general purpose, optimization algorithm that applies the rules of natural genetics to explore a given search space. Knowledge of the basic constitutive properties of concrete and other geological materials is needed to analyze service load characteristics, design, and evaluate strengths. GA can be used to evaluate parameters of a concrete constitutive modeling, which is based on the theory of plasticity. All the parameters are constants for an ultimate (failure) yielding condition. GA also can be used to evaluate parameters of tensile and compressive strengths for frictional materials such as igneous, sedimentary, and metamorphic rocks; ceramics; mortar; polymer concrete; porous limestone; river gravel; dense limestone; and cemented soils. Such parameters are constants for failure (strengths) conditions. Numerical results indicate that GA is capable of optimizing the system parameters quickly and accurately. Resulting parameter values agree well with previous studies.

A constitutive law or model represents a mathematical model that describes the behavior of a material. In other words, a constitutive law simulates physical behavior that has been perceived mentally. The main advantage of establishing a mathematical model is to apply it to solve (complex) events quantitatively. Therefore, the power of a constitutive model depends on the extent to which the physical phenomenon has been understood and simulated.

In this paper, a constitutive model based on the theory of plasticity, described elsewhere (*1–8*), is used that can be used to characterize the stress-deformation behavior of concrete and geological materials. The model allows for factors such as stress hardening, volume changes, stress paths, cohesive and tensile strengths, and variation of yield behavior with mean pressure. To establish the constitutive model, determination of material constants (parameters) is very important. The only rational way to determine parameters to define the constitutive model is to conduct appropriate laboratory and field tests.

GA is a powerful search procedure based on the mechanics of natural selection. It uses operations found in natural genetics to guide it through the paths in the search space. It provides a means to search poorly understood irregular spaces. Because of its robustness, GA has been applied successfully to a variety of function optimizations, self-adaptive control systems, and learning systems.

M. Salami and S. Zhao, Department of Civil Engineering, North Carolina A & T State University, Greensboro, N.C. 27411. A. Homaifar, Department of Electrical Engineering, North Carolina A & T State University, Greensboro, N.C. 27411.

This study uses GAs to solve parameters of a constitutive model and strength models. Test data (*1–6*) was used to check the effectiveness of GA. Finally, parameters obtained by GA are compared with various methods in literature (*1–6*).

CONSTITUTIVE MODEL

Theoretical development of the hierarchical model approach and application to soil, rock, and concrete behavior is given elsewhere (*1–6;9–12*). Application of the model for geological materials, including comprehensive modeling and verifications for various geological materials, is discussed in words by Salami (*1–5*). The hierarchical concept provides a framework for systematic development of models with progressively complex responses: isotropic associative hardening, isotropic nonassociative hardening, anisotropic hardening and strain-softening. As a result, the concept can be sufficiently simplified in terms of material constants that are determined from laboratory tests (*1–6*).

A compact and specialized form, F, of the general polynomial representation (*1–5;9*), adopted herein to describe both the continuous yielding and ultimate (failure) yield behavior, is given by

$$F \equiv J_{2D} - F_b F_s \tag{1}$$

where

J_{2D} = second invariant of the deviatoric stress tensor;
S_{ij} = total stress tensor, σ_{ij};
F_b = basic function; and
F_s = shape function.

The function F is a continuous function in the stress space, and the final curve represents the ultimate behavior. In expanded form, Equation 1 is written as

$$F(J_1, J_{2D}, J_{3D}) \equiv J_{2D} - \left(\frac{-\alpha}{\alpha_0^{n-2}} J_1^n + \gamma J_1^2\right)(1 - \beta S_r)^{-1/2} \tag{2}$$

where

$J_1 = \sigma_1 + \sigma_2 + \sigma_3$, the first invariant of σ_{ij};
S_r = stress ratio = $(J_{3D})^{1/3}/(J_{2D})^{1/2}$, which can also be the Lode angle;
J_{3D} = third invariant of S_{ij}
α, n, γ, and β = response functions;

α_0 = 1 stress unit; and
m = −½ response function.

As a simplification, γ and m are assumed to be constants, whereas β is expressed as a function of mean pressure, J_1, to account for the observed yield behavior of geological materials (*1–5;10–12*).

$$\beta = \beta_0 e^{-\beta_1 J_1} \tag{3}$$

Here, β_0 and β_1 are constants. The constitutive model is developed to represent a wide range of materials. Based on Equation 2, the developed model is proposed to describe both failure and yielding of the concrete and geological materials. The model agrees with the experimental evidence regarding the shapes of yield surfaces on various planes. Moreover, ultimate failure and yielding are defined by a single yield surface.

TENSILE STRENGTH EXPRESSION, f_t

The proposed analytical expression of uniaxial strength f_t, as a function of cylindrical compressive strength for frictional materials, which is based on the experimental results found elsewhere (*13;1–6;14–16*), is given as

$$f_t = -mP_a \left\{ \frac{f_c'}{p_a} \right\}^n \quad \text{(compression positive)} \tag{4}$$

where m and n are dimensionless numbers, and p_a is atmospheric pressure in the same units as those of f_t and f_c'. Values of m and n have been determined by using GA for several frictional materials and are listed in Table 1.

TENSILE STRENGTH, f_{sp}

On the basis of experimental results (*1–6;14*) and also Equation 4, the split tensile strength of concrete is given as

$$f_{sp} = -\lambda P_a \left\{ \frac{f_c'}{p_a} \right\}^\eta \quad \text{(compression positive)} \tag{5}$$

TABLE 1 Values of Parameters m and n Obtained by GA for Various Types of Concrete and Frictional Materials for Equations (4–6)

MATERIALS	m	n
Mortar, *f_t	0.77	0.65
Cemented Soils, f_t	0.39	0.84
Ceramics, f_t	0.70	0.77
Igneous Rock, f_t	0.52	0.72
Metamorphic Rock, f_t	0.21	0.83
Sedimentary Rock, f_t	0.19	0.79
Plain Concrete, f_t	0.61	0.73
Plain Concrete, **f_{sp}	$\lambda = 0.69$	$\eta = 0.65$
Plain Concrete, ***f_r	$\alpha = 0.91$	$\beta = 0.62$
Porous Limestone, f_{sp}	$\lambda = 2.13$	$\eta = 0.43$
Porous Limestone, f_r	$\alpha = 1.96$	$\beta = 0.54$
River Gravel, f_{sp}	$\lambda = 2.28$	$\eta = 0.42$
River Gravel, f_r	$\alpha = 2.32$	$\beta = 0.53$
Dense Limestone, f_{sp}	$\lambda = 0.21$	$\eta = 0.83$
Dense Limestone, f_r	$\alpha = 0.54$	$\beta = 0.76$

*f_t = Direct Tensile Strength **f_{sp} = Split Tensile Strength
***f_r = Beam Flexural Tensile Strength

where λ and η are dimensionless numbers, and p_a is atmospheric pressure in the same units as those of f_{sp} and f_c'. Values of λ and η have been determined by using GA for several frictional materials and are listed in Table 1.

FLEXURAL TENSILE STRENGTH, f_r

On the basis of experimental results (*1–6;14*) and also Equation 4, the flexural tensile strength is given as

$$f_r = \alpha P_a \left\{ \frac{f_c'}{p_a} \right\}^\beta \quad \text{(compression positive)} \tag{6}$$

where α and β are dimensionless numbers, and p_a is atmospheric pressure in the same units as those of f_r and f_c'. Values of α and β have been determined by using GA for several frictional materials and are listed in Table 1.

Polymer concrete materials identified in Figure 1 are used to find parameters of Equation 4 for different temperatures. The values of parameters obtained by GA are presented in Table 2.

GA

GA is a general purpose, optimization algorithm with a probabilistic component. It provides a means to search poorly understood,

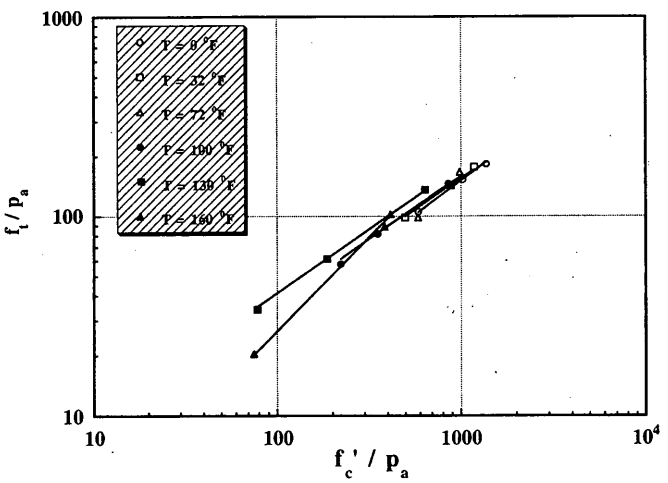

FIGURE 1 Comparison of experimental and predicted results for polymer concrete at different temperatures.

TABLE 2 Values of Parameters m and n Obtained by GA for Polymer Concrete Materials for Equation 4.

TEMPERATURE (^{0}F)	m	n
T = 0	1.29	0.69
T = 32	1.35	0.69
T = 72	2.05	0.63
T = 100	1.93	0.64
T = 130	1.69	0.68
T = 160	0.35	0.64

irregular spaces. GA has been applied successfully to a variety of function optimization, parameter searches, and machine learning applications. Holland (*17*) originally developed GA and provided its theoretical foundations. GA was developed to simulate some of the processes observed in natural evolution, a process that operates on chromosomes (organic devices for encoding the structure of living beings) instead of on living beings. Natural selection links chromosomes with the performance of their decoded structures. The processes of natural selection cause those chromosomes that encode successful structures to reproduce more often than those that do not. Recombination processes create different chromosomes in children by combining material from the chromosomes of the two parents. Mutation may cause the chromosomes of children to be different from those of their parents.

GA appropriately incorporates these features of natural evolution into computer algorithms to solve difficult problems in the way that nature has done, through evolution. GA requires the problem to be maximized (or minimized) in the form of an objective (cost) function. In GA, a set of variables for a given problem is encoded into a binary string, or any other coding structure, analogous to a chromosome in nature. These strings are converted to a numerical value and then linearly mapped over the range allowed for the variable. The value is then used to evaluate the objective function, yielding a "fitness." GA selects parents from a pool of strings (population) according to the basic criterion of survival of the fittest. It reproduces new strings by recombining parts from the selected parents in a random manner.

Repopulation of the next generation is done using three methods: reproduction, crossover, and mutation. Reproduction means simply that strings that are highly fit should receive multiple copies in the next generation, whereas strings with low fitnesses receive fewer if any copies. Crossover refers to splitting a string into two parts at a randomly generated crossover point and recombining it with another string that has been split at the same crossover point. The procedure serves to promote changes in the best strings, those that will produce higher fitnesses. Mutation is the random alteration of a bit in the string, which will assist to preserve diversity in the population of strings.

To explain the mechanisms of GA, a few terms need to be defined. Because binary strings are considered, a notation must be developed to denote similar subsets (schemata). A schema is a similarity subset that has strings containing similarities at some bit positions. Furthermore, the format can be expanded with the introduction of a wild card character, *, in addition to the binary set {0,1}. For example, the set {0001,0101,0011} can be described by the similarity template 0**1. By using this notation, a schema's order and defining length can be specified. For a given schema, h, its order $o(h)$ is defined as the number of fixed bit positions within that schema. The defining length of a schema, $\delta(h)$, is the distance between the outermost fixed positions of a schema. For example, the schema 01****0 has order 3, defining length 5, and can represent 16 different individuals.

With these definitions, one can present the fundamental theorem of GA, the schema theorem (*18*). The schema theorem enables the calculation of lower bound on the expected number of a particular schema, h, following reproduction, crossover, and mutation. The theorem is stated as

$$\lambda(h, t+1) \geq \lambda(h, t)\frac{f(h)}{x}\left[1 - p_c\frac{\delta(h)}{l-1} - p_m o(h)\right] \quad (7)$$

where

λ = expected number of schemata,
t = generation index,
l = overall string length,
$f(h)$ = average fitness of those strings representing the subset h,
x = average fitness of the entire population, and
p_c and p_m = the crossover and mutation probabilities, respectively.

The schema theorem states that a schema will grow when it is short, has low order, and has above average fitness.

GA has many advantages over other methods. Currently most literature defines three main types of search methods: calculus-based, enumerative, and random (*19*). Calculus-based methods can be divided into two classes: indirect and direct. For indirect methods, local extrema are determined by finding where the gradient of the objective function is equal to zero. Direct methods follow along the objective function in a direction related to the local gradient. Both classes share two main disadvantages that greatly limit their usefulness. First, both are local in scope; that is, if a function has multiple local maxima, the method may drive toward one of these values without ever approaching the global maxima. The second deficiency of calculus-based methods is their dependence on the existence of derivatives. However, many real-world functions are discontinuous and noisy and do not work well with a method that prefers smooth, continuous functions.

Enumerative methods offer an attractive advantage, simplicity, but that advantage carries a high cost. Enumerative schemes take a discretized search space and examine the objective function at every point. Although simple in technique, the brute force method is quite inefficient, and its execution time becomes too long as the search space becomes larger.

The last method is the random search method. In many respects, this method might perform as poorly as an enumerative method because of its inefficiency. Randomly searching through a space and saving the best results can be time-consuming as the space becomes large.

The primary advantage of GA is its robustness. GA works through function evaluation, not through differentiation or other such means. Whereas GA begins with a randomly generated set of points, it exploits the information contained in those points to drive it through the search space. Because GA is based on function evaluation, it can be applied to all type of optimization problems: linear, nonlinear, discontinuous, and discrete, as long as the problem is properly coded.

Because of its robustness, GA has been used in optimization problems as diverse as image analysis by Grefenstette and Fitzpatrick (*20*), gaming strategy by Axelrod (*21*), and the traveling salesman problem by Homaifar (*22*). Another practical engineering example of GA's application is Goldberg's study (*23*) of a system of 10 pipes and 10 pumping stations. Also, expert systems can be improved on by using GA, as shown by Davis and Coombs (*24*).

PROBLEM DESCRIPTION AND METHODOLOGY

The constitutive model and strength models that were used have some material constants. Determination of such constants for any material requires a comprehensive series of laboratory tests with a number of loading, unloading, and reloading cycles. In this paper, GA is used to determine material parameters: n, γ, β_0, and β_1 and at

the ultimate yielding conditions of constitutive model, and *m, n* for strength models. The materials that were tested elsewhere (*1–8*) are used in this research.

The basis for software used in this work is the Simple Genetic Algorithm program developed by Goldberg (*19*). The program is rewritten in C language to allow the evaluation of multiple parameters. Multiple parameters are incorporated by dividing each string up into substrings that represent different variables. For example, a string of length 18 could be used to represent three substrings of length 6, each of which could represent a different parameter. Obviously, using multiple parameters requires increasingly longer string lengths, if each variable has an acceptable precision.

The main purpose of this computational experiment is to examine the ability of GA to perform a multiparameter objective function optimization on a real-world problem.

The strings for the GA implementation were formed by concatenating the encoded value of each parameter. The string lengths were chosen as follows: (*a*) a step size of 0.001 was chosen for all parameters of model, and (*b*) the string lengths were chosen to provide appropriate ranges for all parameters. The constraint for choosing the string lengths is given by

$$2^l - 1 = \frac{\text{range}}{\text{stepsize}} \tag{8}$$

where l is string length. The resulting string lengths of parameters for failure, constitutive modeling, and tensile strengths are 8, except n which is 10.

A measure of performance is derived to effectively and accurately compare the performance of the GA. The error, measured over the entire simulation period, is described as

$$E = \sqrt{\sum_i (y_i - x_i)^2} \tag{9}$$

where y is actual data, and x is GA data.

Derivation of the fitness function for the GA is one of the difficult and crucial portions of this study. The fitness function should be formulated to discriminate among different strings. Initial experiments were conducted using a simple mean square error measure

$$\text{Fitness} = \frac{1}{\text{Error}} \tag{10}$$

However, the results provided only a mean square fit, so the fitness function was changed to

$$\text{Fitness} = \frac{\text{number of matched points}}{E} \tag{11}$$

where a matched point is a GA point within a specified tolerance.

Roulette wheel selection and single point crossover are used throughout the experiments. The variables that had to be defined for GA are population size, crossover probability, mutation probability, and maximum number of generations. Their respective values are 1,000, 0.60, 0.01, and 50. Figure 2 shows the flowchart for the implementation. Note that the stopping criterion is usually given in terms of a threshold in improvement or total number of generations. Population sizing is an important requirement in GA. Populations must be large enough to provide adequate diversity. However, the larger the population, the greater the number of calculations.

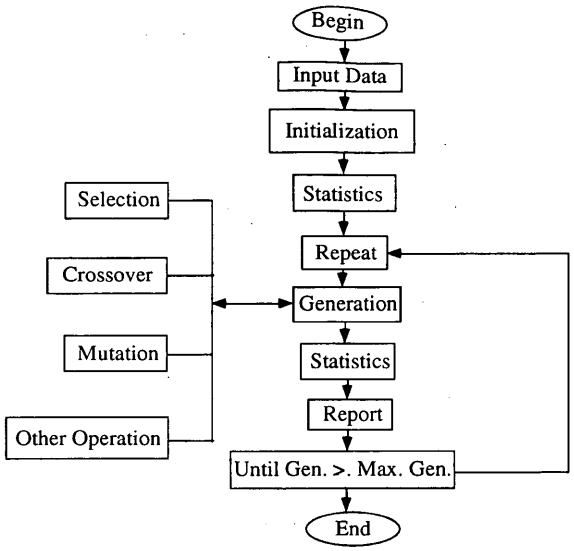

FIGURE 2 The main structure of GA implementation.

ANALYSIS

In this study, parameters for frictional materials, including plain concrete and soapstone, are determined by using GA. Three different cases are considered:

- Case 1: Cemented Soils, Ceramics and Mortar; Igneous, Metamorphic and Sedimentary Rocks are used to analyze the relationships between uniaxial cylindrical compressive strength f_c' and uniaxial tensile strength f_t, as given in Equations 4–6. The parameter values obtained by GA for these materials are shown in Table 1. Graph of typical results is shown in Figure 1 for polymer concrete materials under different temperatures, and demonstrate that parameter values obtained by the GA are compared very well with the experimental data.
- Case 2: The growth (hardening or softening) function α equals zero in Equation 2 of the ultimate condition for concrete materials. Then Equation 2 becomes

$$F(J_1, J_{2D}, J_{3D}) = J_{2D} - \gamma J_1 (1 - \beta S_r)^{-1/2} = 0 \tag{12}$$

where $\beta = \beta_0 e^{-\beta_1 J_1}$

The ultimate constants, n, γ, β_0, and β_1, are obtained by GA when the solutions are reached after 100 generations. Original data obtained by Salami are presented in Table 3 and Table 4, for plain concrete and soapstone, respectively. The GA solutions, along with Salami's solutions, are reported in Table 5. Parameter values obtained by the GA are compared with those obtained by Salami's method (*6*); the precision is 0.068.

- Case 3: The observed ultimate (failure) and preyielding surface for four different values of α is shown in Figure 3. Figures 3(a) and 3(b) express the triaxial compression and simple shear stress path, respectively, where all are assumed to be in an octahedral plane (*1–6*). The GA solutions for triaxial compression and simple shear parameters based on different values of α are given in Tables 6 and 7, respectively. Graphs of typical results are provided

TABLE 3 Ultimate Data for Plain Concrete (6)

Load Path	Spec.	σ_1 (ksi)	σ_2 (ksi)	σ_3 (ksi)	J_1 (ksi)	$\sqrt{J_{2D}}$ (ksi)
Conventional Triaxial Compression (CTC)	B_3	4.8977	0.3944	0.3944	5.6865	2.6000
	B_1	10.864	1.3944	1.3944	13.653	5.4675
	B_2	14.345	2.3944	2.3944	19.134	6.8999
	B_4	17.765	3.3944	3.3944	24.554	8.2971
Triaxial Compression	E_1	6.4144	0.3844	0.3844	7.1832	3.4814
	E_2	8.7944	0.6944	0.6944	10.183	4.6765
SS*	K_1	9.8144	4.8944	-0.0256	14.683	4.9200
Triaxial Extension (TE)	N_2	6.6923	6.6923	-0.2013	13.183	3.9800
	N_1	8.2694	8.2694	-0.356	16.183	4.9799
	N_3	9.7142	9.7142	-0.2451	19.183	5.7500
RTE**	R_1	7.8944	7.8944	4.9444	20.733	1.7032

1.0 psi = 6.89 KPa
* SS = Simple Shear and ** RTE = Reduced Triaxial Extension Compression is Positive.

TABLE 4 Ultimate Data for Soapstone (6)

Load Path	Spec.	σ_1 (ksi)	σ_2 (ksi)	σ_3 (ksi)	J_1 (ksi)	$\sqrt{J_{2D}}$ (ksi)
Conventional Triaxial Compression (CTC)	T_4	1.3533	0.1533	0.1533	1.6599	0.6928
	T_2	5.7143	1.1533	1.1533	8.0209	2.6333
	T_1	7.9873	2.1533	2.1533	12.294	3.3683
	T_3	10.578	3.1533	3.1533	16.885	4.2868
Triaxial Compression (TC)	S_3	4.4873	0.9863	0.9863	6.4599	2.0213
	S_1	6.3353	1.5623	1.5623	9.4599	2.7557
	S_2	7.5473	2.4563	2.4563	12.460	2.9393
Simple Shear (SS)	P_3	3.5623	2.1533	0.7453	6.4609	1.4085
	P_2	4.9293	3.1533	1.3773	9.4599	1.7760
	P_1	6.7013	4.1533	1.6063	12.461	2.5475
Triaxial Extension (TE)	M_3	2.8963	2.8963	0.6683	6.4609	1.2863
	M_2	4.1083	4.1083	1.2443	9.4609	1.6535
	M_1	5.4613	5.4613	1.5373	12.460	2.2655

1.0 psi = 6.89 KPa
Compression is Positive.

TABLE 5 Comparison of Material Parameters for Plain Concrete and Soapstone by Using Two Different Methods for Various Stress Paths (6)

		n	γ	β_0	β_1
Plain Concrete	Salami (6)	7.0	0.113	0.844	0.027
	GA	7.0	0.110	1.830	0.030
Soap-Stone	Salami (6)	7.0	0.047	0.749	0.047
	GA	7.0	0.050	1.460	0.060

in Figures 3 through 6, demonstrating that GA parameters provide a well-shaped curve that closely matches the given curves.

CONCLUSIONS

GA has been applied to find material parameters for a complex failure and constitutive model for concrete material. It also has been applied to find strength material parameters for frictional materials such as concrete, polymer concrete, rocks, and ceramics. Although under most circumstances a multiparameter, multiobjective function optimization problem would be considered a difficult task, GA could handle it successfully. Although the model used here to represent a constitutive model is a relatively simple one, the procedure described would be the same for complex models. Results of assorted runs agreed with experimental and single parameter optimization results. Of course, realistic failure and constitutive models would include many more parameters, but for GA that would only involve increasing the string length to incorporate the additional parameters. The ability of GA to handle a problem of that nature could make it a very important tool in the future of constitutive modeling for geological and engineering materials.

The correlation between the experimental results and analytical predictions was very good and provides a simple approach for developing tensile strength models, failure, and constitutive models for frictional materials.

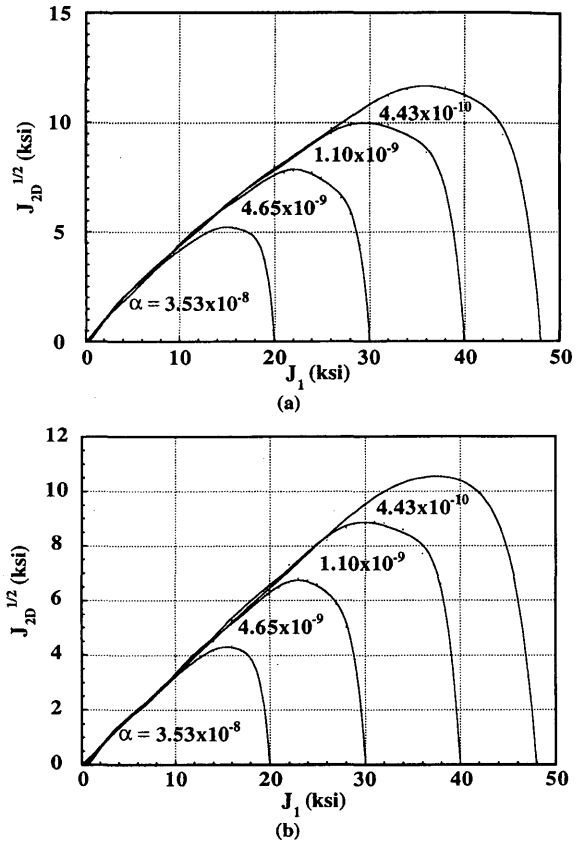

FIGURE 3 Observed ultimate (failure) and preyielding surface in $\sqrt{J_{2D}} - J_1$ plane for (a) triaxial compression test and (b) simple shear test. (1.0 psi = 6.89 kPa).

TABLE 6 Material Parameters for Plain Concrete for Triaxial Compression Tests by GA Method

TC	α	n	γ	β_0	β_1
Plain Concrete (Figure 3)	4.43e-10	7.04	0.13	0.56	0.03
	1.10e-09	7.09	0.15	0.56	0.07
	4.65e-09	7.09	0.15	0.56	0.05
	3.53e-08	7.12	0.16	0.56	0.10

TABLE 7 Material Parameters for Plain Concrete for Simple Shear Tests by Using GA Method

SS	α	n	γ	β_0	β_1
Plain Concrete (Figure 3)	4.43e-10	7.00	0.11	0.39	0.17
	1.10e-09	7.02	0.12	0.42	0.04
	4.65e-09	7.00	0.11	0.41	0.03
	3.53e-08	7.00	0.11	0.12	0.66

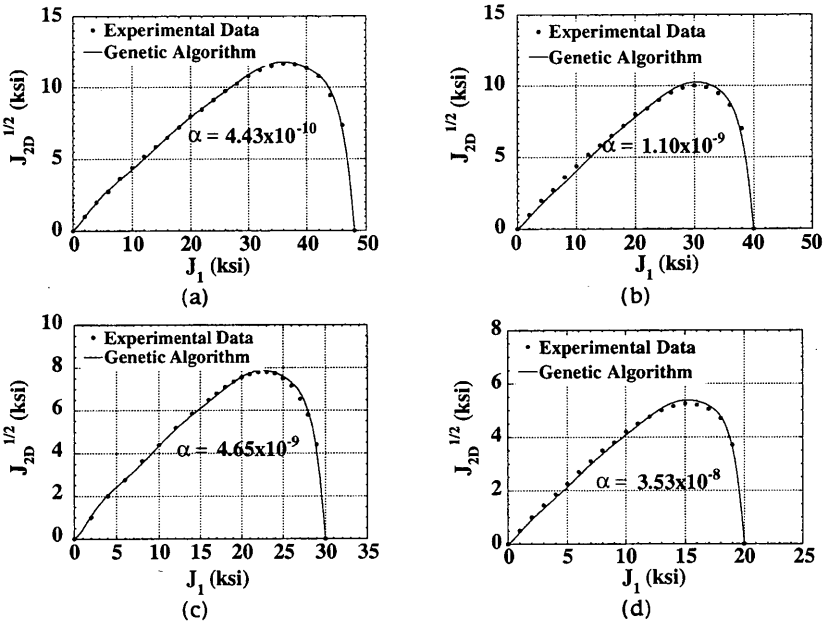

FIGURE 4 Comparison of predicted and experimental results in ultimate and preultimate envelopes in $\sqrt{J_{2D}} - J_1$ planes for triaxial compression test for various α for plain concrete. (1.0 psi = 6.89 kPa).

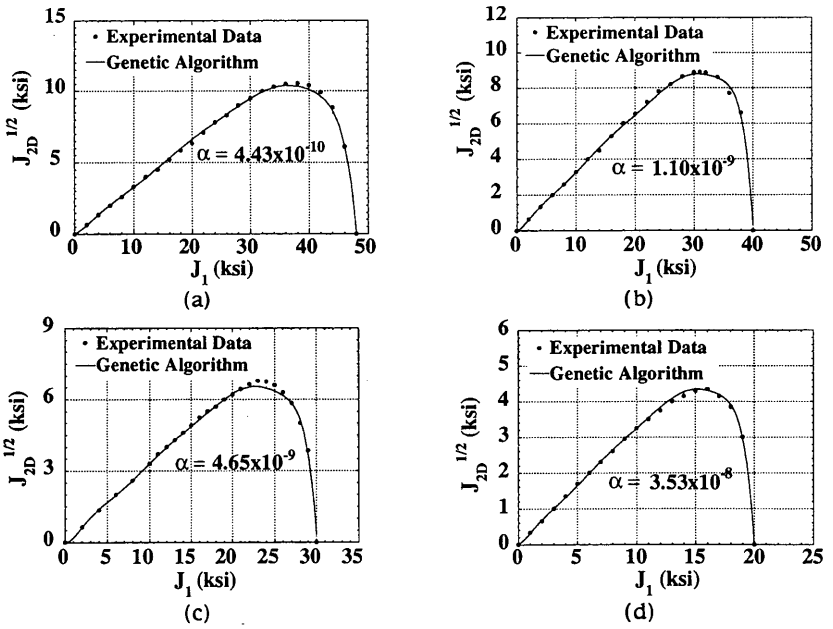

FIGURE 5 Comparison of predicted and experimental results in ultimate and preultimate envelopes in $\sqrt{J_{2D}} - J_1$ planes for simple shear test for various α for plain concrete. (1.0 psi = 6.89 kPa).

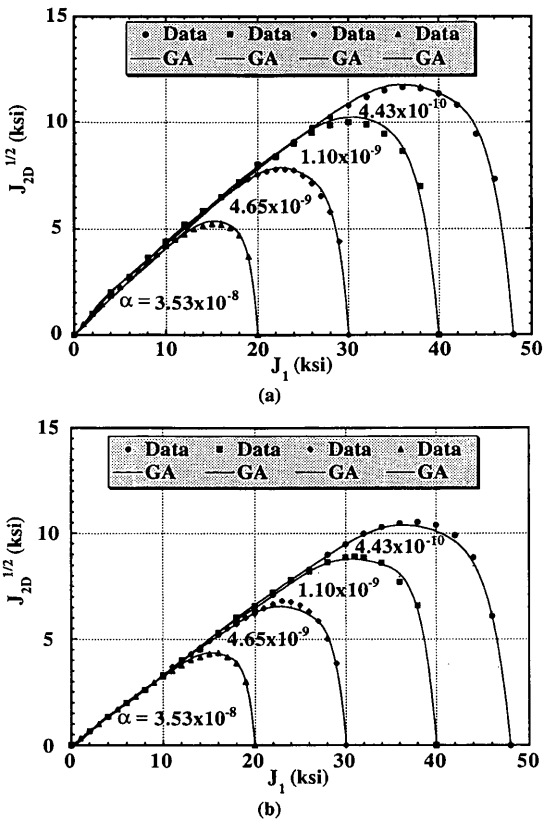

FIGURE 6 Comparison of predicted and experimental results in ultimate and preultimate envelopes in $\sqrt{J_{2D}} - J_1$ planes for (*a*) triaxial compression and (*b*) simple shear tests for various α for plain concrete. (1.0 psi = 6.89 kPa).

ACKNOWLEDGMENTS

The authors appreciate the support of the departments of Civil Engineering and Electrical Engineering at the North Carolina A&T State University. Their work was supported in part by the National Science Foundation, U.S. Department of Army, and AT&T Bell Laboratories.

REFERENCES

1. Salami, M. R. and S. Zhao. Three Dimensional Constitutive and Failure Modeling of Polymer Concrete Materials. Presented at 72nd Annual Meeting of the Transportation Research Board, Washington, D.C., 1993.
2. Salami, M. R. Constitutive Relations and Failure Model for Plain Concrete and Steel-Fiber-Reinforced Concrete. In *Transportation Research Record 1335,* TRB, National Research Council, Washington, D. C., 1992, pp. 40–43.
3. Salami, M. R. Mechanical Properties of Concrete. Presented at 71st Annual Meeting of the Transportation Research Board, Washington, D. C., 1992.
4. Salami, M. R. Failure Criterion for Frictional Materials. *Proc., 21st Midwestern Mechanics Conference,* Vol XV, Michigan Technological University, Houghton, Aug. 13–16, 1989, pp. 171–173.
5. Salami, M. R. and C. S. Desai. Constitutive Modeling (Stress-Strain Behavior) of Concrete Under Multiaxial Compressive Loading. *Proc., 2nd International Conference on Constitutive Laws for Engineering Materials,* Tucson, Ariz., Jan. 5–8, 1987, pp. 447–457.
6. Salami, M. R. Constitutive Modeling of Concrete and Rocks Under Multiaxial Compressive Loading. Ph.D. dissertation. Department of Civil Engineering and Engineering Mechanics, University of Arizona, Tucson, 1986.
7. Salami, M. R. Analytical Expressions for Uniaxial Tensile Strength of Concrete in Terms of Uniaxial Compressive Strength. In *Transportation Research Record 1335,* TRB, National Research Council, Washington, D. C., 1992, pp. 52–54.
8. Salami, M. R., Gary Spring, and Shilong Zhao. Coarse-Aggregate Effect on Mechanical Properties of Plain Concrete. In *Transportation Research Record 1382,* TRB, National Research Council, Washington, D. C., 1993, pp. 46–50.
9. Desai, C. S., and M. O. Faruque. A Constitutive Model for Geological Materials. *J. Eng. Mech. Div.*, Vol. 110, No. 9, ASCE, Sept. 1984, pp. 1391–1408.
10. Desai, C. S., G. N. Frantziskonis, and S. Somasundram. Constitutive Modeling for Geological Materials. *Proc., 5th International Conference on Numerical Methods in Geomechanics*, Nagoya, Japan, April 1985.
11. Desai, C. S., and M. R. Salami. Constitutive Model Including Testing for Soft Rock. *Int. J. Rock Mech. and Min. Sc.,* Vol. 24, No. 5, Oct. 1987, pp. 299–307.
12. Desai, C. S., and M. R. Salami. A Constitutive Model for Rocks. *International Journal of the Geotechnical Engineering Division,* Vol. 113, No. 5, ASCE, New York, May 1987, pp. 407–423.
13. Shah, S. P., and S. H. Ahmad. Structural Properties of High Strength Concrete and Its Implications for Precast Prestresses Concrete. *Journal Prestressed Concrete Institute,* Vol. 30, No. 6, Nov./Dec. 1985, pp. 92–119.
14. Salami, M. R., and C. S. Desai. A Constitutive Model for Plain Concrete. *Proc., 2nd International Conference on Constitutive Laws for Engineering Materials: Theory and Application,* Vol. I, Tucson, Jan. 5–8, 1987, pp. 447–455.
15. Egging, D. E. Constitutive Relations of Randomly Oriented Steel Fiber Reinforced Concrete Under Multiaxial Compression Loadings. M. S. thesis. University of Colorado, 1982.
16. Lade, P. V. Three-Parameter Failure Criterion for Concrete. *Journal of the Engineering Mechanics Division,* Vol. 108, No. EM5, ASCE, Oct. 1982.
17. Holland, J. H. *Adaptation in Natural and Artificial Systems.* University of Michigan Press, Ann Arbor, 1975.
18. Goldberg, D. E. Genetic Algorithms and Walsh Functions. Part I, *A Gentle Introduction, Complex Systems*, Vol. 3, 1989, pp. 129–152.
19. Goldberg, D. E. *Genetic Algorithms in Search, Optimization, and Machine Learning.* Addison Wesley Publishing Co., Reading, Mass., 1989.
20. Grefenstette, J. J., and J. M. Fitzpatrick. Genetic Search with Approximate Function Evaluations. (J. J. Grefenstette, ed.) *Proc., International Conference on Genetic Algorithms and their Applications,* 1985.
21. Axelrod, R. The Evolution of Strategies in the Iterated Prisoner's Dilemma. (L. Davis, ed.) *Genetic Algorithms and Simulated Annealing,* Pitman, London, and Morgan Kaufmann, Inc., 1987.
22. Homaifar, A., S. Guan, and G. Liepins. A New Approach for the Solution of TSP. *Proc., 5th International Conference*, Morgan Kaufmann, San Mateo, Calif., 1993.
23. Goldberg, D. E. *Computer-Aided Gas Pipeline Operation Using Genetic Algorithms and Rule Learning.* Ph.D. dissertation. College of Engineering, University of Alabama, Tuscaloosa, 1983.
24. Davis, L., and S. Coombs. Optimizing Network Link Sizes with Genetic Algorithms. Conference on Computer Simulation and Modeling, Tucson, Ariz. 1987.

Publication of this paper sponsored by Committee on Mechanical Properties of Concrete.

Influence of Loading Type, Specimen Size, and Fiber Content on Flexural Toughness of Fiber-Reinforced Concrete

V. RAMAKRISHNAN AND SATYA S. YALAMANCHI

Results of an experimental investigation to determine the influence of specimen size, fiber type, and fiber content on the flexural behavior of steel fiber-reinforced concrete are presented. Two fiber types and four mixes are investigated. With four series in each mix, there are sixteen series. The effect of the two cross-sectional sizes of 150 × 150 mm and 100 × 100 mm (6 in. × 6 in. and 4 in. × 4 in.) on flexural strength is also studied. Hardened concrete is tested for pulse velocity and flexure. For each series, two specimens are tested for monotonic, and one specimen for cyclic, loading. Loading and unloading rates were the same for both monotonic and cyclic loading. In addition to the load deflection measurements, the crack mouth opening displacements versus load are recorded in the case of notched specimens. Load deformation behavior, post crack load drop phenomenon, and toughness for two types of fibers are evaluated and compared. There is evidence of scatter of results related to the difficulty in achieving a uniform distribution of randomly oriented fibers. The flexural toughness factor, recommended by the Japan Society of Civil Engineers is calculated. A comparison of load deflection curves under monotonic and cyclic loading indicates that the fibers primarily influence the envelope curve and that cyclic loading does not have any appreciable influence on the energy absorption characteristics. The load versus crack mouth opening displacement behavior is similar to the load deflection curve for notched specimens.

Research (*1–16*) has established that the addition of fibers considerably improves the static flexural strength, impact strength, direct tensile strength, fatigue strength, ductility, and flexural toughness of concrete. However, the degree of improvement in such parameters depends on many factors, including size, type, and aspect ratio of fibers. Because fiber-reinforced concrete (FRC), in many applications, is subjected primarily to bending instead of axial loading, performance in flexure is most important. However, lack of sufficient information on fracture toughness and flexural behavior of concretes subjected to static and cyclic loadings with different types and quantities of fibers underscores the need for more research. Such information is essential to design engineers who use FRC in airfield and highway pavements, industrial floors, tunnel linings, and earthquake- and impact-resisting structures.

RESEARCH SIGNIFICANCE

Toughness, a measure of the energy absorption capacity, is used to characterize the FRC's ability to resist fracture when subjected to static, dynamic, and impact loads. Energy absorbed by a specimen is computed using the area under the complete load deflection curve. However, the load deflection curve is observed to be dependent upon the specimen size, the loading configuration, the type of control, and the loading type. The load deflection curve also can be used for determining the modulus of elasticity, first crack strength, and the flexural strength of the composite. Governing the level of these influences are composition parameters, such as the type of fiber, volume content, and aspect ratio of fibrous reinforcement. Currently available test standards for the evaluation of fracture toughness indices, ASTM C1018, Japanese Concrete Institute (JCI) SF4 (17), Japan Society of Civil Engineers (JSCE) SF5 (18), and American Concrete Institute (ACI) 544 (*19,20*), recognize these influences. The research reported in this paper deals with the systematic study of the effects of commonly used fibers on the flexural properties of composites, the volume content, aspect ratio, specimen size, loading system, and test configuration (for notched and unnotched specimens).

EXPERIMENTAL PROGRAM

Two fiber types were selected for the study, the 50.8-mm (2-in.) long hooked-end steel and 50.8-mm (2-in.) long crimped steel fibers. Two volume percentages, 0.5 and 1.0 percent, were investigated for both types of fibers. Two specimen configurations were selected, notched and unnotched. Table 1 provides the mix designations and fresh concrete properties used for different specimens. Four specimens for each series were made. Specimens were cast as large slabs and sawed to size (for flexure tests) to minimize the edge effect. In the case of notched specimens, notch depths for large and small specimens were approximately 18.7 mm (0.75 in.) and 12.5 mm (0.50 in.), respectively. After casting, the slabs were covered with plastic sheets for 24 hr at room temperature. Specimens were then cured in a curing room before being sawed to size and wrapped. Each specimen was wrapped individually in a plastic sheet and was labeled. The specimens remained covered until 1 hr before testing. All mixes were designed for an approximate compressive strength of 34.45 MPa (5000 psi) to 41.34 MPa (6000 psi). All beams were tested for pulse velocity (ASTM C597) at the age of 2 to 3 months.

Beams were tested at the age of 2 to 3 months, as per ASTM C1018, for static flexural strength under third-point loading. For static tests, a dial gauge with an accuracy of 0.0025 mm (0.0001 in.) was used to measure the midspan deflection. The gauge was located at the mid-width point of the specimen to minimize the effect of twisting on the deflection measurements. The rate of loading was maintained in the range .05 mm/min to .1 mm/min (0.002 in./min to 0.004 in./min), as per ASTM C1018. The loads were recorded for every increment of .005-mm (0.0002-in.) deflection until the first crack appeared, and at different intervals thereafter. Specimens

South Dakota School of Mines and Technology, 501 E. St. Joseph Street, Rapid City S.D., 57701,

TABLE 1 Mix Designations and Fresh Concrete Properties

Mix #	Unnotched/ Notched	Specimen Size (mm)	Fiber Type	Fiber Content	Slump (mm)	Unit Weight (kg/m³)	Air Content (%)
A1LU	Unnotched	150x150x525	Hooked-end	0.5	14	2198.7	7.0
A2LU	Unnotched	150x150x525	Hooked-end	1.0	9	2205.1	7.0
A1SU	Unnotched	100x100x350	Hooked-end	0.5	14	2198.7	7.0
A2SU	Unnotched	100x100x350	Hooked-end	1.0	9	2205.1	7.0
B1LU	Unnotched	150x150x525	Crimped	0.5	9	2243.5	5.0
B2LU	Unnotched	150x150x525	Crimped	1.0	8	2240.3	6.5
B1SU	Unnotched	100x100x350	Crimped	0.5	9	2243.5	5.0
B2SU	Unnotched	100x100x350	Crimped	1.0	8	2240.3	6.5
A1LN	Notched	150x150x525	Hooked-end	0.5	14	2198.7	7.0
A2LN	Notched	150x150x525	Hooked-end	1.0	9	2205.7	7.0
A1SN	Notched	100x100x350	Hooked-end	0.5	14	2198.7	7.0
A2SN	Notched	100x100x350	Hooked-end	1.0	9	2205.7	7.0
B1LN	Notched	150x150x525	Crimped	0.5	9	2243.5	5.0
B2LN	Notched	150x150x525	Crimped	1.0	8	2240.3	6.5
B1SN	Notched	100x100x350	Crimped	0.5	9	2243.5	5.0
B2SN	Notched	100x100x350	Crimped	1.0	8	2240.3	6.5

were loaded up to a minimum midpoint deflection of 1/150 of the span, which allowed for computation of ACI, ASTM, and JCI and JSCE fracture toughness indices. In addition to load deflection measurements, the load versus crack-mouth opening displacement readings were measured for notched specimens (ASTM E399). Notched and unnotched specimens were also tested under cyclic loading. Loading and unloading was done at 2, 3, 5.5 and 15.5 times the first crack deflection, using the same unloading/reloading rate as was used for monotonic loading.

TEST RESULTS AND DISCUSSION

Static Flexural Strength

Results of a comparison of the static flexural strengths for unnotched and notched beams are shown in Figure 1. There was a significant fracture strength increase as the fiber content increased from 0.5 to 1.0 percent, in the case of the hooked end fibers, and a much lower increase for the concrete with crimped fibers. The

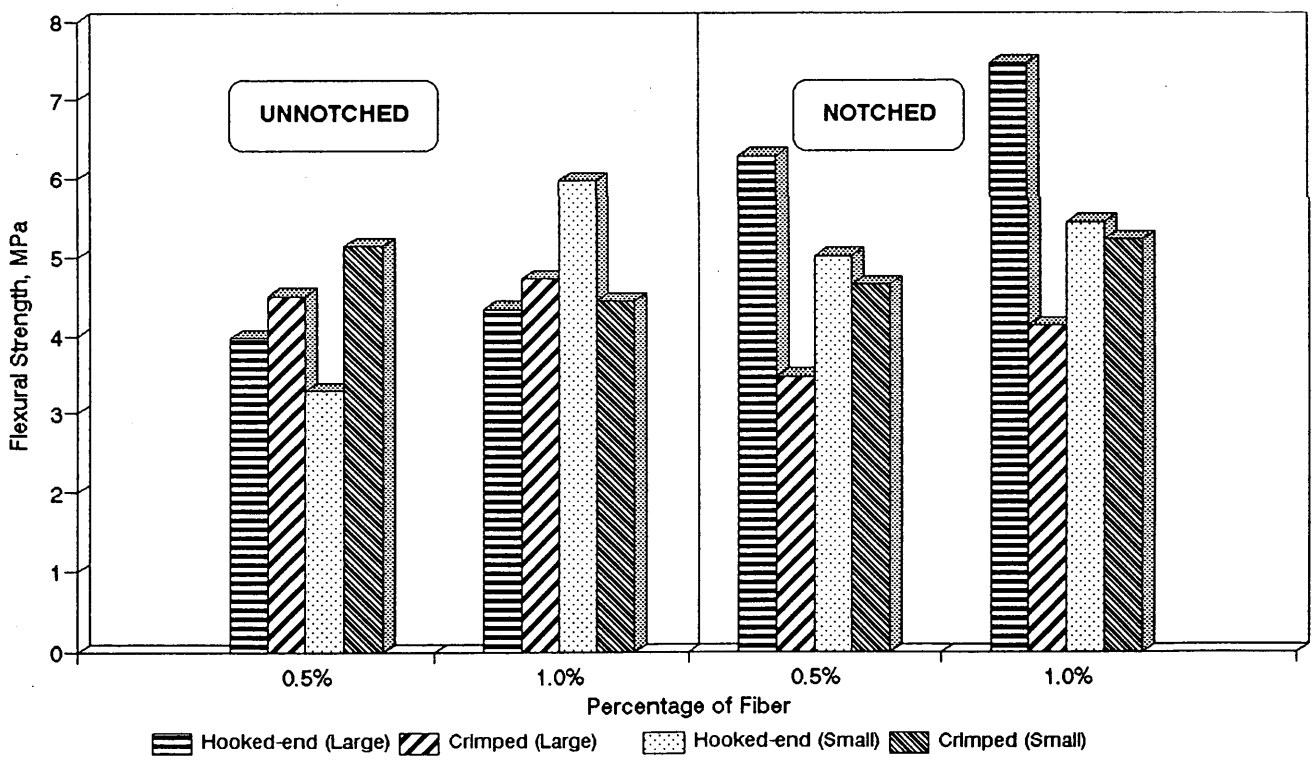

FIGURE 1 Flexural strength versus percentage of fiber.

percentage increases were 74 and 38 percent, respectively, for small and large specimens for hooked fibers. There was no particular trend observed with respect to the size of the beams for both types of fibers, because the distribution of the fibers in the critical tension zone of the beams varied greatly. Flexural strength was more significantly dependent on the actual number of fibers found in the tension block than on the size of the cross section. However, when fiber distribution was fairly uniform, the larger sized specimens had lower flexural strengths.

Flexural Load Deflection Curves

Total area under the load deflection curve is indicative of the energy absorbed by the beam. Load deflection curves were drawn using data from the static flexure test. Load deflection curves for both types of fibers were compared by volume, for 0.5 and 1.0 percent of fiber contents, for both specimen sizes (*21*). Comparison of the static load-deflection curves for FRC with 0.5 and 1.0 percent fiber volumes indicated that the initial elastic part of the curves did not change appreciably. However, the post-crack plastic behavior improved significantly with an increase in fiber content from 0.5 to 1.0 percent. Ultimate loads also increased with an increase in fiber content. An increase in the fracture energy resulted from a greater number of fibers bridging the cracks in FRC with higher fiber content. However, the increase in fracture energy depended greatly on the type of fiber, particularly on the bond and anchorage developed by the geometry of the fiber. Hooked-end fibers had better anchorage and bond than the crimped fibers. Hence, the ultimate loads and the total fracture energy were considerably higher for FRC with hooked-end fibers.

Post-Crack Load Drop Phenomenon

Post-crack load drop is defined as the difference between maximum load and load recorded at a deflection equal to three times the deflection measured at first crack (*2*). Post-crack load drop was less with an increase in fiber content. Typical load drops expressed as a percentage of maximum loads are 20, 10, and 18 and 15 percent for small specimens with 0.5 and 1.0 percent crimped and hooked-end fibers, respectively. Similarly, the load drops were 15, 9, and 21 percent and 3 percent for large specimens with 0.5 and 1.0 percent hooked-end and crimped fibers.

Fracture Toughness and Toughness Indexes

One major objective for adding fibers to concrete is to increase fracture toughness. Various fiber efficiencies can be evaluated by comparing their ability to increase the fracture toughness of concretes. Fracture toughness is a measure of the energy absorption capacity to resist failure when subjected to a flexural load. Tests for the measurement of fracture toughness and toughness indices are recommended by ASTM, JCI (*17*), and ACI (*19,20*). The tests are included in the specifications for FRC to ensure a minimum performance standard when used in construction.

Toughness index, as proposed by ASTM C1018, is a dimensionless parameter that defines or fingerprints the shape of the load-deflection curve. Indexes have been defined on the basis of three service loads, identified as multiples of the first-crack deflection. The index is computed by dividing the total area under the load-deflection curve up to the given service level deflection, by the area under the same curve up to the first-crack deflection. Toughness index I_5 is calculated for a defection of three times the first crack deflection. Likewise I_{10} and I_{30} are the indices up to 5.5 and 15.5 times the first-crack deflection, respectively. First-crack toughness is expressed as the energy absorbed by the standard beam, and it is given by the area of the load-deflection curve up to the first-crack load. Calculated toughness indexes I_5, I_{10}, and I_{30} and first-crack toughness values are presented in Table 2. Results of a comparison of the first-crack toughness values for unnotched and notched beams are provided in Figure 2. Results of a comparison of the toughness indexes I_5, I_{10}, and I_{30} are presented in Figure 3 for unnotched and in Figure 4 for notched beams.

Compared with plain concrete, for which the toughness index is one, FRC had significantly greater toughness, and slightly higher first-crack strength. The increase depended on the type and quantity of fibers added. Toughness increased with the number of fibers, both hooked-end and crimped. Hooked-end fiber–reinforced concrete had higher toughness indexes when it was compared to con-

TABLE 2 Fracture Toughness (ASTM C1018 and JCI SF4)

Mix #	Flexural Strength, MPa	First Crack Toughness, MPa	ASTM C1018					JCI SF4 Fe MPa
			I5	I10	I30	I10/I5	I30/I10	
A1LU	3.97	0.59	6.18	11.87	33.21	1.91	2.85	3.32
A2LU	4.34	1.00	4.48	8.96	27.06	1.74	3.01	3.11
A1SU	3.29	0.28	4.18	8.82	24.89	2.09	2.83	2.69
A2SU	5.96	0.28	5.07	10.51	33.75	2.06	3.24	5.51
B1LU	4.50	1.57	4.33	7.84	20.54	1.81	2.61	1.97
B2LU	4.72	0.71	5.12	10.39	30.79	2.01	2.96	3.05
B1SU	5.13	0.28	4.78	10.00	24.14	2.10	2.41	2.42
B2SU	4.43	0.23	4.80	9.61	26.95	2.00	2.79	3.10
A1LN	6.29	0.85	5.06	10.62	33.19	2.09	3.12	3.76
A2LN	4.47	0.77	5.58	11.08	34.99	2.07	3.00	3.43
A1SN	5.02	0.16	5.76	12.29	39.09	2.13	3.17	3.22
A2SN	5.44	0.20	4.65	9.19	30.02	1.97	3.27	2.57
B1LN	3.48	0.41	4.18	7.72	20.93	1.84	2.69	1.67
B2LN	4.12	0.63	4.61	8.86	30.18	1.95	3.38	2.32
B1SN	4.66	0.15	4.68	9.36	28.22	1.98	2.95	2.64
B2SN	5.22	0.20	4.58	9.40	28.74	2.04	3.05	3.02

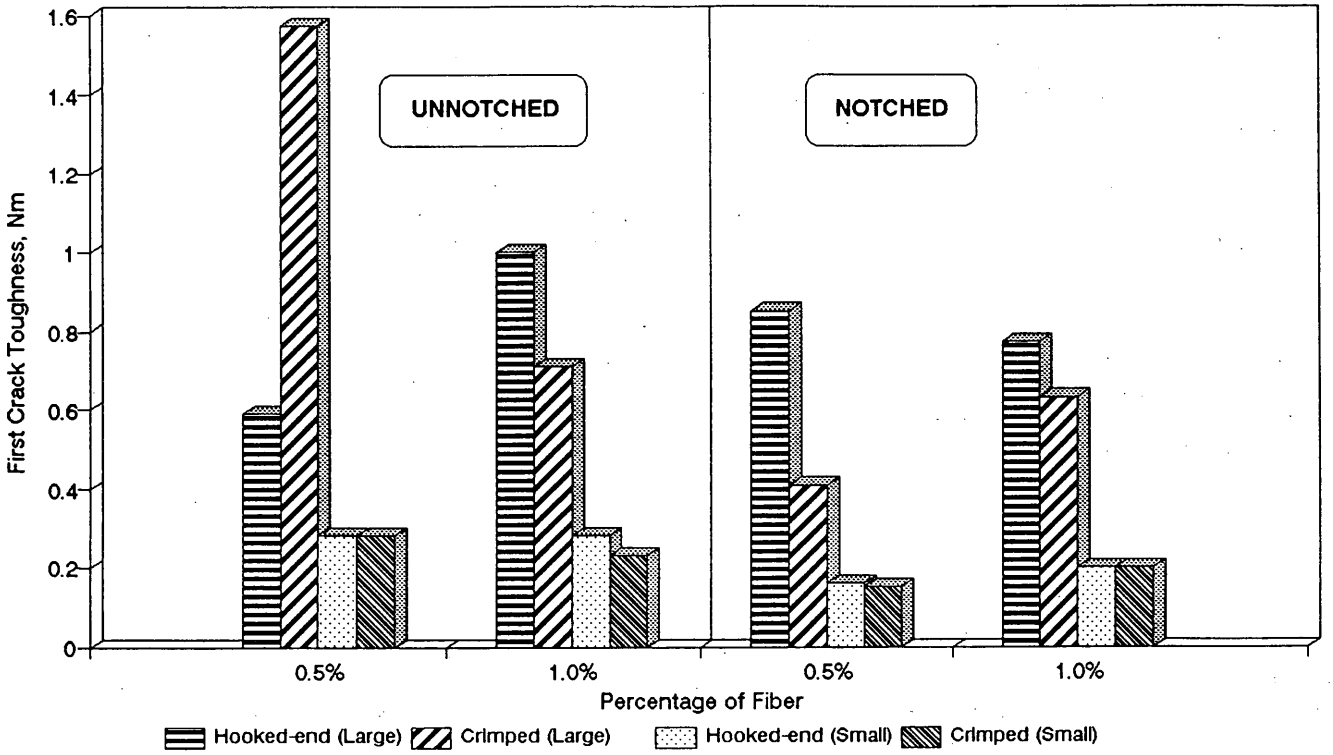

FIGURE 2 First-crack toughness versus percentage of fiber.

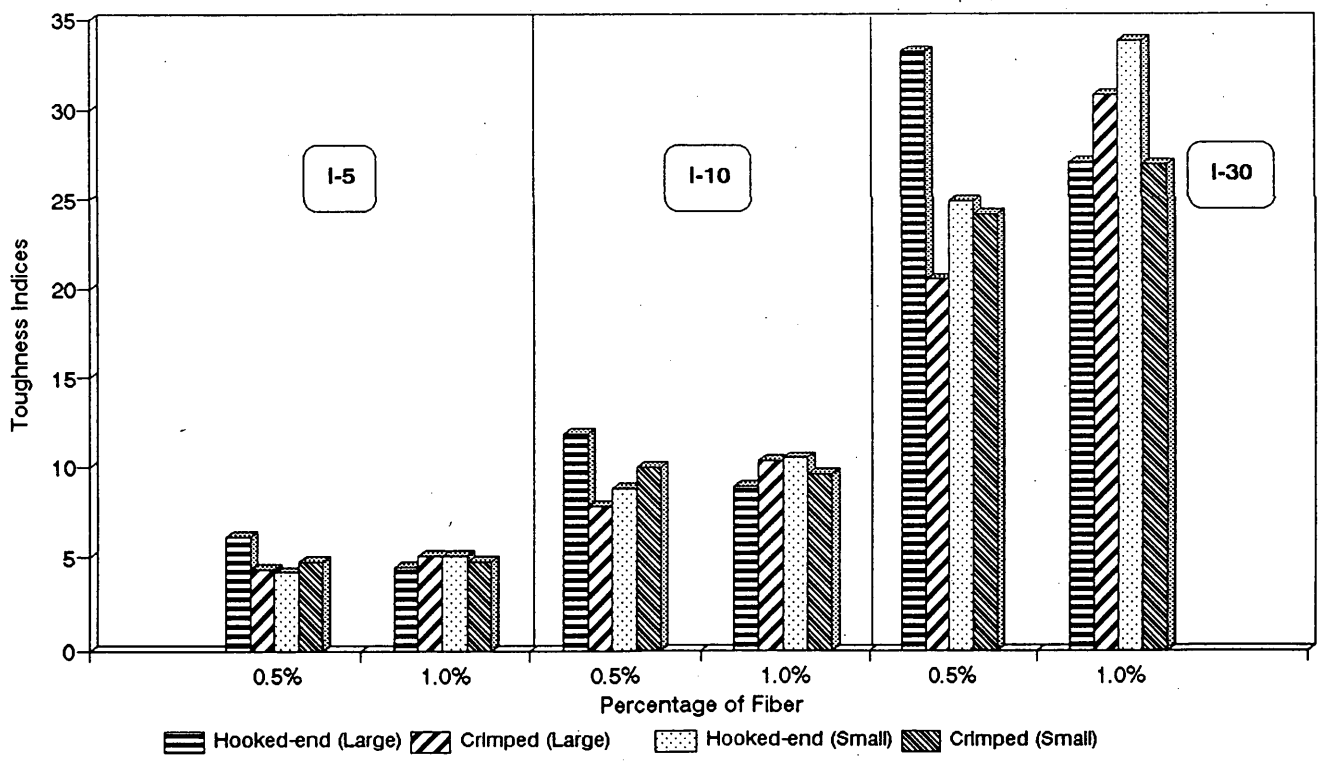

FIGURE 3 Toughness indexes versus percentage of fiber for unnotched specimens.

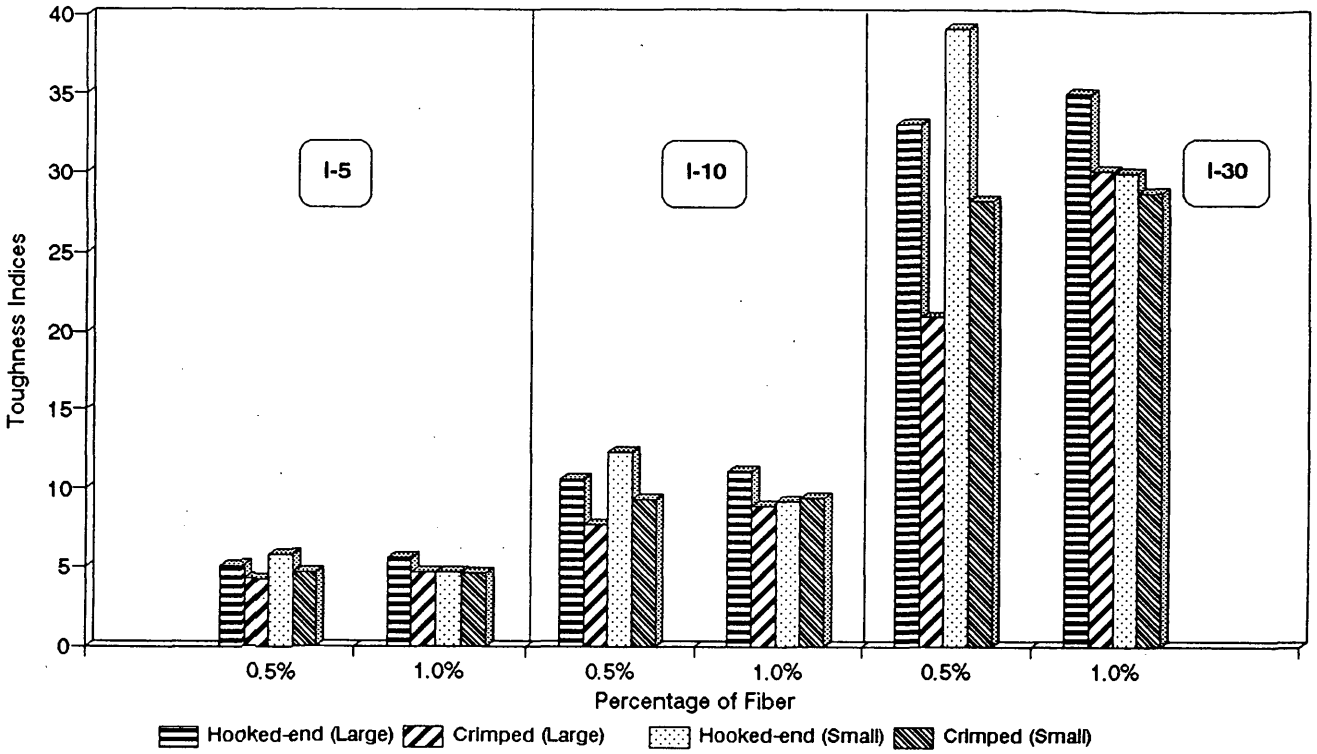

FIGURE 4 Toughness indexes versus percentage of fiber for notched specimens.

crete with an equal quantity of crimped fibers. Better anchorage and bond provided by the hooked-end fibers contributed to the increase in toughness. The influence of the size of the specimens was not clearly indicated because of the inevitable variability in the fiber distribution.

The ratios, I_{10}/I_5 and I_{30}/I_{10} were calculated and are presented in Table 2. The ratios, good indicators of post-crack plastic behavior of the specimens, have values equal to 2 and 3 for I_{10}/I_5 and I_{30}/I_{10}, respectively, and show perfect plastic behavior. Hooked-end fiber reinforced concrete demonstrated almost perfect plastic behavior after the first crack and up to 15.5 times the first crack deflection, because the ratios I_{10}/I_5 and I_{30}/I_{10} are close to two and three.

FRC with crimped fibers showed a decline in the load carrying capacity after a deflection of 5.5 times the first crack deflection. The I_{30}/I_{10} were less than three. The difference in behavior may be attributed to the fiber efficiency.

The most important variable governing the toughness index of steel fiber–reinforced concrete SFRC is the fiber efficiency. Other factors that influence the toughness index are the position of crack, fiber content, and distribution of the fibers. Fiber efficiency is controlled by the resistance of fibers to pull out from the matrix that is developed as a result of bond strength at the fiber-matrix interface. Because the pull out resistance increases with increased fiber length, the longer the fiber the more it improves the properties of composites. Also, because the pull out resistance is proportional to interfacial surface area, nonround fiber cross sections and small diameter round fibers offer more pull out resistance per unit volume than do larger diameter round fibers, because they have more surface area per unit volume.

Hence, a high ratio of length to diameter is associated with fiber efficiency. On that basis, it would appear that fibers should have an aspect ratio high enough to ensure that their tensile strength is approached as a composite fails. Unfortunately, that is not practical. Many investigations indicate that use of fibers with an aspect ratio higher than 100 causes inadequate workability, FRC with nonuniform distribution of fiber, or both (*9*).

In this investigation, the aspect ratio used was 100, and 40 to 65 for type A and B fibers, respectively. Failure of the composites usually was governed by the fiber pull out. The advantage of the pull out type of failure is that it is gradual and ductile compared with a more rapid and possibly catastrophic failure, which can occur if fibers are brittle and break under tension, with little or no elongation. Fiber pull out or fiber fracture depends on the yield strength of the fibers, and the bond and the anchorage between the matrix and the fiber.

Flexural Toughness Factor

The JCI (*17*) and JSCE (*18*) methods for calculating fracture toughness are identical. Toughness is defined in absolute terms as the energy required to deflect the FRC beam at a midspan of 1/150 of the span, δtb. The flexural toughness factor Fe, which is taken as the average flexural strength, is given by the following equation:

$$Fe = Tb \times l/\delta tb \times b \times h^2$$

where

Fe = flexural toughness factor,
Tb = flexural toughness,
δtb = deflection of 1/150 of the span,
l = span,
b = width of failed cross section, and
h = height of failed cross section.

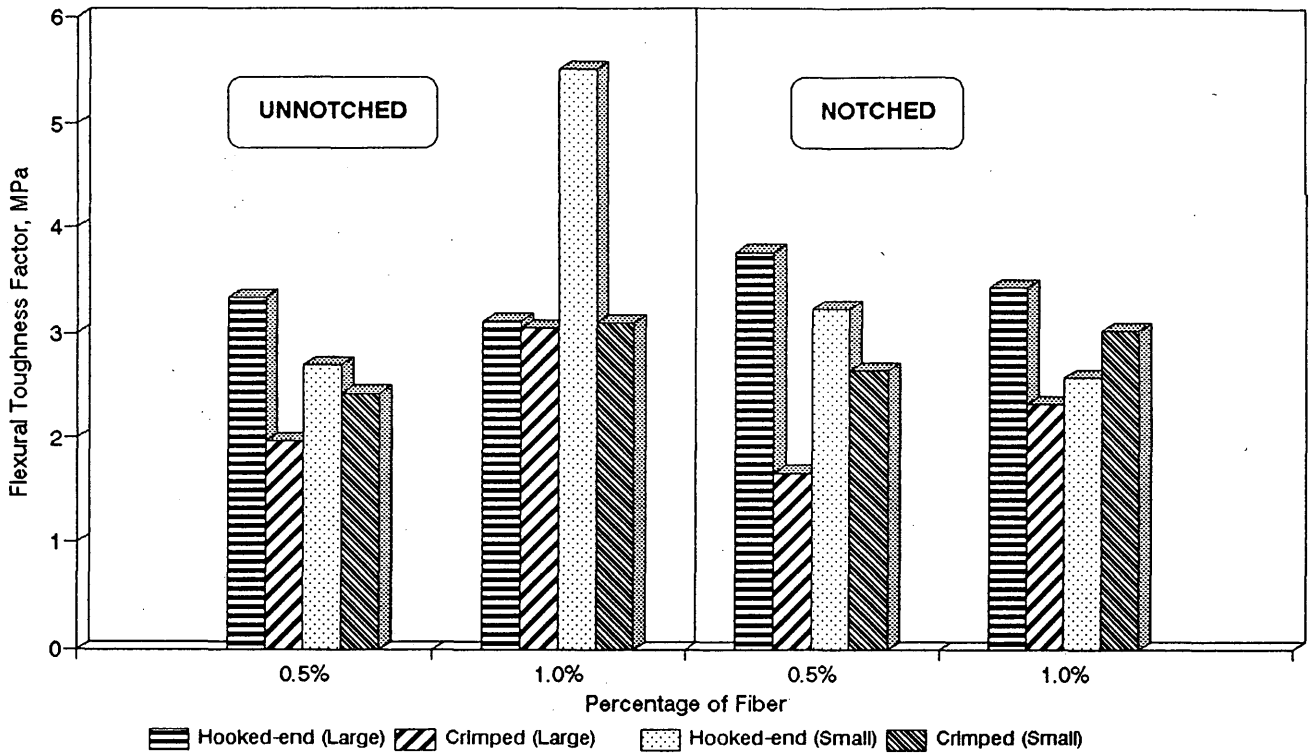

FIGURE 5 Flexural toughness factor versus percentage of fiber.

The flexural toughness factor values are provided in Table 2, and Figure 5 presents comparative results for unnotched and notched beams. The flexural toughness factor had increased as the percentage of the fibers increased, in both types of fibers, except for the large specimens with Type A fiber. Flexural toughness values increased 50 percent for small specimens with Type A fiber, as the percentage of fiber increased from 0.5 to 1.0 percent Similarly, the percentage increases were 20 and 35 percent for small and large specimens with Type B fiber. A detailed analysis presented elsewhere (*21*) indicated that notches in the beams do not influence toughness indexes (ASTM) and flexural toughness factors (JCI).

Cyclic Loading

The ability of structures to resist dynamic loading, such as earthquake loading, depends on the fracture toughness of the material. SFRC with higher fracture toughness and a very high post-crack energy absorption capacity before collapse is a suitable material for the construction of earthquake-resisting structures. The behavior of SFRC and its fracture toughness when subjected to cyclic loading were determined.

Load-deflection curves and complete analysis of results are presented elsewhere (*21*). A typical load-deflection curve obtained in cyclic loading test superimposed by a load-deflection curve obtained under monotonic load for the same SFRC with unnotched beams is shown in Figure 6; the same comparison for notched specimens is shown in Figure 7.

Curves under cyclic loading followed closely the curves for monotonic loading, indicating that the behavior of FRC under cyclic loading can be predicted from the monotonic load curve. Total energy absorbed for collapse appeared to be nearly the same for both loading cases. However, growth of permanent strain and decay in elastic modulus were observed after every cycle, when the loading was higher than the first-crack load. There was not any discernible difference in the behavior of beams with and without notches when subjected to either cyclic loading or monotonic loading.

Crack Mouth Opening Displacement

In addition to the load deformation characteristics, crack mouth opening displacement (CMOD) versus load was recorded under monotonic and as well cyclic loading for notched specimens. A typical load versus CMOD curve is shown in Figure 8. A similar type of behavior was observed for the load versus CMOD curves under both monotonic and cyclic loading. The CMOD was linear, until a crack appeared, then it became nonlinear. The load-CMOD curves and the load-deflection curves were similar for monotonic and cyclic loading.

CONCLUSIONS

- Fracture toughness, as measured by ASTM- and JCI-recommended test procedures, increases significantly with the addition of steel fibers in concrete. With an increase in fiber content, the fracture toughness increases. The degree of increase depends on the type and quantity of fibers added. The hooked-end SFRC had greater toughness than the SFRC with crimped fiber, with an equal quantity of fibers in both. The higher the FRC's fiber content, the lower its corresponding post-crack load drop.

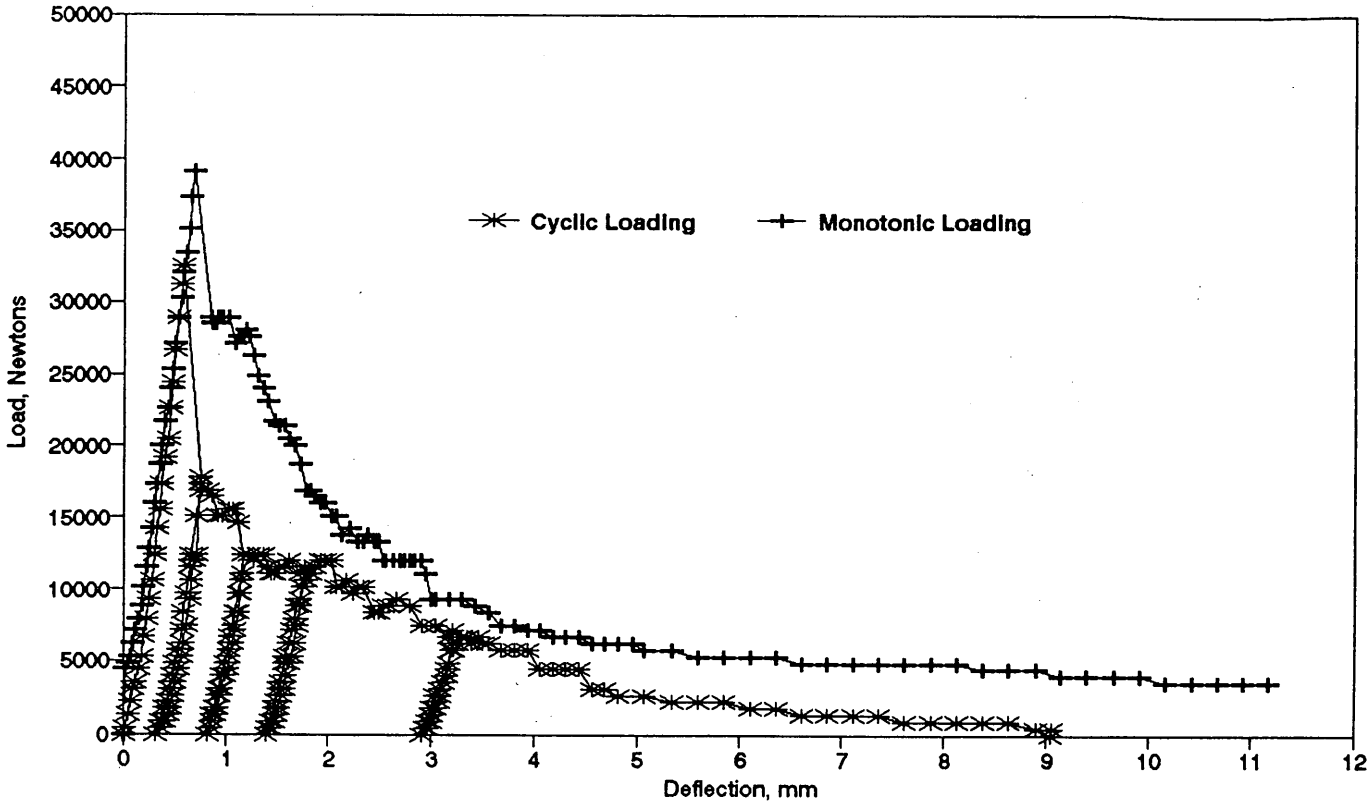

FIGURE 6 Load deflection curves for cyclic and monotonic loading for unnotched specimens.

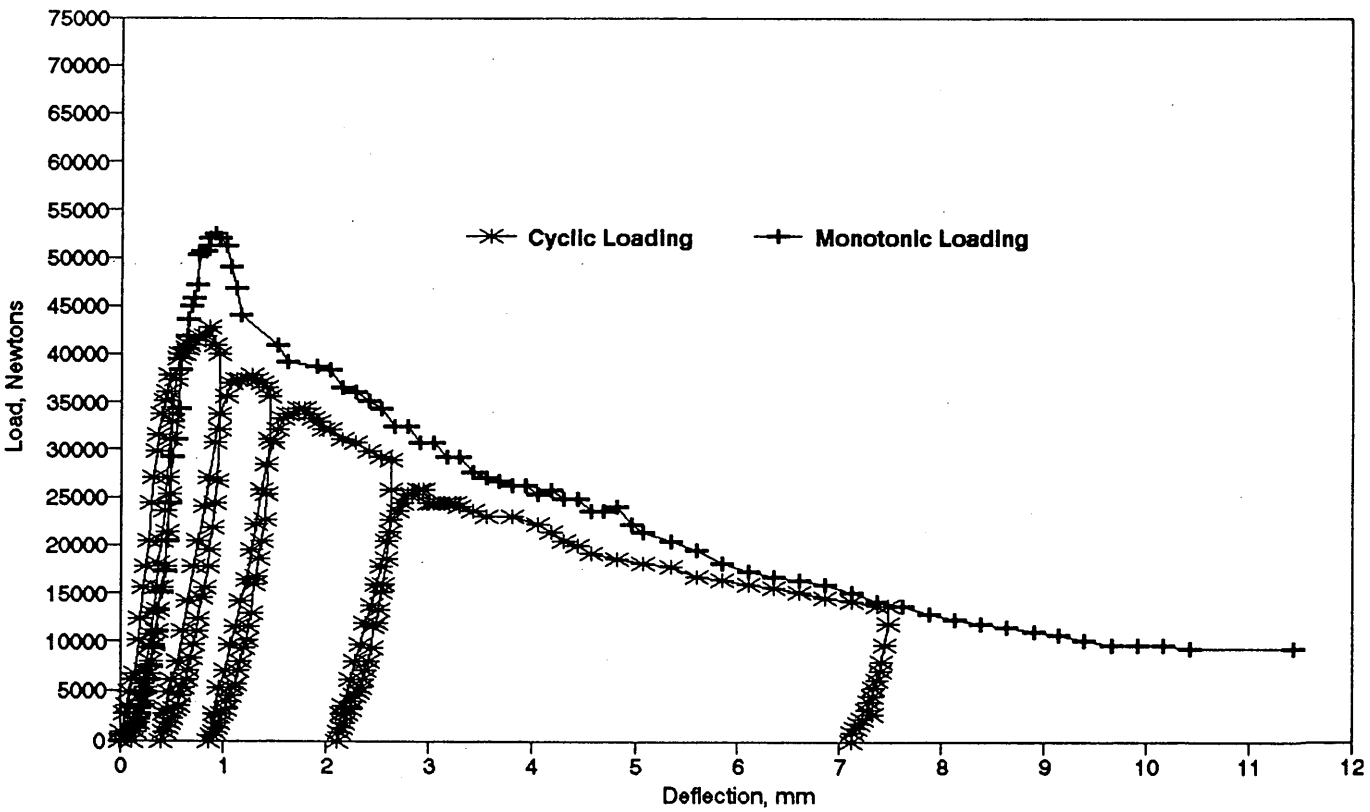

FIGURE 7 Load deflection curves for cyclic and monotonic loading for notched specimens.

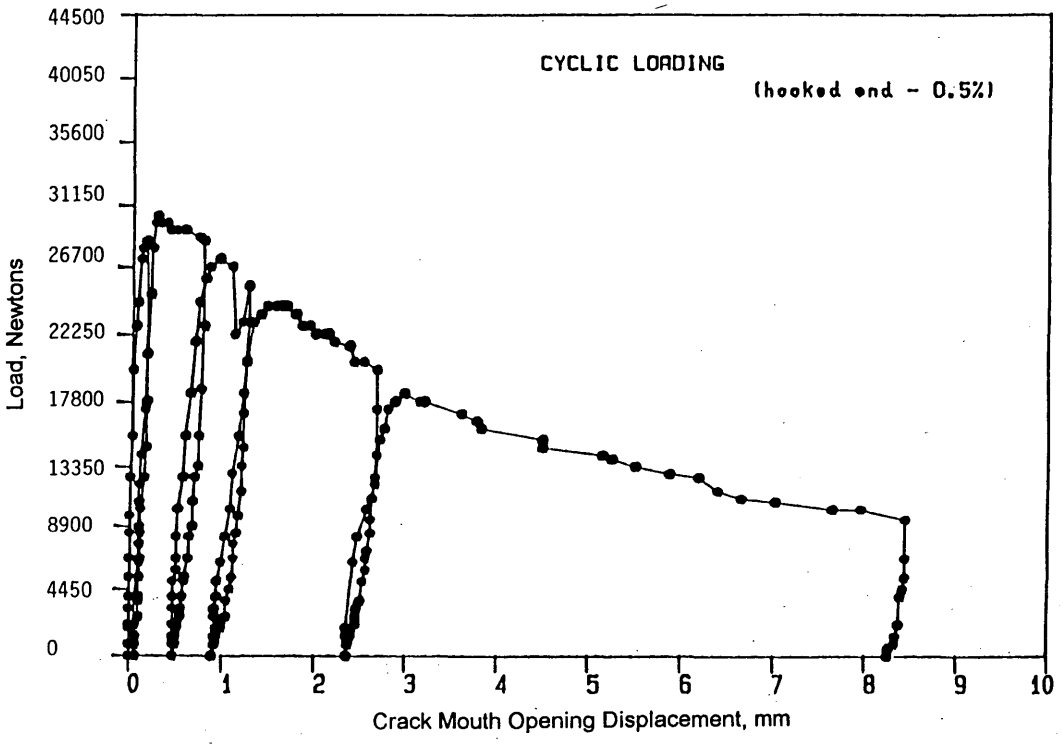

FIGURE 8 Load versus CMOD curve for Beam A1LN-3.

- Significant scatter in the toughness and flexural properties calculated for SFRC is unavoidable because of the inevitable nonuniform distribution of the randomly oriented fibers, particularly in the critical tension zone, both in the laboratory-cast specimens and in concrete in the field.
- In comparing the load-deflection behavior and the flexural properties of FRC specimens subjected to monotonic or cyclic loading, the notch in the specimen did not have any influence on the toughness, other flexural properties, or the behavior of FRC. For the notch-depth/beam-depth ratio used (1:8), the FRC was not notch-sensitive.
- In general, specimen size had an influence on the fracture toughness and the mechanical parameters monitored. The stress at first crack and the ultimate strength were less for the larger specimen size. However, the ultimate strength was more size-dependent than the stress at first crack. Energy absorbed per unit net cross-sectional area, and the initial elastic modulus calculated from the load deflection curves, were both independent of size. For SFRC with hooked-end fibers, the variability of the fiber distribution at the critical section had a much greater influence than specimen size. Therefore, for hooked-end SFRC, the results should be interpreted with caution.
- There was no change in the elastic wave transmission properties of the concrete due to the addition of fibers, as indicated by measured pulse velocities.
- Fracture toughness indexes (I_5, I_{10}, and I_{30}), calculated using ASTM C1018, are not very sensitive to the fiber type, fiber content, or specimen size. The test recommended by the JCI (SF4) is relatively more sensitive to the fiber type and content, and it could be used more effectively to compare fracture toughness of FRC with different fiber types and contents.
- Variability of fiber distribution noticed in the critical sections of the failed specimens cut from a large slab (field concrete), and in those sections of corresponding uncut specimens made in the laboratory in the required sizes, was almost the same. No difference was noticed in performance or mechanical parameters monitored using the specimens cut from the field concrete and the specimens cast in the laboratory.
- Behavior of SFRC under monotonic and cyclic loading indicates that fibers primarily influence the envelope curve; cyclic loading did not have any adverse effect on SFRC's energy absorption capacity or flexural strength.
- Compared with plain concrete, FRC has higher fracture toughness, first-crack strength, static flexural strength, ductility, and post-crack energy absorption capacity.
- For the notched beams, the load versus CMOD curve was very similar to that of the load deflection curve.
- Hooked-end fibers provide greater consistency in terms of toughness index testing. Use of the ASTM C1018 toughness index procedure to derive I_5, I_{10}, and I_{30} is a poor method of determining the end product of the toughness.

ACKNOWLEDGMENT

The authors thank the National Science Foundation's Structures and Building Systems Program Director, Ken P. Chong, for providing financial support for this investigation.

REFERENCES

1. Ramakrishnan, V. Steel Fiber Reinforced Shotcrete; A-State-of-the-Art Report. *Proc., Steel Fiber Reinforced Concrete, U.S. and Sweden Joint Seminar,* Stockholm, June 3–5, 1985, Elsevier, London, England, pp. 7–24.
2. Ramakrishnan, V., G. Y. Wu, and G. Hosalli. Flexural Behavior and Toughness of Fiber Reinforced Concretes. In *Transportation Research*

Record 1226, TRB, National Research Council, Washington, D.C., 1989, pp. 69–77.
3. Ramakrishnan, V. Superplasticized Fiber-Reinforced Concretes for the Rehabilitation of Bridges and Pavements. In *Transportation Research Record 1003,* TRB, National Research Council, Washington, D. C., 1985, pp. 4–12.
4. Ramakrishnan, V., W. V. Coyle, P. A. Kopac, and T. J. Pasko. *Performance Characteristics of Steel Fiber Reinforced Superplasticized Concrete.* ACI SP-68, American Concrete Institute, Detroit, Mich., 1981, pp. 515–534.
5. Ramakrishnan, V., W. V. Coyle, V. Kulandaiswamy, and E. K. Schrader. Performance Characteristics of Fiber Reinforced Concrete With Low Fiber Contents. *American Concrete Institute Journal,* Vol. 78, No. 5, Sept.–Oct. 1981, pp. 384–394.
6. Ramakrishnan, V., T. Brandshaug, W. V. Coyle, and E. K. Schrader. A Comparative Evaluation of Concrete Reinforced With Straight Steel Fibers and Fibers With Deformed Ends Glued Together Into Bundles. *American Concrete Institute Journal,* Vol. 77, No. 3, May–June 1980, pp. 135–143.
7. Ramakrishnan, V., and W. V. Coyle. Steel Fiber Reinforced Superplasticized Concrete for Rehabilitation of Bridge Decks and Highway Pavements. Report DOT/RSPA/DMA-50/84–2, Office of University Research, U.S. Department of Transportation, 1983.
8. Ramakrishnan, V. *Performance Characteristics of Steel Fiber Reinforced Superplasticized Concrete.* Presented at Symposium L, Advances in Cement-Matrix Composites. Materials Research Society, University Park, Pa., Nov. 1980.
9. Balaguru, P., and V. Ramakrishnan. Mechanical Properties of Superplasticized Fiber Reinforced Concrete Developed for Bridge Decks and Highway Pavements. Report SP-93, *Concrete in Transportation,* American Concrete Institute, Detroit, Mich., 1986, pp. 563–584.
10. Ramakrishnan, V. Materials and Properties of Fiber Reinforced Concrete. *Proc., International Symposium on Fiber Reinforced Concrete,* Madras, India, Dec. 1987, pp. 2.3–2.23.
11. Balaguru, P., and V. Ramakrishnan. Comparison of Slump Cone and V-B Tests as Measures of Workability for Fiber Reinforced and Plain Concrete. *Cement, Concrete, and Aggregates,* Vol. 9, No. 1, *CCAGDP,* Summer 1987.
12. Balaguru, P., and V. Ramakrishnan. Properties of Fiber Reinforced Concrete: Workability, Behavior Under Long-Term Loading and Air-Void Characteristics. *American Concrete Institute Materials Journal,* No. 85-M23, May-June 1988, pp. 189–196.
13. State-of-the-Report on Fiber Reinforced Concrete. In *Report 544 IR-82: Concrete International Design and Construction,* May 1982.
14. *Report SP-81: Fiber Reinforced Concrete-International Symposium.* American Concrete Institute, Detroit, Mich., 1986, pp. 563–584.
15. *Report SP-105: Fiber Reinforced Concrete Properties and Applications.* American Concrete Institute, Detroit, Mich., 1987.
16. *Fiber Reinforced Cements and Concretes; Recent Developments.* (R. N. Swamy and B. Barr, eds.) Elsevier, London, England, 1989.
17. Method of Test for Flexural Strength and Flexural Toughness of Fiber Reinforced Concrete. JCI Standards for Test Methods of Fiber Reinforced Concrete (Standard SF4), Japan Concrete Institute, 1983, pp. 45–51.
18. Method of Tests for Steel Fiber Reinforced Concrete. (Standard JSCE-SF4 for Flexural Strength and Flexural Toughness of SFRC, and Standard JSCE-SF5 for Compressive Strength and Compressive Toughness of SFRC) Concrete Library, Japan Society of Civil Engineers, June 1984, pp. 58–66.
19. Measurement of Properties of Fiber Reinforced Concrete. *ACI Journal, Proceedings,* Vol. 75, No. 7, American Cement Institute, Detroit, Mich., July 1978, pp. 283–289.
20. Measurement of Properties of Fiber Reinforced Concrete, *ACI Materials Journal,* Vol. 85, No. 6, American Cement Institute, Detroit, Mich., Nov.–Dec. 1988, pp. 583–593.
21. Yalamanchi, Y. S. *Influence of Specimen Size, Loading Configuration, Fiber Type, and Fiber Content on Flexural Behavior of Steel Fiber Reinforced Concrete.* M.S. thesis. South Dakota School of Mines and Technology, May 1989.

Publication of this paper sponsored by Committee on Mechanical Properties of Concrete.

Performance Characteristics of Monofilament Polypropylene Fiber-Reinforced Concrete

V. RAMAKRISHNAN, JIM SPEAKMAN, SIDHESH KAKODKAR, AND V. R. SURE

Results of an experimental evaluation of the physical and elastic properties of monofilament polypropylene fiber reinforced concretes are presented. Fiber concentrations used were 0.05, 0.067, 0.1, and 0.2 percent by volume. Performance characteristics of the fiber-reinforced concretes were compared with that of a control concrete without fibers. Fresh concrete properties, such as slump, unit weight, vebe time, inverted cone time, and concrete temperature, were measured. For hardened concrete, 7- and 28-day compressive strength, static modulus, modulus of rupture, and 28-day impact strength were determined. Load deflection curves were plotted from the data obtained in the modulus of rupture test to determine the toughness indexes by the ASTM method and the flexural toughness factor and equivalent flexural strength by the Japanese standard method. There was no balling of fibers during mixing and placing for all the concretes. There was less bleeding in the fiber concretes compared to that of the control concrete. There was no segregation and the finishability was good. There was a significant increase in impact strength with the addition of fibers. The toughness calculated according to the ASTM and the Japanese standard methods increased with an increase in fiber content. There is a positive improvement in the concrete's fatigue resistance with the addition of fibers.

Randomly oriented fiber reinforcement is an effective way of improving concrete properties. Fiber-reinforced concrete has a wide range of applications, particularly for airport and highway pavements, bridge deck overlays, curtain walls, sewer pipes, and cavitation and erosion-resistant structures, such as spillways, sluiceways, bridge piers, and navigation locks. Fiber-reinforced concrete also has found its way into precast products, earthquake-resistant structures, and explosion-resistant structures, such as missile silos and energy dissipators, shotcrete for rock-fill stabilization, tunnel linings, and dome structures. Considerable research has been done on the performance characteristics of fibrillated polypropylene fiber-reinforced concrete (*1–12*). An investigation (*5,13*) showed an increase in performance as measured by better resistance to impact loads, and higher toughness and endurance when subjected to fatigue loading. Polypropylene fibers have been proposed as an alternative to using welded fabric wire for crack-control purposes in concrete slabs (*12*).

Polypropylene fibers in general have some unique properties that make them suitable for use in concrete. The fibers are chemically inert, are noncorrosive, and have high chemical resistance to mineral acids, bases, and inorganic salts. They are very stable and do not absorb water. The fibers have high tensile strength and are economical to use. The low-modulus and high-elongation fibers are capable of large energy absorption characteristics.

V. Ramakrishnan, S. Kakodkar, V. Sure, South Dakota School of Mines and Technology, 501 East St. Joseph Street, Rapid City, S.D. 57701-3995. J. Speakman, Dura Fiber, Inc., 2802-A Foster Ave., Nashville, Tenn. 37210.

Most currently available information about properties and performance of polypropylene fiber-reinforced concrete has been obtained for fibrillated polypropylene fibers of lengths varying from 12.7 mm to 63.5 mm (0.5 to 2.5 in.). There is very little information available about the performance of monofilament polypropylene fibers in concrete. Therefore, the authors conducted this study to determine the elastic and mechanical properties of concrete reinforced with monofilament polypropylene fibers.

OBJECTIVES

The primary objective of the investigation was to determine the physical properties of the monofilament polypropylene fiber-reinforced concrete specimens. That was achieved by carrying out tests to determine

- Properties of fresh concrete mixtures reinforced with polypropylene fibers;
- Characteristics of hardened concrete, such as compressive strength, static modulus, static flexure strength, unit weight, and impact resistance;
- Toughness indexes according to ASTM C1018, and flexural toughness and equivalent flexural strength according to the Japanese standard, using deflection-controlled load deflection curves; and
- Qualitative evaluation of flexural fatigue strength and whether there is any increase in the endurance limit with the addition of small amounts of fibers.

EXPERIMENTAL PROGRAM

Materials

Type I/II normal portland cement that satisfies ASTM C150 requirements was used for all mixtures. The maximum size of the coarse aggregate was 19 mm (¾-in.) with absorption coefficient of 0.45 percent and fineness modulus of 6.57. The fine aggregate used was natural sand with a water absorption coefficient of 1.60 percent and a fineness modulus of 2.56. Coarse and fine aggregates satisfy the grading requirements of ASTM C33. Fibers used in this program were monofilament polypropylene fibers manufactured by Dura Fiber Company. The fibers were 19-mm (¾-in.) long.

Mixtures

Basic mix proportions used for the research were as follows: coarse aggregate (926 kg/m^3), fine aggregate (926 kg/m^3), cement

(390 kg/m^3), and water (163.8 kg/m^3). The water cement ratio was maintained at 0.45. Seven mixtures were made, and one mixture was without fibers. The basic mix designations are detailed in Table 1. All the mixing was done according to ASTM C192.

Specimens

The following specimens were cast from each mix: 150 × 300-mm (6- × 12-in.) cylinders for compressive strength and static modulus tests; 100- × 100-mm × 350-mm (4- × 4- × 14-in.) beams for static flexural toughness tests; and 100- × 63.5-mm (6- × 2½-in.) specimens for impact strength. The specimens were covered with plastic sheets for 24 hours at room temperature. They were then demolded and placed in a lime-saturated water tank maintained at 23°C (74°F). They remained in water until they were tested after 7 and 28 days.

TESTS FOR FRESH CONCRETE

Freshly mixed concrete was tested for slump (ASTM C143), air content (ASTM C231), fresh concrete unit weight (ASTM C138), inverted slump cone (ASTM C995), concrete temperature, and vebe time. Results of the tests are presented in Table 1.

TESTS FOR HARDENED CONCRETE

Cylinders were tested for compressive strength at 7 and 28 days, according to ASTM C39. They were also tested for the static modulus (ASTM C469). A pulse-velocity test (ASTM C597) was conducted.

Static Flexure Test

Beams were tested at the age of 7 and 28 days, per ASTM C1018, for static flexural strength under third-point loading. For static tests, a dial gauge with an accuracy of 0.0025 mm (0.0001 in.) was used to measure the midspan deflection. The gauge was located mid-width of the specimen to minimize the effect of twisting on deflection measurements. A specially constructed frame (*13*) was fixed to the specimen over the supports at neutral axis points. The dial gauge was attached to the frame, enabling accurate measurement of the actual midspan deflection and thereby eliminating extraneous deflections caused by crushing at supports and load points, and elastic shortening of the testing machine columns and platens. The device also eliminates the influence of specimen warping from torsion on the measured deflection. Rate of loading was maintained in the range of 0.0508 to 0.101 mm/min (0.002 to 0.004 in./min), per ASTM C1018. Loads were recorded at regular intervals; specimens were loaded up to a minimum midpoint deflection of 1/150 of the span, thereby allowing for computation of ASTM and JCI and JSCE fracture toughness indexes.

Flexural Fatigue Test

In the test for flexural fatigue, third-point loading was used with a span of 304.8 mm (12 in.), and the beams were subjected to a non-reversed fluctuating load. The procedure used for the test was as follows: the lower load limit was set at 10 percent of the average maximum load obtained from the static flexure test. For the first beam in each mix, the upper load limit was set at 90 percent of average maximum flexural load for the set. The fatigue test was run between these limits. If the beam failed before completing 2 million cycles, the upper limit was reduced for the next specimen. If the beam survived, another beam was tested at the same upper load, as a replicate.

The frequency of loading used was 20 cycles/sec (Hz) for all tests. It has been shown elsewhere (*2,3*) that frequency has little or no effect, unless extremely high rates are used. Therefore, for purposes of expediency, a rate of 20 Hz was used. The MTS testing machine was used for all tests. The control and monitor system consists of an MTS 436 control unit, a Hewlett-Packard oscilloscope, and a digital multimeter working with an MTS load cell. There was a counter in the machine that kept track of the number of cycles, and when a beam failed, the counter reading was recorded as the number of cycles at failure. A mechanical cut off switch allowed the operator to turn off the machine when a beam broke.

TEST RESULTS AND DISCUSSIONS

The monofilament polypropylene fiber used for the research performed well. Results of the tests for slump, air content, vebe time, inverted cone time, and unit weight are given in Table 1. The unit weight for all seven mixtures was almost the same, implying that different fiber volumes do not influence the unit weight of concrete. Fiber-reinforced concrete specimens were placed with relative ease and compacted using a vibrating table. Fresh concrete containing fibers had very little or no surface bleeding and no segregation.

TABLE 1 Mix Designations and Fresh Concrete Properties

Mix #	Type of fiber	% Fiber by volume	Slump	Air Content	Unit Weight	Vebe Slump	Vebe Time	Inverted Cone Time
			mm	%	kg/m^3	mm	seconds	seconds
DF1	Monofilament	0.050	32	1.9	2434.5	25	2.6	11.0
DF2	Monofilament	0.067	25	1.8	2434.3	25	2.8	16.0
DF3	Monofilament	0.100	25	1.9	2432.0	25	3.6	20.0
DF4	None	-	57	2.3	2434.1	51	2.0	4.0
DF5	Monofilament	0.067	44	2.1	2464.9	51	2.2	6.8
DF6	Monofilament	0.100	32	2.4	2438.9	25	4.5	6.6
DF7	Monofilament	0.200	19	2.4	2477.6	13	6.0	11.0

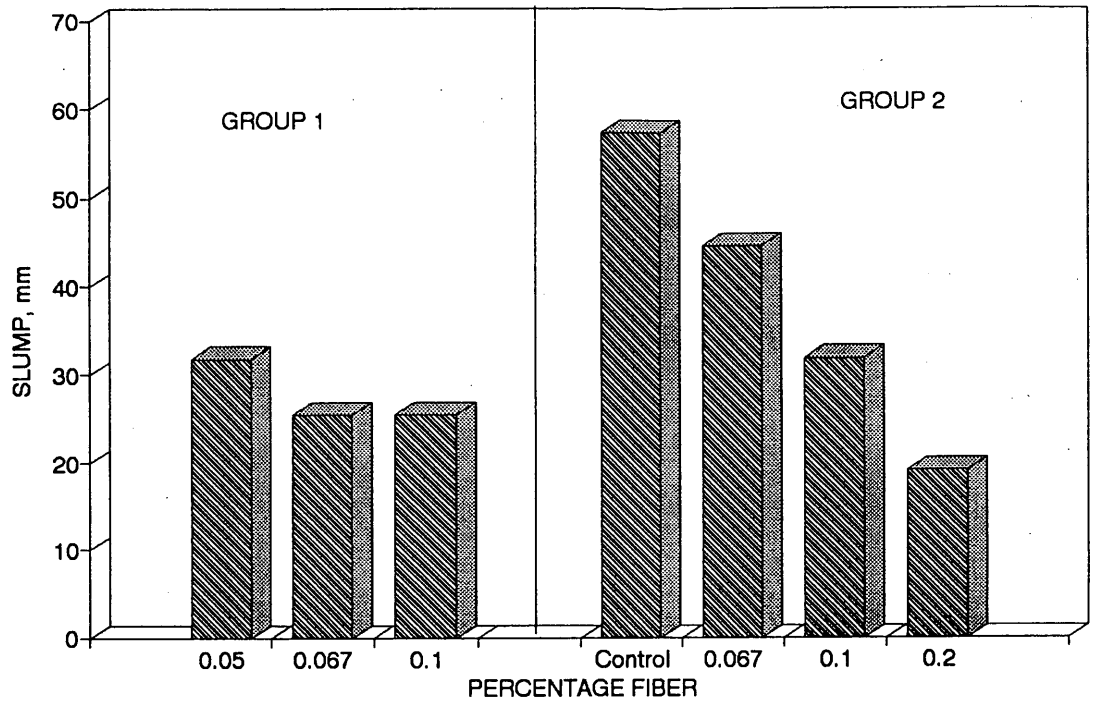

FIGURE 1 Comparison of slump.

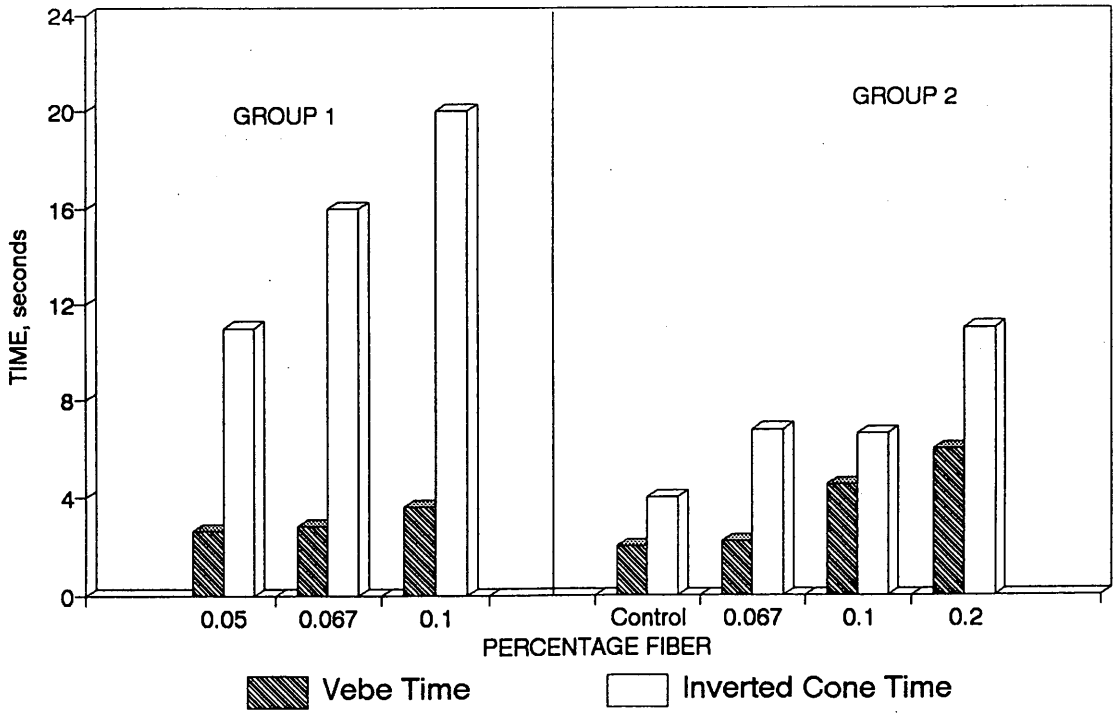

FIGURE 2 Comparison of vebe time and inverted cone time.

Slump, vebe time, and inverted cone time tests were conducted to determine the workability of the concrete mixtures. Results of a comparison of fresh concrete properties are presented in Figures 1 and 2. The water cement ratio was maintained at 0.45, and satisfactory workability was maintained for all the mixtures by adding an approximate amount of superplasticizer. The finishability was good.

HARDENED CONCRETE PROPERTIES

Compressive Strength

Compressive strength test results are shown in Table 2. There was a significant increase in strength from the 7- to the 28-day period. However, the increase of fiber content did not affect the compressive strength of the fiber-reinforced concrete.

There is a slight difference in compressive strength between Group 1 and Group 2 concretes. Group 1 concretes were made in February 1991 and Group 2 concretes were made in July 1992. The difference in compressive strength may have been related to different temperature and humidity conditions at the time the concretes were made. The quality of the cement used may have contributed to the difference in compressive strength between Group 1 and Group 2 concretes.

Static Modulus

Static modulus values are presented in Table 2. The values were reasonably consistent for all the mixtures. There was an increase in static modulus from 7 to 28 days.

Flexural Strength

Static flexural strength test results, also presented in Table 2, indicate an increase in flexural strength from 7 to 28 days. There was no significant increase in the modulus of rupture with an increase in the fiber content from 0.05 to 0.20 percent by volume. Fractured surfaces were inspected visually. Most of the fibers were broken and were not pulled out, indicating that there was a good bond between the fibers and concrete.

Pulse Velocity

Pulse velocity measurements indicated that the addition of fibers to the concrete did not affect the elastic wave transmitting property of the concrete. Measurements also indicated a significant degree of uniformity in the manufactured specimens and consistency in their quality.

Toughness Indexes (ASTM)

Values of calculated toughness indexes are presented in Table 3. Toughness indexes were defined on the basis of three service levels, multiples of first-crack deflection. The toughness index is computed by dividing the total area under the load deflection curve up to the given service level deflection by the area under the same curve up to the first crack deflection. Toughness indexes I_5, I_{10}, and I_{20} are calculated as ratios of the area of the load deflection curve up to deflections of 3, 5.5, and 10.5, respectively, times the first crack deflection divided by the area of the load deflection curve up to the first crack deflection. There was a significant increase in toughness from age 7 to 28 days. A slight increase in first crack toughness with an increase in fiber volume was observed. A comparison of the toughness indexes, I_5, I_{10}, and I_{20} with respect to fiber content is exhibited in Figure 4. The ratios of I_{10}/I_5 and I_{20}/I_{10} were less than 2, as indicated in Table 3. The ratios indicate that even though the concrete was not perfectly elastoplastic, it had adequate ductility and toughness. The toughness index increased with an increase in fiber content, signifying that with a higher percentage volume of fiber, a greater capacity for energy absorption is achieved.

TABLE 2 Compressive Strength, Static Modulus, and Flexural Strength

Mix #	Age, days	Compressive Strength, MPa	Static Modulus, MPa	Flexural Strength, MPa	First Crack Toughness, Nm
DF1	7	32.93	31211	4.18	0.19
	28	42.82	36654	4.79	0.23
DF2	7	32.12	29351	3.91	0.23
	28	40.05	34450	4.89	0.25
DF3	7	32.24	36861	4.19	0.22
	28	39.22	32796	4.82	0.24
DF4	7	34.34	26733	3.51	0.12
	28	49.29	36172	4.32	0.19
DF5	7	30.90	32796	3.85	0.23
	28	52.95	36310	4.68	0.24
DF6	7	35.17	36689	4.13	0.12
	28	52.50	36482	4.41	0.26
DF7	7	29.79	32796	4.68	0.24
	28	47.09	36551	4.82	0.49

TABLE 3 Toughness Indexes

Mix #	Age Days	I5	I10	I20	I10/I5	I20/I10	JCI	
							T[a], Nm	Fe[b], MPa
DF1	7	3.27	5.39	8.87	1.71	1.89	-	-
	28	3.55	6.26	9.29	1.75	1.76	10.51	1.38
DF2	7	3.80	5.62	8.91	1.51	1.57	-	-
	28	3.53	6.45	11.0	1.82	1.70	10.64	1.42
DF3	7	3.55	6.55	10.84	1.85	1.64	-	-
	28	3.95	6.59	11.51	1.65	1.75	11.33	1.55
DF4	7	2.29	3.36	6.29	1.87	1.87	-	-
	28	3.21	5.37	8.27	1.56	1.56	8.41	1.13
DF5	7	2.50	3.93	6.71	1.75	1.75	-	-
	28	3.32	6.75	11.90	1.76	1.76	10.10	1.31
DF6	7	3.53	6.98	10.90	1.56	1.56	-	-
	28	3.60	6.73	11.70	1.73	1.73	10.92	1.47
DF7	7	4.07	8.64	13.64	1.58	1.58	-	-
	28	4.52	8.73	13.93	1.59	1.59	13.42	1.78

a - Toughness (JCI)
b - Equivalent Flexural Toughness Factor (JCI)

Japanese Standard Method

Values for the flexural toughness factor are presented in Table 3. The Japanese standard method, unlike the ASTM method, sets the deflection limit equal to 1/150 of its span. The span for beams used in this program was 304.8 mm (12 in.). The deflection value used for this method is greater than that used for the ASTM method of calculating toughness. Results from a comparison of flexural toughness values for different fiber contents are presented in Figure 5. Equivalent flexural strengths for various fiber contents are indicated in Figure 6. Results show that flexural toughness and equivalent flexural strength increased with an increase in fiber content for Group 1 and Group 2 concretes.

Impact Strength

The American Cement Institute's drop weight test was used in this investigation. The comparison presented in Figure 3 indicates that the number of blows until first crack and the number of blows to failure increase the higher the fiber content.

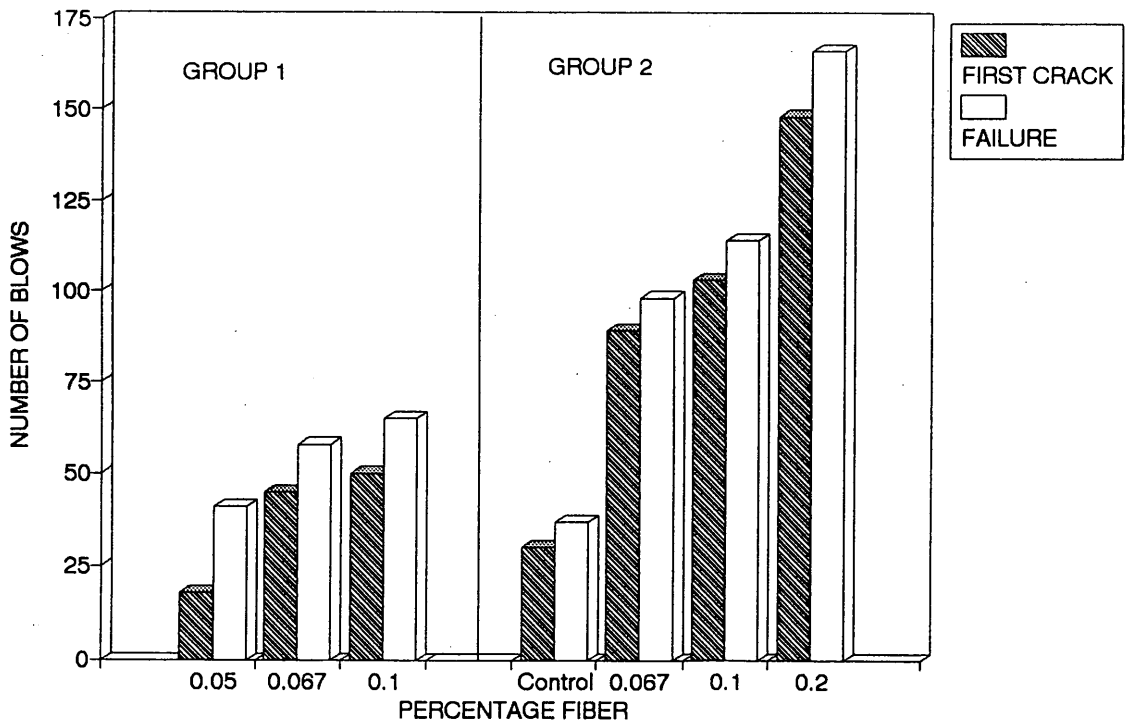

FIGURE 3 Comparison of impact strength.

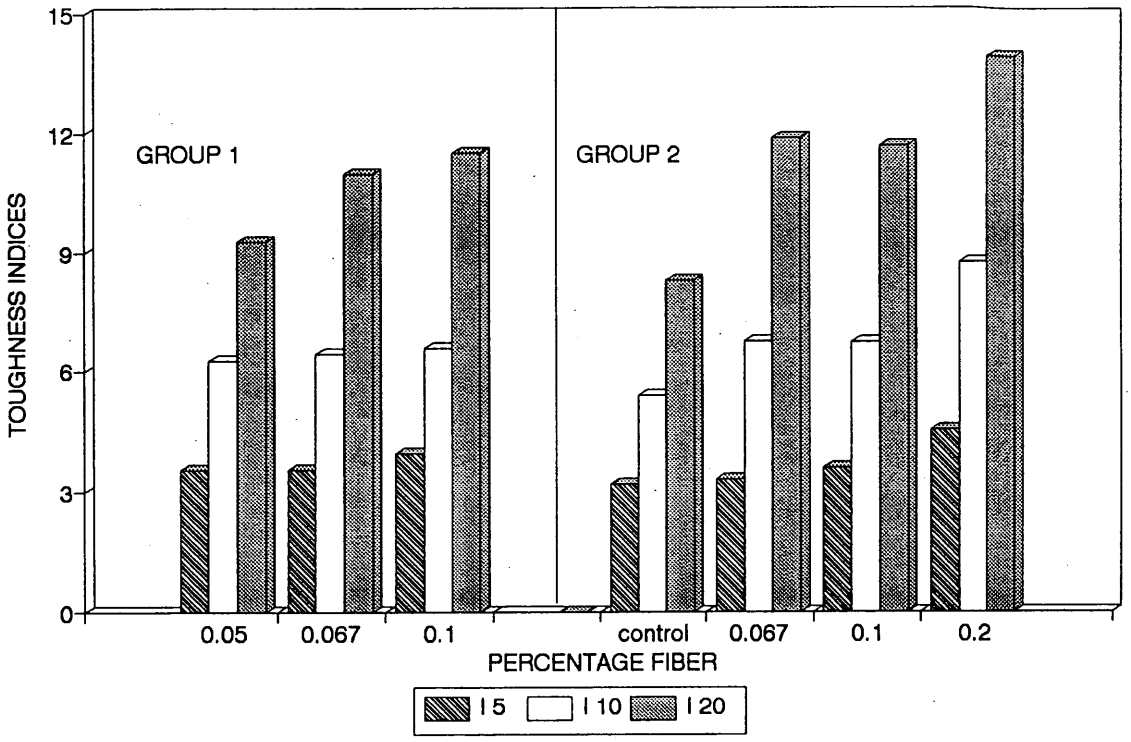

FIGURE 4 Comparison of toughness indexes.

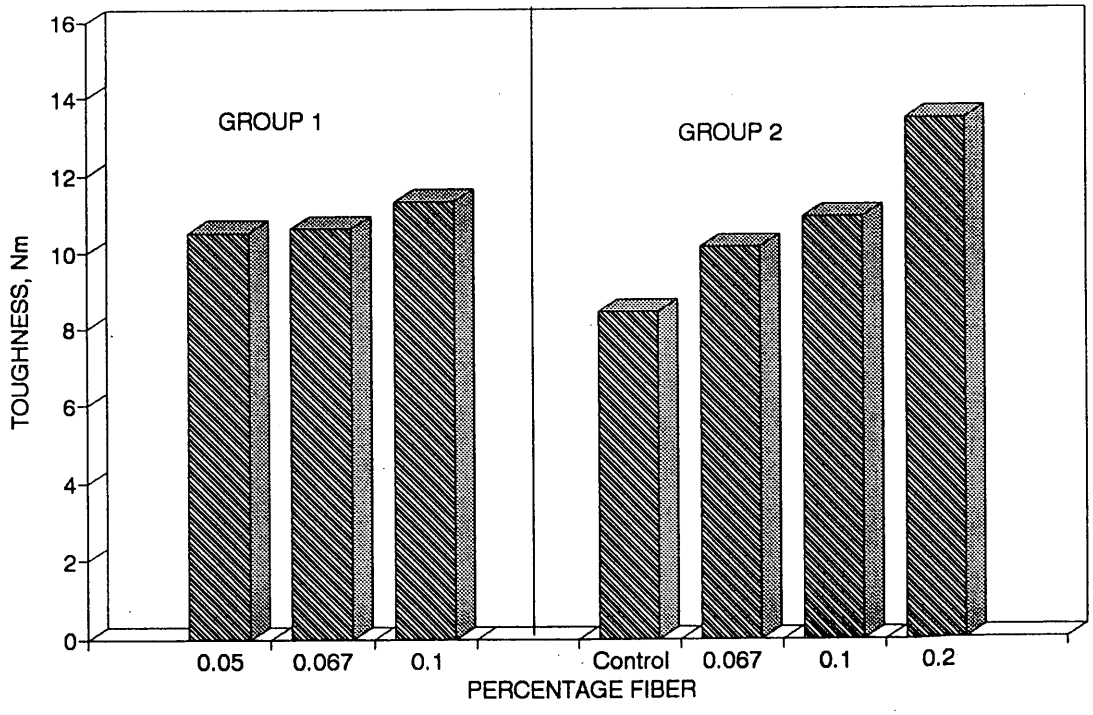

FIGURE 5 Comparison of toughness (JCI).

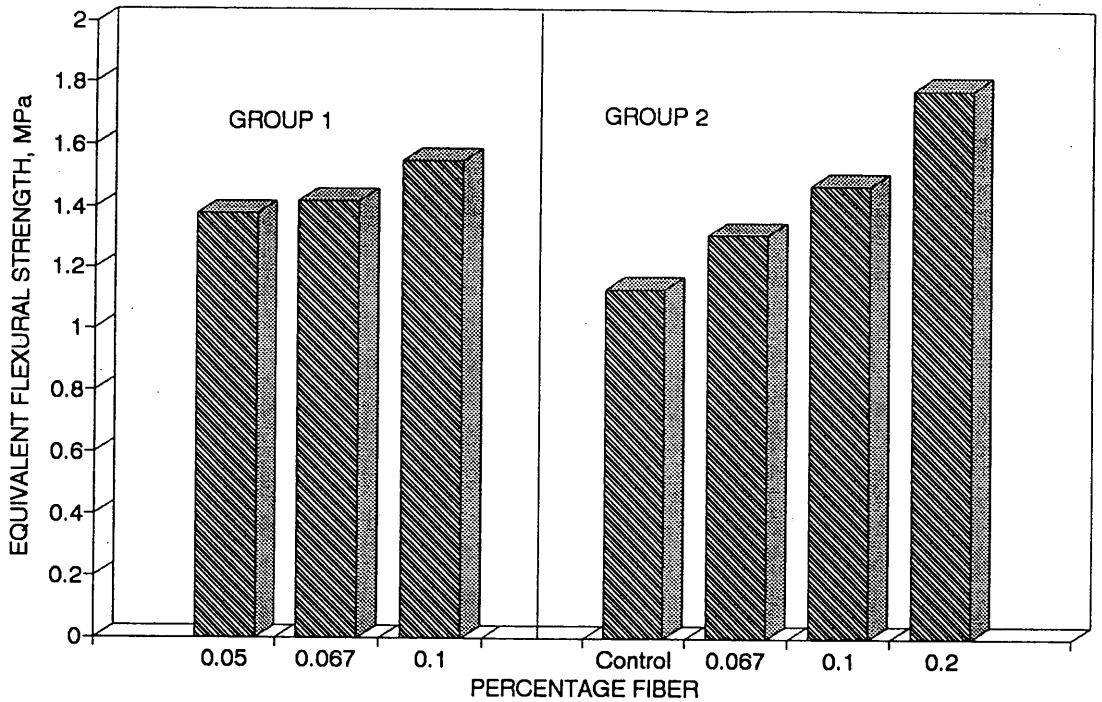

FIGURE 6 Comparison of equivalent flexural strength (JCI).

Comparing earlier investigations with the same amount of fibrillated polypropylene fiber-reinforced concretes with the present study of the monofilament polypropylene concretes, the authors found no significant difference in performance characteristics.

Flexural Fatigue Behavior

A small number of specimens were tested in flexural fatigue (*6*) to evaluate qualitatively the trend in the fatigue performance of monofilament polypropylene fiber-reinforced concrete. Beams made with plain concrete, with 0.1 and 0.067 percent fiber contents by volume, were tested for flexural fatigue. Results of fatigue tests are presented in Figures 7 and 8.

Fatigue Strength

Fatigue strength is defined as the maximum fatigue flexural stress at which point the beam can withstand 2 million cycles of nonreversed fatigue loading.

The authors observed that fatigue strength increased slightly with the addition of monofilament polypropylene fibers to the concrete.

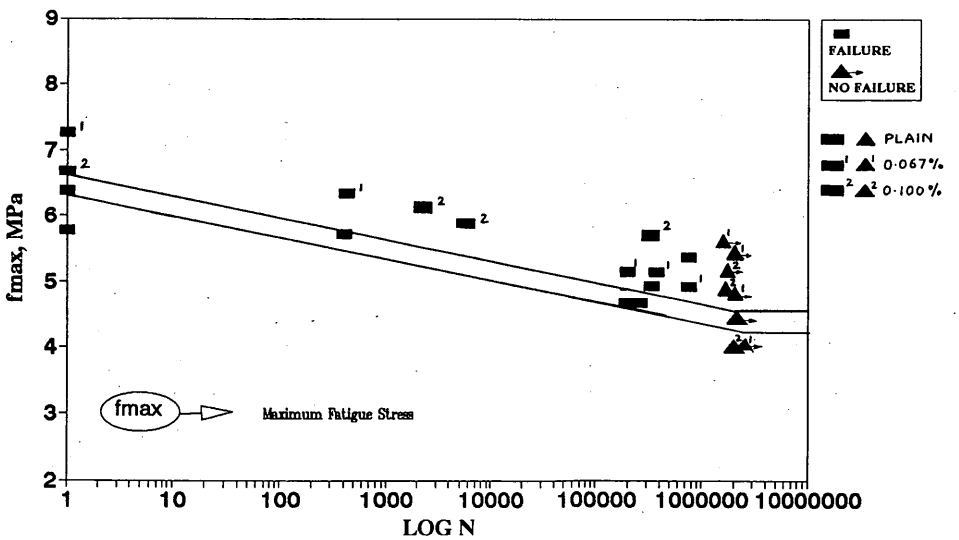

FIGURE 7 Log of number of cycles versus f_{max} for all mixtures.

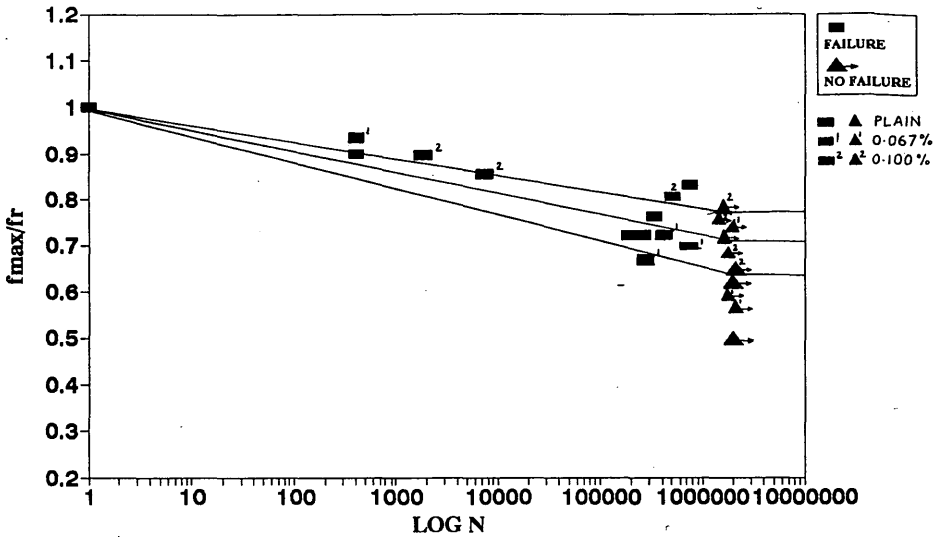

FIGURE 8 Log of number of cycles versus f_{max}/fr for all mixtures.

The fatigue strength was 4.46 MPa (647 psi) for plain concrete; it was 4.49 MPa (652 psi) and 4.86 MPa (705 psi) for 0.067 and 0.1 percent fiber concrete mixtures, respectively—an increase of 1 and 9 percent, respectively. Figure 7 illustrates the relation for fatigue flexural stress versus the logarithm of number of cycles for all the mixtures. Fatigue strength increases with fiber content.

Endurance Limit Expressed as a Percentage of Plain Concrete's Modulus of Rupture

Endurance limit is defined as the maximum fatigue flexural stress at which point the beam could withstand 2 million cycles of nonreversed fatigue loading, expressed as a percentage of modulus of rupture of plain concrete.

For beams made of 0.067 and 0.1 percent of fiber, there is a slight increase in the endurance limit, expressed as a percentage of modulus of rupture of plain concrete. The endurance limit is 69 percent for the mix with the 0.067 percent fiber content. It is 75 percent for the mix with 0.1 percent fiber content. The endurance limit for plain concrete is 65 percent. Thus the endurance limit was increased by 6 and 15 percent, respectively, when 0.067 and 0.1 percent by volume of fibers, respectively, were added to the concrete.

Endurance Limit Expressed as a Percentage of Mixtures Modulus of Rupture

Endurance limit of concrete can also be defined as the fatigue flexural stress at which a beam could withstand 2 million cycles of nonreversed fatigue loading, expressed as a percentage of its modulus of rupture.

The endurance limit for the mix with 0.067 percent fiber content was 70 percent, whereas it was 75 percent for the mix with 0.1 percent fiber content. Hence, the improvement in endurance limit is evident when the endurance limit is expressed as a percentage of its modulus of rupture.

Figure 8 shows the relation between the ratio of the fatigue stress to the average modulus of rupture (fmax/fr) versus logarithm of number of cycles for all mixtures. In this case the relationship is linear for all mixtures. Comparisons of flexural fatigue strength, endurance limit expressed as a percentage of modulus of rupture of plain concrete, and the endurance limit expressed as a percentage of its modulus of rupture are all given in Table 4.

CONCLUSIONS

- Fiber-reinforced concrete mixtures achieve good workability. Placement and compaction is done with relative ease.
- Static modulus, pulse velocity, and compressive strength do not change significantly with an increase in fiber content.
- Toughness indexes (ASTM) indicate improved behavior with an increase in the volume percentage of polypropylene fiber.
- Flexural toughness and equivalent flexural strength increase with a higher volume percentage of fiber.
- Impact strength increases with greater volume percentage of fiber.

TABLE 4 Fatigue Properties

Fiber Content	f max[a], MPa	EL1[b]	EL2[c]
Control	4.45	65	65
0.067%	4.49	69	70
0.100%	4.86	75	75

a - Flexural fatigue strength.
b - Endurance limit expressed as a percentage of modulus of rupture of plain concrete.
c - Endurance limit expressed as a percentage of its modulus of rupture.

- Polypropylene fiber performs well, with no problems with regard to workability, placing, or balling.
- Good finishability is achievable. (No protruding fibers were seen from the finished concrete specimens.)
- No difference in performance characteristics is observable between the monofilament polypropylene fiber-reinforced concrete and fibrillated polypropylene fiber-reinforced concrete.
- There is positive improvement in the fatigue resistance of concrete when monofilament polypropylene fiber is added in small quantities. There is an increase of 6 and 15 percent in the endurance limit for concretes with 0.067 and 0.1 percent fiber by volume, as compared with plain concrete.

REFERENCES

1. Ramakrishnan, V. Materials and Properties of Fiber Reinforced Concrete. *Proc., International Symposium on Fiber Reinforced Concrete,* Madras, India, Dec. 1987, pp. 2.3–2.23.
2. Ramakrishnan, V., S. Gollapudi, and R. Zellers. Performance Characteristics and Fatigue of Polypropylene Fiber Reinforced Concrete. ACI SP-105, *Fiber Reinforced Concrete; Properties and Applications,* American Concrete Institute, Detroit, Mich. 1987, pp. 159–177.
3. Ramakrishnan, V., G. Y. Wu, and G. Hosalli. Flexural Behavior and Toughness of Fiber Reinforced Concretes. In *Transportation Research Record 1226,* TRB, National Research Council, Washington D.C., 1989, pp. 69–77.
4. Ramakrishnan, V., G. Y. Wu, and G. Hosalli. Flexural Fatigue Strength, Endurance Limit, and Impact Strength of Fiber Reinforced Concretes. In *Transportation Research Record 1226,* TRB, National Research Council, Washington D.C., 1989, pp. 17–24.
5. Vondran, G. L., M. Nagabhushanam, and V. Ramakrishnan. Fatigue Strength of Polypropylene Fiber Reinforced Concretes. *Fiber Reinforced Cements and Concretes: Recent Developments,* (R. N. Swamy and B. Basu eds.) Elsevier, London, England, and New York, 1990, pp. 533–543.
6. Gopalaratnam, V. S., S. P. Shah, G. B. Batson, M. E. Criswell, V. Ramakrishnan, and M. Wecharatana. Fracture Toughness of Fiber Reinforced Concrete. *ACI Materials Journal,* Vol. 88, No. 4, July–August 1991, pp. 339–353.
7. Ramakrishnan, V., and Bjorn J. Lovik. Fatigue Strength and Endurance Limit of Plain and Fiber Reinforced Concretes; A Critical Review. *Proc., International Symposium on Fatigue and Fracture in Steel and Concrete Structures,* Madras, India, Dec. 1991, pp. 381–405.
8. Nagabhushanam, M., V. Ramakrishnan, and G. Vondran. Fatigue Strength of Fibrillated Polypropylene Fiber Reinforced Concretes. In *Transportation Research Record 1226,* TRB, National Research Council, Washington D.C., 1989, pp. 36–47.
9. Mindess, S., A. Bentur, C. Yan, and G. Vondran. Impact Resistance of Concrete Containing Both Conventional Steel Reinforcement and Fibrillated Polypropylene Fibers. *ACI Materials Journal,* Vol. 86, No. 6, Nov.-Dec. 1989, pp. 545–549.
10. Yongxin, L. *Properties of Polypropylene Fiber Reinforced Concrete and Effects of Fiber Length; An Experimental Investigation.* M. S. thesis. South Dakota School of Mines and Technology, Rapid City, 1988.
11. Chowdhary, S. G. *Evaluation and Comparison of the Physical Properties of Standard and Modified Polypropylene Fiber Reinforced Concretes.* M. S. thesis. South Dakota School of Mines and Technology, Rapid City, 1991.
12. Malisch, W. R. How Well Do Polypropylene Fibers Control Cracking? *Concrete Construction,* Vol. 31, No. 4, April 1986, pp. 371–378.
13. Ramakrishnan, V., and Satya S. Yalamanchi. Fracture Toughness of Steel Fiber Reinforced Concrete. *Proc., International Symposium on Fatigue and Fracture in Steel and Concrete Structures,* Madras, India, Dec. 1991, pp. 1535–1548.

Publication of this paper sponsored by Committee on Mechanical Properties of Concrete.

Evaluation and Comparison of the Physical Properties of Fibrillated Polypropylene Fiber-Reinforced Concretes

R. C. ZELLERS AND V. RAMAKRISHNAN

A comparative evaluation of physical properties for plain concrete and concrete reinforced with collated fibrillated polypropylene fibers is presented. Three concentrations of fibers, 0.1, 0.2, and 0.3 percent by volume, were evaluated. Evaluation included concretes with the fiber dosages indicated and a plain or control mix in two series: (*a*) fresh concrete properties namely slump, unit weight, vebe time, air content, and concrete temperature and (*b*) hardened concrete properties, such as compressive strength, static modulus, modulus of rupture, and pulse velocity at 7 and 28 days—the second being the replicate. Toughness indexes based on ASTM C1018, as well as the flexural toughness factors, were calculated. In addition, an equivalent flexural strength based on the Japanese standard was obtained. Inspection of plastic mixes and failed test specimens showed that there was no balling of fibers during mixing and fabrication of test specimens. There was a slight increase in the flexural strength as the fiber content increased. Addition of fibers produced less than 5 percent difference in the static modulus, compressive strength, and pulse velocity. On the basis of I_5, I_{10}, and I_{20} toughness index data, the fiber concretes exhibited elasto-plastic behavior.

Concrete has two major deficiencies: low tensile strength and poor ductility. The tensile strength of concrete is very low because plain concrete normally contains numerous microcracks. It is the rapid propagation of these microcracks under applied stress that is responsible for the material's low tensile strength.

Those deficiencies have led to considerable research aimed at developing new approaches to modifying the brittle properties of concrete. Current research has developed a way to increase concrete ductility and energy absorption capacity, as well as to improve concrete's overall durability. The new technology uses discrete steel or synthetic fibers ranging from 19 to 63.5 mm (¾ to 2½ in.) long. The fibers are dispersed randomly throughout the concrete matrix; better distribution of internal and external stresses is provided by using a three-dimensional reinforcing network (*1–8*).

General requirements for fibers used as temperature/moisture shrinkage reinforcement include high tensile strength, high bond strength (typically mechanical), and ease of incorporation into the matrix to insure optimum distribution. The primary role of the fibers in hardened concrete at low volume is to modify the cracking mechanism. By modifying the cracking mechanism, the macrocracking becomes microcracking. The cracks are smaller in width, thus reducing the permeability of the concrete, and the ultimate cracking strain of the concrete is enhanced. Unreinforced concrete will separate at a crack, reducing the load carrying ability to zero across the crack. The fibers are capable of carrying a load across the crack, if all of the characteristics listed are met by the fiber (*1*).

R. Zellers, Forta Corporation, 100 Forta Dr., Grove City, Pa. 16127. V. Ramakrishnan, South Dakota School of Mines and Technology, 501 East St. Joseph Street, Rapid City, S.D. 57701–3995.

Fiber-reinforced concrete specimens, unlike plain concrete specimens that fail at the point of ultimate flexural strength or first crack, do not fail immediately after the initiation of the first crack. After first crack, the load is transferred from the concrete matrix to the fibers. Measuring this load carrying capability of the fibers after the first crack is determined per ASTM C1018.

A major advantage of using fiber reinforced concrete besides reducing permeability and increasing fatigue strength is that fiber addition improves the toughness or residual load carrying ability after the first crack. In addition, a number of studies have shown that the impact resistance of concrete can also increase dramatically with the addition of fibers. Low modulus fibers, like polypropylene, appear to be particularly effective in this regard (5). Combining the technical benefits and in-place costs, synthetic fiber reinforced concrete has been found to meet the prerequisites of value engineering in construction applications.

To demonstrate the validity of this statement, PennDOT had two projects in 1993 where synthetic fibers were specified. One project was a shotcrete application wherein the synthetic fiber reinforced shotcrete was used to protect the active-cathodic protection system on a bridge structure spanning the Lehigh River. The second project in Erie County enlisted the use of synthetic fiber reinforced concrete to replace the arch culvert invert slab. The engineer for both projects found the synthetic fibers filled both the engineering requirements and were cost effective when compared to alternate materials.

The fibers used in this investigation were collated fibrillated polypropylene fibers. These fibers have some unique properties that make them suitable for reinforcement in concrete mixes. The properties of polypropylene fibers are shown in the following:

- Melting point: 160°C–170°C (320°F–338°F),
- Ignition point: 590°C (1094°F),
- Tensile strength: 550–760 MPa (79750–110200 psi),
- Young's modulus: 3.5 GPa (507500 psi),
- Thermal conductivity: low,
- Electrical conductivity: low, and
- Acid and salt resistance: high.

Polypropylene fibers are chemically inert, noncorrosive, and have high resistance to acids, bases, and salts. The surface of the fibers is hydrophobic, which makes it nonabsorbent to water. These fibers have high tensile strength and are economical to use. The high magnitude elongation of these fibers is capable of imparting large energy absorption capacity to concrete, which also improves the ductility of the concrete. Fibrillated polypropylene fiber-reinforced concretes have higher fatigue strength and higher impact resistance.

Adding polypropylene fibers helps reduce early plastic shrinkage and cracking of concrete. The mortar matrix penetrates through the network pattern in the CFP fiber anchoring the fiber network like wire mesh. The mechanical anchorage is called "pegging."

RESEARCH OBJECTIVES

The primary objective of this research program is to study and compare the physical properties of plain concrete and concretes reinforced with collated fibrillated polypropylene fibers. The objective was achieved through determination of the following

1. Properties of the fresh concretes, plain and reinforced with CFP fibers;
2. Characteristics of hardened concrete, such as compressive strength, static modulus, static flexure strength, unit weight, and the pulse velocity;
3. Toughness indexes using the ASTM C1018 standard method and load deflection curves; and
4. Flexural toughness factor and equivalent flexural strength, using the Japanese standard method.

Values of 5.0, 10.0, 20.0 for I_5, I_{10}, I_{20}, respectively, correspond to linear elastic behavior up to the first crack and perfectly plastic behavior hereafter. A value of two for the ratios of I_{10}/I_5 and I_{20}/I_{10} indicates perfectly plastic material behavior between the deflections associated with these indexes.

The observed values of I_5, I_{10}, I_{20} are given in the in-text table.

Index	*Values of Toughness Indexes*		
	Plain concrete	*Elastic plastic material*	*Observed range for fibrous concrete*
I_5	1.0	5.0	1 to 6
I_{10}	1.0	10.0	1 to 12
I_{20}	1.0	20.0	1 to 25

MATERIALS, MIXES, AND TEST SPECIMENS

Materials

- Fiber: Collated fibrillated polypropylene (CFP) fibers produced by Forta Corporation were used. Fiber bundle length was 57 mm (2¼ in.), and the product designation was Type D-15.
- Cement: Type I normal portland cement, satisfying the requirements of ASTM C150, was used for all mixes. The cement was produced by a cement plant in Rapid City, South Dakota.
- Coarse Aggregate: The coarse aggregate used was crushed limestone aggregate obtained locally (Rapid City). The maximum size of the coarse aggregate was ¾ in. and met AASHTO #67 gradation requirements. Its absorption coefficient was 0.45 percent and its fineness modulus was 6.80.
- Fine Aggregate: The fine aggregate used was natural sand obtained locally; it had a water absorption coefficient of 1.64 percent and fineness modulus of 2.95. Both fine and coarse aggregates satisfied the grading requirements of ASTM C33.
- Water: The water used was tap water from the Rapid City, municipal water supply system.
- Superplasticizer: The superplasticizer used was Rheobuild 1000, which was manufactured by Master Builders and met ASTM C494 Type D specifications.

Mixing of Concrete

The basic mix proportions that were used for the research program were as follows:

- Coarse aggregate, 926 kg/m^3,
- Fine aggregate, 926 kg/m^3 Cement;
- Cement, 390 kg/m^3; and
- Water, 163.8 kg/m^3.
- Mix designations are given in Table 1. Three mixes were made using standard D-15 type polypropylene fibers containing 0.1, 0.2, and 0.3 percent by volume. Replicate mixes for the three mixes were also made, and one mix of plain concrete was made. Seven mixes were made for the program. The volume of each mix was 0.077 m^3 (2.75 ft^3). The water to cement ratio was maintained at 0.42. Mixing of concrete was done according to ASTM C192.

Test Specimens

The following specimens were cast from each mix, six 150 × 300 mm (6 × 12 in.) cylinders for the determination of the compressive strength and static modulus tests; six to eight 100 × 100 × 350 mm (4 × 4 × 14 in.) beams for the determination of the static flexural strength and toughness indexes.

The specimens were cast in steel molds immediately after mixing. The specimens were then covered with plastic sheets for 24 hr to prevent evaporation of water from the unhardened concrete. The specimens were then demolded and placed in lime-saturated water tanks in which the temperature of the water was maintained at 23°C (73°F). Specimens used for compressive strength tests and static flexural tests remained in water until they were tested at 7 and 28 days.

TABLE 1 Mix Designation and Properties of Fresh Concrete

Mix	Type of fiber	Percentage of fiber by volume	Superplasticizer Dosage (cc)	Room		Concrete Temp. (°C)	Unit Weight (kg/m^3)	Slump (mm)	Vebe Time (seconds)	Air Content (%)
				Temp. (°C)	Humidity (%)					
FP	No fiber	Plain concrete	150	21	40	22.7	2440	108	1.2	2.2
F1C	Forta D 15	0.10	260	17	65	19.0	2439	38	3.7	2.5
F2C	Forta D 15	0.20	250	21	40	22.4	2435	76	1.5	3.1
F3C	Forta D 15	0.30	380	17	65	19.6	2453	57	3.6	2.5
F1CR	Forta D 15	0.10	110	21	35	20.1	2412	57	1.1	2.4
F2CR	Forta D 15	0.20	140	18	30	20.9	2438	76	1.5	2.3
F3CR	Forta D 15	0.30	170	21	35	20.3	2428	38	3.3	2.2

TESTS FOR FRESH CONCRETE

The freshly mixed concrete was tested for slump (ASTM C143), air content (ASTM C231), fresh concrete unit weight (ASTM C138), as well as concrete temperature and vebe time.

TESTS FOR HARDENED CONCRETE

The cylinders were tested for compressive strength at 7 and 28 days, according to ASTM C39. They were also tested for the static modulus (ASTM C469), pulse velocity (ASTM C597), and unit weight.

Beams were tested for static flexural strength, third-point loading was applied to the beams per ASTM C1018. The span length was 150 mm (12 in.). Deflection was measured at midspan using a dial gauge accurate to 0.002 mm (0.0001 in.). The test was a deflection-controlled test, and the rate of deflection was kept in the range of 0.05 to 0.1 mm (0.002 to 0.004 in.)/min per ASTM C1018. Loads were recorded at every 0.05-mm (0.002-in.) increment in deflection until the first crack appeared, after which loads were recorded at regular intervals. The maximum load reached was called the "first crack load." From loads and deflections obtained from the tests, load deflection curves were drawn and toughness indexes were calculated from the load deflection curves.

The flexural toughness factor and equivalent flexural strength were calculated using the Japanese standard method.

TOUGHNESS

To measure the influence of fibers on flexural strength and the toughness, the United States and Japan prescribed similar bending tests in which the load was to be recorded at specified deflections of the specimen. Both countries used third-point loading configuration. However, the values obtained from these two countries' standards differed considerably. The two methods used were ASTM C1018 and Japanese standard JCI-SF4.

The ASTM method is dependent on the accurate determination of δ, where δ is the deflection up to the first crack. The value of δ is very small, usually in the order of 0.03 to 0.1 mm (0.0019 to 0.0039 in.). The toughness indexes I_5, I_{10}, and I_{20} were calculated using the ASTM method.

When using the Japanese method, the test should be continued until a deflection equal to 1/150 of the span is reached. That deflection is equal to 2 mm (0.08 in.) for a 150-mm (12-in.) span length. The deflection thus obtained is greater than what is measured by the ASTM standard method. The flexural toughness factor and equivalent flexural strength are calculated with the Japanese standard method.

If toughness calculations are made from midpoint deflections, the resultant energy value marginally overestimates the true energy absorbed by the specimen.

RESULTS AND DISCUSSION

Observed Fresh Concrete Properties

The CFP fiber used in the program performed well. Even though the fibers, cement, and water were added into the mixer all at once, no balling occurred. That was because of the low aspect ratio created by the collation of the fibers. The mixing action caused the bundles to open up and expand and form a fiber mesh of individual fibers, which spread uniformly throughout the concrete mix. The fresh concrete with fibers was observed to have very little surface bleeding and no segregation.

Workability

Slump and vebe time tests were conducted to determine the workability of the concrete mixes. Vebe time is used to measure the workability of concrete based on the energy needed to compact the concrete. Test results indicated that satisfactory workability can be maintained even with increased fiber content. Workability was maintained by adjusting the amount of superplasticizer without causing any change in the strength of the concrete. The following amounts of superplasticizer were added to the concrete mixes: 150 cc for plain concrete, 180 cc for 0.1 percent fiber content, 190 cc for 0.2 percent fiber content, and 270 cc for 0.3 percent fiber content. The water to cement ratio was maintained at 0.42. The test results for slump, unit weight, air content, and vebe time are given in Table 1.

The fiber-reinforced concrete was placed with relative ease and compacted using a vibrating table. The tests conducted on fresh fiber-reinforced concrete basically were aimed at determining the workability of each mix with different fiber contents. The room temperature, humidity, and the concrete temperature were noted to make sure that the mixing of the fiber-reinforced concrete mixes was done under similar conditions. The room temperature varied from 17°C to 21°C (64°F to 70°F), the humidity varied from 30 to 65 percent, and concrete temperature varied from 18°C to 22.8°C (64.4°F to 73.2°F).

Slump Versus Air Content

The relationship between the slump and air content is shown in Figure 1. The slump and air content are directly proportional, (i.e., as the slump increases the air content increases.) A linear regression analysis showing the relationship is illustrated in Figure 1.

Slump Versus Vebe Time

Figure 2 shows the relationship between slump and vebe time. The slump and vebe time are inversely proportional, (i.e., as the slump increases the vebe time decreases). A linear regression analysis showing the relationship is illustrated in Figure 2.

Fresh Concrete Unit Weight

The results of the fresh concrete unit weight are given in Table 1. The average unit weight of all mixes with fibers was 2408 kg/m^3 (150 lb/ft^3); whereas the unit weight of fresh concrete without fibers was 2416 kg/m^3 (150.52 lb/ft^3). The average values indicate that there was no significant difference in the unit weight as the fiber content increased from 0.1 to 0.3 percent by volume. It can be presumed that the superplasticizer enhanced consolidation of mixes with higher fiber content. The measured air contents were ranged from 2.2 to 3.1 percent.

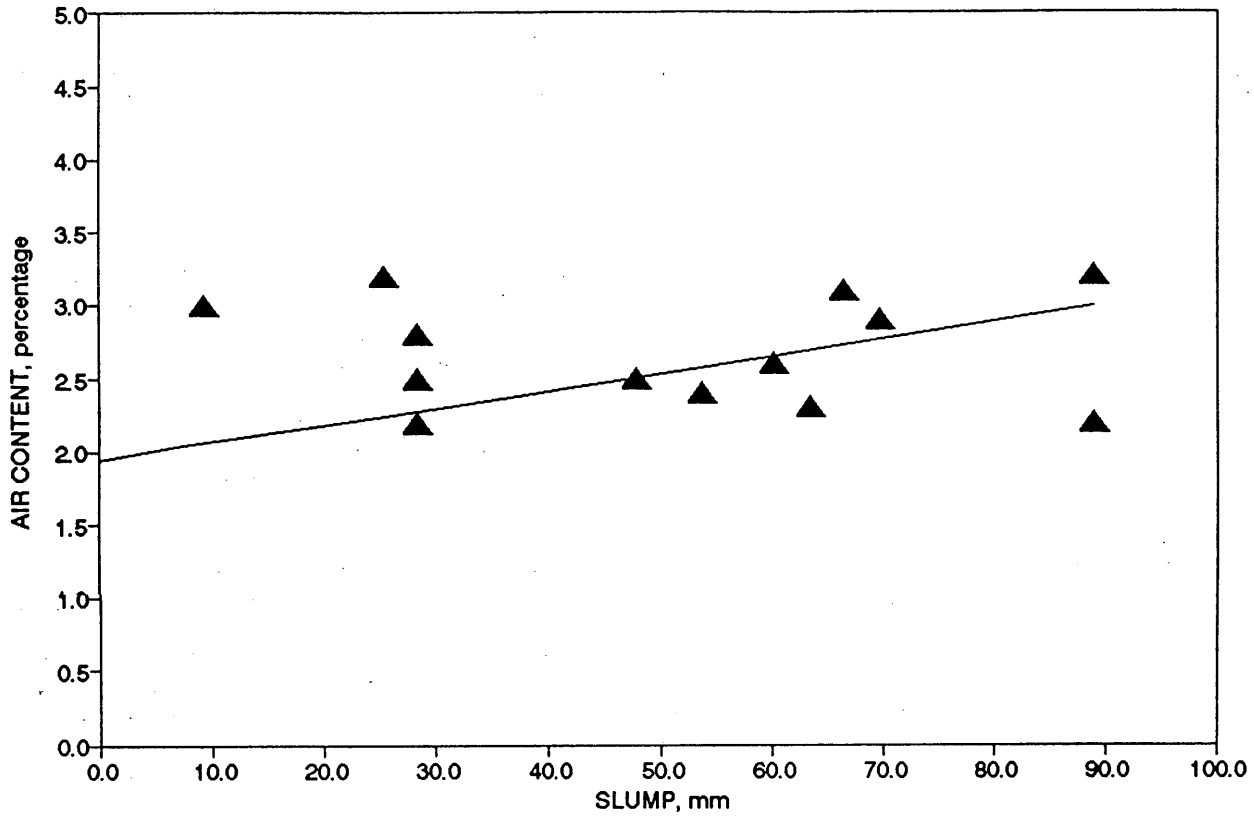

FIGURE 1 Slump versus air content for all mixes.

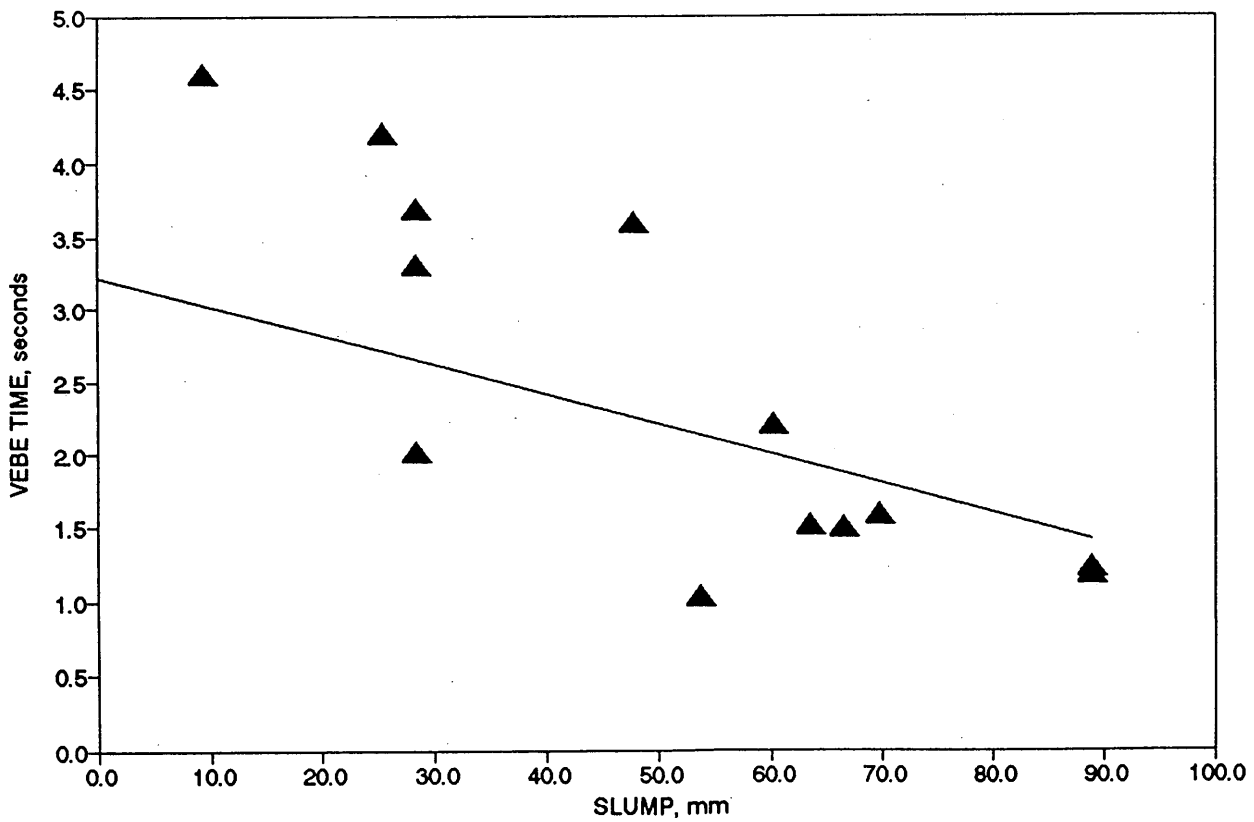

FIGURE 2 Slump versus vebe time for all mixes.

Finishability

Good finishability was obtained with collated fibrillated polypropylene fibers by suitably adjusting the amount of superplasticizer to get the required consistency. As observed, the fibers are coated with the mortar and cement paste. The more fibers introduced to the mix, the greater the mortar portion that is required. The factor does not come into play for the 0.3 percent by volume introduction rate. In fact, no change was required in the mixture proportions for the 0.3 percent by volume fibers.

HARDENED CONCRETE PROPERTIES

Compressive Strength

Compressive strength test results for the plain and fiber-reinforced cylinders are given in Table 2 and Figure 3. The test results indicate the polypropylene fiber-reinforced concrete has slightly higher values than plain concrete except for the 0.2 percent by volume mixes.

As the fiber content increased from 0.1 to 0.3 percent by volume, there was approximately a 5 percent increase in compressive strength. That range is within the experimental variation possible for concrete work. Hence, it can be stated that the addition of fibers did not influence the compressive strength of the concrete.

Flexural Strength

The 7- and 28-day flexural strength results are shown in Table 2 and Figure 3. The flexural strength was slightly higher for polypropylene fiber-reinforced mixes than for the plain concrete in all cases.

Results reported by others indicate there can be a slight reduction in flexural strength with the addition of fibers. The reduction may result from a number of factors, including improper compaction, inadequate mortar, or the lack of bond by fiber, either because of improper length or configuration. The latter would reduce the fibers' ability to modify the cracking and shrinkage.

Static Modulus

The static modulus test results are presented in Table 2 and Figure 3 and indicate that there was less than 5 percent difference between polypropylene fiber-reinforced concrete cylinders and the plain concrete cylinder. The static modulus of plain concrete was the same as that of the fiber reinforced concrete; addition of fibers did not cause any change in the static modulus.

Pulse Velocity

The pulse velocity test served as a good quality-control procedure and produced consistent results.

Pulse velocities are shown in Table 2 and Figure 4. Average pulse velocity for the polypropylene fiber-reinforced beams with 0.1 volume percent fibers was 4909 m/sec (16,096 ft/sec).

There was no difference in the propagation of compressional waves through the beams as the fiber contents were increased from 0.1 to 0.3 volume percent. The average pulse velocity for the plain concrete beams was 4808 m/sec (15,766 ft/sec).

TABLE 2 Hardened Concrete Properties

Mix	Compressive Strength, MPa		Flexural Strength, MPa		Static Modulus, MPa x 10^3		Pulse Velocity m/sec		Unit Weight kg/m^3	
	7- Day	28-Day	7- Day	28-Day	7- Day	28-Day	7- Day	28-Day	7- Day	28-Day
PL	39.13	48.23	3.75	4.06	42.72	36.58	4504.24	4815.03	2435.38	2427.27
	39.73	48.50	4.54	3.99	33.76	35.62	4725.67	4791.85	2437.00	2427.27
	40.65	49.26	4.40	4.61	36.31	36.86	4585.37	4850.72	2425.65	2437.00
Av.	39.89	48.66	4.07	4.51	37.62	36.37	4571.34	4808.63	2432.67	2430.51
F1C	43.46	52.86	4.89	4.87	37.13	36.86	4671.68	4895.86	2454.84	2456.46
	43.77	51.53	4.89	5.66	36.58	33.14	4772.64	4926.36	2466.19	2459.70
	44.11	53.22	5.16	5.37	36.79	36.86	4770.50	4925.14	2458.08	2456.46
Av	43.78	52.54	4.98	5.30	36.86	35.62	4738.17	4915.68	2459.70	2457.54
F2C	37.24	44.29	4.58	4.99	32.58	36.72	4692.73	4795.82	2461.32	2446.73
	36.62	48.91	4.48	5.23	32.86	33.55	4636.91	4908.67	2461.32	2445.11
	38.91	48.04	4.78	4.96	32.31	36.65	4785.75	4902.26	2467.81	2446.73
Av	37.59	47.08	4.61	5.05	32.58	35.62	4705.23	4869.02	2463.48	2446.19
F3C	44.27	52.35	4.92	5.81	35.62	36.03	4784.23	4939.78	2451.60	2456.46
	43.89	48.36	4.96	4.95	36.17	36.65	4718.65	4922.39	2454.84	2448.35
	44.27	51.50	5.13	5.80	36.93	36.79	4725.67	4947.10	2456.46	2461.32
Av	44.14	50.73	5.00	5.52	36.24	36.51	4742.75	5109.66	2454.30	2455.37

Note: The values given are the averages of original and replicate mixes.

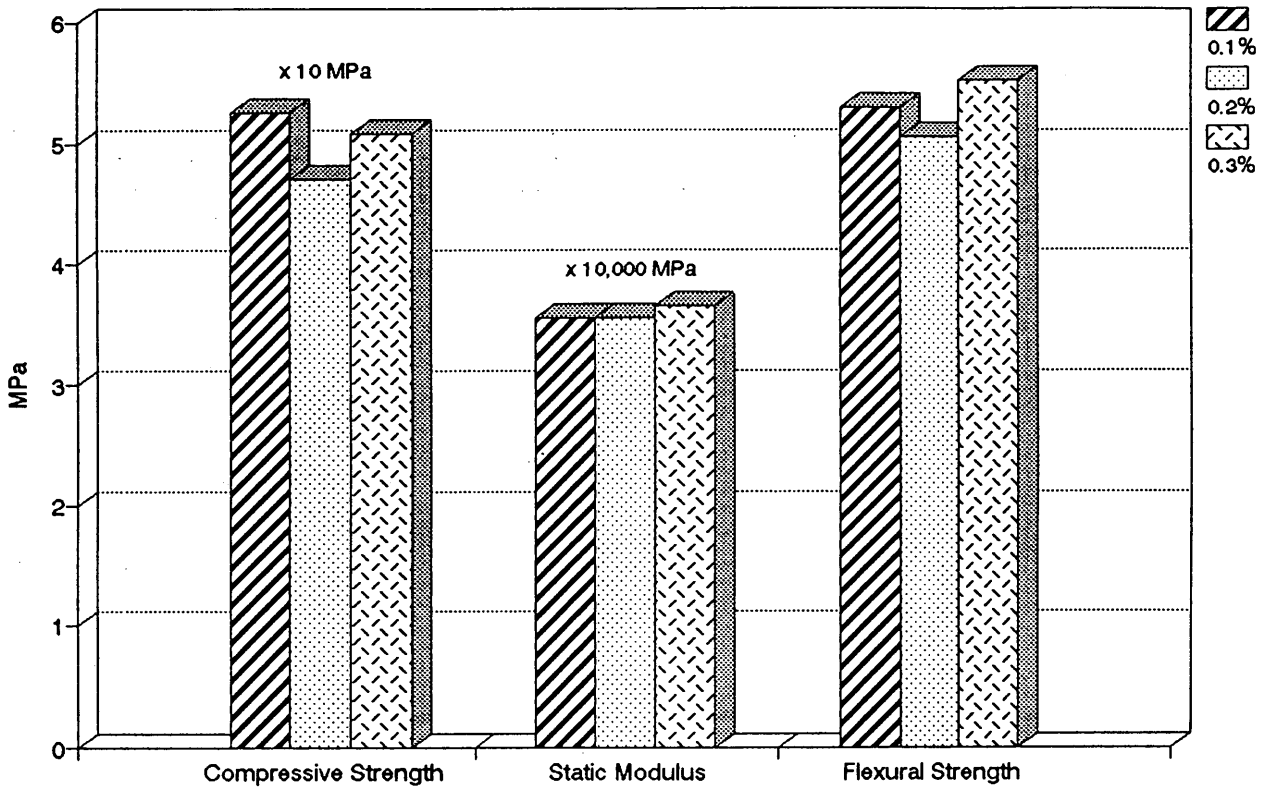

FIGURE 3 Comparison of compressive strength, static modulus, and flexural strength for different fiber contents.

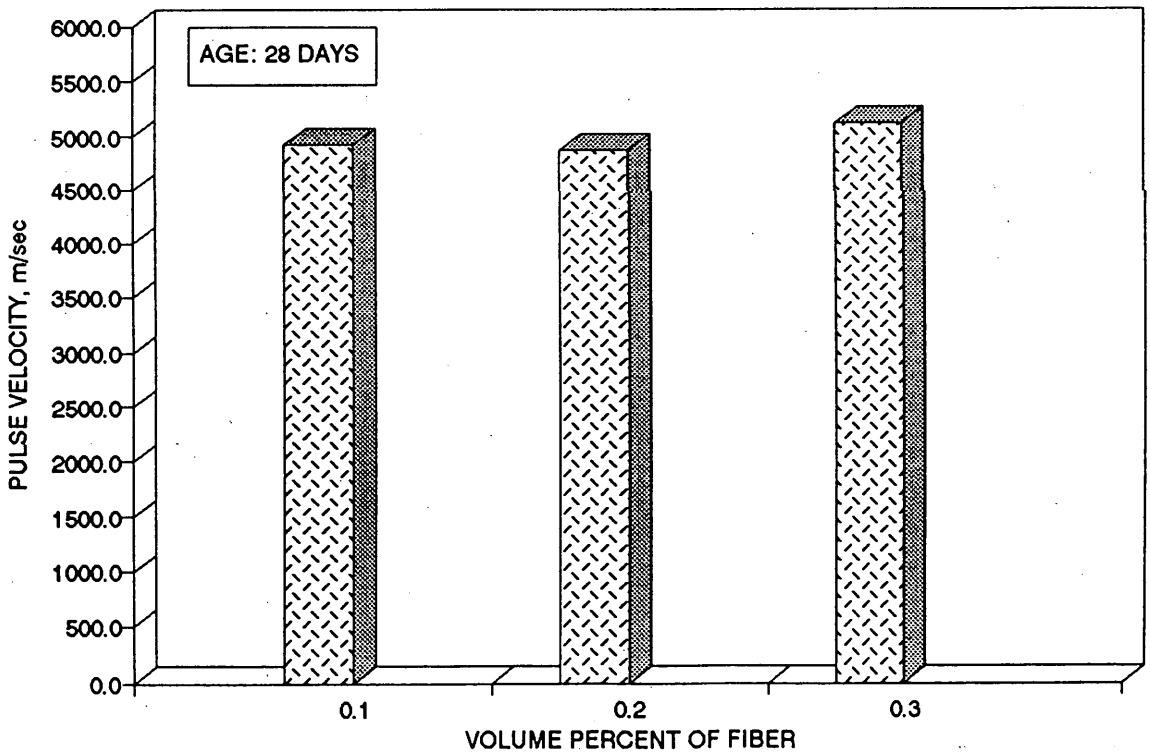

FIGURE 4 Pulse velocity versus fiber content.

Load-Deflection Behavior

Figure 5 shows the load deflection curves for the polypropylene fiber-reinforced concrete beams. The area under the load deflection curve represents the energy absorbed by the beam.

The load deflection curves indicate that elasto-plastic behavior improved as the fiber content was increased. All the plain concrete beams failed immediately after the first crack formed, as would be expected.

Another important observation is that the load deflection curves become nonlinear before any visible signs of material distress. However, the rate at which the moment of inertia deteriorated when the first crack appeared, was lessened by the fibers, because the fibers resisted the propagation of cracks. The crack widths were smaller as fiber content increased. That indicates the energy-carrying capacity or the toughness of the beams increased with an increase in fiber content.

Although only small quantities of fiber were used in this research project, test results and behavior of the load deflection curves indicate that the flexural strengths and toughness indices of fiber-reinforced concrete are approximately 18 percent greater than for plain concrete.

Toughness Indexes (ASTM C1018)

The calculated toughness indexes are given in Table 3 and Figure 6.

The I_{10}/I_5 and I_{20}/I_{10} ratio results (Figure 7) indicate that, even though the specimens were not perfectly elasto-plastic, the fiber reinforced beams achieved a good measure of ductility and post-crack plastic behavior. The results also indicate that there was no significant improvement in the behavior of the beams as the volume percent of fiber was increased from 0.1 to 0.3. That could be because only a small amount of fiber was used in the investigation.

Statistical analysis indicated that good quality control was maintained in the casting and testing operation.

JAPANESE STANDARD METHOD

Flexural Toughness Factor

The values of the flexural toughness factor are given in Table 3 and Figure 8. The Japanese standard method, unlike the ASTM method, specifies the deflection as equal to $1/150$ of its span. The span for beams used in this investigation was 150 mm (12 in.). The deflection measured using this method was much greater than what was measured using the ASTM method.

Equivalent Flexural Strength

The Japanese method provides a better comparison of toughness for concretes with different fiber contents than does the ASTM method. As the fiber content increased, the flexural toughness factor and the equivalent flexural strength values also increased (Figure 9).

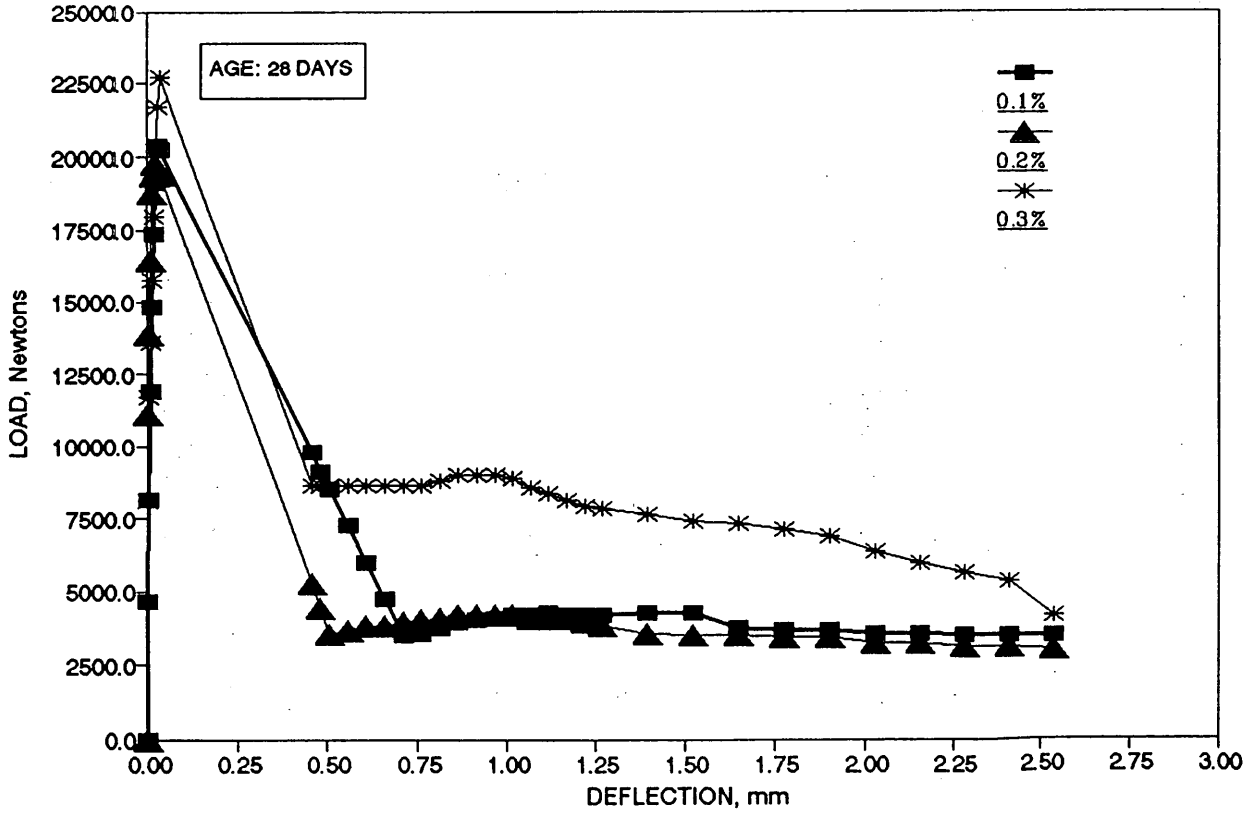

FIGURE 5 Load deflection curves versus fiber content.

TABLE 3 Toughness Indexes (ASTM) and Strength (Japanese Standard)

Mix	Toughness Indexes (ASTM)								Japanese Standard	
	I5		I10		I20		I10/I5	I20/I10	Flexural Toughness x 10^3 N-mm	Equivalent Flexural Strength, MPa
	7-Day	28-Day	7-Day	28-Day	7-Day	28-Day	28-Day	28-Day	28 - Day	28 - Day
F1C	3.64	3.89	6.69	6.45	11.36	11.57	1.69	1.79	13.11	1.72
	3.05	4.38	5.00	8.02	8.48	13.38	1.84	1.68	13.45	1.80
	3.22	3.84	6.33	6.71	11.29	10.88	1.75	1.62	13.56	1.82
Av	3.30	4.04	6.01	7.06	10.38	11.94	1.76	1.70	13.37	1.78
F2C	3.48	4.13	6.17	7.26	9.82	12.26	1.77	1.69	17.40	2.35
	3.57	3.54	6.45	6.60	10.50	10.71	1.85	1.64	13.67	1.86
	3.60	3.71	5.89	7.12	9.74	11.79	1.92	1.65	17.29	2.34
Av	3.55	3.79	6.17	6.99	10.02	11.58	1.85	1.66	16.12	2.18
F3C	3.46	3.50	6.58	6.65	11.51	11.05	1.90	1.67	20.34	2.84
	3.68	3.20	6.88	5.97	11.34	10.47	1.87	1.77	20.23	2.80
	3.90	3.40	7.00	6.42	11.51	10.73	1.89	1.67	18.98	2.62
Av	3.68	3.36	6.82	6.34	11.45	10.75	1.89	1.70	19.85	2.75

CONCLUSIONS AND RECOMMENDATIONS

The workability of the fresh fiber-reinforced concrete mixes can be maintained by adding suitable amounts of superplasticizer. No balling of fibers occurred during mixing. There was no problem in placing and finishing the concrete. The mortar portion of the mix did not need to be increased to accommodate up to 0.3 percent by volume of the CFP fiber (FORTA CR Type D-15).

The compressive strength of the concrete was not significantly affected by the addition of fibers. The static modulus, pulse velocity and unit weight for the fiber-reinforced concrete was less than five percent above that of plain control concrete specimens.

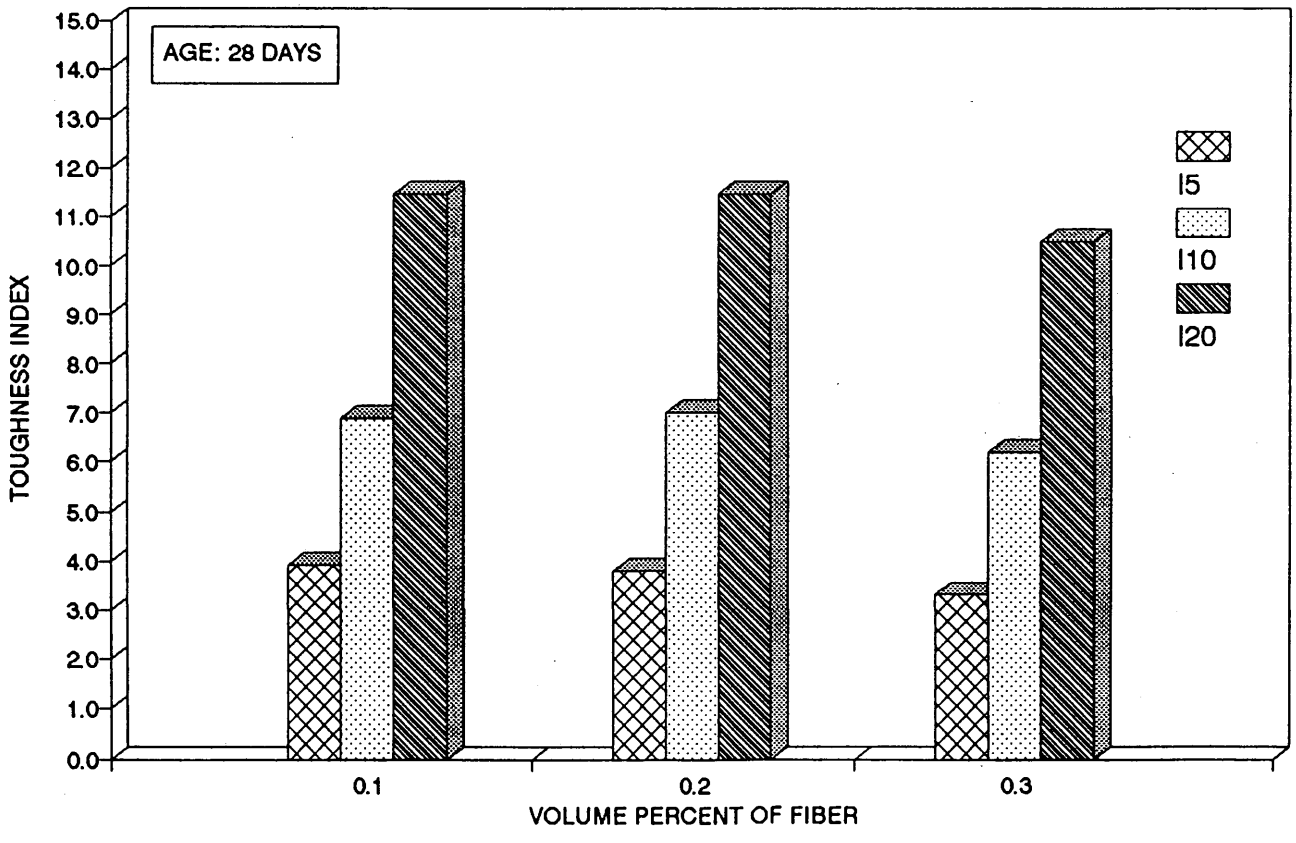

FIGURE 6 Toughness indexes versus fiber content.

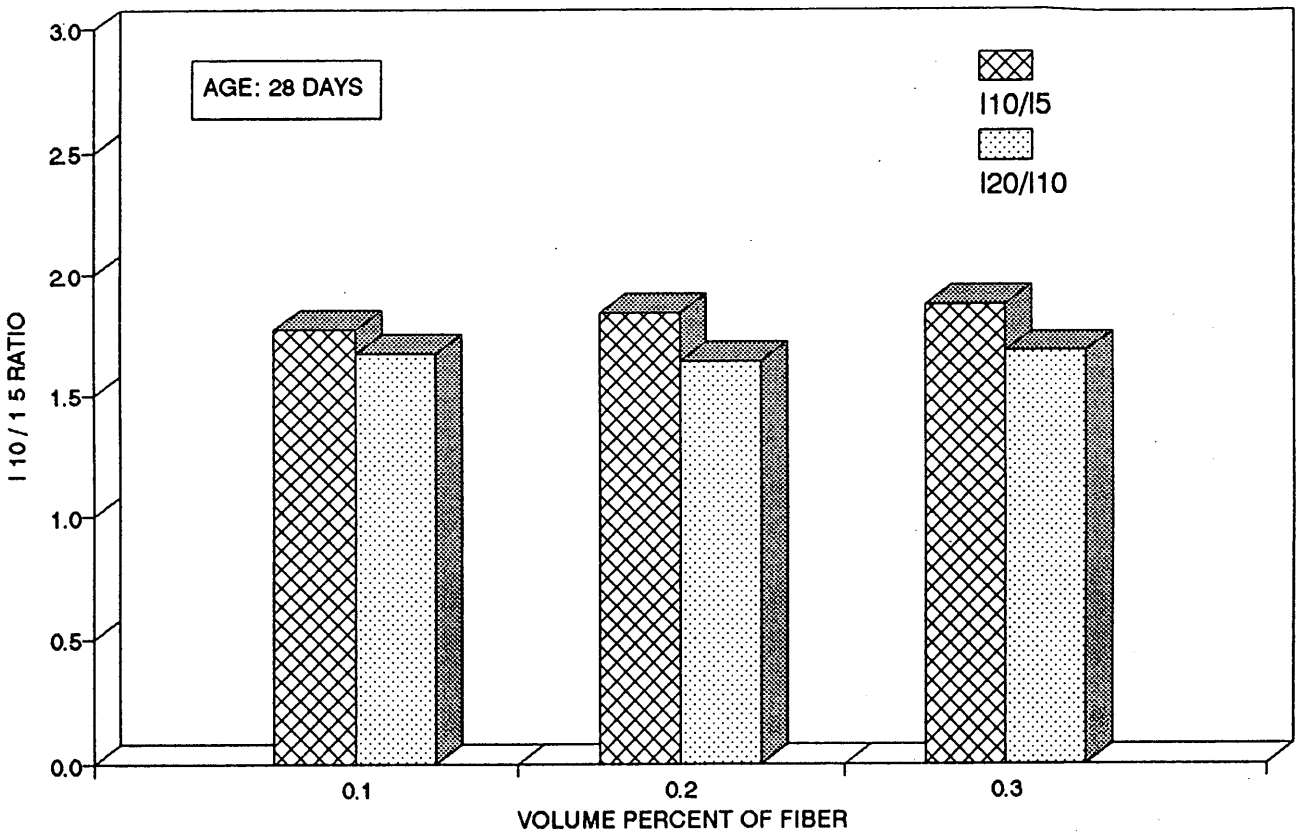

FIGURE 7 Toughness indexes ratios versus fiber content.

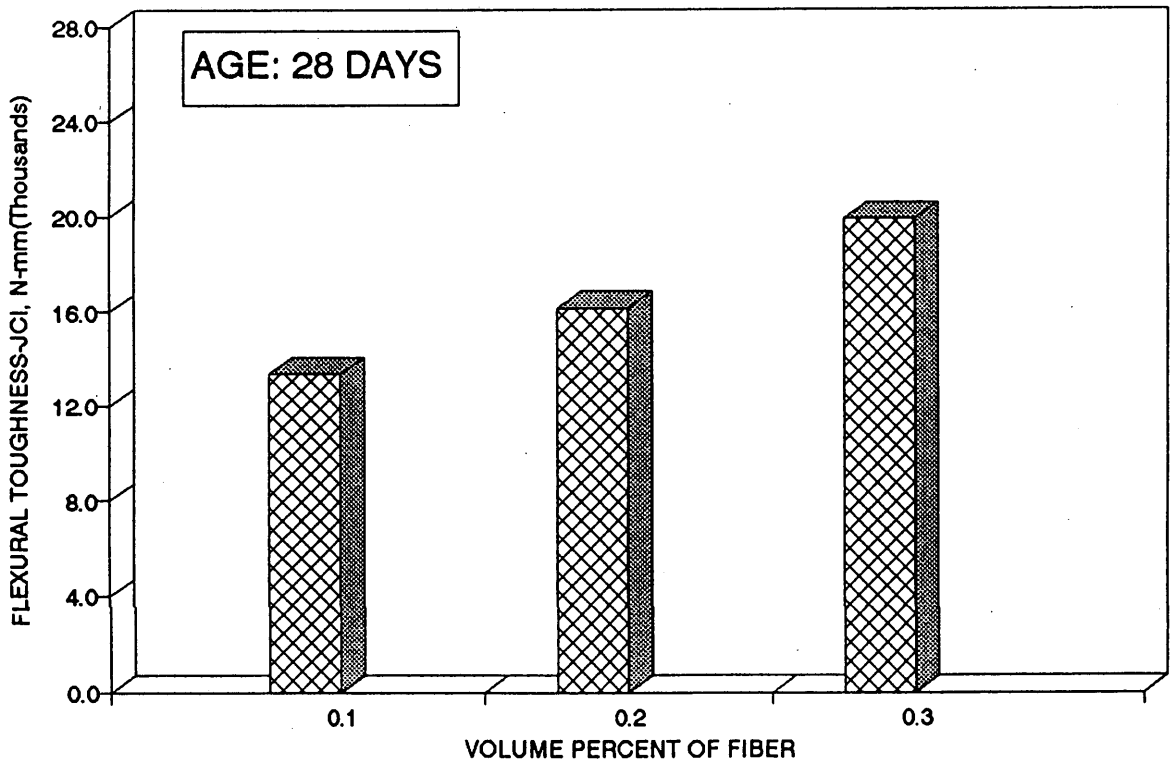

FIGURE 8 Flexural toughness factor (Japanese standard) versus fiber content.

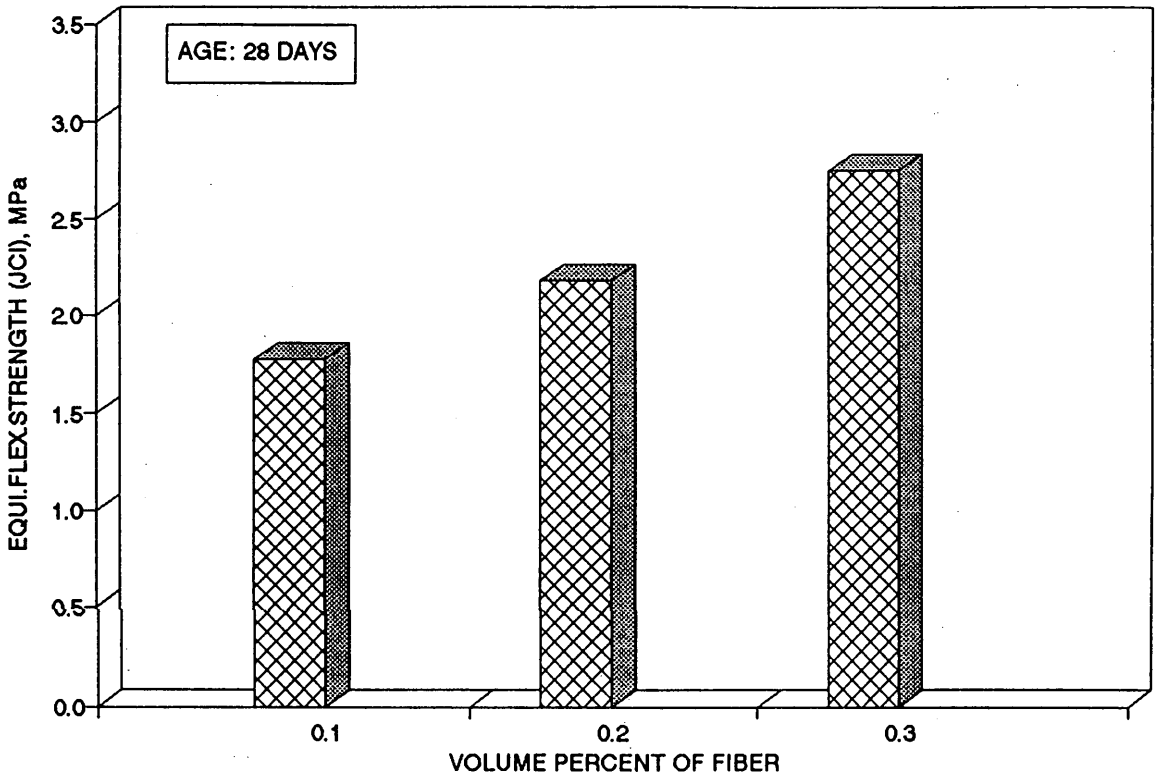

FIGURE 9 Equivalent flexural strength (Japanese standard) versus fiber content.

The ductility of the concrete was increased with the addition of fibrillated polypropylene fiber. The increase in ductility was proportional to the increase in dosage fiber.

The first crack strength and the static flexural strength increased slightly as the volume percent of the fiber was increased from 0.1 to 0.3. The ASTM toughness indexes, I_5, I_{10}, and I_{20}, showed that the fiber-reinforced concrete beams had an elasto-plastic behavior when subjected to flexural loading.

There is no doubt that improvements in the flexural strength and toughness of concrete with the addition of fiber will extend its application in structures such as bridge decks and highway pavements. Nevertheless, addition of fiber represents an additional cost. Therefore the optimum fiber content should be determined by future research.

Effects of fiber length on the performance characteristics of concrete reinforced with standard and modified polypropylene fibers at high fiber volumes merits additional study.

ACKNOWLEDGMENTS

The authors' research was conducted at the Civil Engineering Department of the South Dakota School of Mines and Technology and was partly funded by the Forta Corporation. The authors are grateful to Chowdhary S. Gondy for his help in the experimental work and to Sidhesh Kakodkar for his help in preparing the paper.

REFERENCES

1. Ramakrishnan, V. Materials and Properties of Fiber Reinforced Concrete. *Proc., International Symposium on Fiber Reinforced Concrete,* Madras, India, Dec. 16–19, 1987.
2. Ramakrishnan, V., W. V. Coyle, V. Kulandaiswamy, and E. K. Schrader. Performance Characteristics of Fiber Reinforced Concrete with Low Fiber Contents. *ACI Journal Proceedings,* Vol. 78, No. 5, Sept–Oct. 1981, pp. 384–394.
3. Ramakrishnan, V., S. Gollapudi, and R. Zellers. Performance Characteristics and Fatigue Strength of Polypropylene Fiber Reinforced Concrete. In *Fiber Reinforced Concrete; Properties and Applications,* Special Publication SP105, American Concrete Institute, Detroit, Mich. 1987, pp.159–177.
4. Ramakrishnan, V., G. Y. Wu, and G. Hosalli. Flexural Behavior and Toughness of Fiber Reinforced Concrete. Presented at 68th Annual Meeting of the Transportation Research Board, Washington D.C., Jan. 1989.
5. State of the Art Report on Fiber Reinforced Concrete. Special Publication SP44, American Concrete Institute, Detroit, Mich. 1974, 550 pp.
6. Ramakrishnan, V., G. L. Vandran, and N. Mulphuri. Fatigue Strength of Polypropylene Fiber Reinforced Concrete. In *Fiber Reinforced Cements and Concretes, Recent Developments,* R.N. Swamy, and B. Barr, eds. 1989, pp.533–541.
7. Mulphuri, N. Performance Evaluation of Fatigue Properties of Polypropylene Fiber Reinforced Concrete; An Experimental Investigation. M.S. thesis. South Dakota School of Mines and Technology, Rapid City, 1988.
8. Yongxin, L. Properties of Polypropylene Fiber Reinforced Concrete and Effects of Fiber Length, An Experimental Investigation. M.S. thesis. South Dakota School of Mines and Technology, Rapid City, 1988.

Publication of this paper sponsored by Committee on Mechanical Properties of Concrete.

Stabilization and Solidification of Contaminated Soils and Sludges Using Cementitious Systems: Selected Case Histories

MICHAEL MACKAY AND JOHN EMERY

Practical stabilization and solidification of soils and sludges exhibiting contamination from heavy metals or organic compounds can be accomplished using readily available, conventional, or byproduct cementitious (hydraulic or pozzolanic) materials, such as portland cement, slag cement, cement kiln dust, lime kiln dust, hydrated lime, and fly ash. Case histories are presented documenting the use of various combinations of cements, fly ash, and byproduct kiln dusts, since the mid-1970s to stabilize and solidify a wide range of contaminated materials. Such materials include PCB-contaminated granular road base, steel industry sludges, contaminated lake-bottom sediments, rotary kiln slag from a secondary lead smelter (acid battery reclaimer), and a very wet former fly ash fill site. Stabilization processes developed have enabled treated materials to satisfy environmental and engineering requirements. Field testing, laboratory stabilization process development, and process implementation (pilot and full-scale) are discussed.

Contaminated land is the legacy of the industrial prosperity and urban development of the past century. People, particularly those in industry, are acutely aware that many waste-handling and management practices followed previously and considered appropriate at the time were not adequate. Soil and groundwater in urban areas worldwide are contaminated with a variety of undesirable compounds that result from industrial processes and disposal of municipal refuse: hydrocarbon products; heavy metals; organic compounds; byproducts such as municipal incinerator ash, fly ash, and bottom ash from coal-fired thermal power generation; industrial and sewage sludges; and other more hazardous materials. As public and scientific awareness of the contamination problem increases, and as economic pressures in urbanized areas push up the value of even severely contaminated real estate, site remediation has become a major technical interest. Although there is a wide variety of remediation options available, only two are currently considered established technologies by the United States Environmental Protection Agency (EPA): high-temperature incineration, and stabilization and solidification. The EPA considers all other technologies for site remediation innovative (*1*).

REVIEW OF STABILIZATION AND SOLIDIFICATION TREATMENT TECHNOLOGY

Stabilization of contaminated materials generally involves two distinct components, stabilization, whereby the mobile contaminants are complexed to prevent them from dissolving in the groundwater, and solidification, whereby the stabilized materials are encapsulated to limit exposure and form a monolithic mass protecting them from long-term deterioration in the soil or groundwater in which they are placed. Many concepts involved in stabilization are similar to those involved in the cement and concrete industry, and positive stabilization results can usually be achieved using common cementitious (portland cement, slag cement, hydrated lime), pozzolanic (fly ash, silica fume), or byproduct (cement kiln dust, lime kiln dust) materials.

Methods involved in the stabilization of soils exhibiting high metal concentrations must consider several items to ensure satisfactory stabilization and permanent solidification. Leachable metals must be stabilized by complexing them in their least soluble form. For many common metals, stabilization requires that the pH of the material be limited to a level of minimum solubility for the metals of concern. Most metals are polyvalent, and therefore, amphoteric, which means that the hydroxide compounds formed can act as either acids or bases. At pH levels outside of a relatively narrow band (7 to 11), some hydroxide compounds can break down; the liberated metals become mobile and can enter subsoil or groundwater. Therefore, in stabilizing such a material, it is necessary to provide an environment within a pH band that minimizes solubility of metal hydroxides. The final pH of the stabilized material must remain within this limited pH band also, and the physical characteristics of the stabilized material must resist changes in surface and groundwater conditions and contact water pH to have long-term durability.

In conjunction with the formation of meta-stable metal hydroxide compounds, it may be necessary to complex the metals in more stable forms. For example, metal silicate compounds can be formed that are nearly insoluble across a wide pH range. Several proprietary chemical fixation systems for metals and metal hydroxide wastes involve adding soluble sodium silicates and silicate setting agents to assist the stabilization process (Chemfix, Hazcon, K20/LSC, Sorbond, Petrifix, and Soliditech are some examples). However, portland cement, fly ash, and other supplementary cementitious materials also contain varying amounts of silica; they react with metals and each other to form stable metal silicate compounds. Their interaction is considered in selecting a suitable additive for stabilization. The EPA Superfund Innovative Technology Evaluation program currently is evaluating several stabilization and solidification processes that involve proprietary (silicate-based) additives. Early indications are that the proprietary additives do not significantly improve the effectiveness of stabilization over that of encapsulation (solidification) using cementitious stabilizing agents (*2*).

John Emery Geotechnical Engineering Limited, #1, 109 Woodbine Downs Boulevard, Etobicoke, Ontario M9W 6YI, Canada.

After stabilization of metal-contaminated soils and sludges, solidification or fixation of the material often is necessary to facilitate materials handling and minimize contact between the stabilized material and surrounding environment after landfilling. Relatively loose, dry contaminated material may be difficult to safely handle (because of blowing and dusting problems) and require the addition of water. Water itself may leach heavy metals from material and represents another potential waste stream to be considered. Solidification allows the waste and associated moisture to be treated together. Note that it is often necessary to add additional moisture to adjust pH and assist cementitious reactions (hydration). Resulting material then can be landfilled, forming a large impermeable monolithic mass. By this, it is implied that the contact area of the stabilized material with the surrounding soil and surface groundwater is minimized, which greatly reduces the leaching potential of the contaminated material. Updates from the North Atlantic Treaty Organization Committee on Challenges of Modern Society pilot study indicate that reduced leachability of contaminants after stabilization and solidification treatment is largely the result of entrapment (encapsulation) of contaminants within the cementitious matrix, rather than chemical binding to the matrix (*2*). Encapsulation also can serve to contain organic compounds that may be present in the contaminated soil, although that is a technically controversial issue, particularly with respect to controlling air emissions (volatilization) during treatment, and the lack of standard methods for evaluating the extent to which organics actually have been treated.

Treatment alternatives available for heavy metals contamination are extremely limited. Whereas some reduction of heavy metals using bioremediation and soil washing/metals chelation techniques has been reported, stabilization and solidification methods still represent the best available technology for contamination involving heavy metals.

Various cementitious and byproduct materials are available that have been used successfully in the stabilization of hazardous wastes and contaminated soils. Use of them involves a number of combinations and proportions of contaminated materials, plus stabilizing additives depending on the physical characteristics of the contaminated material (consistency, moisture content, or gradation) and the toxic constituents (solubility potential or concentration). Selecting the process and associated stabilizing agents for a particular material contaminated with heavy metals is largely based on the ability of the fixative to control pH, both in the short-term (for several years) and long-term (for several decades), and thereby minimize solubility of ionic forms of heavy metals and metal hydroxides. Portland cement, slag cement, fly ash, hydrated lime, byproduct kiln dusts, silica fume, and steel slag fines can all be used as stabilizing agents, individually or in combination with other stabilizing agents or chemical fixatives (usually proprietary). The most appropriate stabilizer is selected on the basis of physical and chemical characteristics of the waste and overall treatment economics. The Environment Canada Wastewater Technology Centre, with the support of the EPA and the Ontario Ministry of the Environment, published a proposed evaluation protocol for cement-based solidified wastes (*3*) that represents the most thorough laboratory assessment of the physical and chemical integrity of stabilized and solidified materials, short- and long-term.

CASE HISTORIES

Since the mid-1970s, a number of projects have documented successful use of conventional or byproduct cementitious (hydraulic or pozzolanic) materials for stabilization and solidification of a wide variety of wastes and contaminated materials. Several projects were selected to represent a range of wastes and contaminated materials and to demonstrate the effective use of cementitious systems for stabilization of heavy metals and organic contaminants and the subsequent solidification of a variety of soil and sludge types and moisture conditions (dry to near fluid). Case histories are presented documenting the use of various combinations of cements, fly ash, and byproduct kiln dusts to stabilize and solidify PCB-contaminated road base, steel industry sludges, contaminated lake-bottom sediments, rotary kiln slag from a secondary lead smelter (acid battery reclaimer), and a very wet former fly ash fill site.

PCB-Contaminated Road Base, Lake Clear, Ontario

In 1981 and 1982, investigations of unusually high concentrations of PCB in fish in Lake Clear led to the discovery that PCB-laden waste oil had been used for dust control on several gravel roads adjacent to the lake. Relatively high levels, in the range of 50 to 700 μg/g, were identified in the upper levels of the granular roadbase, shoulders, and ditch of two sections of road, the total length of which is about 8 km. The high PCB concentrations at the surface decreased to about 1 μg/g at a depth of about 0.5 m. The total volume of contaminated material involved was estimated to be about 6 260 m^3 (*4*).

The remediation approach accepted by the Ontario Ministry of the Environment was to subexcavate the contaminated material and incorporate it into a very low permeability monolithic mass and place it in a suitably designed site. The following criteria were established for the remediation:

- Contaminated soil was to be stabilized into a solid mass having a permeability of less than 1×10^{-7} cm/sec;
- Any off-site migration was to be within acceptable limits (PCB concentration in groundwater less than Ontario Drinking Water Quality Objective of 3 μg/1); and
- If considered appropriate after technical evaluation, the disposal site was to be on an identified parcel of crown land about 600 m from the lake.

To meet the disposal criteria for the estimated 6 260 m^3 of contaminated material, a laboratory mix design and bench scale testing program was completed by the authors, with the overall objectives of (*a*) encapsulating the PCB-contaminated soil into a monolithic, durable mass to prevent the loss of free particles and (*b*) reducing the permeability of the mass to less than 1×10^{-7} cm/sec. A series of test specimens was prepared using normal Type 10 portland cement, bentonite, and cement-bentonite as prospective stabilizing and solidification agents. Small samples were mixed by hand in the laboratory and compacted (tamped) into 100-mm high by 100-mm diameter tobacco tins, sealed with a twist lid, placed in double plastic bags to maintain moisture conditions, and allowed to cure. Unconfined compressive strength development at 20°C was monitored using a pocket penetrometer. After a curing period, samples were submitted to an environmental laboratory for distilled water leach and Ontario Regulation 309 (acid) leachate extraction analyses.

On the basis of laboratory tests, it was concluded that satisfactory stabilization and solidification (acceptable reduction of leachable compounds and adequate solidification of the mixture) was achieved using 10 percent of portland cement by mass of dry soil. The mixture, when compacted to at least 95 percent Standard Proctor Maximum Dry Density, exhibited the desired very low perme-

ability and sufficient compressive strength to give good resistance to weathering and erosion. An alternative mix consisting of 12 percent cement kiln dust and 3 percent portland cement was also developed and confirmed to meet the basic design criteria after minor adjustments to the mix proportions.

Following the positive evaluation of the laboratory mix design and bench scale testing, a full-scale remedial work program was implemented. The subexcavation of the contaminated soils and road reconstruction were completed under one contract, and the mixing and disposal of the stabilized material were conducted under a separate contract. Tendering for the mixing and disposal of the contaminated material allowed the bidder to select the stabilization and solidification mixture, and the alternative 12 percent cement kiln dust to 3 percent portland cement mix was used. Contaminated soil was mixed with the stabilizing agents in advance using a central plant, then the mixture was transported, placed, and compacted at the disposal site using conventional soil-cement procedures. Before the contaminated soil was processed in the plant, any oversized rocks and boulders were removed by screening. The screened rocks and grubbing material were placed in layers in the middle of the compacted monofill. Contaminated materials and the stabilization and solidification mixture were monitored continuously using a field laboratory, measuring moisture content, compressive strength development (pocket penetrometer), and field compaction. The 4:1 cement kiln dust to portland cement ratio was maintained throughout, and the total amount of cement kiln dust and portland cement adjusted (increased) to ensure that a satisfactory moisture content was maintained for proper compaction (95 percent Standard Proctor Maximum Dry Density minimum).

The final volume of the stabilized and solidified monofill was measured to be 8 100 m^3, with the increase in volume of 1 840 m^3 (about 29 percent) attributed to the stabilizing agents and some native material picked up when cleaning up the work area. Of the 8 100 m^3, approximately 4260 m^3 was contaminated material processed through the mixing plant, and the remaining 3 840 m^3 was oversized rocks, boulders, and grubbing material.

The average PCB concentration of the contaminated soil after screening was determined to be about 21.5 μg. The monofill was situated at least 2m above the groundwater table in the unsaturated soil zone and, as such, was not in direct contact with the groundwater system. The monofill design promoted surface runoff and minimized infiltration by mounding and construction of a conventional soil-cement cap; solidification prevented the migration of PCB by subsurface movement of fines. The low permeability of the monofill further limits infiltration and hence minimizes the potential for leaching of PCB in the long term.

Theoretical computations were made to estimate the amount of PCB that could move off site under actual site conditions. Based on a PCB solubility of 0.4 μg/l for the average concentrations of contaminated soil representative of the monofill mass, it was calculated that the probable concentration of PCB in the groundwater following beneath the monofill was between 0.01 and 0.05 μg/l, which is well below the Ontario drinking water objective, 3 μg/l. Cost of remediation was about $850,000, using established technology and readily available equipment and procedures. The Ontario Ministry of the Environment considered the remediation an acceptable solution to containing PCB residues in Lake Clear.

Steel Industry Sludges and Contaminated Lake-Bottom Sediments

Expansion of a steel plant in Hamilton, Ontario, required the removal of a large quantity of a very soft, water-laden sludge and sediment mixture from an old harbor area and slip and its replacement with suitable fill to provide a construction site (*5*). Some treatment of the sludge sediment to meet landfill disposal requirements was required, and various stabilization methods were evaluated in the laboratory and small field trials before one was adopted. It was determined that the sludge sediment could be satisfactorily stabilized to meet both environmental (solubility of potential toxic constituents in accordance with Ontario Regulation 309) and engineering (bearing capacity) requirements for industrial fill applications. Thus, the reclamation process adopted for the old harbor area involved removing the sludge sediment by stone fill displacement below the water surface, dredging, stabilization, and either disposal to landfill or return to the site for fill above the water table. Other applications of the process also were developed, for use in stabilizing very soft sediments, basic oxygen furnace clarifier sludge, dust high in trace elements, or contaminated dredge spoils, for example.

Geotechnical studies indicated that the sludge sediment was fairly consistent in appearance along the harbor and slip; it was very loose, oily, black, organic, metallic (mainly from iron oxide) waste mixed with lake-bottom sediment, and its moisture content was highly variable (29 to 75 percent mass of water to total mass), as was its bulk density (1300 to 1650 kg/m^3) and loss on ignition (7 to 31 percent). Although most of the site's contaminants were of industrial origin (rolling mills), at early stages the slip received municipal sewage. The result was a rather unpleasant and variable industrial sludge and sediment mixture.

To give various strengths and rates of strength gain to the highly variable sludge and sediment, stabilization involved a number of possible combinations and proportions of sludges and sediments and stabilizing agents, such as fly ash, byproduct kiln dusts, steel slag fines, portland cement, and slag cement. Byproduct materials were used when possible, and either little or no portland cement was added, to minimize costs. Because the project involved nearly 300,000 m^3 of sludge and sediment, a wide range of byproducts was evaluated to ensure supply continuity.

Construction soil stabilization (soil-cement) concepts were adopted, which involve initial drying of the very wet sludges and sediments using high surface area materials (fly ash, kiln dusts), and then pozzolanic or hydraulic reactions as required. For disposal to landfill, just some drying and fairly low strengths (shear strength $\approx$ 0.01 to 0.02 MPa, equivalent to soft clay) were desirable, whereas for fill, initial handling strength and then high strength development (shear strength $>$ 0.1 MPa, equivalent to a very stiff clay) were required.

A simple laboratory program, similar to that described for the Lake Clear remediation, was developed so that a wide range of stabilizing agents and addition rates could be considered for field trials and costing. The approach is considered more representative of conditions in a large mass of solidifying material than open curing, for which significant strength development may result from simple drying instead of cementitious reactions. Supplemental tests monitored pH, moisture content, temperature and bulk relative density. Typical laboratory stabilization trials for a 46 percent moisture content sludge and sediment are summarized in Table 1.

The laboratory stabilization trial results meeting the strength requirements for landfill or fill indicate that, whereas high organic content was not stopping pozzolanic and hydraulic reactions, it was probably inhibiting them. Quick (unslaked) lime kiln dust is much more efficient in this respect than is ordinary calcitic or dolomitic lime kiln dust, and slag cements require a fair degree of alkaline activation. The 1980 additive costs were $2.00 to $4.00 per tonne of final stabilized material.

TABLE 1 Laboratory Stabilization Trials

Wt. % Sediment (wet)	Mass % Additives	Penetrometer Strength, MPa 1 Day	7 Day	14 Day	21 Day
80	15 lime kiln dust (quick) 5 portland cement	0.29	0.43	>0.43	>0.43
80	15 lime kiln dust (quick) 5 slag cement	0.25	0.31	0.41	0.43
80	15 cement kiln dust (bypass) 5 portland cement	0.04	0.42	0.43	>0.43
80	15 lime kiln dust 5 portland cement	0.12	0.20	0.22	0.24
80	15 fly ash (~ 8% carbon) 5 lime kiln dust (quick)	0.07	0.12	0.17	0.18
75	15 lime kiln dust 10 fly ash (~ 8% carbon)	0.16	0.27	0.30	0.34
75	20 cement kiln dust 5 portland cement	0.02	0.20	0.43	>0.43
75	15 fly ash (~ 8% carbon) 5 lime kiln dust 5 portland cement	0.12	0.24	0.43	>0.43
75	15 fly ash (~ 8% carbon) 5 lime kiln dust 5 slag cement	0.04	0.12	0.15	0.32

Larger bench scale testing was completed; it involved preparation of several large 90-kg samples and various stabilizing agents using an Eirich R-7 mixer that, using only drum rotation, simulated a large stabilization plant pugmill. Sealed curing and curing under a 0.8-m head of water were completed at a 7°C to 13°C temperature range to simulate cooler field conditions. The results supported the smaller-scale test methodology adopted.

Solubility of toxic constituents in the industrial sludge and contaminated sediment was evaluated using a very severe, modified Organization for Economic Cooperation and Development solubility test procedure (*6*) that determines the dissolution rate for each constituent of interest. The procedure involves leaching 1 g of sludge and sediment per 0.05 l of distilled water during five 24-hr cycles of vigorous (3 Hz) shaking, with the supernatant drawn off and filtered between cycles and submitted for chemical analysis.

Solubility test results indicated that stabilization reduced trace element constituent levels in all cases except Cu and Pb, but these were still well below the maximum allowable despite the very severe nature of the test, and the stabilized material was fully acceptable from an environmental viewpoint.

Pilot-scale and full-scale field implementations resulted in a final stabilization and solidification process consisting of (a) a chute that allowed excavated material to be fed into a standard ready-mix truck; (b) central additive storage silos for storing and adding the stabilization agents, with the most reactive agent added last to allow for visual control of initial stiffening; and (c) mixing and transporting for discharge at a designated location where strength monitoring was completed on the stabilized material. The ready-mix truck operation proved so efficient during pilot-scale testing that it was adopted in place of a large base stabilization plant for full scale implementation.

At its peak, six 14-yd^3 ready-mix trucks were used with about 1,000 t of sludge and sediment stabilized in an 8-hr shift. Optimum stabilizing agents (based on economics and availability, after first confirming strength development and stabilization capabilities) were determined to be 8 to 12 percent highly reactive byproduct quick (unslaked) lime kiln dust, and 3 to 5 percent slag cement (replacing portland cement). After successful stabilization of the harbor and slip materials, the process was used to stabilize very soft sediments from another area of the plant, and a similar fixed plant process was developed to stabilize basic oxygen furnace clarifier sludge on a continuous basis. In each case, the stabilized product was approved by the Ontario Ministry of the Environment for fill applications or landfilling, on the basis of a former unsaturated column leachate method (since replaced by the Ontario Regulation 309 Leachate Extraction Procedure). It was estimated that the cost of stabilization and solidification (in 1980 dollars) was about $8.00/t using byproduct stabilizing agents.

Rotary Kiln Slag from Secondary Lead Smelter (Acid Battery Reclaimer)

An acid battery reclaiming plant uses a long rotary kiln and soda ash lead-reduction approach to recover lead from spent batteries. The secondary lead smelting operation has a very low environmental impact; its SO_2 emissions are carefully controlled. Feed materials—primarily lead sulphate, lead oxide, and lead sulphide resulting from crushing of 3.5 million spent lead storage batteries per annum, with soda ash and iron added to capture sulphur in the rotary kiln slag plus coke as a reducing agent/energy source—are fed gravimetrically into the long rotary kiln operating at a temperature of about 1100°C. Resulting molten salt lead is tapped out into 60-tonne holding kettles, with the slag overflowing at the hot end of the kiln and into slag pots to cool. About 31 to 32 percent slag is produced per unit of bullion on average, or about 45 tonnes of rotary kiln slag per day (≈16,500 t/year).

Rotary kiln slag differs from conventional iron silicate lead slag produced by other primary and secondary smelters; it is low in silicates and iron, high in sulphur and sodium, and quite soft and friable. Shortly after being turned out of the slag pot, rotary kiln slag cools to a hard state in large chunks. The fresh slag reacts immediately on contact with air, oxidizing from the surface inward (expending heat). After several weeks of exposure to air and precipitation, rotary kiln slag breaks down to a consistency similar to very moist cohesive soil. The somewhat alkaline rotary kiln slag does not meet Quebec Ministry of the Environment landfill disposal requirements for solid waste (*7*), being slightly high in leachate test lead, and it is physically unstable until fully broken down, that is, after several weeks to months of exposure to air and precipitation. Rotary kiln slag is completely dry when turned out, but it retains about 60 percent moisture when fully broken down in an outdoor stockpile.

A bench scale testing program was developed to stabilize and solidify rotary kiln slag. A series of laboratory trials was completed for the aged, stored slag and the relatively unoxidized fresh slag to determine the optimum stabilization and solidification processes necessary to fully oxidize the slag, reduce the leaching of heavy metals, and durably solidify the material to meet Quebec Ministry of the Environment's requirements.

A series of laboratory trials was completed using several stabilizing agents and solidifiers, including portland cement (Type 10 and Type 50), fly ash, and hydrated lime, in various combinations and proportions. Initially, small samples were prepared in the same fashion as described for the Lake Clear and industrial sludge and

contaminated sediment projects. Because lead, and lead hydroxide solubility is particularly sensitive to changes in pH, as indicated in Figure 1 (*8*), the pH of the stabilized material must be maintained within a narrow range of about 9 to 11. Stabilization trials for the stored slag and fresh slag were completed separately, recognizing that the relatively unoxidized fresh slag had to be pretreated (aged) before stabilization and solidification.

The stored slag was variable in moisture content (approximately 35 to 60 percent by dry mass) and in physical characteristics, suggesting that the degree of aging throughout the stockpiled material was inconsistent. Forty stabilization trials were conducted to develop an optimum stabilization recipe based on pH, unconfined compressive strength development, appearance (density, porosity, permeability), and durability.

As a result of the trials, stabilization and solidification mixes incorporating fly ash were eliminated, (pH was too high and it had inadequate strength development. Larger 2-kg samples were prepared by mechanical mixing, using mixtures incorporating Type 10 portland cement with and without hydrated lime. For these trials, the moisture content of the stored slag was increased to 60 percent by mass to control pH and provide additional moisture to assist in oxidizing any unreacted slag pieces that were still present in the stored slag.

Throughout the testing program, samples were subjected to environmental analysis in accordance with Quebec Ministry of the Environment's leachate extraction test procedures. It is an agitated acid leachate extraction procedure similar to the USEPA EPTox procedure and the Ontario Regulation 309 Leachate Extraction Procedure. Test results indicated that stabilization and solidification using 10 percent Type 10 portland cement by wet mass of stored slag resulted in a material satisfying the Quebec ministry's requirements for solid waste.

Fresh slag presented a separate set of challenges. The presence of unreacted pieces in the fresh slag required that a prestabilization and solidification step be introduced into the process to rapidly age the slag before treatment, otherwise the material would not be stable, and subsequent slag expansion destroyed the cementitious matrix. Laboratory testing indicated that the fresh slag could be quickly broken down by adding water in stages (a maximum of about 90 percent by dry mass), in conjunction with regular mixing of the wetted slag to expose it to air. After about one week, the condition of the fresh slag was similar to that of the stored slag, allowing the fresh slag to be stabilized and solidified in the same way as the stored slag, using 10 percent Type 10 portland cement.

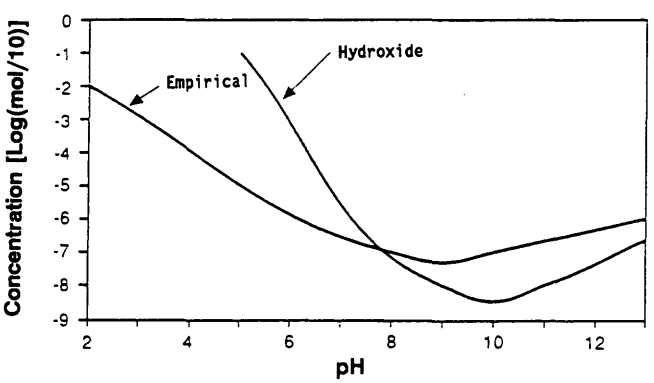

FIGURE 1 Solubility of lead versus pH in a cement/fly ash stabilization and solidification system (*8*).

The laboratory bench scale testing program was completed in June 1991. Pilot-scale field testing was completed at the plant in the fall of 1991, with similarly positive results for the stabilization and solidification. Results of the pilot-scale field testing indicated that the process for aging fresh slag needed refinement.

Former Fly Ash Fill Site

In 1967 or thereabouts, approximately 100,000 m^3 of Type C (low CaO) fly ash from Ontario Hydro's coal-fired thermal generating station was placed in a former sand and gravel pit situated in the northeast corner of metropolitan Toronto. The fly ash was innocuous from an environmental point of view (almost inert fill, with the exception of slightly elevated arsenic and boron levels). However, under Ontario Regulation 309 and its nonregistrable, nonhazardous limits, the fly ash is very loose and wet; as such, it is not suitable for the proposed construction of a large and prestigious commercial/industrial development. Reconditioning the fly ash fill is necessary if the material is to be used as engineered fill below road and parking lot areas.

Testing of the fly ash confirmed that its in situ moisture content was about 45 to 50 percent, and its consistency ranged from dry to near fluid.

Because of its relatively low CaO content, the fly ash fill material, although pozzolanic, does not possess significant hydraulic properties. Laboratory trials were conducted in spring 1991 to determine a reconditioning process for the material so that it could be used economically for engineered fill applications at the site.

Laboratory trials were conducted on large, bulk samples of the fly ash obtained from the site with a large backhoe. Field samples were double bagged to preserve their moisture condition, then carefully split into smaller representative subsamples for laboratory trials. A series of small-scale trials was completed using portland cement, hydrated lime, and lime kiln dust initially identified as potential stabilizing and solidifying agents. The test method used was similar to that previously described using 100-mm high × 100-mm diameter cans, with strength development (rate and unconfined compressive strength using a pocket penetrometer) of interest for engineered fill use, and pH measured for environmental reasons. Note that the fly ash fill area was already alkaline, and a significant increase in pH was not desirable.

Test observations indicated that portland cement and hydrated lime were not suitable stabilizing and solidifying agents. At even low addition levels (<5 percent), the fly ash mixtures set very rapidly (within hours) to strengths greater than 0.4 MPa. For engineered fill applications at this site, it was desirable to have a mixture that remained workable until it could be placed and compacted using conventional construction equipment with a final, unconfined compressive strength similar to stiff clay, so it could be excavated later if future construction was necessary.

Byproduct dolomitic lime kiln dust proved most effective. Additional trials were completed to refine the addition levels, and it was determined that 8 percent lime kiln dust (by wet mass) resulted in a satisfactory engineered fill mixture that could be readily handled (placed and compacted using conventional equipment), which possessed adequate strength (approximately 0.3 MPa after about 2 days and 0.4 MPa after four weeks). The reconditioned fly-ash mix, although possessing relatively high unconfined compressive strength, could be broken up by hand, indicating that it could be re-excavated easily using conventional construction equipment.

A sample of the reconditioned fly ash was subjected to environmental analysis (Ontario Regulation 309 Leachate Extraction Procedure) for comparison with Ontario requirements for drinking water and wastes. Although the boron level was slightly elevated, fluoride and selenium, the leachate from the stabilized and solidified reconditioned fly ash, satisfied Ontario drinking water standards and was well within the nonregistrable, nonhazardous designation for wastes.

On the basis of the reconditioning results and leachate analyses, the fly ash was classified as a special waste and accepted by the Ontario Ministry of the Environment for use as engineered fill at the site. The reconditioned fly ash may be used beneath parking lot and roadway areas outside the building footprint. It is anticipated that pilot-scale and full-scale reconditioning of the fly ash will proceed on-site in 1992, as the site is developed.

CLOSING COMMENTS

Results of more than 15 years of experience confirm that cementitious systems—portland cement, fly ash, hydrated lime and byproduct materials, such as cement and lime kiln dusts, silica fume and slag cement—can be used to durably stabilize and solidify a wide variety of soils, sludges, sediments, and other wastes containing unacceptable levels of organic and inorganic toxic constituents. Such systems can be designed using relatively simple laboratory procedures, based on a thorough understanding of the cementitious components involved and their reactions with the waste materials and toxic constituents. The systems also can be practically implemented using conventional, readily available materials and equipment. New protocols for evaluating cement-based solidified wastes will greatly assist in the assessment of the longevity of stabilization and solidification remediation (particularly with respect to contaminated materials containing organic compounds); such protocols are expected to further support EPA current position that stabilization and solidification is an accepted technology for the treatment of contaminated materials.

REFERENCES

1. Kovalick, W. W. *Innovative Remediation Technologies: Implementation Successes and Challenges.* U.S. Environmental Protection Agency; Presented at Clean-Up of Contaminated Sites:Regulations and State-of-the-Art Technologies Conference. Insight Educational Services, Toronto, Ontario, Canada, Nov. 5 and 6, 1991.
2. Hinsenveld, M. *Stabilization/Solidification of Contaminated Soil.* Update to the NATO/CCMS Pilot Study Committee, Oct. 29, 1991.
3. *Proposed Evaluation Protocol For Cement-Based Solidified Wastes.* Wastewater Technology Centre, Environment Canada; U.S. Environmental Protection Agency, Office of Research and Development; and Ontario Ministry of the Environment, Waste Management Branch, Ottawa, Ontario, Canada, Sept. 1991.
4. Cornfield, H. W., and G. E. Owen. Control of Polychlorinated Biphenyl Residues In Road Soils; Lake Clear Case History. *Proc., 32nd Ontario Industrial Waste Conference,* Toronto, Ontario, Canada, June 16–19, 1985.
5. Emery, J. J. Stabilizing Industrial Sludge for Fill Applications. *Proc., 7th International Congress on the Chemistry of Cement,* Vol. IV, Paris, France, 1980.
6. *Use of Waste Materials and Byproducts in Road Construction.* Organization for Economic Cooperation and Development, Paris, France, Sept. 1977.
7. Regulation Respecting Solid Waste, Q-2, r.14. Excerpt from the *1981 Revised Regulations of Quebec,* Quebec, Canada, (updated), Dec. 18, 1990.
8. *Solidification and Stabilization of Wastes Using Portland Cement.* Portland Cement Association, Skokie, Ill., 1991.
9. *Cement Industry Solutions to Waste Management.* Canadian Portland Cement Association, Calgary, Alberta, Canada, Oct., 7–9, 1992.

Publication of this paper sponsored by Committee on Chemical Additions and Admixtures for Concrete.

Recycling Contaminated Spent Blasting Abrasives in Portland Cement Mortars

BRYAN K. SALT, ANDRÉ G. GARNER, DAVID W. FOWLER, RAYMOND C. LOEHR, AND RAMON L. CARRASQUILLO

Use of abrasive blasting to remove paint containing lead, cadmium, and chromium from steel bridges is producing contaminated spent blasting abrasives that may be classified by the Environmental Protection Agency as hazardous, because of their toxicity. Transportation and disposal of spent abrasives is difficult and costly. A potentially inexpensive and practical solution is to recycle contaminated spent blasting abrasives at the construction site in an environmentally safe manner using solidification and stabilization technology. A further benefit of recycling spent blasting abrasives is that there is no need to use landfills or hazardous waste disposal sites. The use of portland cement to solidify and stabilize spent abrasives to produce usable construction material is investigated. Recommendations provided to the Texas Department of Transportation were applied at the Rainbow Bridge in Beaumont, Texas, where the mix designs were used successfully to recycle more than 3,000 55-gal drums of spent blasting abrasives produced at the site. Recycling involved producing concrete blocks that were subsequently used as filler material in the dolphins around the bridge piers.

Use of abrasive blasting to remove lead-based paints results in contaminated spent blasting abrasives that may be classified as hazardous by the Environmental Protection Agency (EPA). Contaminated spent blasting abrasives are considered hazardous waste if they exhibit a "characteristic of toxicity," as defined in the Resource Conservation and Recovery Act. If the Toxicity Characteristic Leaching Procedure (TCLP) leaching of lead, cadmium, or chromium is more than the maximum levels set by EPA, the material must be treated and rendered nonhazardous before land disposal. A preferable alternative to land disposal, however, would be to recycle the waste material in an environmentally sound application at the construction site.

To produce a usable construction material from spent blasting abrasives, the solidification/stabilization (S/S) process must satisfy environmental and construction concerns. The S/S process must be able to render the spent blasting abrasives nonhazardous by reducing the leaching of the lead, cadmium, and chromium to levels below the maximum levels set by EPA. At the same time, the S/S process must be able to produce an end product of adequate strength and durability.

Contaminants resulting from abrasive blasting of lead-based paints can cause problems for portland cement S/S systems. Lead can act as a retarder on the hydration of cement, causing longer set times and lower strengths (*1*). Aluminum, although not considered toxic, is present in many paints. It reacts with the cement to produce hydrogen gas, resulting in lower strength and more permeable mortars.

B. Salt, A. Garner, Hunt & Joiner, Inc., 4300 N. Central Expressway, Suite 206, Dallas, Tex. 75206. D. Fowler, R. Loehr, R. Carrasquillo, Department of Civil Engineering, University of Texas at Austin, 10100 Burnet Road, #18B, Austin, Tex. 78578.

This study addresses the effectiveness of portland cement mortars in rendering spent blasting abrasives nonhazardous through the S/S processes and in recycling the spent blasting abrasives in portland cement mortars for use as a construction material.

EXPERIMENTAL PROGRAM

Introduction

More than 160 different portland cement mortar mixes have been tested to investigate the S/S capabilities of portland cement mortars on spent blasting abrasives. The spent material either was spent blasting sand, spent blasting dust, or a combination of the two. The main elements of concern found in the spent material were lead, chromium, cadmium, and aluminum.

The test variables to be studied were

- Water/cement (W/C) ratio;
- Cement content;
- Amount of fly ash;
- Amount of silica fume;
- Dosage of superplasticizer;
- Dosage of calcium nitrite as an accelerator;
- Spent material type, composition, and amount;
- Strength gain over time;
- Leaching of lead, chromium, and cadmium as per TCLP; and
- Permeability.

Materials

Most S/S mixes were made with spent blasting sand, which was processed in several forms: separated spent blasting sand and separated spent blasting dust. Each results from spent blasting sand that has been run through a particle separator after blasting. A particle separator isolates larger sand particles to be reused for further blasting and removes the dust and paint chips to waste barrels. The separated spent blasting sand and spent blasting dust can be combined in the desired proportions for recycling in concrete. Unseparated spent blasting sand/dust is spent blasting sand that has not been run through a particle separator before being placed in waste barrels. Spent blasting sands have a fine gradation because of the blasting process. Fineness moduli for the spent blasting sands used in this study ranged from 2.25 to 2.39.

Except for the spent blasting abrasives, all other materials used in the study are commercially available and currently used in the production of portland cement concrete in Texas. Materials used

TABLE 1 TCLP and TCA Results for Spent Blasting Abrasives

Material Type and Origin	TCLP (mg/L)				TCA (mg/kg)				% Lead
	Pb	Cr	Cd	Al	Pb	Cr	Cd	Al	by wt.
Separated Spent Blast Sand A Rainbow Bridge Barrel # 1	2.02	0.58	0.57	0.54	367.0	54.5	15.5	192.5	0.04
Separated Spent Blast Sand B Rainbow Bridge Barrel # 2	1.13	1.42	0.53	1.38					
Separated Spent Blast Dust A Rainbow Bridge Barrel # 1	9.48	5.36	1.07	2.54	2896.0	724.5	68.0	1946.0	0.29
Separated Spent Blast Dust B Rainbow Bridge Barrel # 2	1.14	9.51	1.08	4.95					
Unseparated Spent Blast Sand/Dust A Rainbow Bridge Barrel # 1	0.48	2.09	0.62	0.56	981.5	389.5	34.0	711.0	0.10
Unseparated Spent Blast Sand/Dust B Odessa Bridge Barrel # 1	1.33	0.56	0.29	0.65	125.4	52.9	11.9	688.7	0.01

include Type I/II portland cement, siliceous river sand with a bulk specific gravity (BSG) at SSD of 2.58 and an absorption capacity of 1.44 percent, an ASTM Class C fly ash with a BSG of 2.58, a condensed silica fume with a BSG of 2.20, a high-range water reducer, and a calcium nitrite accelerator.

Table 1 presents the results of TCLP and total constituent analysis (TCA) for the spent blasting abrasives used in the project. TCLP results are given in terms of milligrams of contaminant per liter of acid leachant, and TCA results are given in milligrams of contaminant per kilogram of spent blasting abrasives. The percentage of lead by weight in the spent blasting abrasives is also indicated.

Mix Proportions

Tables 2–6 contain detailed information on the specimen designations and corresponding mix proportions for selected mixes. When mineral admixtures were used, fly ash was used as a volumetric replacement for portland cement in the amount of 30 percent, and silica fume was used in addition to the portland cement in the amount of 12 percent of the weight of portland cement. All mix proportions were based upon a cubic-yard batch of concrete, less the volume of coarse aggregate.

TABLE 2 Proportions for Mixes with Separated Spent Blast Sand A

Mix #	Cement (kg)	Concrete Sand (kg)	Blast Sand (kg)	W/C Ratio by wt.
1	213	499	0	0.38
2	213	299	200	0.37
3	213	100	399	0.40
4	320	499	0	0.35
5	320	299	200	0.37
6	320	100	399	0.38

TABLE 3 Proportions for Mixes with Separated Spent Blast Dust A

Mix #	Cement (kg)	Concrete Sand (kg)	Blast Dust (kg)	W/C Ratio by wt.
7	213	499	25	0.40
8	213	499	175	0.57
9	320	499	25	0.38
10	320	499	175	0.50

1 kg = 2.205 lbf

Mix Procedure

All batches were mixed using the following procedure:

- All raw materials were weighed to the nearest one-tenth of a pound;
- The mixer was charged with the dry materials, followed by mixing for 10 sec;
- The water and superplastisizer were added, followed by mixing for 3 min;
- The batch was allowed to rest without mixing for 2 min;
- If needed, additional superplastisizer was added to achieve the required workability; and
- The batch was mixed for 3 min more.

Mixes containing mineral admixtures normally required a slightly longer mixing time for adequate distribution of the fine particles.

Casting and Curing

Specimen molds were filled in two equal layers and vibrated on a vibrating table for 20 sec according to ASTM C192-88. Specimens were then finished using aluminum trowels.

Curing consisted of placing specimens under wet burlap and polyethylene for the first 24 hr after casting, per ASTM C192-88, after which they were removed from the molds and placed in a moist curing room. Mixes taking longer to set than 24 hr because of lead retardation were kept under the wet burlap and polyethylene until they set, at which time they were removed from the molds and placed in a moist curing room. Mixes that had not set within 7 days of curing were discarded. The moist curing room was kept at 23°C and 100 percent relative humidity until testing, in conformance with ASTM C511-85.

Testing Procedures

Workability of fresh mortar mixes was measured according to ASTM C109-87. A targeted workability was established on the basis of the control mixes, and all subsequent mixes were batched to have similar workability, as indicated by the flow table test.

Compressive strength of hardened mixes was determined using cylinders 76 mm (3 in.) in diameter and 152 mm (6 in.) tall, which

TABLE 4 Proportions for Mixes with Unseparated Spent Blast Sand/Dust A

Mix #	Cement (kg)	Blast Sand/Dust (kg)	HRWR[a]	Fly Ash (kg)	Silica Fume (kg)	W/C Ratio by wt.
11	213	499	15.8	0	0	0.35
12	213	499	9.4	0	0	0.35
13	320	499	7.8	0	0	0.35
14	320	499	6.2	0	0	0.35
15	320	499	14.2	0	38	0.35
16	320	499	7.8	96	38	0.35
17[b]	320	249	7.8	0	0	0.35

[a] In mL per kg of cement
[b] Includes 249 kg of Concrete Sand
1 kg = 2.205 lbf

TABLE 5 Proportions for Mixes with Separated Spent Blast Sand B and Separated Spent Blast Dust B

Mix #	Cement (kg)	Blast Sand (kg)	Blast Dust (kg)	HRWR[a]	Calcium Nitrite (L/m^3)	Silica Fume (kg)	W/C Ratio by wt.
18	320	499	0	0.0	0	0	0.35
19	320	499	25	12.3	0	0	0.35
20	320	499	75	25.5	0	0	0.35
21	320	499	125	39.6	0	0	0.35
22	320	499	0	0.0	9.9	0	0.35
23	320	499	25	1.7	9.9	0	0.35
24	320	499	75	5.5	9.9	0	0.35
25	320	499	125	11.2	9.9	0	0.35
26	320	499	0	2.4	0	38	0.35
27	320	499	25	6.3	0	38	0.35
28	320	499	75	17.4	0	38	0.35
29	320	499	125	21.1	0	38	0.35

[a] In mL per kg of cement
1 kg = 2.205 lbf

TABLE 6 Proportions for Mixes with Unseparated Spent Blast Sand/Dust B

Mix #	Cement (kg)	Blast Sand/Dust (kg)	HRWR[a]	Calcium Nitrite (L/m^3)	Silica Fume (kg)	W/C Ratio by wt.
30	320	499	7.8	0	0	0.35
31	320	499	10.8	0	38	0.35
32	320	499	7.8	9.9	0	0.35

[a] In mL per kg of cement
1 kg = 2.205 lbf

were tested according to ASTM C39-79, at 7, 28, and 90 days. Cylinders were capped using unbonded neoprene caps inside steel restraining rings.

Permeability of hardened mixes was determined according to AASHTO T-277, Rapid Determination of the Chloride Permeability of Concrete, at 28 days with the following exceptions:

1. Tests were conducted on 102-mm (4-in.) diameter mortar cylinders instead of 95-mm (3.75-in.) diameter concrete core specimens (2).
2. Two 51-mm (2-in.) thick specimens were cut from the interior of each cylinder instead of using two specimens cut from the ends of a cored specimen (2).
3. Specimens were kept saturated in a sealed vacuum for an hour after evacuation, in lieu of a forced vacuum (2).

TCLP testing was performed as per 40 CFR 261, Appendix II-Method 1311 (7-1-90 Edition) at 7 or 28 days or both. TCLP is designed to simulate the leaching potential of waste disposed of in a municipal landfill. The waste is subjected to an acetic acid solution to simulate the organic acids produced at a landfill during decomposition of organic material in refuse. TCLP concentration limits have been set for 25 organic compounds, eight metals, and six pesticides. Metals of concern in this study are lead, cadmium, and chromium, as they are used in the manufacturing of paints and pigments. EPA's TCLP concentration limits for these three metals are indicated in Table 7.

TEST RESULTS

Compressive Strength and Rapid Chloride Ion Permeability

The compressive strengths and rapid chloride ion permeabilities for the S/S mixes detailed in tables 2–6 are presented in Table 8. Com-

TABLE 7 7-Day TCLP Leaching Results for Selected Mixes

Mix #	Lead (mg/L)	Chromium (mg/L)	Cadmium (mg/L)
1	0.09	0.46	0.18
2	0.09	0.52	0.15
3	0.13	0.54	0.12
4	0.12	0.39	0.11
5	0.10	0.42	0.15
6	0.02	0.44	0.16
7	0.10	0.59	0.17
8	-	-	-
9	0.07	0.56	0.16
10	0.05	1.00	0.16
11	-	-	-
12	-	-	-
13	-	-	-
14	-	-	-
15	0.07	2.36	0.13
16	0.04	4.15	0.13
17	0.06	1.07	0.14
18	0.09	2.17	0.04
19	0.12	2.16	0.07
20	-	-	-
21	-	-	-
22	0.18	1.72	0.15
23	0.19	1.92	0.19
24	-	-	-
25	-	-	-
26	0.08	1.87	0.06
27	0.07	1.92	0.09
28	0.08	1.79	0.10
29	0.12	1.77	0.09
30	0.17	0.67	0.11
31	0.07	0.79	0.03
32	0.00	0.53	0.05
EPA Limits	5.00	5.00	1.00

- Not tested due to no set

pressive strength is given as the average strength of two companion cylinders at 7, 28, and 90 days, and permeability is given as the average chloride ion permeability of four companion specimens cut from two cylinders at 28 days. Unless otherwise noted, mixes set within 24 hr of mixing.

TCLP Leaching Results

The TCLP leaching results of the S/S mixes detailed in Table 2–6 are presented in Table 7 along with the EPA TCLP leaching limits. Leachability is given as the average of TCLP leaching values from three 50-mg samples tested at 7 days. TCLP leaching tests were conducted for lead, chromium, and cadmium (*3*).

DISCUSSION OF RESULTS

All raw materials used in the study were characterized by TCLP and TCA. That information is necessary to determine how much background contamination exists in the portland cement, water, or mineral admixtures, as well as the contamination level of the spent blasting abrasive.

The effectiveness of portland cement S/S systems depends greatly on the contamination level of the spent blasting abrasives. The contamination level of the spent blasting abrasives could vary greatly along the span of a bridge because of differences in paint systems. Particle size of pulverized paint also affects portland cement mortar. As a result, characterization of the spent blasting abrasives for each job is important in determining the most suitable mix design.

Likewise, because of the variability of background contamination of portland cement, water, and chemical and mineral admixtures, the characterization of these materials is necessary. If the materials contain large amounts of contaminants, their use should be questioned, and a material with less contaminants might have to be used.

The effect of contamination level on set times is an important consideration; it can affect the success of portland cement S/S systems. In summary, the effect of contamination level on set times can be stated as follows: the higher the amount of contamination in a portland cement mortar, the longer the set time; the higher the cement content, the shorter the set time. As reflected in Table 5, Mixes 18–21 had an increasing spent blasting dust content which effectively increased their level of contamination. As Table 8 indicates, set times increase the greater the spent blasting dust content. Mixes with the higher dust contents were not set within 7 days. The mixes with higher cement contents set faster, apparently because of a lower lead/cement ratio when the amount of spent blasting abrasives is constant.

Silica fume and calcium nitrite effectively reduced the set times of the mixes. Mixes 22–25 were identical to Mixes 18–21, except

TABLE 8 Compressive Strength and Rapid Chloride Ion Permeability for Selected Mixes

Mix #	Average Compressive Strength (MPa)			Permeability[a]	Set Time
	7 Day	28 Day	90 Day	coulombs	
1	43.2	50.5	56.7	7460	
2	21.8	28.2	28.8	8110	
3	20.2	18.7	25.3	N/A	
4	60.6	70.5	77.1	3300	
5	37.0	39.0	47.5	8100	
6	31.4	33.9	29.6	8410	
7	14.2	17.5	19.8	7460	
8	0.0	0.0	0.0	N/A	NO SET
9	20.6	27.5	26.9	5620	
10	8.7	10.8	10.3	8810	
11	0.0	0.0	0.0	N/A	NO SET
12	0.0	0.0	0.0	N/A	NO SET
13	0.0	0.0	0.0	N/A	NO SET
14	0.0	0.0	0.0	N/A	NO SET
15	15.4	21.0	21.0	5270	
16	4.3	18.5	19.9	10070	
17	23.1	27.6	32.4	10080	
18	21.5	21.0	32.0	11130	SET 3D
19	8.0	5.3	5.2	16460	SET 6D
20	0.0	0.0	0.0	N/A	NO SET
21	0.0	0.0	0.0	N/A	NO SET
22	22.1	27.1	33.0	21110	SET 1D
23	16.1	23.0	21.6	18260	SET 2D
24	0.0	0.0	0.0	N/A	NO SET
25	0.0	0.0	0.0	N/A	NO SET
26	11.7	16.9		4450	SET 1D
27	13.7	19.4		6990	SET 1D
28	18.0	25.9		6450	SET 1D
29	10.9	14.1		11790	SET 4D
30	11.9	16.3	15.4	12800	
31	13.9	16.1	18.3	2450	
32	43.2	54.5	58.7	6880	

[a]28-Day Test Age
N/A - Not applicable due to no set
1 MPa = 145.0 lbf/in^2

that the former contained a 9.9 L/m^3 (2 gal/yd^3) dosage of calcium nitrite as an accelerator. The calcium nitrite effectively reduced set times for mixes with lower dust contents; however, mixes with the higher dust contents still would not set within 7 days. Silica fume was most effective in reducing set times; its use resulted in the higher dust content mixes (Mixes 26–29) setting within 7 days. Future research will study the effect of other accelerators, such as calcium chloride and sodium silicate, on the set times of mixes.

The effect of contamination level on compressive strength can be drawn from Figures 1–3; by observing: the more spent blasting abrasive used instead of clean concrete sand, the lower the compressive strength; the greater the cement content, the higher the compressive strength; and, the lower the W/C ratio, the higher the compressive strength. Silica fume and calcium nitrite generally were found to increase compressive strength.

The effect of contamination level on permeability can be summarized by referring to Figures 4–6, which reflect that the lower the W/C ratio and the higher the cement content, the lower the permeability. Mixes containing silica fume, fly ash, and calcium nitrite had lower permeabilities. Finally, the greater the clean fine-aggregate replacement with spent blasting abrasives, the higher the permeability.

The effect of composition on TCLP results is reflected in Figures 7 and 8. The higher the W/C ratio, the higher the leaching of contaminants; the higher the cement content, the lower the leaching of contaminants. Mixes containing silica fume showed lower leaching. Those trends also depend on the background composition of the binder materials, such as portland cement, clean fine aggregate, mix water, and mineral admixtures.

The compressive strength effect on TCLP results can be observed in the trend toward decreased leaching of contaminants with in-

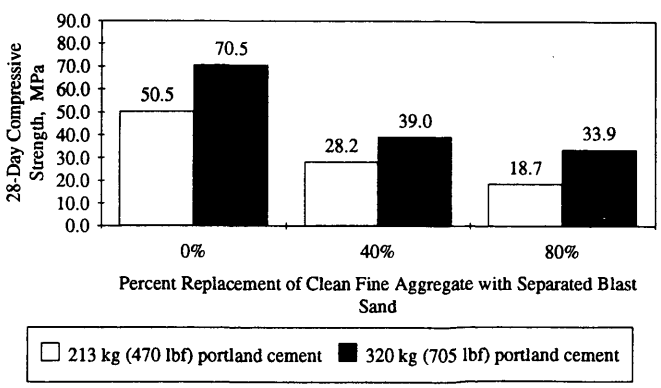

FIGURE 1 28-day compressive strength versus percent replacement of clean fine aggregate for separated Sand A mixes.

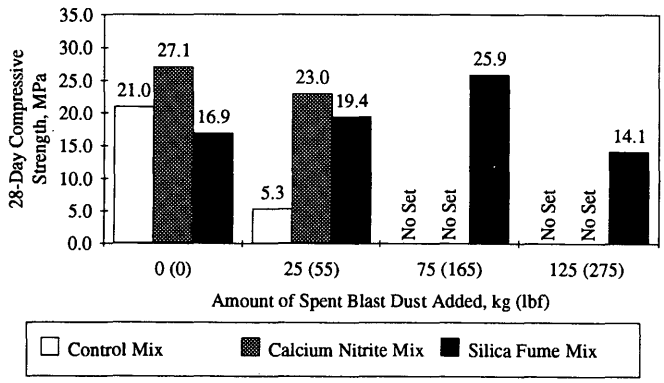

FIGURE 2 28-day compressive strength for separated Sand B/Separated Dust B mixes.

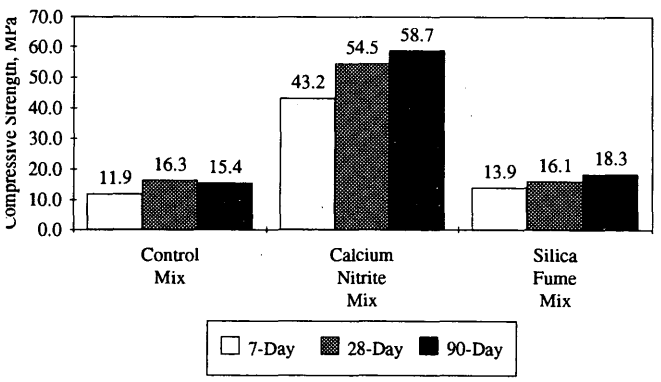

FIGURE 3 Compressive strength for unseparated Sand B mixes.

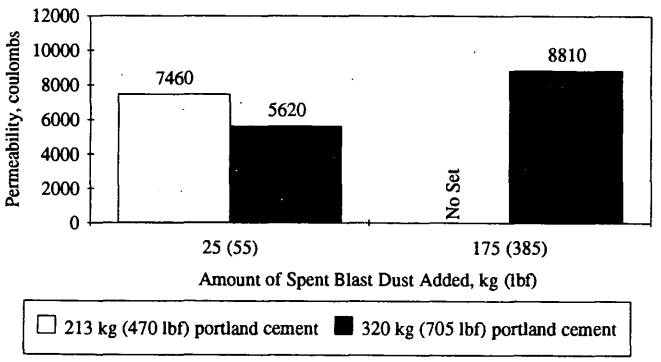

FIGURE 4 Permeability versus amount of spent blast dust for Separated Dust A mixes.

creased compressive strength. However, in many mixes, no correlation is observed. Two variables that affect compressive strength, W/C ratio and cement content, are the most important factors affecting TCLP leaching. Lower W/C ratios and higher cement contents produce mixes with higher compressive strengths and lower contaminant leaching.

The effect of permeability on compressive strength is, in general, that the compressive strength of the S/S matrices decrease as permeability of the matrices increases, regardless of the type of spent blasting abrasives or if whether chemical or mineral admixtures are used.

Factors contributing to the success of a portland cement mortar are the mixing sequence and the time used during the batching procedure. The importance of mixing sequences and times was determined from laboratory observations. Stabilized mortar mixes, batched using the following mixing procedure, were the most uniform and gave the most predictable results. The mixing procedure is as follows: (*a*) mix most of the dry materials first, (*b*) add the water and chemical admixtures, (*c*) add the remaining dry material and (*d*) continue mixing. As a rule of thumb, S/S mixes should be mixed approximately two to three times—as long as ordinary concrete and mortar mixes. S/S mixes that were mixed for short periods of time were not uniform and had pockets of unmixed material. Pockets of unmixed material either had an accelerated or a delayed set, depending on the mix constituents in the areas of concentration.

FIELD APPLICATION

Recommendations based on this study were provided to the Texas Department of Transportation for use at the Rainbow Bridge in Beaumont, Texas (*4*). Table 9 gives the mix proportions recommended for recycling the spent blasting abrasives generated at this particular site.

The recommendations were followed successfully in recycling more than 3,000 55-gal drums of spent blasting sand produced at

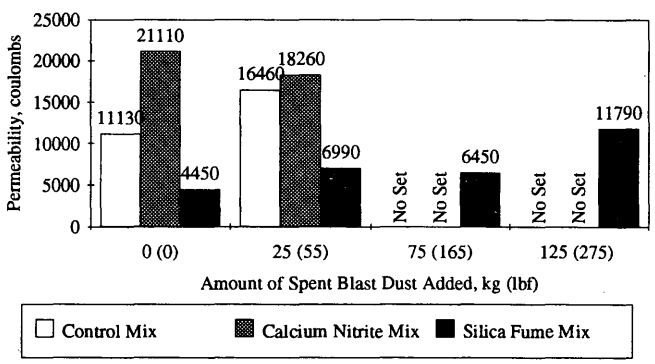

FIGURE 5 Permeability for Separated Sand B/Separated Dust B mixes.

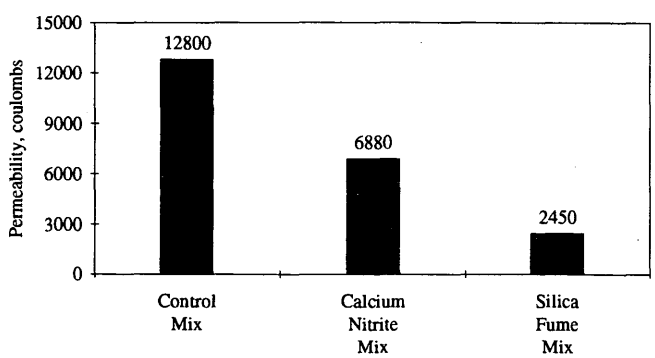

FIGURE 6 Permeability for Unseparated Sand B mixes.

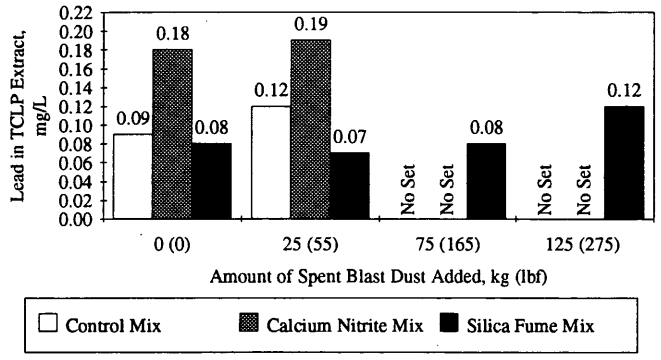

FIGURE 7 TCLP lead leaching for Separated Sand B/Separated Dust B mixes.

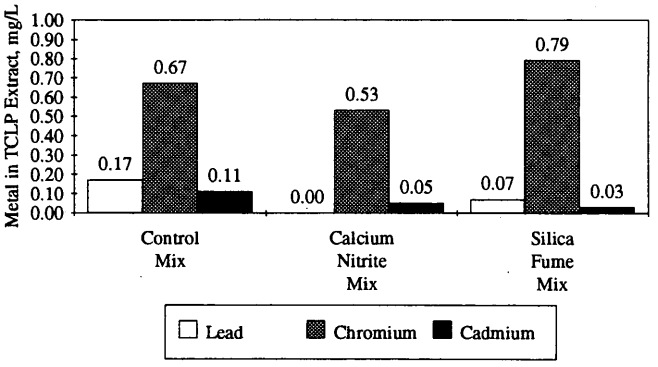

FIGURE 8 TCLP leaching for Unseparated Sand/Dust B mixes.

this site. The mix was used to produce approximately 50,000 12-in. square by 6-in. thick blocks. The blocks were placed as filler material in dolphins around the bridge piers to protect them from ship collisions.

The mix designs not only provided an environmentally sound way to recycle the spent blasting abrasives as a construction material but also resulted in a cost savings to the Texas Department of Transportation. Future research will be to acquire field specimens for compressive strength, permeability, and TCLP testing.

CONCLUSIONS

The following conclusions are made on the basis of this study:

- A portland cement-based S/S system that has adequate compressive strength and permeability and meets EPA's and the Texas Department of Transportation's environmental guidelines can be produced using the contaminated spent blasting abrasives investigated in this study.
- The most important factors governing TCLP leaching, compressive strength, and permeability are W/C ratio and cement content. The lower the W/C ratio and the higher the cement content, the lower the leaching and the higher the compressive strength, regardless of the admixtures used.
- The higher the contamination level of an S/S mix, the longer the set times and the lower the compressive strength. Silica fume and calcium nitrite are effective in reducing set times and increasing compressive strength.
- S/S mixes exhibiting lower permeability also had lower TCLP leaching, not because of the permeability of the matrix, but because the factors that affect leaching the most—because of W/C ratio and cement content—also affect permeability. Silica fume effectively reduces permeability and therefore TCLP leaching.
- The trend is toward decreased leaching with increased compressive strength; however, in many mixes, no such correlation was observed.
- Setting times did not affect TCLP leaching or compressive strength. S/S mixes with a delayed set because of lead retardation exhibited adequate strength and leaching characteristics at later ages.
- Mixing sequence and times are important for the success of S/S systems. Best performance was obtained when the majority of the dry components were mixed thoroughly before adding water or chemical admixtures.
- As shown in the Rainbow Bridge project, portland cement mortars can be effective in treating and recycling spent blasting abrasives, as an alternative to land disposal, thereby reducing the burden to landfills and resulting in a significant cost savings compared with disposal.

TABLE 9 Recommended Mix Proportions for Rainbow Bridge Spent Abrasive Recycling

Cement	320 kg (705 lbf)
W/C ratio	0.35
Superplastisizer	13.7 mL/kg (21 oz./cwt)
Silica Fume	12% by weight addition to cement
Spent Blasting Sand	499 kg (1100 lbf)

ACKNOWLEDGMENTS

TCLP analyses were performed by Matthew Webster and Douglas Brabrand of the Department of Civil Engineering at the University of Texas at Austin. Without their help, this research would not have been possible. The authors are grateful to the University of Texas at Austin, the Texas Department of Transportation, and the FHWA for their support.

REFERENCES

1. Thomas, N. L., D. A. Jameson, and D. D. Double. The Effect of Lead Nitrate on the Early Hydration of Portland Cement. *Cement and Concrete Research,* Vol. 11, No. 1, Jan. 1981, pp. 143–153.
2. Whiting, D. *Rapid Determination of the Chloride Permeability of Concrete.* Report FHWA/RD-81/119. FHWA, U.S. Department of Transportation, 1981.
3. Brabrand, D. J. *Solidification/Stabilization of Spent Blasting Abrasives with Portland Cement for Nonstructural Concrete Purposes.* M. S. thesis. University of Texas at Austin, Dec. 1992.
4. Garner, A. G. *Solidification/Stabilization of Contaminated Spent Blasting Media in Portland Cement Concretes and Mortars.* M. S. thesis. University of Texas at Austin, Dec. 1992.

Publication of this paper sponsored by Committee on Chemical Additions and Admixtures for Concrete.

Mechanical Properties of Lightweight Concrete Incorporating Recycled Synthetic Wastes

PARVIZ SOROUSHIAN, ABDULRAHMAN ALHOZAIMY, AND ALY I. ELDARWISH

An experimental program was conducted on partial substitution of lightweight aggregates with recycled plastics in lightweight concrete. Bridging cracks in the brittle concrete matrix by soft synthetic inclusions led to the material's enhanced toughness and increased resistance to shrinkage cracking. Plastics also enhanced the impact resistance of lightweight concrete and produced desirable permeability characteristics and acceptable compressive strength-to-unit weight ratios. Because of the desirable performance characteristics of concrete materials incorporating mixed recycled plastics, such materials are expected to have environmental, economic, and technical benefits.

The most widely used construction material is concrete, which is commonly made by mixing portland cement with aggregates and water. Concrete consumption in the United States is close to 2 ton/year for each resident. No other material except water is consumed in such tremendous quantities. There are some key advantages associated with recycling in concrete construction: (*a*) potential development of large-volume markets for waste products, (*b*) reduced need for purification of waste, and (*c*) long-term removal of recycled materials from the waste stream, considering that concrete products typically have a service life exceeding 40 years.

Improvements in some key aspects of concrete performance can make important contributions to developing a more reliable infrastructure. Recycling of plastics in concrete can help overcome problems with the brittleness and relatively high unit weight of concrete. Plastics also can help control shrinkage cracking of concrete. The study presented evaluates recycled plastics as lightweight reinforcing inclusions in concrete.

It is now well known that before application of external load microcracks exist in the transition zone between the mortar matrix and coarse aggregates in concrete (*1*). The number and width of these cracks in concrete would depend, among other factors, on bleeding characteristics, the strength of a transition zone, and the curing history of concrete. Under ordinary curing conditions (whereby a concrete element is subjected to drying shrinkage or thermal strains), differences in dimensional movements and elastic moduli will set up differential strains between the matrix and coarse aggregates, generating microcracks in the transition zone. Under load and environmental effects, the transition zone, microcracks begin to increase in length, width, and number—initially within the transition zone and later into the matrix and, in the case of lightweight aggregates, through the aggregates. The relatively low fracture energies required for propagation of cracks in brittle concrete matrices result in relatively low toughness, impact resistance, and tensile strength for concrete.

Michigan State University, Department of Civil and Environmental Engineering, A349 Engineering Building, East Lansing, Mich. 48824.

In concrete composites containing plastics, the propagating microcracks encounter of with tough, well-bonded plastics relaxes the intensity of stresses at the crack tips, a phenomenon that increases the fracture energy, and thus the toughness and impact resistance, of the composite as well as its resistance to shrinkage cracking. Delayed propagation of microcracks encountering the plastic inclusions would take place mainly within the transition zone instead of through the plastic inclusions [Figure 1 (a)]. Eventually, when increased load levels lead to the interconnection and rapid growth of microcracks, bridging of plastic inclusions across the resulting microcracks [Figure 1 (b)] helps maintain the integrity of the composite at large post-peak deformations and control the crack widths (e.g., under restrained shrinkage movements).

The main objective of this study is to validate these hypotheses regarding microcrack arrest and deflection, and the bridging of cracks by plastic inclusions in concrete—and consequent improvements in toughness and shrinkage crack control. These hypotheses have been validated for lightweight concrete (in terms of toughening effects) and normal-weight concrete (in terms of shrinkage crack control). (*2,3*)

EXPERIMENTAL PROGRAM

An experimental program was designed on the basis of statistical concepts of factorial analysis of variance (2^2 factorial design). The program investigated the following two variables: plastic type (HDPE and "MIXED," as will be defined later) and plastic content. Plastic content was evaluated for two different levels: 20 and 40 percent replacement of fine lightweight aggregate by volume corresponding to 7.5 and 15 percent by total volume of concrete. Control mixtures with no plastics added were also considered.

MATERIALS AND MIX PROPORTIONS

The basic mix ingredients used were Type I portland cement, lightweight coarse aggregate, lightweight fine aggregate, recycled HDPE, water, and air-entraining agent. The lightweight aggregate used in the investigation, Tufflite, is a volcanic rock-based aggregate with a maximum aggregate size of 0.5 in. (12 mm). Specific gravity of lightweight coarse and fine aggregates were 1.2 and 1.5, respectively.

Recycled "MIXED" plastic is a combination of high density polyethylene (HDPE), polystyrene (PS), polypropylene (PP), polyvinyl chloride (PVC), polyethylene terephlthalate (PET), and acrylonitrile butadiene styrene (ABS). Table 1 shows the percent-

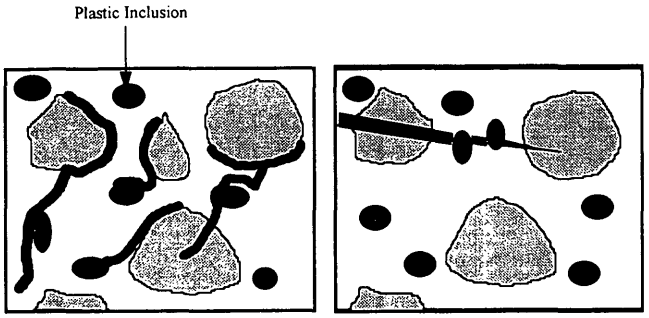

(a) Arrest and Deflection of Microcracks (b) Bridging of Cracks

FIGURE 1 Mechanisms of action of plastic inclusions in concrete.

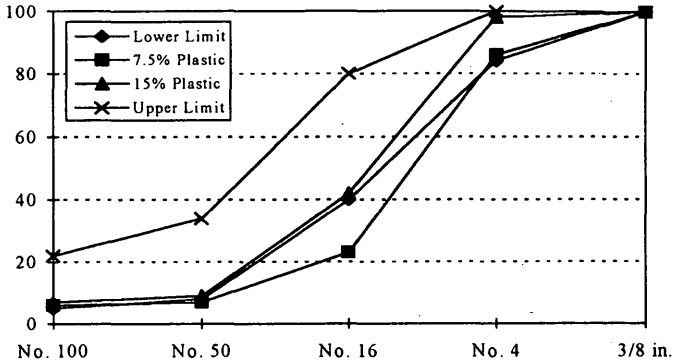

FIGURE 2 Gradation of plastic-fine aggregate combinations.

ages, by weight, of these plastics in municipal solid waste and those used in this investigation.

Recycled HDPE and MIXED plastic particles are irregular (relatively flat) in shape. Specific gravity of different types of plastics ranged from 0.9 to 1.1. HDPE and MIXED plastic have a nominal planar dimension of 3/8 in. (10 mm).

Figure 2 shows the gradation of fine aggregates and plastic-fine aggregate combinations at two replacement levels (20 and 40% replacement of fine aggregate by volume corresponding to 7.5 and 15 percent, respectively, of total volume of concrete).

Different trial mixtures were produced to optimize the cement content, and the fine aggregate to coarse aggregate ratio, to achieve the maximum replacement level of fine aggregates with HDPE or MIXED plastics without adversely influencing fresh mix workability (*2*) The cement content and fine aggregate to coarse aggregate ratio were 750 lb/yd^3 (450 kg/m^3) and 4 (by volume), respectively. It should be noted that a relatively high fine aggregate to coarse aggregate ratio was necessary to achieve the desired workability, compactability, and finishability when part of the lightweight fine aggregate was replaced with HDPE or MIXED plastic. Both the cement content and fine aggregate to coarse aggregate ratio were kept constant in all mixtures. Water content was adjusted to give comparable slumps of 1.5 to 2.0 in. (38 to 51 mm). An air-entraining agent (water-based) was used at 0.06 percent by weight of cement to produce resistance against frost attack. Table 2 presents the optimized mix proportions.

Conventional mixing and curing procedures (ASTM C-192) were used to prepare control mixtures and the plastic-concrete composites. External vibration was found to be suitable for producing concretes incorporating recycled plastics. Optimum vibration time was found to be 25 ± 5 sec at a frequency of 80 Hz. All the specimens (except the drying shrinkage test) were continuously moist-cured [73°F (23°C)] up to the test age of 28 days.

TABLE 1 Types and Percentages of MIXED Plastics by Weight

Plastic Type	MSW*	Used
HDPE	21	31
PP	16	24
PS	16	24
PVC	7	10
PET	4	6
ABS	3	5

*MSW: Municipal Solid Waste

TEST PROCEDURES

The fresh mix workability was assessed by the slump test (ASTM C-143), and the hardened unit weight was measured following ASTM C-567 procedures.

For hardened materials, flexural strength and toughness, compressive strength, impact resistance, restrained shrinkage cracking characteristics and chloride permeability properties were investigated experimentally to develop an overall understanding of various aspects of material behavior.

The flexural test specimens tested were 4 × 4 × 14 in. (100 × 100 × 350 mm), and the compressive strength test specimens were 3 × 6 in. (75 × 15-mm) cylinders. Flexural and compression tests were conducted following ASTM C-78 (four-point loading) and C-39 procedures. Midspan deflection as well as loads were monitored in flexure tests. The Japanese Concrete Institute specification was followed in calculating flexural toughness, defined as the area underneath the load-deflection curve up to a deflection equal to the span length divided by 150 (*4*). The impact test was conducted following the procedures recommended by the American Concrete Institute (Committee 544). That test measures the amount of impact energy (represented by the number of blows) necessary to start a visible crack in concrete and then continue the opening of crack until failure.

Ring type specimens are used for restrained drying shrinkage test on mortar (*5*). The specimen is cast in two equal layers, leveled by a trowel, and then covered with plastic sheets for 6 hr. Specimens are then exposed to air at approximately 68°F (23°C) and 40 percent relative humidity. Restraint of shrinkage movements by the steel ring inside the specimen creates internal tangential tensile stresses that cause cracking.

Permeability tests were conducted using AASHTO T-277 (Rapid Determination of the Chloride Permeability of Concrete (*6*). That test measures the amount of charge passed through a concrete spec-

TABLE 2 Optimized Mix Proportions lb/yd*

Matrix Comp.	Cement	Coarse Agg.	Fine Agg.	Recycled Plastic	Water	AEA %
Control	750	170	850	-	735	0.06
20% Plastic	750	180	719	120	698	0.06
40% Plastic	750	193	579	258	638	0.06

* 1 lb/yd^3 = 0.594 kg/m^3; AEA = Air Entraining Agent, by weight of cement

imen subjected to permeation of chloride ions at 60 VDC for 6 hr. The total charge passed (in coulombs) is related to chloride ion permeability. The more permeable the concrete, the higher the coulombs. A cylindrical specimen, 4 in. (102 mm) in diameter by 2 in. (51 mm) in thickness, is used for this test.

DISCUSSION OF TEST RESULTS

Hardened Unit Weight

The hardened unit weight test results are presented in Figure 3. The addition of recycled plastics tends to reduce the hardened unit weight that adds value to concrete properties. Reduction in hardened unit weight can be attributed to the fact that the lightweight sand used in this investigation had a higher specific gravity than that of the recycled plastics used.

Flexural Performance

Typical 28-day flexural load-deflection curves for lightweight concrete and plastic concretes incorporating 7.5 and 15 percent plastics—HDPE and MIXED performed similarly—are shown in Figure 4. Figure 5 presents the flexural strength test results, and Figure 6 presents flexural toughness test results.

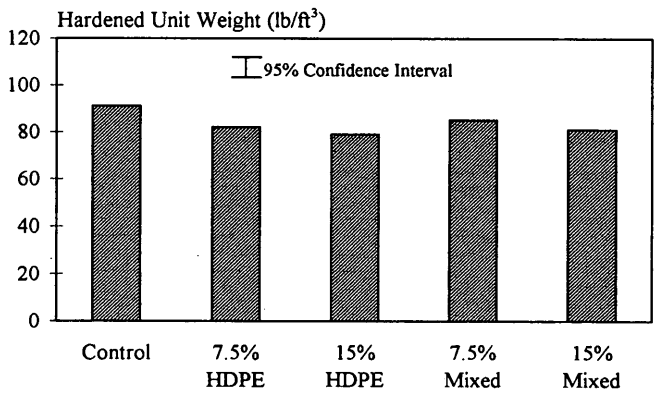

FIGURE 3 Hardened unit weight (means and 95 percent confidence interval).

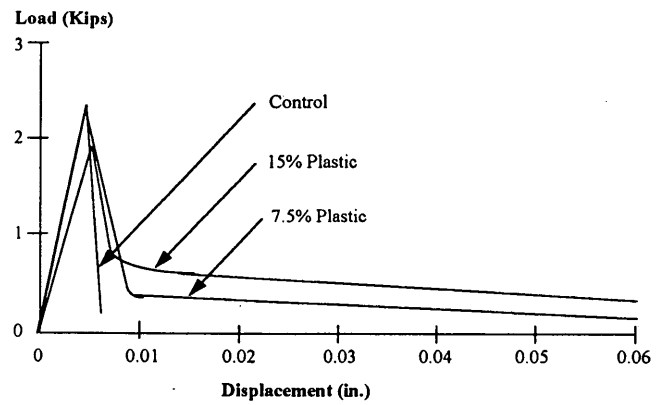

FIGURE 4 Typical flexural load-deflection curves at 28 days.

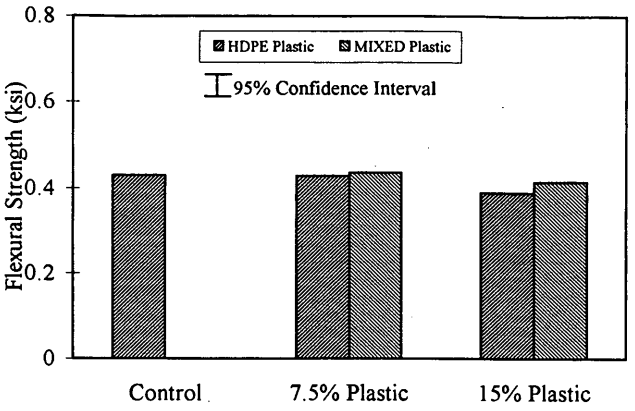

FIGURE 5 Flexural strength test results (means and 95 percent confidence interval).

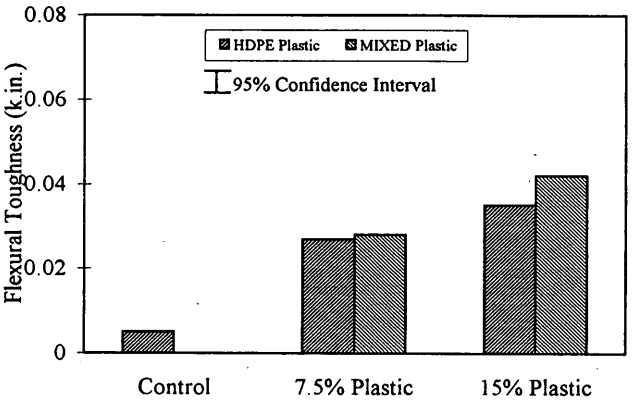

FIGURE 6 Flexural toughness test results (means and 95 percent confidence interval).

For the lightweight concrete mix composition used in this study, the addition of plastics up to a certain level (7.5 percent of total volume) produced a flexural strength comparable to that of the control mixture without plastics. At 15 percent plastic content, however, flexural strength dropped by 6 and 12 percent for MIXED plastic and HDPE, respectively, compared with the control mixture. Two-way analysis of variance and comparison of means of flexural strength test results indicate that, at plastic contents of 7.5 and 15 percent, flexural strength was comparable at 95 percent level of confidence with that of control concrete, except for HDPE with 15 percent plastic content.

Two-way analysis of variance confirmed (95 percent level of confidence) that plastic content influenced flexural toughness. Flexural toughness increased with HDPE and MIXED plastic to 4.5 and 8 times that of the control light lightweight concrete at plastic contents of 7.5 and 15 percent, respectively. That was confirmed statistically (using the separation of means technique between recycled plastics and control) at a 99 percent level of confidence. In general, the positive effects of plastics on flexural toughness reflect their capability to bridge the cracks and mitigate brittle modes of failure in concrete materials by their pull-out resistance across cracks.

Compressive Strength

Figure 7 presents the 28-day compressive strength test results for lightweight concrete. It was confirmed statistically (95 percent level of confidence) that plastics have adverse effects on compressive strength. The situation would be somewhat improved if one considered the compressive strength-to-weight ratio, because plastics also reduce unit weight. A drop in compressive strength with the addition of plastics may be attributed to the relatively low modulus of elasticity of plastics, which would lead to a redistribution of stresses into the more rigid inorganic matrix. It should be noted, however, that limits on load carrying capacity and service life of concrete structures are generally provided by the resistance of concrete of cracking and failure under tensile stress systems. Concrete is fairly strong in compression, and concrete structures rarely fail because of material failure in compression.

Impact Resistance

Figure 8 gives the mean values of the 28-day impact resistance test results for lightweight concrete, presented as the number of blows to first crack and failure. Statistical analysis (comparison of means) indicated, at 95 percent level of confidence, that recycled plastics have a significant positive effect on the impact resistance of concrete beyond the initial crack up to failure.

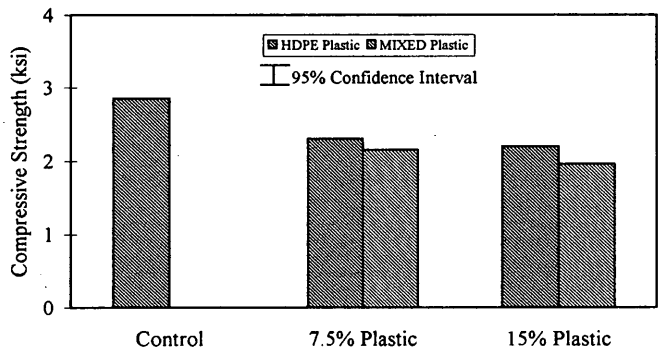

FIGURE 7 Compressive strength test results (means and 95 percent confidence interval).

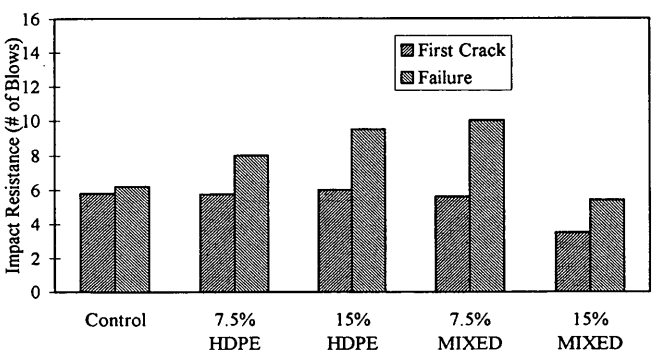

FIGURE 8 Impact resistance test results (means).

Improvements in ultimate impact resistance in the presence of plastics further validate the hypothesis that tough plastic inclusions help to enhance fracture energy and toughness characteristics of concrete materials through bridging across cracks.

Restrained Drying Shrinkage

Figure 9 indicates the maximum crack width versus time in a restrained shrinkage test of lightweight concrete. The addition of recycled plastics to lightweight concrete helps to control the drying shrinkage cracks because recycled plastics (HDPE or MIXED) act as reinforcing inclusions that arrest microcracks and bridge across cracks to restrain their widening.

Permeability

The chloride permeability test results (means and 95 percent confidence intervals) for lightweight concrete and plastic-concrete materials incorporating 20 and 40 percent recycled HDPE or MIXED plastics are presented in Figure 10. Two-way analysis of variance at a 99 percent level of confidence, confirmed that the two variables investigated (replacement level of sand with plastic, and plastic

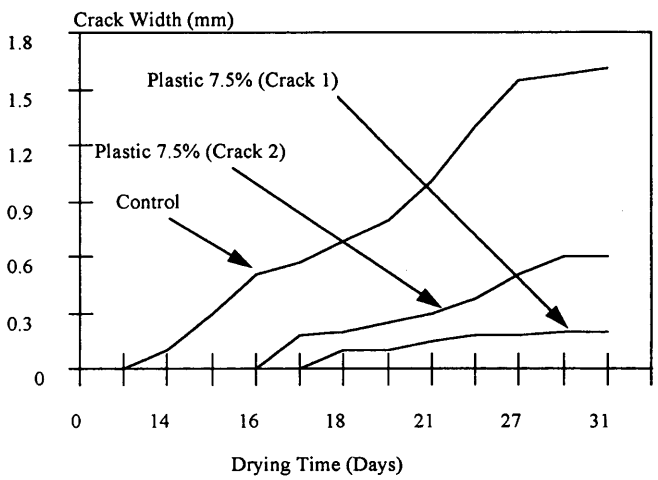

FIGURE 9 Crack width versus drying time.

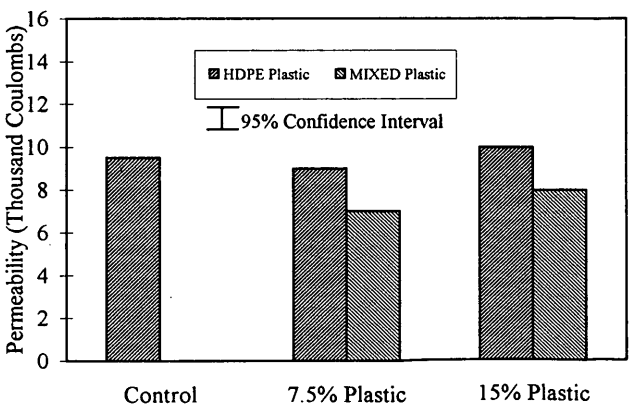

FIGURE 10 Chloride permeability test results (means and 95 percent confidence interval).

type), but not their paired interactions, influenced the permeability of lightweight concrete. Separation of means of the test results confirmed, at a 95 percent level of confidence, that the permeability of control concrete (without plastics) was statistically comparable to that of plastic concrete composites with 20 percent plastic replacement levels when HDPE was used. Increasing the HDPE content to 40 percent led to a slight increase in permeability. However, MIXED plastic at 20 and 40 percent replacement levels reduced permeability by 25 and 17 percent, respectively, when compared to the control (95 percent level of confidence). Hence, plastic concrete presents permeability characteristics comparable or superior to that obtained with conventional lightweight concrete materials.

To understand the effects of plastic on concrete permeability, one should consider that while plastics, as low-permeability inclusions that may reduce microcrack intensity, are expected to reduce permeability, porous or microcracked plastic cement interfaces may cause an increase in permeability. Hence, with improved interface characteristics, one may potentially reduce concrete permeability by adding recycled plastics.

To ensure the environmental safety of recycled plastic-concrete materials, leaching TCLP tests were conducted and it was concluded that the recycled plastic concrete materials are environmentally safe (*3*).

SUMMARY AND CONCLUSIONS

The effects of partial substitution of lightweight aggregate with recycled plastics on concrete properties were investigated. Two plastic types, HDPE and MIXED, and two levels of replacement of fine aggregate (7.5 and 15 percent plastics by total volume of concrete) were used.

The hardened material mechanical properties were assessed through flexure, impact compression, and restrained drying shrinkage tests. Long-term durability characteristics, represented by chloride permeability tests, were evaluated. The following conclusions were derived from analyses of the generated data:

- Addition of recycled plastics to lightweight concrete helps to reduce and control the drying shrinkage cracks.
- Recycled plastics at 7.5 and 15 percent volume fractions gave comparable flexural strengths to that of a control concrete mix. However, flexural toughness was 4.5 and 8 times higher, respectively. The finding was confirmed statistically at a 99 percent level of confidence.
- Compressive strength test results were indicative of the adverse effects of recycled plastics. It should be noted that concrete is fairly strong in compression, and rarely fails because of material failure in compression. Furthermore, because reduction in compressive strength is accompanied by reduction in unit weight, the situation would be somewhat improved if one looked at the compressive strength-to-weight ratio.
- Recycled plastics have a significant and positive effect on the impact resistance of concrete beyond the initial crack up to failure.
- Chloride permeability test results indicate that HDPE's permeability is statistically comparable to that of control concrete. However, MIXED plastic reduced permeability characteristics at 7.5 and 15 percent volume fraction of plastic compared with control concrete.

ACKNOWLEDGMENTS

The authors gratefully acknowledge the financial support of EPA, Coalition Technologies Ltd., and the Research Excellence Fund of the State of Michigan. Technical support of the Composite Materials and Structures Center at Michigan State University is also acknowledged. Tufflite Inc. of Arizona is acknowledged for supplying the lightweight aggregate, and Scrap Masters of Michigan for supplying the recycled plastics.

REFERENCES

1. Hsu, T. C., F. O. Slate, G. M. Struman, and G. Winter. Microcracking of Plain Concrete and Shape of the Stress-Strain Curve. *Journal of the American Concrete Institute,* Vol. 60, No. 2, 1963, pp. 209–223.
2. Alhozaimy, A. *Recycling of Reactive and Reinforcing By-Products in Concrete Construction: New Developments and Assessment of Long-term Performance,* thesis. Michigan State University, 1993.
3. Eldarwish, A. I. *Recycling of Synthetic Wastes in Concrete Materials* thesis, Michigan State University, 1993.
4. *JCI Standards for Test Methods of Fiber Reinforced Concrete.* Report No. JCI-SF-1984-6800, Japanese Concrete Institute, Japan, 1984.
5. Grzybowski, M., and S. P. Shah. Shrinkage Cracking of Fiber Reinforced Concrete. *ACI Materials Journal,* Vol. 87, No. 2, 1990, pp. 138–148.
6. *Rapid Determination of the Chloride Permeability of Concrete.* AASHTO Designation: T-277-83, AASHTO Part II, Washington, D. C., 1987, pp. 1229–1234.

Publication of this paper sponsored by Committee on Chemical Additions and Admixtures for Concrete.

Use of Maturity and Pulse Velocity Techniques To Predict Strength Gain of Rapid Concrete Pavement Repairs During Curing Period

P.A. OKAMOTO AND D. WHITING

Rapid strength gain concrete repair mixtures that cure within 4 to 12 hr were used to carry out full-depth slab repairs on a section of Interstate highway. The mixtures included a calcium-chloride accelerated mix, a very early strength mix developed by the Strategic Highway Research Program, and a "fast-track" mix previously used for early opening of concrete intersections. Before carrying out the repairs, job materials and mix designs were obtained and used to develop correlations between pulse velocity, maturity, and early strength of concrete. Maturity functions based both on Nurse-Saul and Arrhenius (equivalent age) approaches were developed. To account for heat rise of the concretes in actual sections, laboratory correlations were carried out by curing test cylinders in a specially insulated curing box. Pulse velocity and maturity functions were used to predict in situ strength gain of concrete in instrumented test repair sections. Temperatures were monitored through the depths of the test slabs during the initial 8 hr of curing. Temperatures at mid-depth ranged from 60°C to 70°C (140°F to 160°F) for these mixes. After 4 hr of curing, the very early strength mix exceeded 14 MPa (2,000 psi) compressive strength, as determined by in situ methods. The other two mixes gained strength at a slower rate.

In recent years, early opening of concrete pavements to traffic has been given much emphasis. As documented in a synthesis (*1*) published by the Strategic Highway Research Program (SHRP), many recent developments in materials and processes for concrete paving focus on early opening. "Fast track" technology (*2*) allows concrete pavements to be constructed or repaired and opened to traffic within 4 to 24 hr. That is especially useful when full depth pavement repairs are being carried out along critical segments of highway where traffic disruption must be kept to a minimum.

In recognition of the importance of this technology, FHWA initiated a demonstration project on accelerated rigid paving techniques in 1988 to promote the development of fast track techniques. Several pilot projects have been completed with the assistance of the FHWA under this program. As a result of these advances, many states now allow early opening when fast track mixes are used (*3*). The high-early strength gain typically is obtained by using high cement content, a low water to cement ratio, and accelerating admixtures. A rich, low-water-content mix containing 1 to 2 percent calcium chloride produces adequate strength and abrasion resistance for opening to traffic in 4 to 5 hr at temperatures above 10°C (50°F) (*4*). Accelerators are added at either the ready-mix plant or at the jobsite, depending on the temperature and distance to the plant. Other admixtures commonly used in repair mixes include air-entraining agents, water-reducers, and superplasticizers.

Concrete used for rapid repair applications must meet minimum strength levels before the pavement can be opened to traffic. To obtain on-site estimates of strength gain rapidly, in situ techniques for strength measurement are very helpful, as it is not necessary to remove cores from the pavement—a time-consuming and destructive process.

A variety of methods for in situ strength measurement is available (*5*). Two methods that are widely used, pulse velocity measurements and maturity monitoring, were chosen for evaluation in this research program.

The use of ultrasonic pulse velocity measurements is described in the ASTM standard test method for pulse velocity through concrete. The method involves measuring the travel time of an ultrasonic pulse passing through concrete. Pulses are generated by an electro-acoustical transducer held in contact with one surface of the concrete being tested. The pulses are received and converted into electrical energy by a second transducer located a distance L from the transmitting transducer. The transit time is measured electronically, and the direct path length, L, between the transducers is divided by the travel time to obtain the pulse velocity through the concrete. Pulse velocity is proportional to the square root of the elastic modulus and inversely proportional to the square root of the density of concrete. Assuming the elastic modulus is proportional to the square root of compressive strength, pulse velocity is proportional to the fourth root of compressive strength.

Maturity monitoring is based on the fact that strength of concrete is the result of a chemical reaction (hydration) between cement and water. Because the rate of hydration depends on temperature, the strength of concrete may be evaluated from the concept of maturity, which is expressed as a function of time and curing temperature (*6*). By monitoring concrete temperature after casting, maturity can be calculated and compressive strength estimated—if a relationship between maturity and compressive strength for a given mixture has been established previously.

Maturity is most often calculated by the formulas first developed by Nurse (*7*) and Saul (*8*).

$$M(t) = \Sigma\,(T - T_o)\,\Delta t \qquad (1)$$

Where

$M(t)$ = maturity at age t, degree-days or degree-hours;
Δt = time interval, days or hours;

Materials Research and Consulting, Construction Technology Laboratories, Inc., 5420 Old Orchard Road, Skokie, Ill. 60077.

T = average concrete temperature during time interval (Δt, °C); and
T_o = datum temperature (°C).

Datum temperature is the temperature at which concrete ceases to gain strength in time (hydration stops). Datum temperature reportedly ranges from −10.6°C to 0°C (14°F to 32°F) but could fall outside that range depending on the specific materials used. The formula is based on the assumption that maturity increases linearly with temperature. However, it is known from chemical reaction kinetics that the rate of chemical processes increases with temperature, not linearly, but exponentially, according to the Arrhenius equation.

$$K = A \cdot \exp\left(\frac{-E}{RT}\right) \tag{2}$$

where

K = rate constant (1/time),
A = constant (1/time),
E = activation energy (J/mol),
R = gas constant (J/°K·mol), and
T = temperature (°K).

Based on this equation, the variation in maturity or the "equivalent age" at specified temperature can be computed (*9*)

$$t_e = \Sigma \exp -Q\left(\frac{1}{T_a} - \frac{1}{T_s}\right)\Delta t \tag{3}$$

where

t_e = equivalent age at a specified temperature T_s, days or hours,
Q = activation energy divided by the gas constant, °K,
T_a = average temperature of concrete during time interval Δt, °K,
T_s = specified temperature, °K and
Δt = time interval, days or hours.

Equations 1 and 3 are considered in ASTM standard practice for estimating concrete strength by the maturity method C 1074. To estimate the in-place strength of concrete in highway or other structures on the basis of maturity concepts, the concrete temperature should be monitored continuously, and the in-place maturity computed using either the temperature-time factor (Equation 1) or equivalent age (Equation 3). Temperature monitoring starts as soon as practicable after concrete placement; according to ASTM (C 1074), the recording time interval should be ½ hr or less for the time 48 hr, and 1 hr or less thereafter.

SCOPE OF INVESTIGATION

Field Site Description

A test site for installation of full-depth pavement repairs was located on I-20 west of Augusta, Georgia, between Mileposts 189 and 192. Test sections were added to a contract that was in progress for the full-depth repair of working cracks on I-20 in that vicinity. The project involved making full-depth repairs on existing 230-mm (9-in.) thick jointed plain concrete pavement with 9-m (30-ft) joint spacing. Repair lengths varied from 2 to 9 m (6 to 30 ft). Ongoing repairs were carried out each night, and the state required the road to be opened by 6 a.m. each morning. Work involved full-depth saw cutting, removal of the slab by lift-out, drilling of dowel holes by automatic ganged dowel bar drills, and dowel insertion and epoxy grouting. Plastic grout-retention disks were used. Approximately 20 patches were made each night. Concrete deliveries started about 10 p.m. and continued until about 2 a.m. Investigators used the first patch of each night for their main materials test program (*10*) allowing all testing and coring to be carried out before opening the highway.

Concrete Materials and Mixes

Materials used for pavement repair mixes at this site consisted of: (*a*) Type I and III cements; (*b*) an angular quartz natural sand having specific gravity of 2.68, absorption of 0.56 percent, and FM of 2.62; and (*c*) a crushed siliceous natural gravel having a maximum topsize of 19 mm ¾ in.), specific gravity of 2.66, and absorption of 0.5 percent. Admixtures included: (*a*) a chloride-free (nitrite-based) Type C accelerator, (*b*) an organic-acid salt-based air-entraining agent (*c*) a lignosulfonate-based Type A water reducer (*d*) a melamine-base Type F high-range water reducer, and (*e*) a 40 percent solution of calcium chloride.

Mixes used for the repairs are presented in Table 1. "Very Early Strength" (VES) concrete was developed by the investigators on an SHRP project (*11*) with the objective of opening concrete pavements approximately 4 to 6 hr after placement. "Fast Track I" was developed originally by Iowa DOT (*3*) for opening times of 12 to 24 hr. Finally, the mix being used by the contractor on the I-20 repair project, which was designed for opening 4 hr after placement of the last patch, was designated "GADOT" by the investigators.

Laboratory Correlations

Before carrying out the field experiment, representative materials were shipped from the Georgia ready-mix concrete supplier to the investigators' laboratories for preparation of trial batches. Mix quantities were adjusted to achieve the desired opening strengths [13.8 MPa (2,000 psi)] at 4 hr for VES and 13.8 MPa (2,000 psi) at 12 hr for fast track. Because the GADOT mix could not be changed, the mix was prepared using the supplied design. Compressive strengths of only 2.75 MPa (400 psi) were recorded for the GADOT mix after 4 hr, and the 13.8 MPa (2,000 psi) level was reached at 8 hr under laboratory curing conditions. However, it was noted during the subsequent field trials that the mix temperatures in Georgia were higher than 32 °C (90°F), which would tend to increase early strengths over those recorded in the room-temperature lab trial mixes. In all cases, cylinders were stored in an insulation box (*12*) constructed out of expanded polystyrene, which was cored to accept individual 100 × 200-mm (4 × 8-in.) cylinders immediately after casting. Each box holds a maximum of 28 such cylinders. This process served to simulate curing in a thick section of pavement.

A series of "correlation" batches was produced. From these batches, cylinders were cast to establish maturity relationships and relationships between pulse velocity and compressive strength. Mortar cubes also were prepared by wet screening mortar from the concrete batches from which datum temperature and activation energy were determined following ASTM C 1074 procedures. Temperatures monitored in the cylinders during curing in the insu-

lation box were used to calculate maturity at the curing times chosen for the calibration: 4, 6, 8, 15, 18, 20, and 24 hr. Compressive strengths were determined also on the cylinders at these preselected times. For details of the maturity procedures, one is referred to the ASTM C 1074 method. Pulse velocity was determined on 100 × 200-mm (4 × 8-in.) cylinders using a commercially available pulse generator operating at 54kHz. Compressive strengths of the test cylinders were then determined after obtaining pulse velocity readings at the selected curing times noted previously.

Regression analyses were performed on each of the nine sets of data (i.e., three concrete mixes times three predictors). Various data transforms were applied to each data set to maximize the fit of the transformed relationships to a linear equation. Predictive equations developed by these techniques are presented in Table 2. The equations represent the best linearized fits obtained for each data set. Maturity values (MAT) for the Nurse-Saul approach were obtained using Equation 1, those for the Arrhenius predictor were obtained using Equation 3.

Field Instrumentation

After the first slab was removed each night, the open hole was instrumented to allow in-place testing to be carried out. Instrumentation for maturity monitoring consisted of a thermocouple tree containing thermocouples placed at depths of 13, 130, and 230 mm [0.5, 5 (i.e., mid-depth), and 9 in.] below the surface of the pavement. The thermocouple tree was positioned approximately 305 mm (12 in.) from the slab edges to minimize edge cooling effects. Additional thermocouples were placed in ambient air and in one of the test cylinders contained within the insulated curing box. Temperatures were monitored every 30 min using a portable datalogger. An average through-slab temperature was computed for each temperature increment for purposes of strength prediction from the maturity equations.

To facilitate pulse velocity measurements, expanded polystyrene blocks 152 × 152 mm (6 × 6 in.) in dimension were staked to the grade 200 mm (8 in.) apart. After the concrete had reached final set,

TABLE 1 Mixes Used at I-20 Full-Depth Pavement Repair Site

Material - Cubic Meter Basis	VES	Fast Track	GADOT
Cement (kg)	516[a]	439[a]	446[b]
Fine Aggregate (kg)	490	783	608
Coarse Aggregate (kg)	1,020	843	1,071
Water (kg)	199	155	169
Water reducer (ml)	(—)	1,301	(—)
Accelerator (L)	22.7	(—)	(—)
$CaCl_2$ solution (L)	(—)	(—)	6.0
HRWR (ml)	1,286	(—)	(—)
AE agent (ml)	1,286	355	290
w/c ratio	0.39	0.35	0.38

[a]Type III cement used.
[b]Type I cement used.
(—) Material not used in this mix.
Note: 1 m^3 = 1.308 yd^3 ; 1 kg = 2.205 lb ; 1 L = 0.264 gal ; 1 ml = 0.0338 fl.oz.

TABLE 2 Developed Predictive Relationships for I-20 mixes

Mix	Predictor	Equation	R^2
VES	Pulse Velocity	$\log f'c = 1.27 \times 10^{-4}$ PV + 1.844	0.98
	Nurse-Saul	$1/f'c = 0.062/MAT + 1.72 \times 10^{-4}$	0.99
	Arrhenius	$1/f'c = 6.06 \times 10^{-3}/MAT + 1.68 \times 10^{-4}$	0.99
Fast Track	Pulse Velocity	$\log f'c = 5.47 \log PV - 19.09$	0.99
	Nurse-Saul	$f'c = -22.69 \times 10^3/MAT + 5161$	0.99
	Arrhenius	$f'c = -59.44 \times 10^3/MAT + 5163$	0.99
GADOT	Pulse Velocity	$1/f'c = 30.48PV - 1.91 \times 10^{-3}$	0.99
	Nurse-Saul	$\log f'c = -203.4/MAT + 3.717$	0.97
	Arrhenius	$\log f'c = -6.762/MAT + 3.705$	0.98

the blocks could be removed to leave square cavities in which to place an ultrasonic transmitter and receiver. As was done with the thermocouple trees, the blockouts were positioned away from slab edges to minimize edge cooling effects. The pulse velocity transmitter and receiver were placed at mid-depth of the slab in the cavities in order to obtain the direct transmission pulse velocity readings.

FINDINGS AND DISCUSSION

Temperature Development in Test Slabs

To estimate strength gain from maturity data, the temperature of the patches was monitored throughout the period of cure. Temperature profiles for the VES slab are shown in Figure 1. It can be seen that the mid-depth of the slab reached the highest temperatures at any point during the monitoring, as would be expected from the relatively stable nighttime air temperature range of 21°C to 26°C (70 °F to 80 °F), which allowed heat to escape from the top of the slab. The insulated cylinders at first lagged the slab, but then gained in temperature and eventually exceeded the slab temperature. About 5 hr after placement, the slab temperature stabilized at about 60°C (140°F) and then began to go downward, whereas the insulated cylinder temperature continued to rise to close to 70°C (160°F). Temperature profiles for the fast track slab are shown in Figure 2; peak temperatures are about 10°C (20°F) cooler than for the VES mix. That is to be expected considering the lower cement content and absence of accelerating admixtures. The fast track mix took longer to reach its peak (5.5 hr as opposed to 4 hr for VES). Again, the insulated box temperatures continued to rise after the slab had reached peak temperature. Finally, temperature profiles for the GADOT mix are shown in Figure 3. Peak temperature of 50°C (122°F) at 4 hr is very similar to that of the fast track mix.

Strength Gain Prediction Using Maturity and Pulse Velocity Techniques

Temperature data acquired from the test sections were used to develop plots of time versus predicted compressive strength using maturity and pulse velocity predictive functions (Table 2). Note that the strength that is predicted will be dependent on the location within the slab from which the temperature data are taken. As compressive strengths were to be compared with cores taken through the depth of the pavement, an average through-depth pavement temperature was calculated at each time increment. Two 100 × 200-mm (4 × 8-in.) cores were removed from each of two of the three test sections for field testing and comparison with predicted values. It was not possible to remove cores from the GADOT section, as construction activities prevented coring operations at this location.

Predictions of early compressive strength for the three mixes, VES, fast track, and GADOT are shown in Figures 4–6, respec-

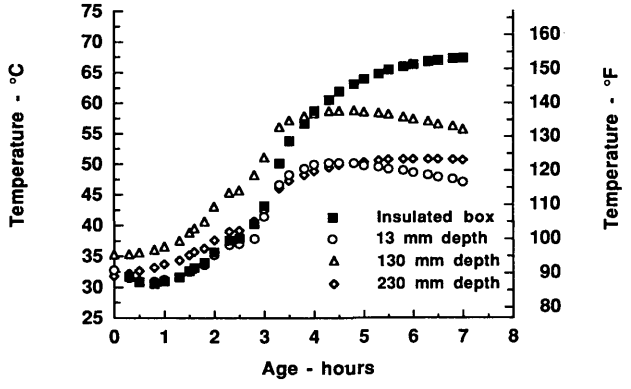

FIGURE 1 Temperature profiles for VES mix.

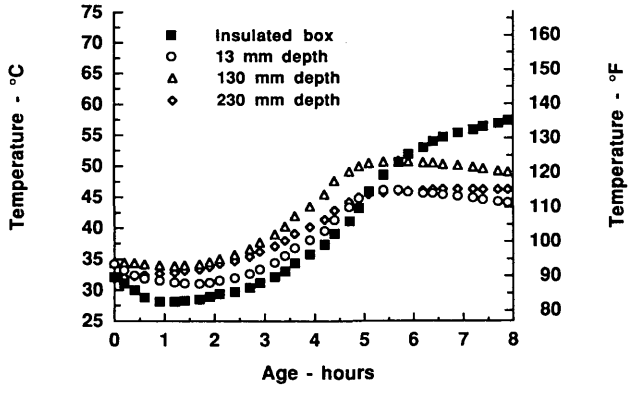

FIGURE 2 Temperature profiles for fast track mix.

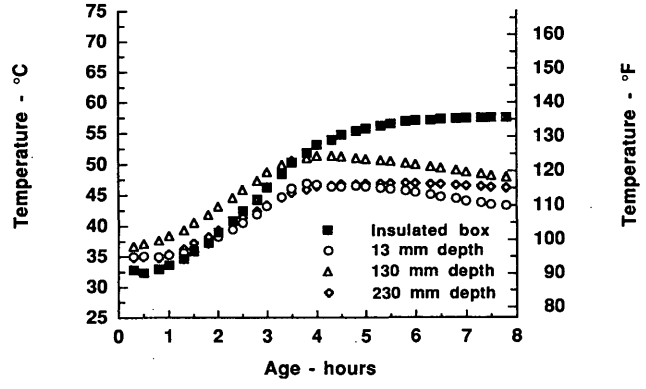

FIGURE 3 Temperature profiles for GADOT mix.

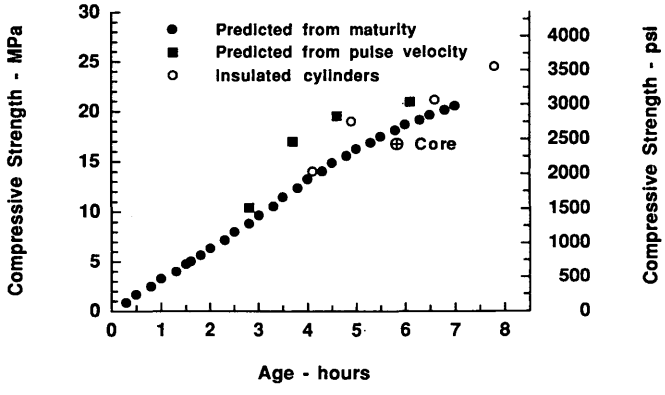

FIGURE 4 Compressive strength predictions for VES mix.

tively. Strengths predicted via maturity are shown for the approach (Equation 1 or 3) yielding the best prediction as measured by cores extracted from the test sections. For VES, the Nurse-Saul function (Equation 1) gave predicted values closest to core strengths. For fast track, the Arrhenius function (Equation 3) was more successful. Finally, for the GADOT mix, although no comparison core data were available, strengths predicted via the two approaches were within an average of 5 percent of each other. In addition to strengths predicted via maturity and pulse velocity, the strengths of cylinders stored in the insulated curing box are also presented.

For the VES mix (Figure 4) strengths predicted by maturity calculations were similar to strengths predicted by pulse velocity at early ages, but lower than both the pulse velocity predicted strengths and the strengths measured on cylinders taken from the insulated curing box at later times. At the time selected for sampling from this section (5.8 hr after casting), strength predicted from maturity was 18 MPa (2,600 psi) and that from pulse velocity was 20 MPa (2,900 psi). These values are 6 and 20 percent higher, respectively, than the measured core strengths of 17 MPa (2,450 psi). The somewhat higher strength predicted by the pulse velocity technique is reasonable, as pulse velocity transducers were placed near the middle of the pavement [a 130-mm (5-in.) depth], where the higher temperatures (Figure 1) would lead to a higher local strength at that elevation.

Similar data for the fast track mix are presented in Figure 5. There is a large discrepancy between the techniques at ages up to 8 hr. In fact, up to about 6 hr the maturity function predicts that the concrete will not gain any strength, although the ability to obtain pulse velocity readings on the actual slab indicates that the concrete as-placed was indeed gaining strength during that time. The reason for this most likely relates to the procedure used in the laboratory to establish the maturity function for this mix. As the fast track mix was placed into the 12- to 24-hr opening category in terms of the overall SHRP research project, initial strength measurements made for purposes of developing the maturity function (Arrhenius) were not obtained until after 12 hr of curing. Therefore, it appears that although the function should be applicable to all time/temperature combinations in theory, in actual practice, its range of applicability may be more restricted. Eight hr after casting, however, the methods tend to converge. At the time of sampling (7.8 hr) core strength was 8 MPa (1,150 psi), strength predicted by maturity was 7.6 MPa (1,100 psi), and strength predicted by pulse velocity was 10 MPa (1,450 psi). Again, as for the VES mix, the best predictor of strength appears to be the maturity function, as the core strength lies exactly on the line of prediction.

Finally, Figure 6 shows data developed on the GADOT mix. Here again, maturity predicts somewhat lower strengths at early ages, but after about 5 hr all methods fall within the same general band. Unfortunately, as previously noted, cores could not be retrieved from this slab.

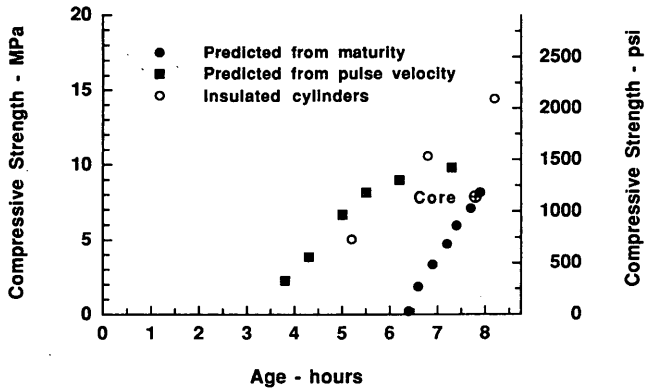

FIGURE 5 Compressive strength predictions for fast track mix.

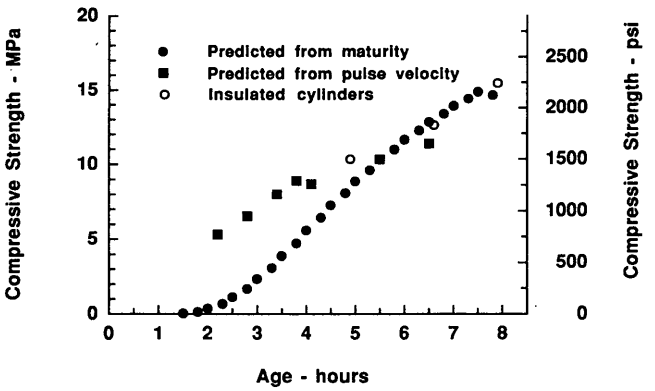

FIGURE 6 Compressive strength predictions for GADOT mix.

CONCLUSIONS

Based on the results of the study described in this paper the following conclusions may be drawn:

- NDT readings must be calibrated to strength before construction. Strength as a function of NDT reading must be established using job materials and proposed mix designs. Changes in mix design or materials during construction can lead to significant predictive errors.
- Both maturity and pulse velocity techniques can be used to monitor early strength gain during the curing period in pavement repair slabs. Results obtained using these techniques agree favorably with strengths of cores extracted from repair sections before opening to traffic.
- The maturity approach offers a more exact prediction of strengths close to time of opening. At earlier ages, however, the maturity approach appears to significantly underestimate strength in some instances.
- Both techniques employed in this study are practical and well suited to field operations. However, significant amounts of calibration must be done in the laboratory before either method is used on a particular job. It is likely then, that the methods will have their greatest application on larger and longer-term projects for which the same mix is repeated many times and rate of strength gain must be verified in the field.

ACKNOWLEDGMENTS

This research was carried out under the SHRP. The authors would like to acknowledge the Georgia Department of Transportation's assistance in making field sites available for the study. The authors also would like to thank Tom Yu of ERES Consultants, Inc., for assistance in site selection and field activities, and Inam Jawed, SHRP program manager, for advice and encouragement throughout the course of the study.

REFERENCES

1. Whiting, D., A. Todres, M. Nagi, T. Yu, D. Peshkin, M. Darter, J. Holm, M. Andersen, and M. Geiker. *Synthesis of Current and Projected Concrete Highway Technology.* SHRP-C-345, Strategic Highway Research Program, National Research Council, Washington, D.C., 1993.
2. Pearson, R. I. Fast-Track Concrete Paving. *Concrete International.* Vol. 10, No. 8, Aug. 1988, pp. 33–35.
3. Grove, J. D., K. B. Jones, K. S. Bharil, A. Abdulshafi, and W. Calderwood. Fast Track and Fast Track II, Cedar Rapids, Iowa. In *Transportation Research Record 1282,* TRB, National Research Council, Washington, D. C., 1990, pp. 1–7.
4. NCHRP Synthesis of Highway Practice No. 45: *Rapid-Setting Materials for Patching of Concrete.* TRB, National Research Council, Washington, D.C ., 1977.
5. In-Place Methods for Determination of Strength of Concrete. ACI Committee Report 228.1R. *ACI Materials Journal,* Vol. 85, No. 5, 1988, pp. 446–472.
6. Carino, N. J., H. S. Lew, and C. K. Volz. Early Age Temperature Effects on Concrete Strength Prediction by the Maturity Method. *ACI Journal Proceedings,* Vol. 80, No. 2, 1983, pp. 199–208.
7. Nurse, S. W. Steam Curing of Concrete. *Magazine of Concrete Research,* Vol. 1, No. 2, 1949, pp. 79–88.
8. Saul, A. G. A. Principles Underlying the Steam Curing of Concrete at Atmospheric Pressure. *Magazine of Concrete Research,* Vol. 2, No. 6, 1951, pp. 127–140.
9. Hansen, F. P., and J. Pederson. Maturity Computer for Controlled Curing and Hardening of Concrete. *Nordisk Betong,* Vol. 21, No. 1, 1977, pp. 19–34.
10. Whiting, D., M. Nagi, P. Okamoto, T. Yu, D. Peshkin, K. Smith, M. Darter, J. Clifton, and L. Kaetzel. *Optimization of Highway Concrete Technology.* SHRP-C-373. Strategic Highway Research Program, National Research Council, Washington, D. C., 1994.
11. Zia, P., M. L. Leming, and S. H. Ahmad. *Mechanical Properties of High Performance Concrete* Strategic Highway Research Program, National Research Council Washington, D.C., (forthcoming).
12. Burg, R. G., and B. W Ost. *Engineering Properties of Commercially Available High-Strength Concretes.* Research and Development Bulletin RD 104T. Portland Cement Association, Skokie, Ill., 1992.

Publication of this paper sponsored by Committee on Chemical Additions and Admixtures for Concrete.

Influence of Early Heat Curing on Properties of 100-MPa Air-Entrained Concrete

K.H. KHAYAT AND M. LESSARD

An air-entrained, high-strength concrete was prepared in a precasting plant to evaluate the effect of initial heat treatment and subsequent outdoor storage on concrete characteristics. One set of standard specimens was cured in lime-saturated water at 23°C until testing. Another set of specimens and a large panel were heat cured on a steel bed heated by 50°C water circulating underneath it. Heating began 6 hr following concrete casting and lasted for 8 hr. Heated concrete remained on the bed for an additional 6 hr before demolding; it was then cured indoor at 15°C until the age of 7 days before outdoor storage. Investigated properties included temperature rise, compressive, splitting tensile, and flexural strengths, modulus of elasticity, chloride ion permeability, and frost durability. Mechanical properties were evaluated at 1, 4, 28, 91, and 365 days. Test results indicate that the investigated concrete can secure high early strength without early heat curing. Initial heating increased compressive strength; however, such heat treatment coupled with subsequent outdoor storage had a deleterious effect on ultimate strength, especially for concrete from the precast panel where initial peak temperature was 56°C, compared with 42°C for accompanying heated specimens. Maximum reductions in compressive, splitting tensile, and flexural strengths and modulus of elasticity of concrete subjected to early heat curing and subsequent outdoor storage compared with standard-cured specimens were approximately 15, 35, 40, and 15 percent, respectively. Regardless of curing history, the concrete exhibited excellent frost durability. Mercury intrusion porosimetry of 1-yr old samples demonstrated that heated concrete had greater porosity than standard-cured concrete and higher concentrations of pores with 1–5 μm diameter. That was confirmed by microscopical examination; however, no particular increase in microcracking in the paste or transition zone of heated concrete, as compared with moist-cured concrete, was observed.

In recent years, there has been a growing interest in the use of high-strength concrete (HSC) in the precasting industry. The increase in compressive and tensile strength capacities enable the application of greater service loads or the production of more slender and lighter structural elements at reduced cost. The use of HSC can improve the bond strength to prestressed strands and reduce the transfer and development lengths of pretensioned strands. Similarly, the relatively low creep of HSC can decrease long-term deformations and prestressing losses. The increase in the modulus of elasticity also can reduce elastic deflections and shortening losses. Finally, the improved durability of HSC can lower the maintenance cost of precast structural and architectural elements.

Soon after casting, precast concrete elements are often heated by low- or high-pressure steam, radiant heat from hot oil or water pipes, or electric-resistance heating. This is done to accelerate early-strength development and enable the early release of prestressing strands and the rapid stripping and reuse of precasting molds. Such accelerated curing increases early-age compressive strength and modulus of elasticity developments (*1–6*) and to a lesser degree splitting tensile strength (*5,6*). Whenever the concrete is subjected to elevated curing temperatures for a few hours at very early ages or cured at elevated temperatures for longer periods, the development in long-term mechanical properties may be adversely affected (*1–6*). For example, conventional concrete with a water-to-binder ratio of 0.41 to 0.55 that was cured continuously at 50°C developed 20 to 30 percent lower strength after 28 days and one year, respectively, compared with similar concrete cured at 20°C (*6*).

What causes long-term reduction of mechanical properties from early exposure to elevated temperatures is not well understood. Richartz (*7*) observes that high initial temperature affects the morphology of the hydration products. Accelerated heat curing is reported to result in rapid formation of short-fibered calcium silicate hydrate (C-S-H) instead of long-fibered C-S-H. That could occur whenever the initial hydration rate was slowed down, either by low temperature curing or by incorporating a set retarder. Unlike the long-fibered phase, the short-fibered C-S-H did not appear to span the available gel pore space in the early hydration phase. The formation of short-fibered C-S-H then could reduce the interlock between C-S-H fibers and restrict subsequent development of longer fibers; hence, it could limit ultimate strength (*7*).

High initial curing temperatures accelerate the rate of cement hydration that can exceed the rate of diffusion of hydration products. Dense hydration products then can precipitate near cement grains and decrease the rate of subsequent diffusion and precipitation of additional hydration products throughout the interstitial space between cement grains (*8*). The resulting increase in large pore volume was observed by Goto and Roy (*9*), as total porosities of cement pastes made with water-to-cement ratios of 0.35, 0.40, and 0.45 cured at 60°C were considerably greater than those of pastes hydrated at 27°C. The difference in porosity is attributed to spreads in volume of pores with diameters 150–460 nm. Pastes with substantial volumes of pores with diameters greater than 150 nm also were found to exhibit higher water permeability values. Similar observations were reported by Kjellsen et al. (*10,11*), who compared the pore structure and microstructure of two identical cement pastes made with a water-to-cement ratio of 0.50, one cured at 5°C and another at 50°C. Greater total porosity and an increase in the volume of relatively coarse pores were observed in paste subjected to the higher curing temperature after approximately 70 percent of hydration. That was especially true for pores of diameters 40–200 nm. Using a backscatter electron microscope and image analysis techniques to examine relative densities of various microstructures, cement paste cured at 5°C was reported to have a more uniform

Université de Sherbrooke, Faculty of Applied Science, Department of Civil Engineering, Sherbrooke, Quebec, J1K 2R1, Canada.

C-S-H phase than that cured at 50°C. The latter was reported to have a dense and strong C-S-H "shell" around cement grains but porous C-S-H in the interstices between cement particles. The presence of such porous C-S-H and the observed coarsening of capillary pores can detrimentally affect the development of mechanical properties and durability. Detwiler et al. (*12*) further reported that increase in capillary porosity in the cement paste resulting from curing at 50°C versus 5°C causes an increase in chloride ion diffusion, especially in low water-to-cement ratio systems. (0.40 versus 0.50 and 0.58).

Unlike conventional concrete, there is limited information on the effect of early-age heat curing on the long-term characteristics of HSC. Laamanen et al. (*4*) tested the effect of early heat curing on the loss of compressive strength of concrete mixtures made with water-to-binder ratios of 0.30, 0.45, and 0.60, which contained 0 or 8 percent silica fume replacements. The beginning of heat treatment was varied to allow concrete to attain initial strength varying between 0 and 15 MPa. Samples first were stored in 40°C water baths for one hour before transferring them to 60°C water baths. The heat curing lasted for 6 days, then the specimens were stored in 20°C baths until the age of testing at 28 days. The authors reported that HSC can undergo less reduction in strength from early heat curing than can conventional concrete, and that silica fume concrete can exhibit smaller reduction in compressive strength than can non-silica fume concrete. The delay period before heat treatment was found to have no significant effect on the development of compressive strength at 28 days, providing that the strength of the concrete exceeded 3 MPa before heating.

Kanda et al (*13*) investigated HSC made with 12 percent silica fume replacement and a water-to-binder ratio of 0.25. Heat treatment started 8 to 10 hours after casting and consisted of curing concrete under temperature-match conditions in water baths in which temperatures were adjusted to reflect those recorded in cast and insulated concrete blocks. Maximum curing temperatures varied between 45 and 75°C. Following a 5-day accelerated curing period, the specimens were sealed and cured at 20°C until the age of testing at 28 days. The study showed that the 28-day compressive strength of heat-treated HSC can be 10 ± 5 percent less than that of concrete cured at 20°C.

Lindgard and Sellevold (*14*) examined the influence of heat curing on compressive strength of HSC made with water-to-binder ratios of 0.30 to 0.33. Heat treatment was started 6 hr after casting and lasted for 3 days at either 40 or 60°C. Specimens gradually were cooled before storage in 20°C water bath. Reduction in strength development was found to decrease with the reduction in water-to-binder ratio and the decrease in curing temperature. Compared with concrete continuously cured in water at 20°C, HSC had 15 to 25 percent reduction in uniaxial tensile strength and 10 to 20 percent reduction in flexural strength at 60 days. No significant differences were observed for compressive strength, elastic modulus, strains at maximum compression and tensile stresses, fracture energy, and durability.

Gjørv and Martinsen (*15*) demonstrated that up to 28 days, curing HSC made with lightweight aggregate at temperatures up to 90°C had no adverse effect on compressive strength, modulus of elasticity, capillary absorption, porosity, or resistance to water permeability. However, elevated curing temperatures of 50°C and 90°C had detrimental effects on rapid chloride ion permeability, suggesting that the concrete had a more open and porous microstructure than that cured at 20°C. Similar observations were reported by Sandvik and Gjørv (*16*) on 65-MPa lightweight concrete made with 4 percent silica fume with a water-to-binder ratio of 0.43. Core samples obtained from a slab for which maximum recorded temperatures reached 85°C showed no drops in compressive strength or elastic modulus. However, rapid chloride ion permeability values were found to increase whenever the peak temperature exceeded 50°C.

Soon after production, precast elements often are put to use at early ages, or they can be stockpiled outdoor before shipment to job sites without any additional moist curing. The limitation of moist curing can affect the ultimate characteristics of HSC. Asselanis et al. (*17*) compared the gains in compressive strength and modulus of elasticity of HSC subjected to various durations of moist curing. The concrete had a water-to-binder ratio of 0.28 and incorporated 9 percent silica fume replacement. Compressive strength and elastic modulus values of air-dried concrete were found to be 18 and 15 percent lower, respectively, than moist-cured concrete after 28 days of curing. Similar results were obtained at 56 days. A minimum duration of moist curing of 7 days was recommended for such HSC (*17*).

As more construction is done using precast HSC, it is important to investigate the combined impact of accelerated early heat curing and subsequent exposure to the atmosphere without further moist curing on the development of engineering properties and potential durability to provide information on possible consequences and practical implications of such practices. In this research, methods are assessed by evaluating any reduction in compressive, flexural, and splitting tensile strengths: modulus of elasticity; chloride ion impermeability; and resistance to freezing and thawing of HSC.

EXPERIMENTAL PROGRAM

Concrete Mixture

An optimized, air-entrained HSC with an approximate 91-day compressive strength of 100 MPa was cast. A 530 kg/m^3 of a blended silica fume cement containing approximately 7.5 percent silica fume by mass was used. The concrete had a water-to-binder ratio of 0.22. The fine aggregate was a natural sand with specific gravity and absorption values of 2.67 and 0.9 percent, respectively. The coarse aggregate was a crushed dolomitic limestone with a nominal size of 10 mm and specific gravity and absorption values of 2.75 and 0.8 percent, respectively. The contents of the sand and coarse aggregate were 700 and 1080 kg/m^3, respectively.

A sulfonated napththalene-based high-range water reducer (ASTM C494, Type F) was used at 19 L/m^3. The concrete incorporated a hydroxylated carboxylic acid-based set retarding admixture (ASTM C494, Type D) and a neutralized vinsol resin-based air-entraining admixture (ASTM C260) at 0.74 and 0.30 L/m^3, respectively. The panel and standard specimens were cast from a single batch. The concrete had an initial slump of 220 mm.

Curing Conditions

The concrete was cast indoors in a precast concrete plant in Montreal, Quebec. Reference specimens were cast and covered with wet burlap and a polyethylene sheet to minimize evaporation. The specimens were demolded after one day and stored in lime-saturated water at approximately 23°C, in accordance with ACNOR CAN3-A23.2-3C and ASTM C192. The specimens were kept moist until the time of testing and were tested under moist conditions.

A second series of molded specimens was cured under an insulating blanket on a steel bed heated with 50°C water circulating

underneath through a dense network of pipes. The concrete began to harden after approximately 4.5 hr. The heat treatment was delayed for approximately 6 hr following casting, or 6.5 hr after the beginning of mixing. The circulation of hot water lasted for 8 hr, but the concrete remained on the hot steel bed for approximately 6 additional hr before demolding and removal. A concrete panel measuring 2.7 × 1 × 0.3 m was also cast on the same heating bed and subjected to early temperature curing identical to that of heated specimens. The heat rise of concrete was monitored for approximately one day using thermocouples placed in the centers of 100 × 200-mm standard-cured and heat-cured cylinders and precast panel.

After demolding, the panel along with heated specimens were kept indoors at approximately 15°C without supplemental water curing until they were aged 7 days. This was to allow gradual cooling and to minimize the formation of hairline cracks and crazing that can result from thermal and drying shrinkage. All heat-treated cast specimens were sealed using aluminum and plastic wrapping before outdoor storage to minimize water loss. The curing sequence was done in compliance with the precasting plant's standard practice for manufacturing structural elements and architectural panels using conventional concrete. Heated specimens and precast panel were stored outdoors where the concrete could be exposed to substantial temperature differentials and drying winds until testing time.

A few days before testing, molded specimens and samples from the panel were sealed and brought to the laboratory. Core ends were cut to obtain 200-mm long samples corresponding to concrete from the center of the panel, which can be less affected by drying than can surface concrete.

Test Specimens

The concrete was sampled for compressive strength, elastic modulus, flexural and splitting tensile strengths, chloride ion permeability, and frost durability. Table 1 indicates the various tests performed along with specimen dimensions. A total of 110 molded specimens and 55 cored and sawn samples obtained from the precast panel were tested. All cylinder and core ends used to evaluate compressive strength and elastic modulus were ground to ensure smooth and perpendicular end surfaces.

For each concrete, mercury intrusion porosimetry was done on two cores measuring 38 mm in length and 19 mm in diameter. The cores were taken from 1-year old specimens. Effort was made to avoid high concentrations of coarse aggregate in the cores. The samples were submerged into acetone for 6 hr then oven dried at 105°C until they reached constant mass to ensure complete drying. Water absorption was measured on similar specimens by measuring weight losses of water-saturated specimens following oven drying. The mercury intrusion porosimetry apparatus permitted the intrusion of pores with apparent pore diameters ranging between approximately 5 nm and 5μm.

TEST RESULTS

Tested mechanical properties are summarized in Table 2 along with their corresponding coefficients of variations. Results of the air-void systems of the hardened concrete, chloride ion permeability, and frost durability are also compiled in Table 2. Figure 1 shows the temperature-time history of the three concretes.

Figures 2 and 3 show cumulative pore size distributions of dry samples measured by mercury intrusion porosimetry. Figures 4 and 5 compare compressive strength, elastic modulus, flexural strength, splitting tensile strength of heated specimens and samples obtained from the panel to those of standard-cured concrete. Figures 6 and 7 compare normalized strength ratios of heat-treated concrete to those obtained for standard-cured concrete. The normalization was done by dividing the ratios of flexural-to-compressive strength, splitting tensile-to-compressive strength, and modulus of elasticity-to-

TABLE 1 Testing Program

	Dimensions of Specimens (mm)	Number of Specimens	Type of Specimens	Standard
Compressive Strength	100 x 200	30	Cast	ASTM C39
	95 x 190	15	Cored	
Modulus of Elasticity	100 x 200	16	Cast	ASTM C469
	95 x 190	8	Cored	
Flexural Strength	100 x 100 x 400	24	Cast	ASTM C78
		12	Sawn	
Splitting Tensile Strength	150 x 300	24	Cast	ASTM C496
		12	Cored	
Spacing Factor	100 x 200	4	Cast	ASTM C457
	95 x 190	2	Cored	
Chloride Ion Permeability	100 x 200	8	Cast	AASHTO T277
	95 x 190	4	Cored	
Freeze/thaw Durability	75 x 75 x 350	4	Cast	ASTM C666
		2	Sawn	(Procedure A)

TABLE 2 Summary of Test Results

	Standard Curing					Accelerated Heat Curing									
	ACNOR CAN3-A23.2-3C					Heated Specimens					Cores from Panel				
Age	33 h	4 d	28 d	91 d	1 yr	33 h	4 d	28 d	91 d	1 yr	33 h	4 d	28 d	91 d	1 yr
F_c (MPa)	36.1	63.5	89.1	103.3	108.8	53.0	57.4	76.1	87.3	109.3	55.2	63.6	75.4	82.6	102.5
C.O.V. (%)	2.9	0.5	1.5	2.0	0.1	0.9	6.5	0.8	0.7	6.9	7.3	4.3	3.5	1.2	3.1
E_c (GPa)	–	35	44	46	49	–	36	38	41	48	–	35	37	40	44
C.O.V. (%)	–	0.4	3.1	4.9	0.7	–	5.3	4.5	0	0	–	3.8	1.9	3.4	0.8
MR (MPa)	–	8.3	10.0	10.8	–	–	5.8	6.1	7.2	7.6	–	4.9	6.1	6.3	7.9
C.O.V. (%)	–	7.9	5.0	2.8	–	–	11	1.6	13.7	--	–	7.6	6.6	4.8	4.8
F_{sp} (MPa)	–	4.5	5.2	6.1	6.9	–	3.9	4.3	4.9	4.9	–	3.4	3.3	4.1	4.7
C.O.V. (%)	–	19.8	3.3	8.7	4.2	–	7.5	11.1	11.4	6.1	–	6.2	7.6	22.3	4.3
MR/F_c (%)	–	13.1	11.2	10.5	–	–	10.1	8.0	8.3	7.0	–	7.7	8.1	7.6	7.7
F_{sp}/F_c (%)	–	7.1	5.8	5.9	6.3	–	6.8	5.7	5.6	4.5	–	5.3	4.4	5.0	4.6
							Strength Ratio of Standard-Cured Concrete								
MR/F_c (%)							77	71	79			59	72	73	
F_{sp}/F_c (%)							96	97	95	71		75	75	84	72
$E_c/(F_c)^{0.5}$							108	93	97	99		100	92	97	93
Cl^- Per. (coulombs)	1450	560	210	100			1250	1070	590	160		1050	1120	760	150
Initial Current (mA)	64	28	13	7			60	51	28	13		47	54	37	9
Water Absorb. (%)				2.7						2.9					3.3
Total Porosity (mm^3/g)				22.4						24.1					29.5
							Frost Durability								
Air Vol. Hard. Conc. (%)			4.7				4.7					5.9			
Spacing Factor (μm)			380				380					370			
Specific Surface (mm^{-1})			14				15					13			
Pulse Velocity (% V_o)			100				103					100			
Durability Factor (%)			100				106					100			
Elongation After 300 Cycles (μm/m)			460				200					400			

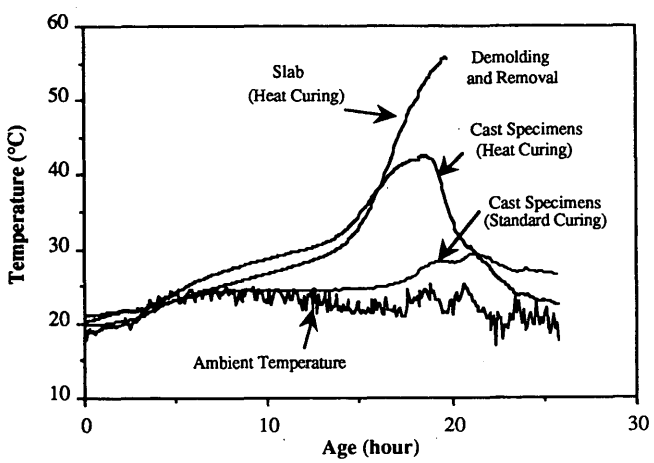

FIGURE 1 Initial temperature rise.

square root of compressive strength of heated concrete by corresponding ratios obtained from the moist-cured concrete.

Figures 8 and 9 show backscattered electron images of 1-year old standard-cured concrete as well as that taken from the precast panel.

DISCUSSION OF RESULTS

Temperature Rise

Peak concrete temperatures measured in the panel and in 100- × 200-mm specimen at the time of demolding were 56°C and 42°C, respectively. The moist-cured specimen exhibited a delay in temperature rise and had a peak temperature of 29°C. The sharp increase in temperature recorded in heated concrete after approximately 15 hr of age coincided with the increase in hydration rate of cement. Such initial temperature rise can accelerate the rate of

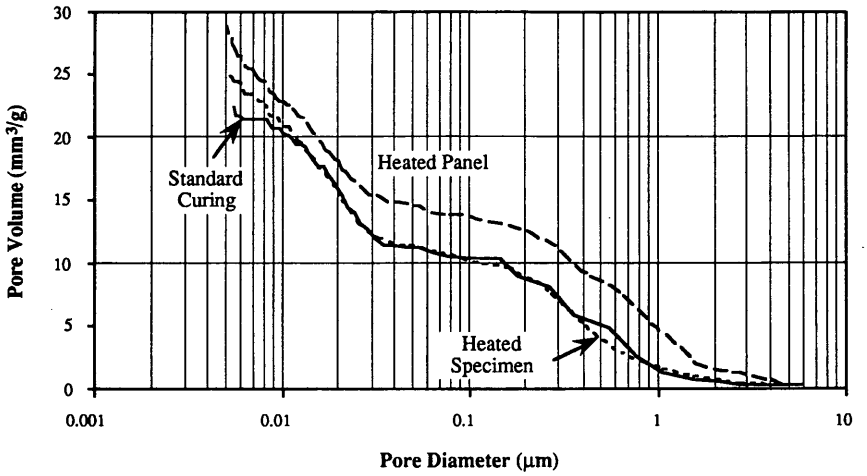

FIGURE 2 Cumulative pore size distribution.

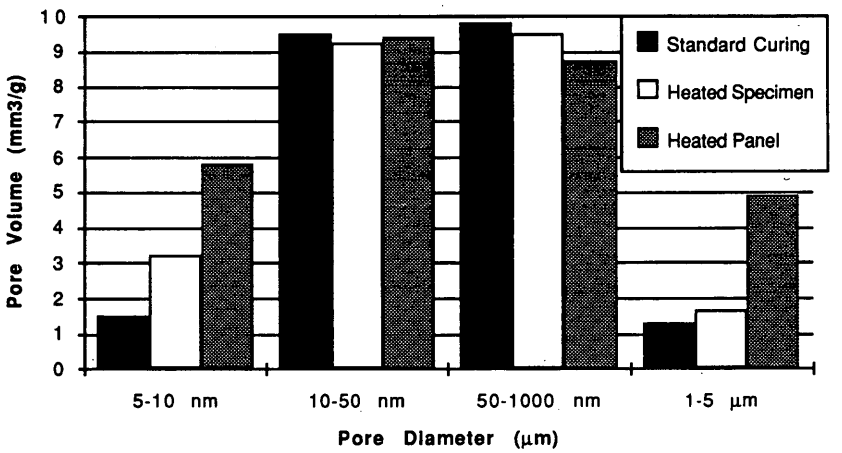

FIGURE 3 Pore size distribution.

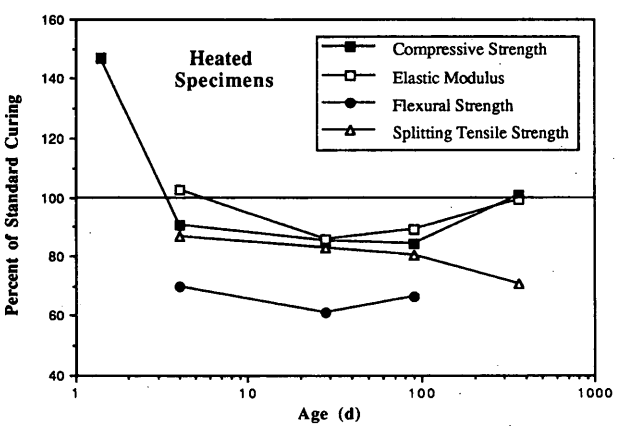

FIGURE 4 Mechanical properties of heated specimens versus standard specimens.

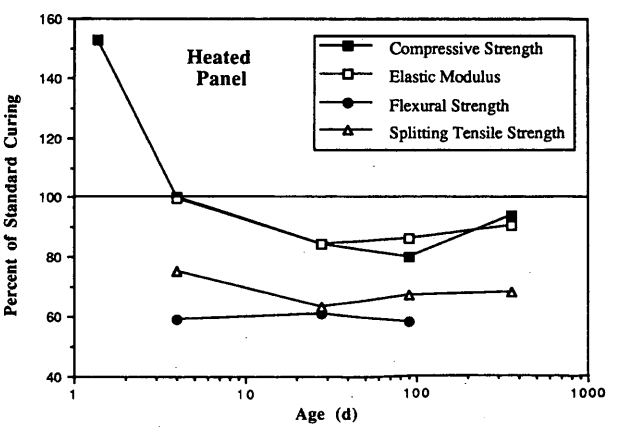

FIGURE 5 Mechanical properties of heated panel versus standard specimens.

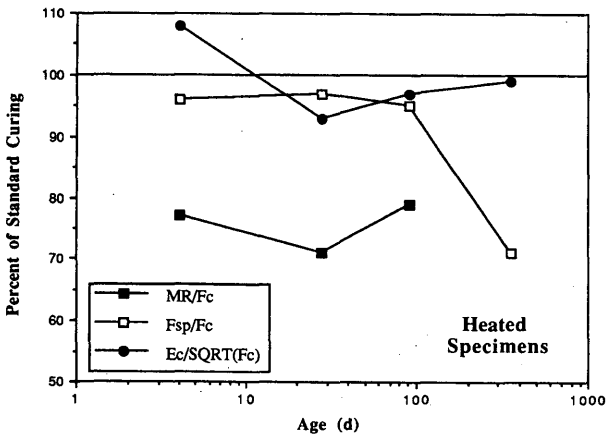

FIGURE 6 Normalized properties of heated versus standard specimens.

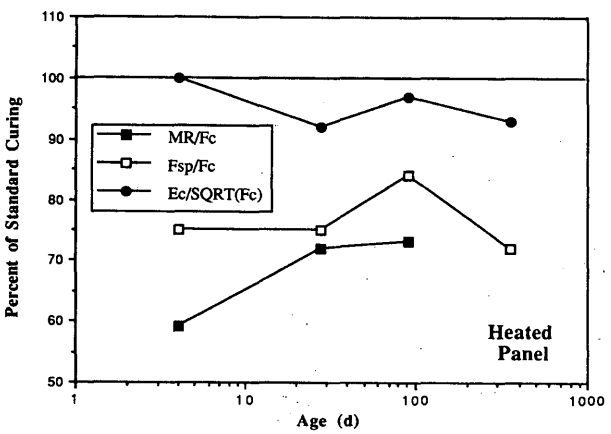

FIGURE 7 Normalized properties of panel samples versus standard specimens.

hydration of cement, which may adversely affect the development of engineering properties.

Mercury Intrusion Porosimetry

Cumulative pore size distribution curves indicate that concrete from the heat-treated panel developed greater total porosity and coarser pore volume than standard-cured and heated specimens. The latter two concretes had almost identical porosity and pore-size distribution values. The mean measured total porosity of 1-year old samples taken from the moist-cured concrete, heated-cylinders, and heated-panel were 22.4, 24.1, and 29.5 mm^3/g, respectively. Similarly, the mean values of water absorption were 2.7, 2.9, and 3.3 percent, respectively.

A comparison of pore size distribution of capillary pores indicates that an increase in total measured capillary porosity is mostly the result of increases in pores with diameters 5–10 nm and 1–5 μm. Mehta and Manmohan (*18*) suggest that capillary pores measured by mercury intrusion porosimetry with diameters greater than 100 nm can be considered to be relatively large pores, ones that can affect permeability and strength. The greater volume of large pores with diameters 1–5 μm in the heat-treated panel can therefore be expected to have a deleterious effect on permeability and strength.

Compressive Strength and Elasticity Modulus

Heat-cured cylinders and core samples had mean compressive strengths of 53.0 and 55.2 MPa, respectively, at 33 hr of age compared to 36.1 MPa for standard-cured concrete. However, beyond 4 days of age, the compressive strength of the standard-cured concrete was greater than that of heat-cured concrete. Both types of heat-treated concrete developed similar compressive strengths up to 91 days. Their compressive strengths at 28 and 91 days, respectively, were approximately 15 and 15–20 percent lower than those of standard-cured concretes. Between 91 days and 1 year, the moist-cured concrete had a slower rate of strength gain than heat-treated concretes. Both control and heated cylinders tested similar compressive strengths after 1 year; their strength was approximately 6 percent greater than the mean strength of cores from the heated panel.

As in the case of compressive strength, early temperature curing had no significant effect on the modulus of elasticity after 4 days of

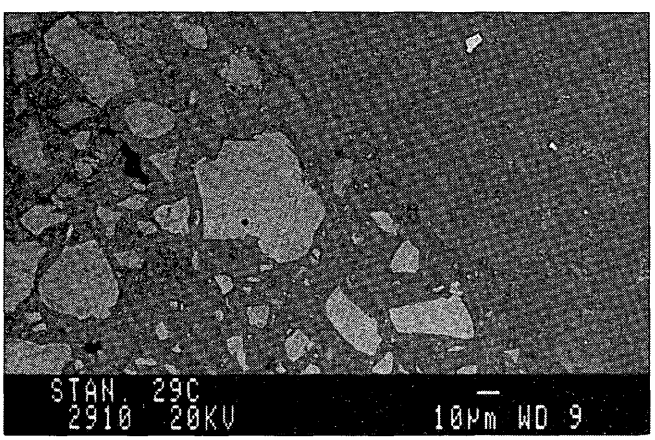

FIGURE 8 Backscattered electron images of standard-cured concrete.

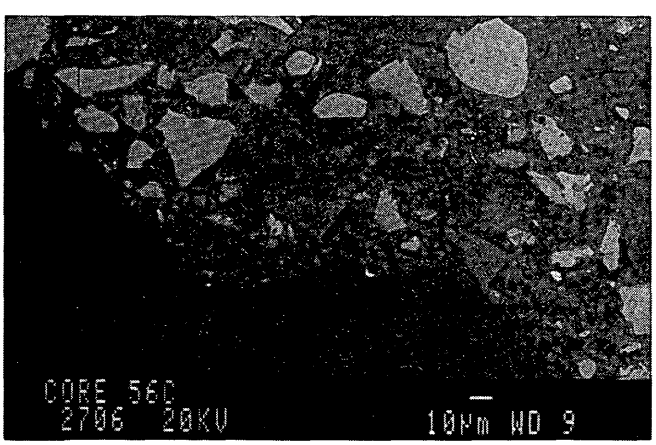

FIGURE 9 Backscattered electron images of precast panel concrete.

curing. However, there was a significant spread between the modulus of elasticity of heat-treated and standard-cured concretes at 28 and 91 days. The spread was approximately 15 and 10–15 percent at 28 and 91 days, respectively. After one year, the modulus of elasticity values of standard-cured and heat-treated molded specimens were identical, measuring approximately 9 percent more than those of cores obtained from the panel.

Flexural and Splitting Tensile Strengths

The initial increase in curing temperature and subsequent outdoor storage of the HSC had detrimental effect on flexural and splitting tensile strengths. Rates of gains in flexural strength were similar for the three concrete types. Molded specimens subjected to early heat curing and subsequent outdoor storage exhibited approximately 30 to 40 percent reduction in flexural strengths and 15 to 30 percent in splitting tensile strength, compared with standard-cured specimens. Samples obtained from the precast panel indicated approximately 40 percent reduction in flexural strength and 25 to 35 percent reduction in splitting tensile strength. In general, the spread between splitting tensile strength of heat-treated and standard-cured concretes increased with age, indicating a slowing down in the rate of strength gain of the latter concrete.

Chloride Ion Permeability

Standard-cured concrete had a slightly greater initially permeability to chloride ions than heat-treated concrete. However, after 28 and 91 days of curing the chloride ion permeabilities of standard-cured concrete were considerably lower than those of heated concrete. These differences are important since precast elements can be put into service before 91 days. The greater chloride ion permeabilities of the heated concrete may be mostly due to the greater capillary porosity and the coarser pore structure detected by mercury porosimetry compared to that of moist-cured concrete. Chloride ion permeability measurements of 1-year-old concrete showed that all three concretes had negligible chloride ion permeability levels that ranged between 100 and 160 coulomb indicating a highly discontinuous pore structure.

Frost Resistance

All concretes had similar spacing factors (370 to 380 μm) and specific surface values of air bubbles (13 to 15 mm^2/mm^3). Regardless of the temperature history and curing mode, all tested concretes exhibited excellent durability to freezing and thawing and had durability factors ranging between 100 and 106 percent.

Reduction in Mechanical Properties and Microstructure

Early heat curing appears to have a more lasting and significant effect on splitting tensile strength and modulus of rupture than on compressive strength or modulus of elasticity. That may be because of changes in the microstructure of the bulk cement paste or in the interface between aggregate and cement paste.

Using normalized strength ratios (Figures 6 and 7), it is possible to determine the percentage reduction in mechanical properties compared with those obtained for standard cured concrete. For heated specimens that developed a peak temperature of 43°C and were sealed before outdoor storage, maximum reductions in flexural strength, splitting tensile strength, and modulus of elasticity were 29, 29, and 7 percent, respectively. On the other hand, these values were 41, 28, and 7 percent, respectively, for samples obtained from the heated panel for which the recorded maximum temperature was 56°C.

In general, mechanical properties of heat-treated molded samples were superior to those obtained for the precast panel. The former concrete had a peak temperature of 14°C lower than that measured in the panel. The variation in peak temperature at early ages may have resulted in some reduction in the rate of initial cement hydration that could have improved the pore structure of the cement paste (*7–11*). The lower peak temperature also can reduce initial differential thermal expansions that adversely affect the quality of the interface between aggregate and cement paste. Furthermore, molded specimens were sealed before exposure to the atmosphere to minimize drying a method that can favor cement hydration and assure longer gains in strength.

Backscattered electron imaging of polished concrete samples was carried out on 1-year-old samples to examine differences in microstructure. However, such examination did not reveal any specific difference in the concentrations of microcracks, either at the interface between cement paste and coarse aggregate, or in the paste itself. Comparison of the microstructure of polished concrete surfaces did reveal greater concentrations of relatively large pores in the case of concrete from the precast panel compared with other two concretes. The pores appear as black areas in the micrographs shown in Figures 8 and 9. This finding is in agreement with the increase in the volume of large capillary pores detected by mercury intrusion porosimetry.

Secondary electron microscopy was used also to observe fractured surfaces at very high magnifications. Again, no specific differences in the densities of microcracking were observed. All three concretes appeared to have excellent interface regions between the aggregate and paste and a minimum of microcracking and calcium hydroxide deposits. The microstructure also was observed to examine any changes in the morphology of hydration products between the various concretes, in particular the form of the C-S-H. High initial temperature can be expected to increase the rapid formation of short-fibered C-S-H, instead of long-fibered C-S-H, which can reduce the interlocking between C-S-H fibers and reduce ultimate strength development (*7*). However, careful examination of the morphology of the C-S-H revealed that all three concretes had similar types of C-S-H gel.

Except for variations in pore size distribution and total porosity, it is not clear from the microstructural examination whether there are other significant differences in the concentrations of microcracking or hydration reaction morphology that could explain the large spreads in splitting and flexural strengths. Further research is warranted.

CONCLUSION

The combination of initial heat curing of a 100-MPa air-entrained concrete at approximately 50°C and subsequent air drying for 6 days at 15°C before exposure to harsh climatic conditions can

result in significant reductions in mechanical properties. On the basis of test results, the the following conclusions can be drawn:

- The evaluated air-entrained HSC developed high initial strength without heat curing.
- Higher strengths were obtained in heat-treated concrete after approximately 1 day of age. However, beyond 4 days, standard-cured concrete developed approximately 15 percent greater compressive strength and modulus of elasticity than heat-treated precast concrete (peak temperature of 56°C). The spread was approximately 10 to 15 percent and 15 to 20 percent, respectively, for heat-treated and subsequently sealed samples (peak temperatures of 42°C).
- Heat-treated concrete exhibited a 30 to 40 percent reduction in flexural strength compared with standard-cured prisms, samples from the panel showing lower relative strength than heat-molded prisms.
- The spreads in splitting tensile strengths between heated and standard-cured specimens varied from 15 to 30 percent and from 25 to 35 percent, respectively, for concretes from the panel and those tested on heated cylinders.
- Heat-treated and subsequently air-dried concrete had greater capillary porosity than did moist-cured concrete. Additional porosity mostly was attributed to increases in pores with diameters 5–10 nm and 1–5 μm.
- Heat-treated concrete developed a lower initial chloride ion permeability compared with standard-cured concrete but higher values after 4 days. No significant difference existed after 1 year of curing.
- Regardless of the heat treatment and mode of curing, the evaluated air-entrained concrete developed excellent resistance to freezing and thawing.

ACKNOWLEDGMENTS

The authors would like to thank the industrial partners of the Industrial Chair on Concrete, Université de Sherbrooke, and the National Research Council of Canada for their support.

REFERENCES

1. Hot Weather Concreting (ACI 305R-91). *ACI Materials Journal,* Vol. 88, No. 4, American Concrete Institute, Detroit, Mich. July-Aug. 1991, pp. 417–447.
2. Schideler, J. J., and W. H. Chamberlin. Early Strength of Concrete as Affected by Steam Curing Temperatures. *Journal of the American Concrete Institute,* Vol. 46, No. 6, 1949, pp. 273–288.
3. Higginson, E. C. Effect of Steam Curing on Important Properties of Concrete. *Journal of the American Concrete Institute,* Vol. 58, No. 3, 1961, pp. 281–298.
4. Laamanen, P. H., K. Johansen, B. P. Kyltveil, and E. J. Sellevold. Heat Curing of Concrete With and Without Condensed Silica Fume; Effect of Early Temperature History on Compressive Strength. *Proc., 4th CANMET/ACI International Conference on Fly Ash, Silica Fume, Slag and Natural Pozzolans in Concrete,* Vol. 2, Istanbul, Turkey, 1992, pp. 1045–1059.
5. Oluokun, F. A., E. G. Burdette, and J. H. Deatherage. Concrete Physical Property Development at Early Ages: the Influence of Steam Curing. In *Transportation Research Record 1284,* TRB, National Research Council, Washington, D.C., 1990, pp. 31–36.
6. Klieger, P. Effect of Mixing and Curing Temperature on Concrete Strength. *Journal of the American Concrete Institute,* Vol. 54, June 1958, pp. 1063–1081.
7. Richartz, W. On the Development of Structure and Strength in Cement Paste. *Beton,* Vol. 19, Nos. 5 and 6, Dusseldorf, Germany, May and June 1969, pp. 203–206 and 245–248.
8. Verbeck, G. J., and R. H. Helmuth. Structures and Physical Properties of Cement Paste. *Proc., 5th International Symposium on the Chemistry of Cement,* Tokyo, Japan, 1968, pp. 1–32.
9. Goto, S., and D. Roy. The Effect of W/C Ratio and Curing Temperature on the Permeability of Hardened Cement Paste. *Cement and Concrete Research,* Vol. 11, No. 4, July–Aug. 1981, pp. 575–579.
10. Kjellsen, K. O., R. J. Detwiler, and O. E. Gjørv. Backscattered Electron Imaging of Cement Pastes Hydrated at Different Temperatures. *Cement and Concrete Research,* Vol. 20, No. 2, March–April 1990, pp. 308–311.
11. Kjellsen, K. O., R. J. Detwiler, and O. E. Gjørv. Pore Structure of Plain Pastes Hydrated at Different Temperatures. *Cement and Concrete Research,* Vol. 20, No. 6, Nov. 1990, pp. 927–933.
12. Detwiler, R. J., K. O. Kjellsen, and O. E. Gjørv. Resistance to Chloride Intrusion of Concrete Cured at Different Temperatures. *ACI Materials Journal,* Vol. 88, No. 1, Jan.–Feb. 1991, pp. 19–24.
13. Kanda, T., F. Sakuramoto, and K. Suzuki. Compressive Strength of Silica Fume Concrete at Higher Temperatures. *Proc., 4th CANMET/ACI International Conference on Fly Ash, Silica Fume, Slag and Natural Pozzolans in Concrete,* Vol. 2, Istanbul, Turkey 1992, pp. 1089–1103.
14. Lindgard, J., and E. J. Sellevold. Is High-Strength Concrete More Robust Against Elevated Curing Temperatures? *Proc., Utilization of High-Strength Concrete,* Vol. 2, Lillehammer, Norway, June 1993, pp. 810–821.
15. Gjørv, O. E., and J. Martinsen. Effect of Elevated Curing Temperature on High-Strength Lightweight Concrete. *Proc., Utilization of High-Strength Concrete,* Vol. 2, Lillehammer, Norway, June 1993, pp. 706–712.
16. Sandvik, M., and O. E. Gjørv. High Curing Temperatures in Lightweight High-Strength Concrete. *ACI Concrete International,* Vol. 14, No. 12, Dec. 1992, pp. 40–42.
17. Asselanis, J. G., P. C. Äitcin, and P. K. Mehta. Effect of Curing Conditions on the Compressive Strength and Elastic Modulus of Very High-Strength Concrete. *ASTM Cement, Concrete, and Aggregates Journal,* Vol. 11, No. 1, Summer 1989, pp. 80–83.
18. Mehta, P. K. and D. Manmohan. Pore Size Distribution and Permeability of Hardened Cement Pastes. *Proc., 7th International Congress on the Chemistry of Cement,* Paris, France, 1980, Vol. 3, pp. VII-1–5.

Publication of this paper sponsored by Committee on Chemical Additions and Admixtures for Concrete.

Effect of Curing on Durability of Fly Ash Concrete

M.D.A. THOMAS AND J. D. MATTHEWS

Findings of a 5-year laboratory investigation on the effect of curing on the durability of fly ash concrete are summarized. Three series of concrete mixes were cast such that concretes within a given series were of similar strength grade (nominally 25, 35, or 45 MPa) but varied in fly ash replacement level (0 to 50 percent). Following casting, concrete specimens were subjected to various curing treatments and subsequently were stored at a range of temperatures and relative humidities before testing. To assess the influence of the various curing and storage regimes on concrete performance, concrete specimens were tested for (*a*) compressive strength, (*b*) oxygen permeability, (*c*) carbonation in both internal and external storage, and (*d*) resistance to chloride ingress and steel corrosion. Results indicated that, whereas all concretes required adequate curing to achieve their potential properties, concretes containing fly ash were more sensitive to poor curing. The difference was especially marked at higher levels of replacement (50 percent fly ash), where curtailing the moist-curing period resulted in a large increase in the rate of carbonation and permeability and a marked reduction in compressive strength. Concretes with lower levels of ash (15 to 30 percent) carbonated at slightly higher rates than the control concretes but generally offered lower permeability. Resistance to the penetration of chloride ions increased as fly ash content increased, irrespective of the level of curing applied to the concrete. Poorly cured, low strength grade (C25) concretes with 50 percent fly ash provided greater resistance to chloride than higher grade (C45) concretes without ash. Concretes with moderate levels of fly ash (15 to 30 percent) require no additional curing to provide equal, if not improved, durability compared with opc concrete of the same strength grade. Concretes with higher levels of ash may require extended curing compared with opc concrete, especially if the design of the structure and conditions are conducive to carbonation. Adequately cured, high fly ash content concretes are likely to offer substantially improved durability because of their low permeability and high resistance to chloride ion ingress compared with opc concrete.

It is well established that the use of fly ash in concrete can considerably improve concrete durability. As with all concrete, adequate curing is essential for fly ash concrete if its potential properties are to be realized. However, because long-term benefits associated with a pozzolanic reaction are more evident in well-cured concrete, it generally has been thought that fly ash concrete has a greater susceptibility to poor curing than plain portland cement concrete. Consequently, there is some concern about the durability of fly ash concrete under conditions of curing more closely representative of the range of treatments concrete typically receives on site. Treatment may vary from early stripping of formwork (at low temperatures) with no further curing to keeping concrete covered or spraying with water or curing compounds for longer periods.

This paper reports results from an ongoing laboratory investigation of the effect of curing on the durability of fly ash concrete. Concretes with a range of fly ash levels were subjected to a wide range of curing and subsequent storage conditions before strength and durability testing. Durability testing included (*a*) carbonation, (*b*) permeability, and (*c*) chloride diffusion and corrosion of reinforced concretes in a marine environment (*1*). The results are summarized and demonstrate the effect of curing on the durability of fly ash concrete exposed to different environments.

M. Thomas, Department of Civil Engineering, University of Toronto, 35 St. George St., Toronto, Ontario, M5S 1A4, Canada. J. Matthews, Building Research Establishment, Garston, Herts, United Kingdom, WD4 7JR.

EXPERIMENTAL

Three series of concrete mixes were designed using a range of fly ash levels. The mixes' characteristic design strengths were 25 MPa, 35 MPa, and 45 MPa (designated as C25, C35, and C45, respectively) and their slumps ranged from 30 to 60 mm. Mix proportions are presented in Table 1. Cement used for this study was complied with BS 12 for ordinary portland cement (*2*). Three sources of fly ash were selected to provide ashes with a range of 45 microns sieve retention values (5 to 20 percent retained by mass) and otherwise complied with BS 3892: Part 1 (*3*). The chemical compositions of the cement and fly ashes are given in Table 2.

Following casting, specimens were cured for 24 hr in moulds under damp sacking and polyethylene, either in the laboratory at 20°C or in an environmental cabinet at 5°C. After 24 hr, all the specimens were demoulded, kept at the same temperature, and subjected to one of the following curing treatments:

- 1-day cure: air-stored immediately after demoulding,
- 3-day cure: moist-cured under damp sacking and polyethylene for an additional 2 days before air-storage,
- 7-day cure: moist-cured under damp sacking and polyethylene for an additional 6 days before air-storage, and
- water-cured: immersed in water for 28 days.

After curing, specimens were stored in air at various temperatures (5°C or 20°C) and relative humidities (40 to 90 percent relative humidity for 28 days. The following air-storage conditions were used:

Mix Series	*Temperature (°C)*	*Relative Humidity (percent)*
A, G, and H	20	65
B	20	40
C	20	80
D	20	90
E	5	65
F	5	80

At 28 days, the following series of test was carried out:

- Strength: compressive strength testing of 100 mm cubes.
- Carbonation: concrete prisms, 75 × 75 × 200 mm, stored in the laboratory (20°C and 65 percent RH) or outside (sheltered from

TABLE 1 Details of Concrete Mixes

Mix series	Fly ash content	Mix proportions (kg/m³) OPC	Fly ash	Total water	Thames Valley aggregate < 5 mm	5-10 mm	10-20 mm	Free w/c	Slump (mm)	CF	Density (kg/m³)	28-day strength (MPa)
A-F	-	300	-	188	655	405	810	0.57	50	0.89	2365	41.5
(C35)	15% P1	271	48	180	635	411	822	0.51	45	0.89	2370	44.5
	30% P1	242	104	173	603	418	835	0.45	40	0.87	2375	45.5
	50% P1	196	196	162	577	418	836	0.37	30	0.85	2370	41.5
	30% P2				As mix A3			0.45	50	0.87	2370	49.5
	30% P3				As mix A3			0.45	50	0.88	2375	47.0
G	-	250	-	189	691	402	819	0.68	60	0.91	2335	32.5
(C25)	15% P1	226	40	181	653	423	845	0.61	55	0.88	2360	33.0
	30% P1	202	87	174	633	428	855	0.54	30	0.88	2375	34.5
	50% P1	162	162	162	590	438	876	0.44	40	0.87	2370	33.0
	30% P2				As mix G3			0.54	35	0.89	2360	33.5
	30% P3				As mix G3			0.54	55	0.88	2370	33.5
H	-	350	-	188	564	419	839	0.49	40	0.88	2365	50.0
(C45)	15% P1	314	55	180	564	418	836	0.44	35	0.88	2360	50.0
	30% P1	280	120	173	541	420	841	0.39	50	0.88	2375	53.0
	50% P1	226	226	162	514	419	838	0.32	30	0.80	2370	48.0
	30% P2				As mix H3			0.39	35	0.87	2360	50.5
	30% P3				As mix H3			0.39	35	0.85	2370	50.5

TABLE 2 Chemical and Physical Properties of OPC and Fly Ashes

Oxide	OPC	Fly Ash P1	Fly Ash P2	Fly Ash P3
SiO_2	20.55	48.2	48.1	52.4
Al_2O_3	5.07	26.7	24.0	26.0
Fe_2O_3	3.10	11.6	10.6	9.4
CaO	64.51	1.71	6.12	1.69
MgO	1.53	1.62	1.61	1.54
K_2O	0.73	3.18	1.83	2.87
Na_2O	0.15	0.65	0.79	1.32
TiO_2	0.26	0.88	1.00	0.94
P_2O_5	0.19	0.33	0.63	0.21
Mn_2O_3	<0.01	0.02	0.1	0.04
BaO	0.01	0.15	0.14	0.11
SrO	0.18	0.05	0.07	0.03
SO_3	2.53	0.83	0.90	0.85
Cr_2O_3	n.d.	0.03	0.03	0.03
LOI	1.58	4.34	4.49	2.80
Total	100.39	100.41	100.53	100.34
Free lime	0.96	-	-	-
Total C (included in LOI)	-	3.83	4.10	1.98
45 μm sieve residue	-	11.34	19.45	5.53
Relative density	-	2.46	2.44	2.46
Bogue composition				
C_3S	57			
C_2S	16			
C_3A	8			
C_4AF	9			

direct sunlight and rainfall). Depth of carbonation determined by spraying freshly fractured surfaces with phenolphthalein indicator at 90 days, 1, 2, and 4 years (*4*).

- Permeability: oxygen permeability tests on discs 150 mm in diameter and 50 mm thick cut from 150 × 300 mm cylinders. Specimens conditioned at 20°C and 65 percent RH for 28 days before testing (*5*).
- Corrosion: reinforced concrete prisms, 100 × 100 × 300 mm, placed in tidal zone of marine exposure site (*1*). Composition of seawater: 2.6 g/l SO_4, 18.20 g/l Cl, 0.40 g/l Ca, 1.20 g/l Mg, 9.74 g/l Na, and 0.40 g/l K. Specimens removed at 1, 2, and 4 years. Chloride concentration profile determined by incremental drilling and chemical analysis of collected powder samples. Corrosion of reinforcement determined gravimetrically.

TABLE 3 Summary of Results

Ambient Conditions (to 28 days)		Concrete Grade	Fly ash Content	28 day Strength (% 28 day water-cured strength)			90 day Strength (% 28 day water-cured strength)			Indoor Carbonation depth @ 4 years (mm)			Outdoor Carbonation depth @ 4 years (mm)			Oxygen Permeability (x $10^{-17}m^2$)			Marine Exposure	
																			D* (x10^{-8} cm^2/s)	C** (wt. % cement)
Temp °C	R.H. (%)			days curing			day curing			days curing			days curing			days curing			days curing	
				1	3	7	1	3	7	1	3	7	1	3	7	1	3	7	1	1
20	40-65	C25	none	89	91	92	91	102	107	25	18	15	13	10	10	65	36	25	15.1	1.7
			15-30	77	93	98	84	102	112	23	17	14	15	12	10	47	23	16	3.2	0.4
			50	70	90	99	73	101	117	>38	22	18	20	15	12	41	11	10	2.5	0.2
		C35	none	82	97	106	84	104	114	16	12	9	10	6	4	56	32	25	9.3	1.7
			15-30	72	91	96	75	96	107	16	13	10	10	7	6	31	22	15	2.5	0.2
			50	61	87	97	63	91	110	23	17	14	13	11	8	31	14	7	2.0	0.2
		C45	none	77	94	102	81	102	105	11	10	9	5	1	1	44	24	20	4.5	0.7
			15-30	73	91	100	77	100	111	12	9	8	6	4	2	18	14	9	1.4	0.1
			50	63	97	109	60	97	112	14	10	8	8	6	2	16	3	3	1.4	0.1
	80	C35	none	82	95	99	92	100	107	12	10	10	7	6	3	43	30	17	N.D	
			15-30	79	97	100	92	107	116	12	11	10	8	6	6	23	14	12		
			50	77	97	103	86	110	131	16	12	11	10	7	5	23	6	6		
	90	C35	none	85	97	101	98	113	119	12	10	8	7	5	4	19	14	12	N.D	
			15-30	86	101	105	104	116	128	11	10	9	7	5	4	13	12	7		
			50	85	96	102	99	114	123	12	11	11	9	9	7	11	8	5		
5	65	C35	none	53	82	102	N.D			16	11	9	9	6	4	45	26	9	N.D	
			15-30	42	83	98				20	13	9	11	7	5	38	19	7		
			50	40	69	96				22	16	12	14	9	7	65	15	7		
	80	C35	none	70	85	91	N.D.			16	14	11	11	8	6	42	16	13	N.D	
			15-30	63	86	95				15	11	8	9	6	5	28	10	10		
			50	56	76	97				17	10	9	10	7	5	22	8	5		

N.D. - not determined

D* - chloride diffusion coefficient calculated from chloride concentration profile after 2 years exposure; C** - chloride content at depth 26-31mm after 2 years exposure.

RESULTS

Results for tests for three types of concrete are summarized in Table 3: (*a*) no fly ash (control mixes), (*b*) normal fly ash replacement levels (average results for concretes with 15 to 30 percent fly ash), and (*c*) high fly ash content (50 percent).

Strength

The strength of all concretes decreased as their curing period was curtailed (Table 3); however, the strength of fly ash concrete was more adversely affected by inadequate curing, especially at higher levels of fly ash (50 percent and for those concretes exposed to low temperatures or low relative humidities after curing. Other researchers have observed similar trends for fly ash concrete and mortars (*6–9*).

Concretes with traditional levels of fly ash (15 to 30 percent) generally exhibit comparable strength loss to opc concretes, provided the concretes are cured for at least 3 days. Fly ash concretes cured for only 1 day before exposure to low relative humidities (or low temperatures) lose more strength than similarly treated opc concretes.

Under favorable exposure conditions (20°C and 80 or 90 percent relative humidity), fly ash concrete requires no additional curing to achieve strength comparable to opc concrete, even at high levels of replacement.

In practice, only the surface of large sections of concrete will lose moisture at rates similar to those of small specimens used in this study. The internal bulk of the concrete will retain its moisture for a much longer period. Consequently, the strength of large sections are less affected by the quality of curing. In addition, the temperature rise caused by the heat of hydration plays an important part in determining the in situ strength of large concrete sections. Except in slender sections, the effect of a temperature rise is likely to overshadow the effect of low ambient temperatures, which retard fly ash concrete strength development more severely than opc concrete. Therefore, additional curing required by fly ash concretes in order to achieve similar strength as opc concretes may be necessary only in slender sections.

Permeability

The permeability of concrete is an important parameter in determining its durability, because it provides a measure of the concrete's physical resistance to the ingress of deleterious agents (carbon dioxide, chlorides, and sulphates) and the movement of oxygen and water, which is required for corrosion. Although there is no single test for assessing the durability of concrete exposed to different conditions, permeability is generally considered the best parameter for characterizing the ability of the concrete to resist deterioration (*10*).

The oxygen permeability results in Table 3 indicate a very marked dependence on the duration of curing. Increasing the period

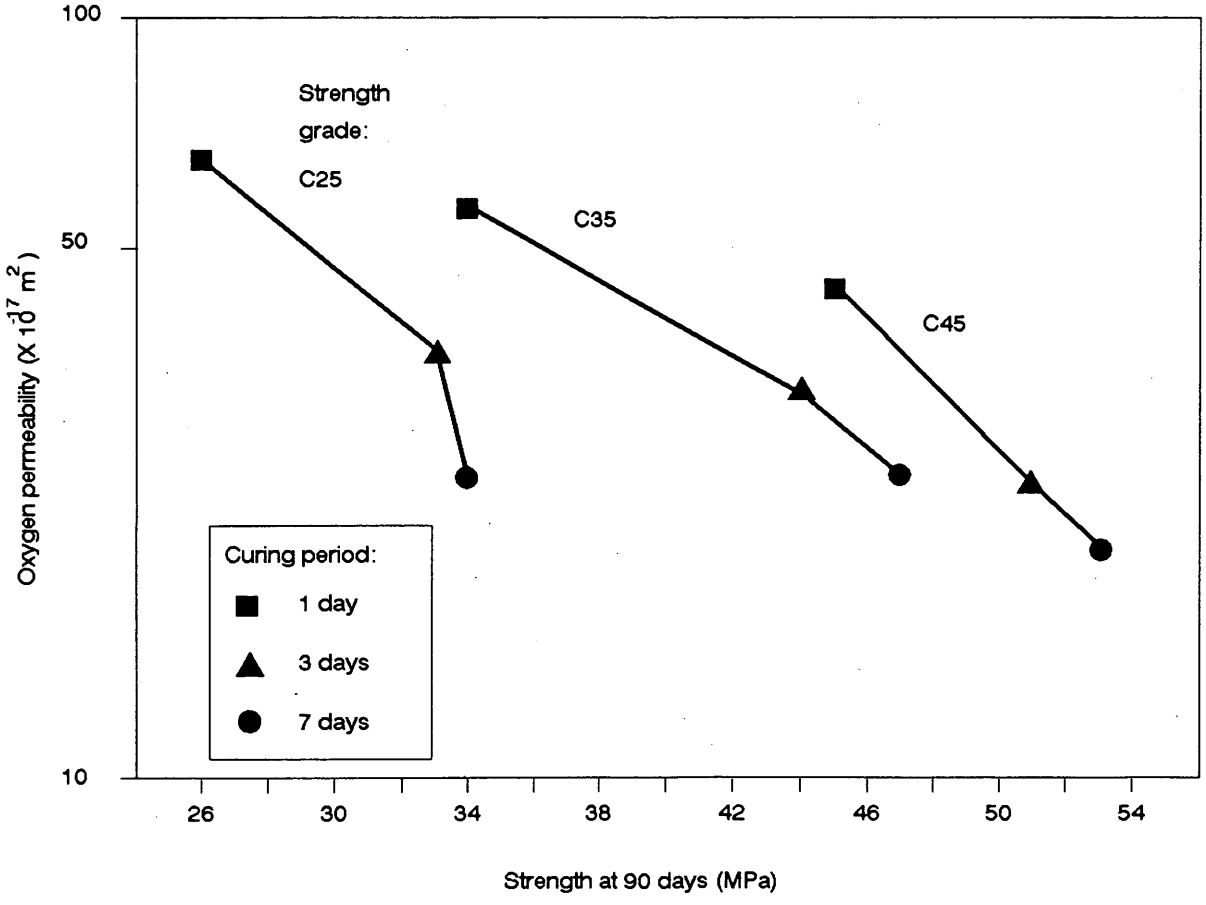

FIGURE 1 Effect of curing on the strength and permeability of opc concrete.

of curing from 1 to 7 days reduced permeability by a factor ranging from 2 (for concrete exposed to high temperature and relative humidity after curing) to more than 9 (for concrete exposed to low temperature and relative humidity).

Generally, fly ash concretes exhibit greater dependence on curing; concretes with higher levels of fly ash had greater reductions in permeability after extended curing. However, fly ash concretes generally were less permeable than opc concrete of the same strength grade, irrespective of the level of curing applied. Similar findings have been reported by others testing gas permeability (*11*), water sorptivity (*11*), and initial surface absorption (*12*). In the present study, low strength concretes (C25) with 50 percent fly ash were less permeable than higher strength concretes (C45) without ash.

The only condition that produces a higher permeability in fly ash concrete than in similar grade opc concrete is inadequate curing, (1 day at 5°C) before exposure to low temperature (5°C) and relative humidity (65 percent relative humidity). If the curing period is extended to 3 days the fly ash concrete is less permeable. The behavior of the concretes at 5°C is interesting. Providing adequate curing was given (3 to 7 days), concretes stored at 5°C are less permeable than comparable specimens stored at 20°C. Although the hydration of portland cement is retarded at low temperature, after sufficient curing periods the quality of concrete is increased because of the improved dispersion of hydration products.

Figure 1 shows the effect of the curing period on both the strength and the permeability of opc concrete. Increasing the initial curing period has a much more pronounced effect on the concrete's permeability than its strength. Ballim (*11*) suggested that increasing the duration of moist curing may be a more efficient way of extending the durability of concrete than increasing the cement content (and design strength). There is no unique relationship between strength and permeability (and hence durability). The relationship is dependent on the level of fly ash replacement, the degree of curing, and the exposure conditions following curing. Consequently, neither design nor in situ strength can be expected to provide a reliable indication of concrete durability. Similar conclusions have been reached by others (*13,14*).

Protection of Steel Reinforcement

Durability of reinforced concrete is controlled largely by the capability of the concrete cover to protect steel reinforcement from corrosion. In hardened concrete, the pH of the pore solution typically is in excess of 13, and at such levels of alkalinity, steel is normally protected from corrosion by a thin surface layer of oxide. However, the steel may become susceptible to corrosion in the presence of chlorides, or if it becomes depassified when the alkalinity of the concrete at the location of the steel is reduced as a result of carbonation. Consequently, it is desirable for the concrete cover to adequately resist penetration of chlorides and carbon dioxide.

Carbonation

Figure 2 indicates the effect of the curing period and storage conditions immediately following curing, on carbonation. Results compiled in Figure 2 and Table 3 indicate that curing has a pronounced

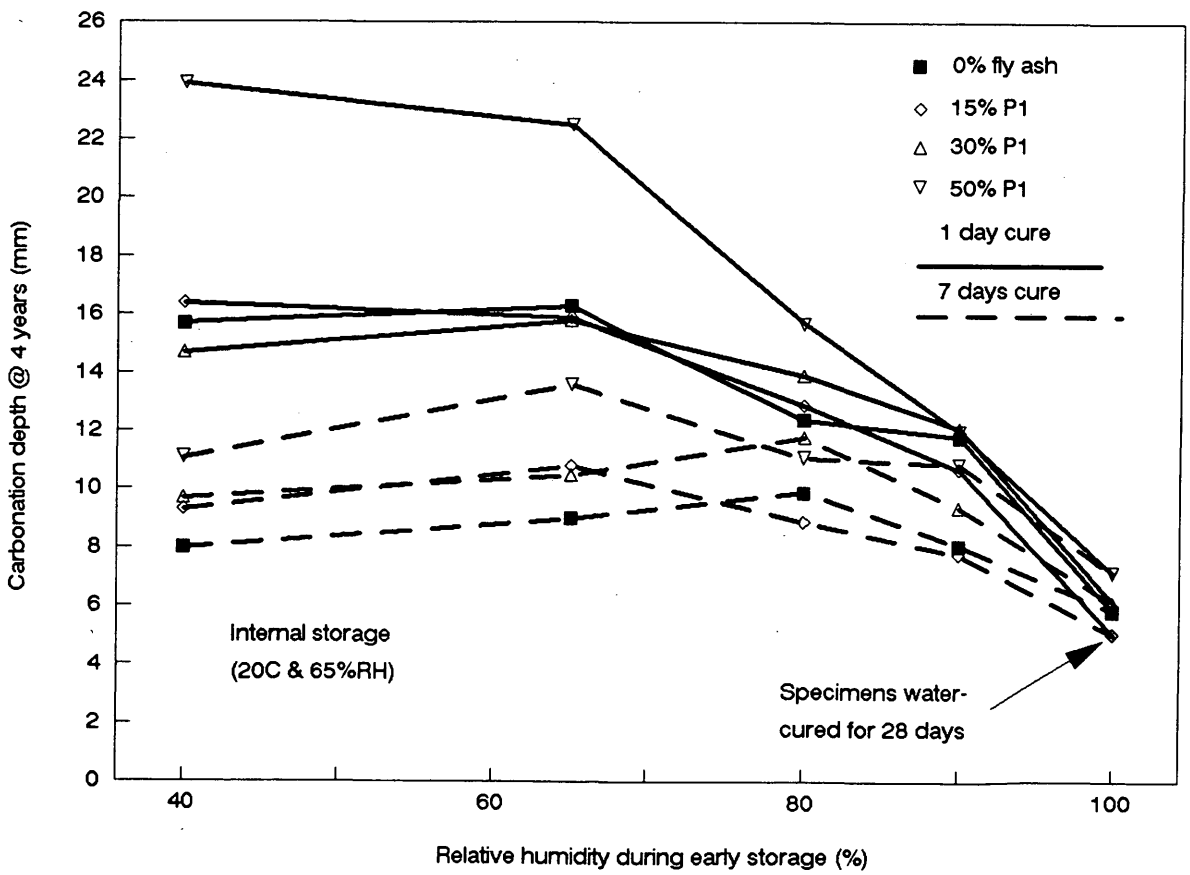

FIGURE 2 Effect of relative humidity during curing on carbonation of concrete.

effect on the carbonation of concrete. Fly ash concretes carbonate at a faster rate than opc concretes of the same strength grade; the effect is more marked at higher replacement levels and under poor curing conditions.

For concretes with a moderate level of fly ash (15 to 30 percent) the differences are small, generally less than 2 mm after 4 years in most cases, compared with the differences resulting from changes in curing or ambient conditions. The results support the view of other researchers (*15–22*) that concretes containing fly ash carbonate to a similar or slightly higher degree compared with opc concrete of the same strength grade, even when the concretes are poorly cured.

At higher levels of fly ash, differences in carbonation rate are more significant, especially for poorly cured lower grade concretes. Increases of more than 12 mm were observed for 25N concretes with 50 percent fly ash compared with equal grade opc concrete stored internally for 4 years.

Figure 3 illustrates the relationship between the carbonation depth of a concrete specimen at 2 years and the actual compressive strength at 28 days of identically cured companion specimens from the same mix. There is a single relationship between these two properties for each exposure environment for all the concrete mixes tested, and the relationships are independent of the level of fly ash and the conditions of curing and early storage.

Carbonation results appear to be in conflict with the permeability results; fly ash concrete carbonates at an increased rate despite being less permeable compared with opc concrete of similar strength (Figure 4). This may be explained by the process of carbonation, which occurs mainly by gaseous diffusion of CO_2, accompanied by chemical interaction between the CO_2 and the cement hydrates, particularly $Ca(OH)_2$. The reduced $Ca(OH)_2$ content of fly ash concrete means that there is less CO_2 consumed; consequently, CO_2 may diffuse more quickly compared with an opc concrete of similar permeability. However, as there is little chemical interaction between oxygen and cement hydrates, permeability to oxygen is a function of the pore structure.

Chloride ion penetration

Table 3 gives chloride diffusion coefficients for concretes cured for 1 day. The coefficients were calculated from chloride concentration profiles after 2-years' exposure, using Crank's solution to Fick's second law (*1*). The duration of initial curing was observed to have little effect on chloride penetration (*1*), and diffusion coefficients calculated from concentration profiles indicated little variation with duration of curing. Those results are in contrast to the permeability and carbonation test results, which show a marked dependence on the initial curing period. The marine-exposed concretes remained in a saturated condition for the duration of the test, and the continued cement hydration and pozzolanic reaction tended to mask the initial differences between specimens because of initial curing conditions. The reduced impact of curing on diffusion results compared with other permeation properties has been observed by others (*23,24*).

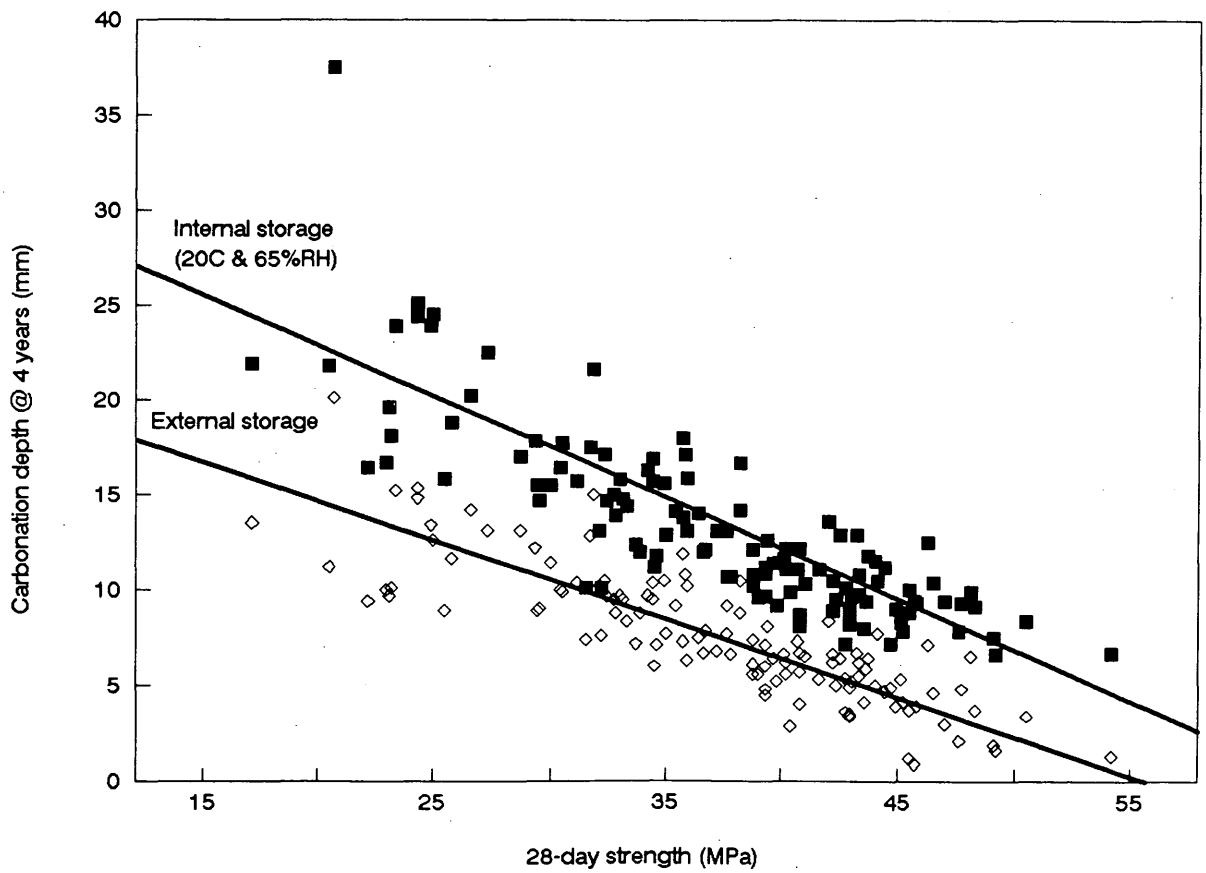

FIGURE 3 Relationship between 28-day strength and carbonation for all concrete mixes.

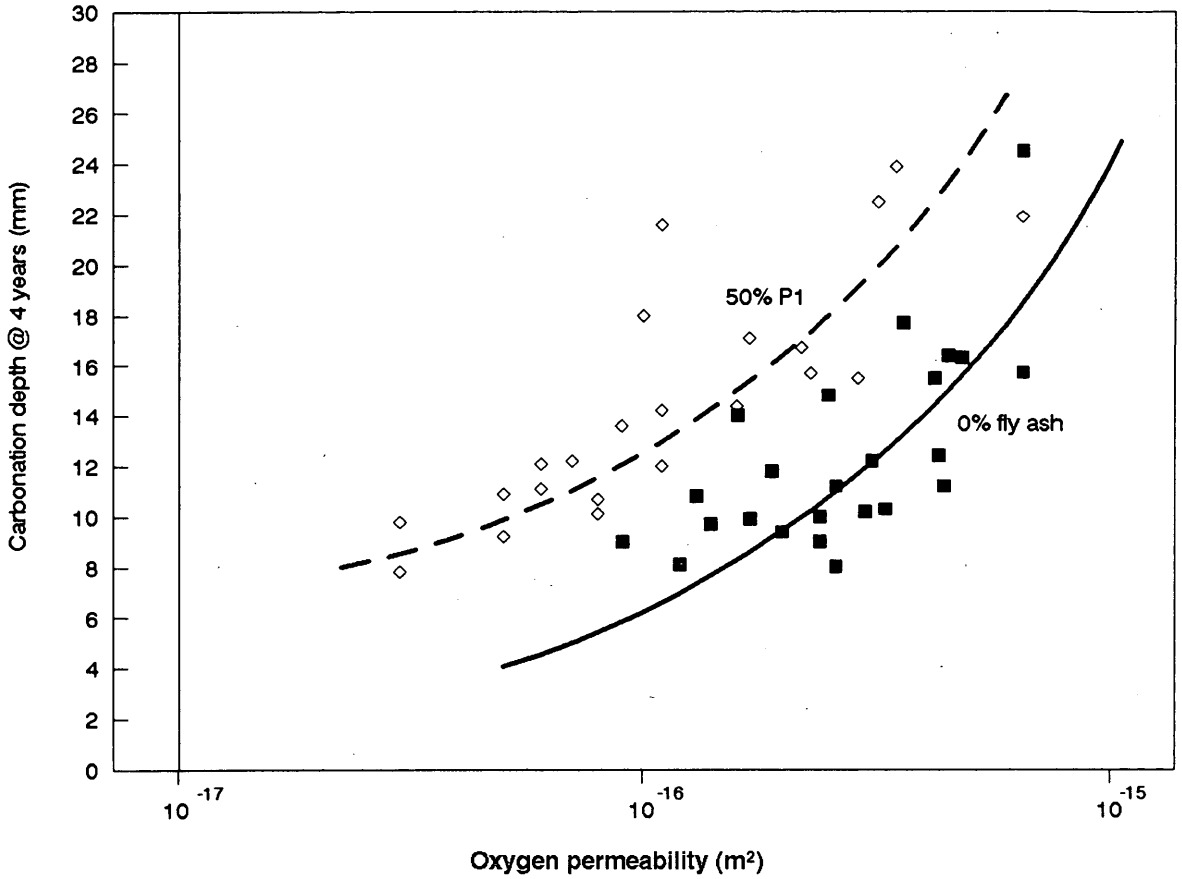

FIGURE 4 Relationship between carbonation and permeability.

In addition to chloride diffusion coefficients, the chloride concentration at depth (26 to 31 mm) is also given in Table 3. The results indicate that the fly ash concrete has a much greater resistance to the penetration of chloride ions than does opc concrete, especially at high replacement levels. Indeed, low grade concretes (C25) with moderate or high levels of fly ash perform better in this environment than (C45) opc concretes.

Figure 5 shows the effect of strength grade and fly ash content on chloride penetration. Increasing the strength or fly ash content reduces chloride penetration. However, increasing the level of fly ash is far more effective; low strength (C25) concretes offer greater resistance than higher strength (C45) opc concrete. Figure 6 shows the change in chloride concentration with time. Differences between fly ash and opc concrete become more marked with time; chloride levels at all depths increase with exposure for opc concretes. The increase in chloride content at a given depth between 1 and 4 years is of the order of 2 times for opc concrete [i.e., the chloride content increases proportionally with the square root of time consistent with Fickean law (*25*)]. In contrast, there is little ingress of chlorides beyond the first year for concretes with high levels of fly ash. A chloride content below 26 mm indicates no significant increase between 1 and 4 years. This finding does not conform with Fickean diffusion, and it has been suggested that the initial profile may be the result of the absorption of chlorides because of the unsaturated condition of the concretes before exposure (*1*). Consequently, the diffusion coefficients for fly ash concretes actually may be lower than those reported in Table 3.

Increased resistance to the penetration of chlorides in fly ash concrete led to substantially reduced corrosion of the reinforcing steel in marine exposed specimens (*1*).

Reduced chloride diffusion of fly ash concretes observed in the present study is consistent with previous studies that have indicated lower diffusion rates for pastes (*26–29*), mortars (*30*), and concretes (*30–34*).

PRACTICAL SIGNIFICANCE OF RESULTS

Curing has a significant influence on the strength and durability of laboratory-size concrete specimens. In practice, only the outer surfaces of larger elements will be affected by early curing, the internal bulk of the concrete will retain its moisture for longer periods (*35*). Consequently, the overall strength of a concrete element may not be adversely affected, and the greater susceptibility of fly ash concrete strength is of practical significance in thin sections exposed to adverse curing environments. Recent studies by the authors (*36*) of fly ash and opc concretes in the field have shown fly ash concrete to invariably have a greater in situ strength than comparable opc concrete (equal design strength or cementitious material content) taken from the same structure. Furthermore, studies of high-volume fly ash concrete structures (up to 56 percent ash), examples of which have existed in the United Kingdom for more than a decade, show these concretes to have strengths considerably in excess of the design strength or measured 28-day strength (*37*).

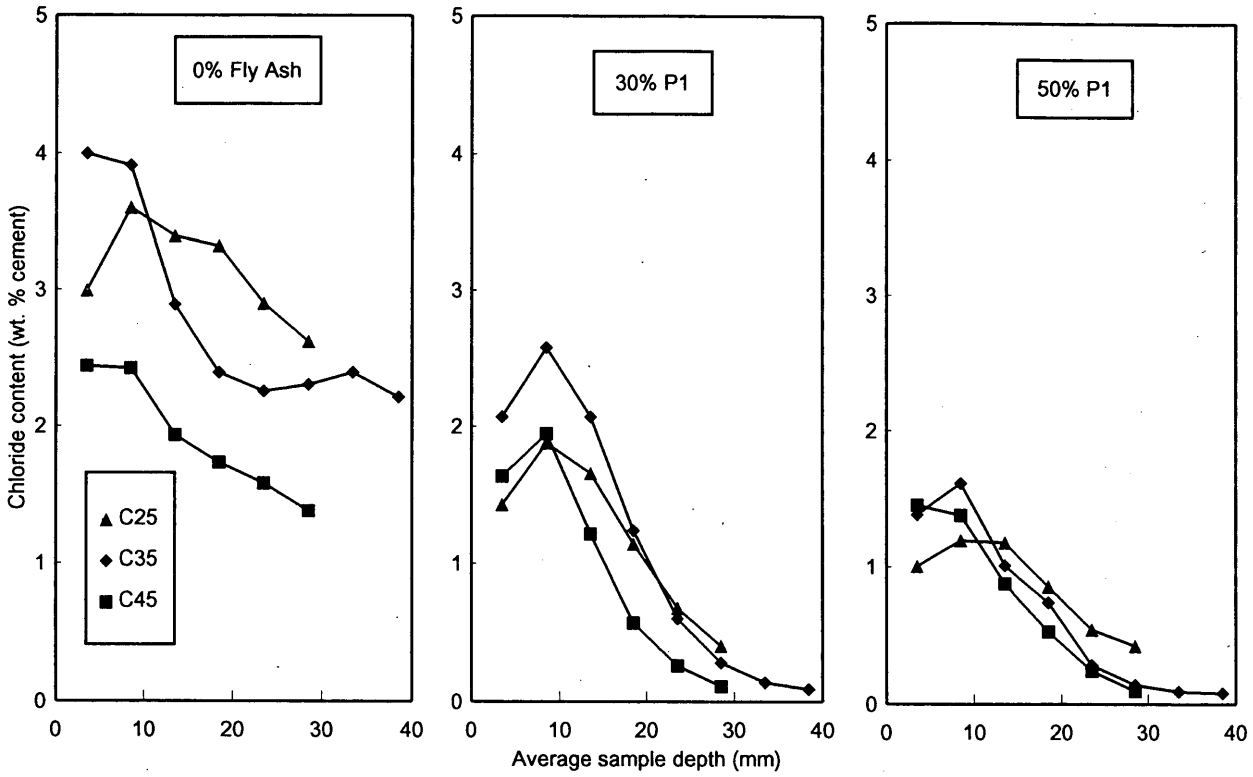

FIGURE 5 Chloride concentration profiles for opc and fly ash concretes after 4 years marine exposure.

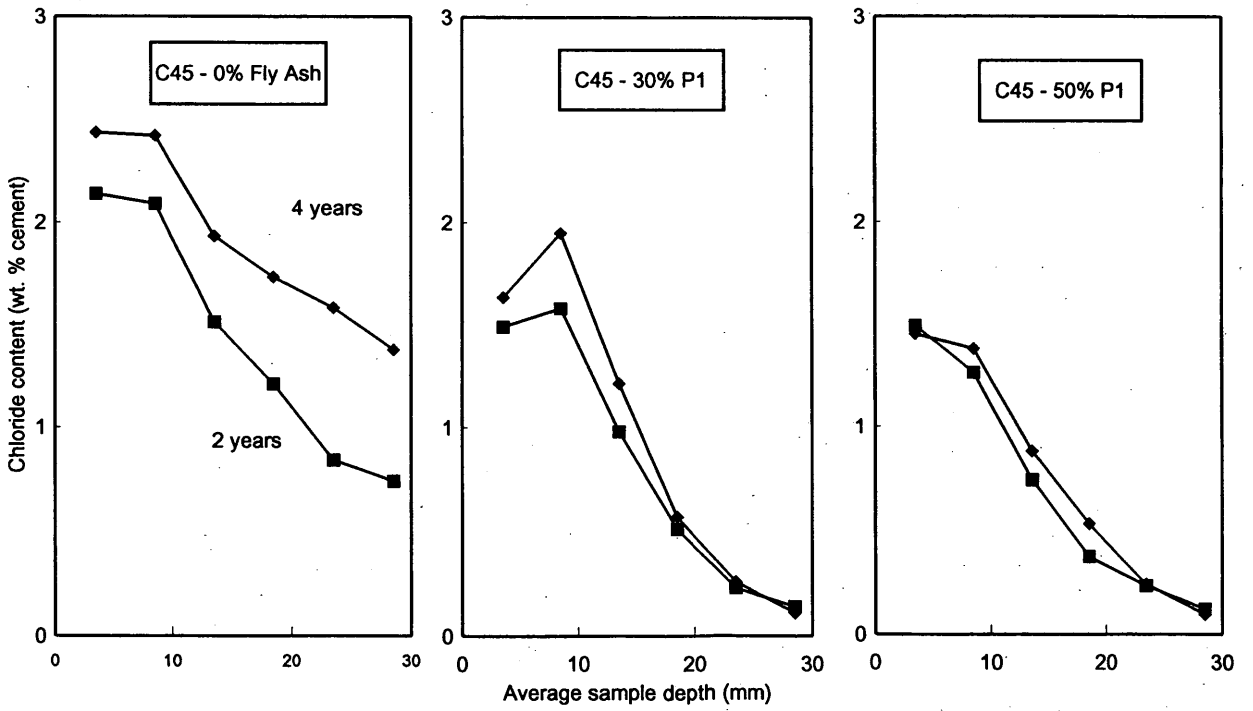

FIGURE 6 Effect of age and fly ash content on chloride concentration profiles in concrete.

Properties of the outer surfaces or "covercrete" of concrete elements have a major influence on the durability of the structure, as such surfaces provide protection to the steel reinforcement and bulk concrete. The results of this study indicate that fly ash concrete may be less permeable and considerably more resistant to the penetration of chloride ions than opc concrete of the same strength grade, irrespective of the level of curing provided. Differences in carbonation depths were not marked for concretes with fly ash contents between 0 and 30 percent. The results correlate well with field studies (*36*), which show fly ash concrete to be less permeable and more resistant to the penetration of chlorides from deicing salts or seawater than is comparable opc concrete with the same exposure. Fly ash concretes in the field exhibit slightly higher carbonation also. Overall, the results indicate that concretes with normal levels of fly ash (15 to 30 percent require no additional curing, as compared with opc concretes of the same strength grade.

High fly ash content concretes (50 percent) show excellent durability properties, for increased carbonation rates. The differences can be significant under certain curing and exposure conditions, so particular attention should be paid to the curing fly ash concretes if the design of the structure and conditions of exposure are conducive to carbonation.

All the concretes studied had improved durability when the curing period was extended. The importance of providing adequate curing protection cannot be overemphasized. Although, inadequate curing may be compensated for by decreasing the water to cementitious material ratio of the concrete, this will usually result in higher cement contents and concomitant increases in shrinkage, hydration temperature, alkali contents, and material costs.

ACKNOWLEDGMENT

This work was carried out at the Building Research Establishment in collaboration with National Power, PowerGen, and Imperial College. The authors thank Charles Haynes for carrying out the laboratory work.

REFERENCES

1. Thomas, M. D. A. Marine Performance of pfa Concrete. *Magazine of Concrete Research,* Vol. 43, No. 156, 1991, pp. 171–185.
2. *Specification for Portland Cements.* (BS12), British Standards Institution. London, England, 1989.
3. *Specification for Pulverized-Fuel Ash for Use as a Cementitious Component in Structural Concrete.* (BS3892: Part 1), British Standards Institution. London, England, 1982.
4. Thomas, M. D. A., and J. D. Matthews. Carbonation of Fly Ash Concrete. *Magazine of Concrete Research,* Vol. 44, No. 160, 1992, pp. 217–228.
5. Thomas, M. D. A., and J. D. Matthews. The Permeability of Fly Ash Concrete. *Materials and Structures,* Vol. 25, 1992, pp. 388–396.
6. Matthews, J. D. Pulverized-Fuel Ash; Its Use in Concrete. *Material Properties, British Standards and Concrete strength.* BRE information paper, Part I, Building Research Establishment, Garston, 1987.
7. Haque, M. N., M. K. Goplan, R. C. Joshi, and M. A. Ward. Strength Development of Inadequately Cured High Fly Ash Content and Structural Concrete. *Cement and Concrete Research,* Vol. 16, 1986, pp. 363–372.
8. Thomas, M. D. A., J. D. Matthews, and C. A. Haynes. The Effect of Curing on the Strength and Permeability of PFA concrete. *Proc., 3rd International Conference on Fly Ash, Silica Fume, Slag and Natural Pozzolans in Concrete,* ACI SP–114, Vol. I, American Concrete Institute, Detroit, Mich. 1989, pp. 191–217.
9. Vandewalle, L., and F. Mortelmans. The Effect of Curing on the Strength Development of Mortar Containing High Volumes of Fly Ash. *Proc., 4th International Conference on Fly Ash, Silica Fume, Slag and Natural Pozzolans in Concrete,* ACI SP-132, Vol. I, American Concrete Institute, Detroit, Mich. 1992, pp. 53–63.
10. Schonlin, K., and H. K. Hilsdorf. Permeability as a Measure of Potential Durability of Concrete; Development of a Suitable Test Apparatus. *Permeability of Concrete,* ACI SP-108, American Concrete Institute, Detroit, Mich. 1988.
11. Ballim, Y. Curing and the Durability of OPC, Fly Ash, and Blast-Furnace Slag Concretes. *Materials and Structures,* Vol. 26, 1993, pp. 238–244.
12. Dhir, R. K., and E. A. Byars. PFA concrete: Near Surface Absorption Properties. *Magazine of Concrete Research,* Vol. 43, No. 157, 1991, pp. 219–232.
13. Bamforth, P. B. The Water Permeability of Concrete and Its Relationship with Strength. *Magazine of Concrete Research,* Vol. 43, No. 157, 1991, pp. 233–241.
14. Hooton, R. D. High-strength Concrete as a By-product of Design for Low Permeability. *Proc., Concrete 2000,* Dundee, Scotland, Sept. 1993.
15. Nagataki, S., H. Ohga, and E. K. Kim. Effect of Curing Conditions on the Carbonation of Concrete with Fly Ash and the Corrosion of Reinforcement in Long-Term Tests. *Proc., 2nd International Conference on Fly Ash, Silica Fume, Slag and Natural Pozzolans in Concrete,* ACI SP-91, Vol. I, American Concrete Institute, Detroit, Mich., 1986, pp. 521–540.
16. Matthews, J. D. Carbonation of Ten-Year-Old Concretes With and Without PFA. *Proc., 2nd International Conference on Ash Technology and Marketing,* CEGB, London, England, 1984.
17. Hobbs, D. W. Carbonation of Concrete Containing PFA. *Magazine of Concrete Research,* Vol. 40, No. 143, 1988, pp. 69–78.
18. Schubert, P., and W. vom Berg. Coal Fly-Ash with Test Mark as an Additive for Concrete in Accordance with DIN 1045. *Betonwerk und Fertigteil-Technik,* No. 11, 1979, pp. 692–696.
19. Lewandowski, R. Effect of Different Fly-Ash Qualities and Quantities on the Properties of Concrete. *Betonwerk und Fertigteil-Technik,* No. 1–3, 1983.
20. Gebauer, J. Some Observations on the Carbonation of Fly Ash Concrete. *Silicates Industriels,* No. 6, 1982, pp. 155–159.
21. Tsukayama, R., H. Abe, and S. Nagataki. Long-Term Experiments on the Neutralization of Concrete Mixed with Fly Ash and the Corrosion of Reinforcement. *Proc., 7th International Congress on the Chemistry of Cement,* Vol. III, Paris, France, 1980, pp. 30–35.
22. Dhir, R. K., et al. Near-Surface Characteristics of Concrete: Prediction of Carbonation Resistance. *Magazine of Concrete Research,* Vol. 41, No. 148, 1989, pp. 137–143.
23. Dhir, R. K., and E. A. Byars. PFA Concrete: Chloride Diffusion Rates. *Magazine of Concrete Research,* Vol. 45, No. 162, 1993, pp. 1–9.
24. Bamforth, P. B., and D. C. Pocock. Minimising the Risk of Chloride-Induced Corrosion by Selection of Concreting Materials. In *Corrosion of Reinforcement in Concrete Construction* (CL Page et al. ed.), Elsevier, London, England, 1990, pp. 119–131.
25. Barrer, R. M. *Diffusion in and Through Solids.* Cambridge University Press, London, England, 1951.
26. Collepardi, M., A. Marcialis, and R. Turriziani. Penetration of Chloride Ions into Cement Pastes and Concretes. *Journal of the American Ceramic Society,* Vol. 55, No. 534, 1972, pp. 534–535.
27. Page, C. L., N. R. Short, and A. El Tarras. Diffusion of Chloride Ions in Hardened Cement Pastes. *Cement and Concrete Research,* Vol. 11, No. 3, 1981, pp. 395–406.
28. Li, S., and D. M. Roy. Investigations of Relations Between Porosity, Pore Structure and Cl^- Diffusion of Fly Ash and Blended Cement Pastes. *Cement and Concrete Research,* Vol. 16, No. 5, 1986, pp. 749–759.
29. Byfors, K. Influence of Silica Fume and Fly Ash on Chloride Diffusion and pH Values in Cement Paste. *Cement and Concrete Research,* Vol. 17, No. 1, 1987, pp. 115–130.
30. Malek, R. I. A., et al. The Diffusion of Chloride Ions in Fly Ash/Cement Pastes and Mortars. *Proc., Materials Research Society Symposium,* Vol. 85, Materials Research Society, Pittsburgh, Pa., 1987.
31. Jackson, P. J., and P. Brookbanks. Chloride Diffusion in Concretes Having Different Degrees of Curing and Made Using Portland Cements and Blended Cements Containing Portland Cement, Pulverized Fuel Ash and Ground Granulated Blast Furnace Slag. Supplementary Papers of the 3rd International Conference on Fly Ash, Silica Fume, Slag and

Natural Pozzolans in Concrete, American Concrete Institute, Detroit, Mich., 1989, pp. 641–655.
32. Dhir, R. K., M. R. Jones, H. E. H. Ahmed, and A. M. G. Seneviratne. Rapid Estimation of Chloride Diffusion Coefficient in Concrete. *Magazine of Concrete Research,* Vol. 42, No. 152, 1990, pp. 177–185.
33. Marusin, S. L. Influence of Fly Ash and Moist Curing Time on Concrete Permeability. *Proc., 4th International Conference on the Use of Fly Ash, Silica Fume, Slag and Natural Pozzolans in Concrete,* ACI SP-132, Vol. I, American Concrete Institute, Detroit, Mich., 1992, pp. 257–269.
34. Zhang, Y., and J. D. Matthews. The Effect of PFA on the Quality of the Concrete Cover to Reinforcement. *Proc., Hong Kong Concrete Technology and Construction Conference,* Hong Kong, 1990, pp. 399–432.
35. Parrot, L. J. Moisture Profiles in Drying Concrete. *Advances in Cement Research,* Vol. 1, No. 3, 1988, pp. 164–170.
36. Thomas, M. D. A., and J. D. Matthews. Performance of Fly Ash Concrete in U.K. Structures. *ACI Materials Journal,* Dec. 1993.
37. Dunstan, M. R. H., M. D. A., Thomas, J. B. Cripwell, and D. J. Harrison. Investigation into the Long-Term In-Situ Performance of High Fly Ash Content Concrete Used for Structural Applications. *Proc., 4th CANMET/ACI International Conference on Fly Ash, Silica Fume, Slag and Natural Pozzolans in Concrete,* Vol. 1, ACI SP-132, American Concrete Institute, Detroit, Mich., 1992.

Publication of this paper sponsored by Committee on Chemical Additions and Admixtures for Concrete.

Addition of Class C Fly Ash To Control Expansions due to Alkali-Silica Reaction

SIDHESH KAKODKAR, V. RAMAKRISHNAN, AND LON ZIMMERMAN

Results of a study to determine the influence of five different Class C fly ashes on inhibiting expansion due to alkali-silica reaction (ASR) are presented. Five different sands with varying degrees of ASR, combined with the five different fly ashes, were investigated. An accelerated test method (ASTM P214) was used to detect potentially deleterious expansion of mortar bars due to ASR. Replacement levels of 0, 10, 15, 20, 25, and 30 percent of cement by weight were investigated for all five fly ashes and for all five sands. Four of the fly ashes were effective in reducing to negligible levels ASR expansions. Varying amounts of fly ashes were needed for effective control of deleterious expansion. Some fly ashes at lower levels of blending (10 and 15 percent) actually increased expansion. One fly ash was not effective in inhibiting expansion as a result of ASR, even at 30 percent replacement. Fly ashes with high alkali contents (1.92 percent) were effective in inhibiting expansion related to ASR. Test results indicated that some Class C fly ashes at adequate replacement levels effectively reduced expansion to negligible levels, even in highly reactive sands.

Alkali-reactive sands or coarse aggregates, when used in concrete structures, can produce severe deterioration. Certain internal chemical reactions between the cement alkalies and the aggregates produce reaction products that can cause harmful expansion. Highly variable and different expansions develop within concrete in the long-term as a result of alkali-silica reactions (ASR), for example. The ASR expansion reaction, characterized by production of a gel-like reaction product, occurs in concrete structures if three requirements have been met: (*a*) reactive forms of silica or silicate in the aggregates; (*b*) sufficient alkali (sodium and potassium), primarily from the cement; and (*c*) sufficiently available moisture in the concrete. If one is not present, then expansion from ASR cannot occur.

The potential ASR problem has gained a lot of attention from product suppliers and state highway departments in nearly every state. Even though the problem has had worldwide attention for the past 50 years, effective measures for inhibiting the alkali-silica reactions have not been available until recently (*1–21*). Such measures are important to improving the durability of concrete structures.

To prevent deleterious expansion the following three options are available: (*a*) use low alkali cement, (*b*) avoid reactive aggregates, and (*c*) partially replace cement with fly ash or other fine siliceous materials.

Low-alkali cements have been used nationwide to mitigate ASR in concrete; however, low-alkali cements also have been associated with severe ASR in pavements exposed to salts used for highway deicing, the salts having increased total available alkali in the concrete. Further, low-alkali cement may not always be available.

S. Kakodhar and V. Ramakrishnan, South Dakota School of Mines and Technology, 501 E. St. Joseph Street, Rapid City, S. D. 57701. L. Zimmerman, Midwest Fly Ash and Materials, Inc., 2220 Hawkeye Drive, Sioux City, Iowa 51105.

Depletion of good quality aggregate near construction sites has created a need to develop methods that will permit the successful use of marginal aggregates, making the third option more attractive. There is an abundant supply of fly ash. A perusal of the proceedings of three international conferences (7–9) on the use of pozzolans in concrete indicates that fly ashes can effectively control ASR. Factors that influence the ability of fly ash to control ASR are the chemical composition of fly ash, mixture proportions, type of reactive aggregates and amount of fly ash used. Some investigators, using low levels of fly ash replacement, have determined that the alkalies in fly ash participate in ASR (*3,4,18*).

OBJECTIVES

The primary objectives of this investigation were to determine the

- Potential effectiveness of different Class C fly ashes in reducing the deleterious expansions related to ASR in highly reactive and nonreactive sand mortar bars,
- Level of effectiveness for different amounts of fly ash additions,
- Influence of alkali and oxide contents of fly ashes on ASR expansion,
- Reactive potential of various sands currently used in construction of pavements using ASTM P214 test method,
- Influence of selected levels of cement replacements with fly ash on the compressive strength of mortar at different ages and, finally,
- To establish the pessimum limits for fly ash replacement.

RESEARCH PROGRAM

The ASTM P214 test method for accelerated detection of potentially deleterious expansion of mortar bars due to alkali-silica reaction was used throughout the investigation. Five different sands ranging from innocuous to highly reactive were selected, and the chemical and mineral compositions of these sands were determined using reference intensity method (RIM) analysis.

Five ASTM Class C fly ashes were selected, their oxide and alkali contents varying from the low to high levels permitted by ASTM. The chemical and mineral composition of the fly ashes were determined using two different procedures, the atomic absorption inductively coupled plasma method and scanning electron microscope method. Physical properties, such as density, fineness, autoclave expansion, and specific gravity, were determined (ASTM C311). Mortar cubes were made with a standard control sand and cements with 0, 10, 15, 25, and 30 percent fly ash replacement by

weight, and then tested at 3, 7, and 28 days to determine the influence of fly ash replacement on their compressive strength.

TEST METHODS FOR ASR DETERMINATION

Alkali-silica reactivity is a slow process. Several test methods, such as the ASTM C227 mortar bar method, the ASTM C289 chemical test, the ASTM C586 rock cylinder test, and CAN/CSA-A23.2-14A concrete tests (*15*) are used to predict ASR in aggregates.

Many researchers report that ASTM C227 procedure does not adequately identify potential alkali reactive aggregates (*10–14*), particularly slowly reacting aggregates. Therefore, on the basis of ASTM C227 alone, a firm recommendation cannot be made that an aggregate is nonreactive. There is a need for an accelerated method that is more severe and would identify all potential aggregates, including slowly reacting aggregates. Among the various methods tried, the one selected by Canadian researchers and recommended as a proposed Canadian standard (*10*) is the best one available. Named the "Standard Test Method for Accelerated Detection of Potentially Deleterious Expansion of Mortar Bar Due to Alkali-Silica Reaction," the method also has been adopted as the ASTM P214 test. Using that method, it is possible to detect within 16 days potentially deleterious expansion of mortar bars due to alkali-silica reactivity. The test procedure is based on the NBRI accelerated test method, and it provides a good supplement to ASTM C227. ASTM P214 is particularly useful for aggregates that react slowly or produce expansion late in the reaction. Berube and Fournier (*13*) recommended accelerated test procedure mentioned above as more appropriate than the other rapid test procedures. The test method has been used successfully to determine the effectiveness of mineral additives, such as fly ash, silica fume, and blast furnace slags.

It is claimed that all potentially reactive aggregates can be identified using this method. However, one drawback is that it also indicates expansions for some nonreactive aggregates. Therefore, the following procedure is recommended. First, identify all potentially reactive aggregates by the accelerated method. Aggregates shown to be reactive would be further investigated using ASTM C227, other tests (ASTM C289 and C856), petrographic analysis (ASTM C295), and by examining field service records.

TEST METHODS FOR IDENTIFYING REACTIVE AGGREGATES

All five sand samples were tested for mineralogical contents. The RIM of quantitative X-ray diffraction analysis was used. Each of the sand samples was powdered, and a thin layer was collected on to a glass filter. The X-ray beam was passed through the sample. Because the layer within the filter was thin, corrections were applied to transform the diffracting layer into one that is infinitely thick. Analysis of the diffracting layer and computations were done by computer, and weight fractions for all components, crystalline and amorphous, were obtained from the print-out. These were then recombined into whole-sample oxide and the element composition of the sand that was analyzed (Table 1). Sand samples also were analyzed for chert content using polarizing light microscopy.

TABLE 1 Mineralogical Content of Sands

SAMPLE NAME	CROFT SAND	EVERIST HAWARDEN	AKRON IA	CONCRETE MATERIALS	OPPERMAN HERRICK PIT
QUARTZ (%)	9.06	34.68	8.71	23.31	33.11
CALCITE (%)	16.47	19.37	24.54	29.17	1.55
OLIGOCLASE (%)	7.17	-	0.089	13.70	26.38
MICROCLINE (%)	5.33	-	0.086	11.23	38.95
DOLOMITE (%)	54.23	12.38	40.16	16.33	-
HEULANDITE (%)	0.64	-	2.31	1.50	-
HORNBLENDE (%)	2.33	0.93	1.70	1.70	-
ILLITE (%)	1.37	0.29	2.69	-	-
KAOLINITE (%)	-	1.59	2.25	1.23	-
ALBITE (%)	-	15.14	-	-	-
HEMATITE (%)	-	-	-	-	-
ORTHOCLASE (%)	-	12.91	-	-	-
CHLORITE (%)	3.33	-	-	1.78	-
CHERT (%)	-	7.7	-	-	13.90

(-) - Unavailable

MATERIALS

- Cement: the cement used was ASTM Type I/II (ASTM C150), obtained from a plant in Rapid City, South Dakota. Its chemical analysis and physical properties are given in Table 2.
- Fly ash: five different fly ashes were obtained from the Midwest. The chemical and mineral compositions of the fly ashes are given in Table 3. The physical properties determined also are given in Tables 2 and 3. According to ASTM C618 classification, all five are Class C fly ashes.
- Sands: five sands currently used in the construction of highway structures in the Midwest were obtained. The mineral composition of the sands was determined by RIM analysis and findings are given in Table 4. Fine aggregates were separated into different sized fractions, thoroughly washed and dried, and recombined to meet specific gradations given in ASTM P214.
- Water: the water used was tap water from the Rapid City municipal supply system.

MIXTURE PROPORTIONS

Accelerated Test Method

Mixture proportions were fixed according to ASTM P214: 1 part of cement and fly ash and 2.25 parts by weight of the test aggregate was used for all the five sands. The water to cement and fly ash ratio was kept at 0.44 for all the mixes. For all mixes without fly ash, 600 g of cement, 1 350 g of fine aggregate and 264 ml of water was used. According to the procedure adopted by the South Dakota Department of Transportation, 10 percent replacement with fly ash is increased to 1.5 times the percent replacement. Similarly, 15, 20, 25, and 30 percent are increased by 1.25 times the percent replacement. Therefore, with fly ash addition, for 10 percent by weight, 90 g of fly ash and 540 g of cement were mixed uniformly, but the same quantities of the fine aggregates and water were used. Similarly, for replacement levels of 15, 20, 25, and 30 percent, the appropriate amount of cement was replaced by fly ash.

The specimens (mortar bars) used for this method were made according to ASTM C227. Molds were stripped at one day and the bars placed in water heated to 80°C. On the second day, initial measurements were taken and the bars stored in 1N NaOH solution at 80°C. The bar expansions were measured when they were hot, within 15 sec of removal from the container. Expansions were monitored for 14 days.

TABLE 2 Chemical and Physical Properties of Cement

CHEMICAL COMPOSITION	WEIGHT (%)
Silicon dioxide (SiO_2) %	22.63
Aluminium oxide (Al_2O_3) %	4.81
Ferric oxide (Fe_2O_3) %	3.17
Magnesium oxide (MgO) %	1.14
Sulfur trioxide (SO_3) %	2.09
Bogue Potential Compounds	
Tricalcium Silicate (C_3S)	47.36
Tricalcium Aluminate (C_3A)	7.39
Tetracalcium Alumino Ferrite (C_4AF)	9.64
Alkalies	0.55
Loss on Ignition	1.40
Insoluble Residue	0.54

PHYSICAL TEST RESULTS

Blaine Fineness (m^2/kg)	387
Autoclave Expansion (%)	0.01
Gillmore Initial set time	2.15
Gillmore Final set time	4.00
Vicat setting time	1.40
3 Day Compressive Strength (MPa)	24.08
7 Day Compressive Strength (MPa)	34.19
Air Content of Mortar (vol.)	8.5

Cube Compressive Strength

Standard test method for compressive strength of hydraulic cement mortar (ASTM C109) was adopted for the procedure, but the cement was replaced with fly ash by 10 to 30 percent by weight and testing was done for compressive strength. Mix proportions were one part of cement and fly ash and 2.75 parts of sand, proportioned by weighing. The water to cement and fly ash ratio was maintained at 0.485 for all mixes. The molds were 50-mm (2-in.) cubes with three compartments.

TEST SPECIMEN

Four mortar bar specimens were prepared for each mix for the accelerated test method. Specimen sizes were 25 × 25 × 290.625 mm (1 × 1 × 11.625 in.). For cube compressive strength with fly ash replacement, 9 cubes of 50-mm (2 in.) were cast for testing—3 cubes each at ages 3, 7, and 28 days.

CHECKING THE ACCURACY OF OUR TEST PROCEDURE

To validate and confirm the accuracy of the work done, crushed Spratts aggregate of known expansion was acquired from the Engineering Materials Office, Ministry of Transportation, Ontario, Canada. It was tested in our laboratory, using the same procedure and equipment. The Spratt aggregate was from a horizontally bedded limestone quarry, containing 3 to 4 percent microscopic chalcedony and black chert with a conchoidal fracture. Results obtained were compared with known results obtained from Ministry of Transportation, Canada, laboratories. A comparison of the measured expansions is given in the in-text table.

Days	*Canadian Lab*	*SDSM&T Lab*
3	0.08	0.10
7	0.29	0.29
11	0.36	0.36
14	0.42	0.41

TABLE 3 Chemical Composition and Physical Properties of Fly Ashes

	FLY ASH #1	FLY ASH #2	FLY ASH #3	FLY ASH #4	FLY ASH #5
CHEMICAL COMPOSITION					
Silicon oxide (SiO_2)	36.5	32.8	29.9	35.1	46.7
Aluminium oxide (Al_2O_3)	20.8	20.0	17.7	20.3	13.4
Iron oxide (Fe_2O_3)	6.6	5.9	5.7	6.4	8.3
($SiO_2 + Al_2O_3 + Fe_2O_3$)	63.9	58.7	53.3	61.8	68.4
Sulfur Trioxide (SO_3)	1.3	3.5	4.3	1.9	1.4
Calcium oxide (CaO)	23.5	26.9	30.1	23.6	18.7
Magnesium oxide (MgO)	4.3	4.7	7.1	4.2	-
Available Alkalies as Na_2O	1.12	0.77	1.70	1.92	-
Moisture Content	0.0	0.1	0.1	0.0	0.02
Loss on Ignition	0.1	0.4	0.2	0.2	0.02
PHYSICAL TEST RESULTS					
Fineness retained on #325 sieve	11.0	11.4	13.2	16.9	16.7
Soundness					
Autoclave Expansion (%)	0.02	0.04	0.12	0.02	0.09
Specific Gravity	2.61	2.61	2.72	2.66	2.51

The measured expansions were reasonably close, confirming the degree of agreement of our test procedure.

EXPANSION LIMITS FOR ACCELERATED TEST METHOD

Expansion limits for the accelerated test method, as suggested by Berube and Fournier (*13*) are as follows:

- If the aggregates show expansion lower than 0.1 percent at 14 days, they are innocuous.
- If the aggregates show expansion between 0.1 and 0.25 percent, they are slowly expansive.
- If the aggregates show expansion above 0.25 percent, they are rapidly expansive aggregates.

These limits were modified by Hooton and Rogers (*10*), who suggested the following classification in their CSA draft proposal:

- Less than 0.10 percent is innocuous,
- Between 0.10 and 0.20 percent is inconclusive, and
- Greater than 0.20 percent is deleterious.

ASTM P214 suggests the same classification that Hooton and Rogers recommend (*10*). When mortar bar expansions greater than 0.10 percent develop within 16 days from casting, it is strongly recommended that supplementary information be developed to confirm that the expansion is actually due to alkali-silica reactivity. Sources of such supplementary information include (*a*) petrographic examination of the aggregate (ASTM C295) to determine if known reactive constituents are present, (*b*) tests of the aggregate for potential reactivity by chemical methods (ASTM C289), and (*c*) examination of the specimens after tests to identify the products of alkali-silica reactivity (ASTM C856).

The 0.20 percent expansion level recommended for reactive aggregates has to be investigated further in relation to the field performance history of an aggregate. However, that limit is too liberal and it should be reduced to 0.15 or 0.10 percent expansion.

TEST RESULTS AND DISCUSSION

Sand Classification by ASTM P214

The total percentage expansion of mortar bars made from the five different sands and the same Type I/II cement is shown in a bar chart (Figure 1). Results represent the average of four specimens. Sands 1 to 4 could be classified as "not conclusive" because the expansions are above 0.10 percent and below 0.20 percent. Sand 5 is a highly reactive sand. Field observation of pavements built with Sand 5 confirms that classification.

Evaluation of Fly Ashes

Mortar bar length measurements and subsequent expansions measured at 3, 7, 11, and 14 days, and the calculated percentage expansions for all fly ashes and sands and their combinations, are given elsewhere (*24*). Figures comparing expansions at 3, 7, 11, and 14 days for mortar bars without and with 10, 15, 20, 25, and 30 percent by weight of cement replacements with fly ash are given elsewhere (*24*).

TABLE 4 Chemical Composition of Sands

SAMPLE NAME	CROFT SAND	EVERIST HAWARDEN	AKRON IA	CONCRETE MATERIALS	OPPERMAN HERRICK PIT
SiO2 %	50.58	55.71	45.38	50.98	74.61
Si %	23.65	26.05	21.22	23.83	34.89
Al2O3 %	5.442	7.040	5.385	4.780	13.33
Al %	2.881	3.720	2.850	2.530	7.050
Na2O %	1.541	2.010	1.602	1.405	2.710
Na %	1.102	1.490	1.146	1.005	2.010
K2O %	1.198	1.950	1.360	1.154	5.860
K %	0.995	1.610	1.129	0.957	4.870
CaO %	10.44	14.46	12.00	10.54	1.950
CaO %	7.468	10.33	8.578	7.534	1.390
FeO %	-	0.650	-	-	0.050
Fe %	-	0.040	-	-	0.040
Fe2O3 %	0.872	0.220	0.859	0.784	0.140
Fe2 %	0.610	0.150	0.601	0.548	0.090
MgO %	1.716	2.700	1.364	1.222	0.040
Mg %	1.035	1.630	0.820	0.737	0.020
H2O %	-	0.540	-	-	0.230
H %	-	0.060	-	-	0.068
CO2 %	-	14.32	-	-	0.682
C %	-	3.900	-	-	0.180
MnO %	0.044	0.250	0.084	0.036	0.100
Mn %	0.034	0.200	0.065	0.028	0.010
TiO2 %	0.095	0.020	0.075	0.177	0.099
Ti %	0.057	0.010	0.045	0.106	0.050
NiO %	-	0.020	-	-	-
Ni %	-	0.010	-	-	-
BaO %	0.039	0.010	0.040	0.035	0.020
Ba %	0.035	0.010	0.035	0.031	0.010
OXIDE TOTAL	71.96	98.99	68.15	68.30	99.74
ELEMENT TOTAL	37.86	49.75	36.49	37.30	50.71

NOTE : Results for all Sand Samples were obtained by Reference Intensity Method (RIM) of Quantitative X-Ray Analysis.

Bar charts comparing the total percentage expansions at 14 days for all fly ashes at various levels of cement replacement with fly ashes for all sands are given elsewhere as well (*24*). A typical bar chart for Sand 1 is given in Figure 2, and a similar bar chart for the most reactive, Sand 5, is provided in Figure 3.

Effect of Fly Ash Addition on Expansion

Earlier investigations (*3,4,18–20*) indicated that replacement of a portion of cement with fly ash reduces expansion caused by the reactivity between alkalies and reactive silica in the aggregate, provided the proper amount of fly ash is added. The amount depends on the type of fly ash used and its mineralogical contents, in particular, its calcium oxide content. For some fly ashes with more than 1.5 percent available alkali content, a "pessimum limit" was observed (*20*). The pessimum limit is the specific percent replacement of cement with fly ash, for which the expansion reaction due to the alkali-aggregate is the greatest. If the percent of cement replaced with fly ash is below the pessimum limit, then the addition of fly ash causes equal or greater expansion in mortars with fly ash than in those without fly ash. The reason for this is the percentage of alkali in the fly ash (all fly ashes contain alkalies) is released into the pore solution, increasing the degree of alkali-silica reactivity in the mortar. Therefore, the higher the alkali content of the fly ash, the larger the mortar bar expansion.

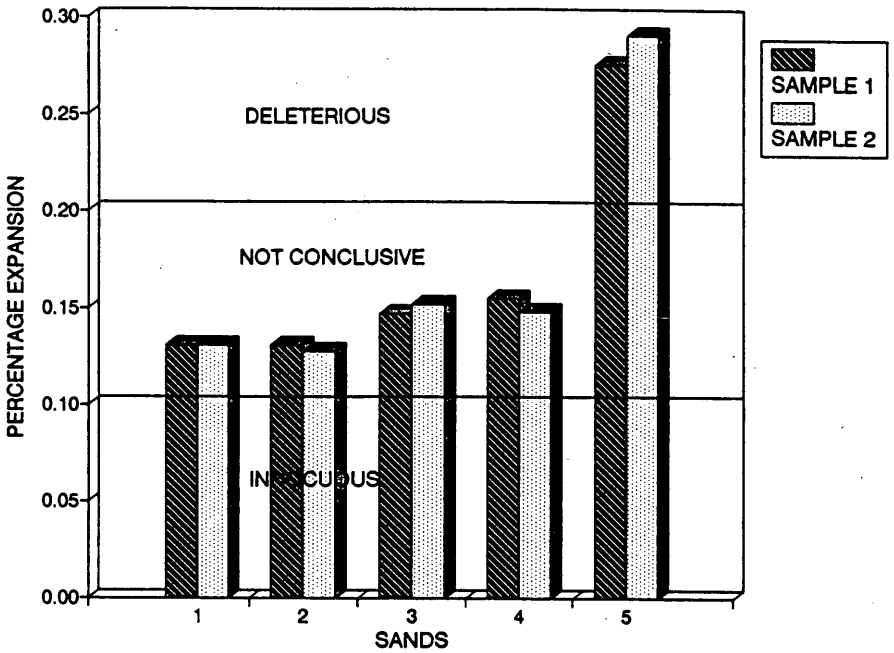

FIGURE 1 Comparison of expansions of five sands using two samples.

The actual mechanisms by which fly ash reduces alkali-aggregate expansions are not clearly understood. The shape and size of fly ash particles affect the watertightness, workability, and mixing water demand of fly ash concrete. Generally, fly ash concretes have reduced permeability, and hence the moisture available for the alkali-aggregate reactivity is less than is available in non-fly ash concrete. That results in reduced expansion in fly ash concretes.

Regarding the chemical composition, it has been suggested that pozzolans reduce or eliminate alkali-aggregate expansion by pozzolanic reaction and by producing lower C/S mole ratio calcium silicate hydrates by reacting with high C/S mole ratio hydrates (*20*). These new hydrates can incorporate large amounts of alkali in their structure, retaining the alkalies and therefore reducing their availability for reaction with silica in the aggregate. However, alkalies

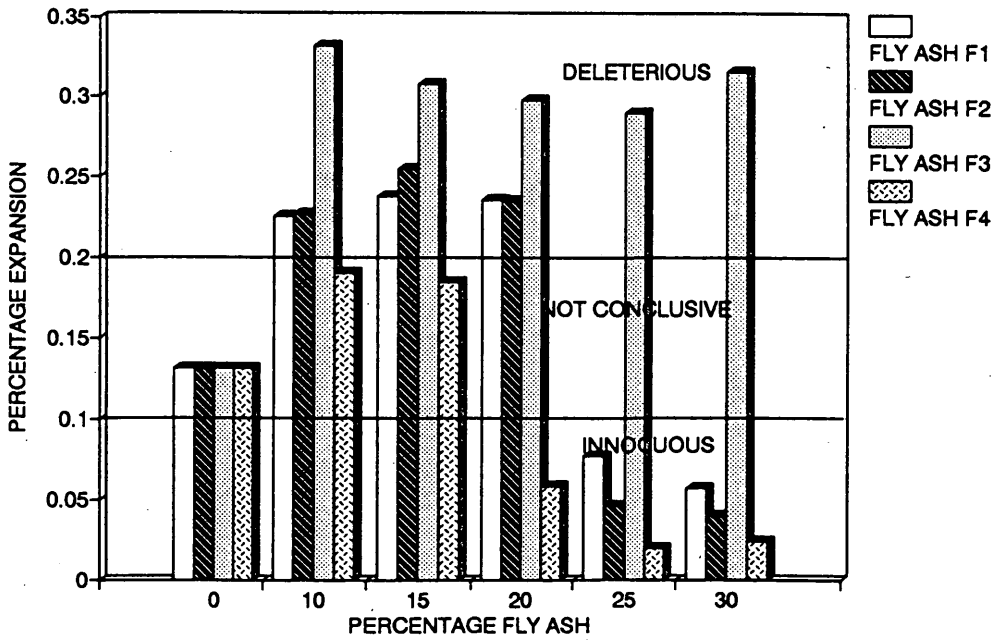

FIGURE 2 Comparison of expansion from accelerated test method for Sand 1 using different fly ashes at 14 days.

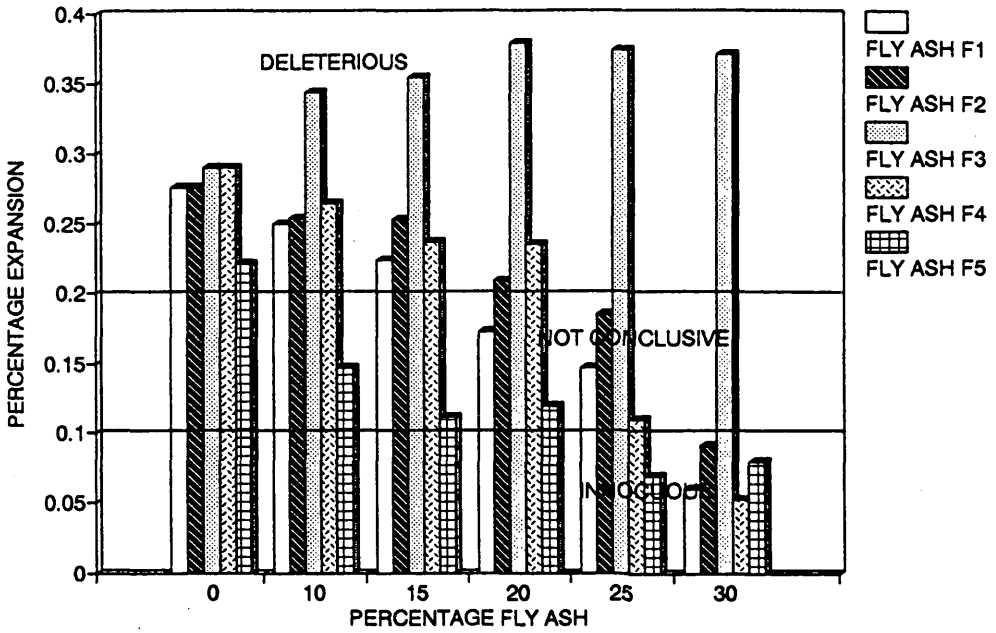

FIGURE 3 Comparison of expansion from accelerated test method for Sand 5 using different fly ashes at 14 days.

in fly ash are also released into the pore solution. Therefore, a balance between the amount of alkalies released by both cement and fly ash into the pore solution and the reduction in expansion related to the combined effect of improved physical properties of concrete and retention of alkali by the pozzolanic activity, and lowered C/S mole ratio silicate hydrates in the mixture, should be achieved (*20*).

Nixon and Gaze (*19*) reported that when low alkali cement and high alkali fly ash are combined, the alkalies in the fly ash contribute to the reactions with the pore solutions at all ages up to 1 year. Hobbs (*18*) observed that, for 30 percent replacement of fly ash, the alkalies in the fly ash contributed to the alkali-silica reaction, which resulted in higher expansion. However, for 50 percent cement replacement, he found that the expansions were negligible. Hobbs stated, therefore, that for 50 percent replacement of cement by fly ash, either no alkali contribution by the fly ash to the reaction appeared to have taken place or the fly ash had effectively neutralized the alkalies of the pore solution (*18*). A similar finding was reported by Alasali (*3*). Alasali observed that in mortars with low level of cement replacement by fly ash, the presence of additional free alkalies had a significant effect on alkali-silica expansion; at higher replacement levels, however, the effect was negligible.

Analysis of the results and observation of the figures indicate clearly that four fly ashes, if added in appropriate quantities, reduced deleterious expansions to a negligible (innocuous) level in mortar bars made with highly reactive Sand 5. However, one fly ash (#3) had slightly increased expansion at all levels of fly ash addition. Results clearly indicate that the addition of any quantity of the four Class C fly ashes (#1, 2, 4, and 5) significantly reduces expansion due to ASR when reactive sands are used. At 30 percent cement replacement with fly ash, the expansions are innocuous. All mortar bar specimens containing one of these four fly ashes had a significant reduction in expansion compared with those specimens without fly ash. However, the influence of fly ash #3 on ASR expansions is the opposite. The reason for that is unknown; further investigation is necessary.

In the case of nonreactive sands (Sand 1, for example 1) a pessimum effect is seen when fly ashes are added. The addition of smaller quantities of fly ash (less than 20 percent for fly ashes #1 and 2, and 15 percent replacement for fly ash #4) had actually increased the total expansion. Above a certain level of replacement, 20 percent for fly ashes 1 and 2, and 15 percent for fly ash 4, expansions due to ASR are reduced. The pessimum limits for these fly ashes are 20, 20, and 15 percent, respectively, for #1, 2, and 4. When fly ashes are added above these pessimum levels, 25 percent for #1 and 2 and 20 percent for #4, deleterious expansions are reduced to innocuous.

The influence of fly ash #3 on ASR expansion in mortar bars made with nonreactive sands (Sand 1), is opposite to that of the other four fly ashes. At every level of fly ash addition up to 30 percent replacement, the expansions are increased. In this case, there is no pessimum limit. Again, the phenomenon cannot be explained without further study.

Influence of Oxide Content of Fly Ashes

Oxide contents of the fly ashes varied from 53.3 to 68.4 percent. Fly ash 3, which had the lowest oxide content (53.3 percent), was not effective in controlling deleterious expansion due to ASR in mortar bars made with reactive and nonreactive sands. Fly ashes with oxide contents of 58.7 percent (#2), 61.8 percent (#4), 63.9 percent (#1) and 68.4 percent (#5) were effective in inhibiting expansion due to ASR, in mortar bars made with reactive and nonreactive sands. Fly ashes with higher quantities of oxides appear to more effectively inhibit expansion; however, the difference is not very significant. As anticipated, the pessimum effect is seen only in nonreactive sands.

Influence of Alkali Contents in Fly Ashes

Alkali contents varied from 0.77 to 1.92. Fly ash 4, which had the highest alkali content of 1.92 percent, was fully effective in inhibiting expansion due to ASR in mortar bars made with reactive and nonreactive sands. Whereas fly ash 3, which had a lower alkali content of 1.70 percent, was not effective in controlling expansion related to ASR.

Effect of Fly Ash Addition on Cube Compressive Strength

Compressive strengths at 3, 7, and 28 days for mortar cubes made either with or without blended cements are given in Table 5. Five fly ashes (1 to 5) were blended with the same cement (Type I/II) at 10, 15, 20, 25, and 30 percent by weight replacement levels. Strengths at 3, 7, and 28 days are compared with the corresponding strengths of mortar cubes made with nonblended cements. The comparison indicates that the replacement of cement, 10 to 30 percent by weight, with fly ash did not adversely affect the compressive strength or the rate of compressive-strength development for all four fly ashes. In some cases the compressive strengths were actually slightly higher for the mortar cubes made with blended cements.

TABLE 5 Compressive Strengths of Cubes With and Without Different Percentages of Fly Ashes

TYPE OF FLY ASH & PERCENTAGE	COMPRESSIVE STRENGTH MPa		
	3 DAYS	7 DAYS	28 DAYS
Fly Ash - F1			
F1 - 0% (Control)	20.96	34.50	39.79
F1 - 10%	23.42	30.94	44.26
F1 - 15%	22.90	28.88	46.90
F1 - 20%	20.27	33.12	49.49
F1 - 25%	18.72	26.75	47.25
F1 - 30%	24.28	24.74	44.32
Fly Ash - F2			
F2 - 0% (Control)	20.96	34.50	39.79
F2 - 10%	26.23	35.43	36.39
F2 - 15%	28.02	27.61	37.49
F2 - 20%	27.27	28.65	38.98
F2 - 25%	27.33	30.08	39.10
F2 - 30%	23.59	34.05	37.84
Fly Ash - F3			
F3 - 0% (Control)	20.95	34.50	39.78
F3 - 10%	31.35	39.21	39.21
F3 - 15%	31.46	39.61	39.78
F3 - 20%	31.46	34.91	37.60
F3 - 25%	32.50	37.60	37.55
F3 - 30%	28.42	39.96	40.42
Fly Ash - F4			
F4 - 0% (Control)	20.95	34.50	39.78
F4 - 10%	30.71	37.77	40.07
F4 - 15%	31.00	37.49	39.84
F4 - 20%	29.62	33.07	37.43
F4 - 25%	29.28	32.55	37.08
F4 - 30%	27.44	32.43	36.39
Fly Ash - F5			
F5 - 0% (Control)	11.98	24.68	36.14
F5 - 10%	8.88	28.11	43.15
F5 - 20%	7.51	23.24	35.29
F5 - 30%	11.45	30.59	25.07
F5 - 40%	14.51	23.46	32.12
F5 - 50%	20.48	27.07	42.04
F5 - 60%	12.80	25.42	40.32
F5 - 70%	15.81	20.34	41.08

CONCLUSIONS

- Accelerated test method results indicate that one sand (Sand 5) is reactive (deleterious) and the other four sands are slow or late to affect expansion (inconclusive).
- Some ASTM Class C fly ashes are effective in inhibiting expansion due to ASR in mortar bars made with reactive and nonreactive sands.
- When nonreactive sands are used, there is a pessimum level below which the fly ash addition slightly increases the expansion related to ASR. However, when fly ashes are added above this pessimum limit, ASR expansions are reduced to negligible innocuous levels. The pessimum levels were 15 or 20 percent for the fly ashes tested.
- When reactive sands are tested, the addition of Class C fly ash at any level considerably reduces ASR expansion. ASR expansions are innocuous, negligible, when appropriate quantities of fly ash are added.
- For the five fly ashes studied, the oxide content of the fly ash seems to have an influence on expansion related due to ASR. Fly ash (3) with low oxides content (53.3 percent) was not effective in inhibiting the expansion from ASR in mortar bars made with reactive and nonreactive sands. The effectiveness improved the higher the oxide content; however the improvement was not significant.
- Alkali content of fly ash did not seem to influence its effectiveness in inhibiting expansion due to ASR in mortar bars made with reactive and nonreactive sands. Additional investigation is necessary to confirm that finding.
- The mortar setting behavior, early strength development characteristics, and their ultimate cube compressive strengths were not affected when part of the cement, (up to 30 percent by weight) was replaced with fly ash and when the fly ash was properly preblended with the cement.

REFERENCES

1. Alasali, M. M., and V. M. Malhotra. Role of Concrete Incorporating High Volumes of Fly Ash in Controlling Expansion Due to Alkali-Aggregate Reaction. *ACI Materials Journal,* Vol. 88, No. 2, American Concrete Institute, Detroit, Mich., March-April 1991, pp. 159–163.
2. Oberholster, R. E., and G. Davies. Effect of Mineral Admixtures on the Alkali-Silica Expansion of Concrete Under Outdoor Exposure Conditions. *Proc., 7th International Conference on Concrete Alkali-Aggregate Reactions,* Ottawa, Ontario, Canada, 1986, pp. 60–65.
3. Alasali, M. M. Alkali-Aggregate Reaction in Concrete: Investigations of Concrete Expansions from Alkali Contributed by Pozzolans or Slag. (V. M. Malhotra, ed.) *Proc., 3rd International Conference on Fly Ash, Silica Fume, Slag, and Natural Pozzolans in Concrete, ACI,* SP-114, Vol., 1, Trondheim, Norway, 1989, pp. 431–451.
4. Carrasquillo, R. L., and P. G. Snow. Effects of Fly Ash on Alkali-Aggregate Reaction in Concrete (V.M. Malhotra, ed.), *Proc., 2nd International Conference on the Use of Fly Ash, Silica Fume, Slag and Natural Pozzolans in Concrete,* Madrid, Spain, April 1986.
5. Swamy, R. N., and M. M. Alasali. Effect of Alkali-Silica Reaction on the Structural Behavior of Reinforced Concrete Beams. *ACI Structural Journal,* Vol. 86, No. 4, July-Aug. 1989, pp. 451–459.

6. Tenoutasse, N., and A. M. Marion. Influence of Fly Ash in Alkali-Aggregate Reaction. *Proc., 7th International Conference on Concrete Alkali-Aggregate Reactions,* 1980, pp. 45–54.
7. *Proc., 3rd International Conference on the use of Fly Ash, Silica Fume, Slag, and Natural Pozzolans in Concrete.* ACI Special Publication SP 114, (V. M. Malhotra, ed.), 2 vols. Trondheim, Norway, 1989.
8. *Proc., 2nd International Conference on the use of Fly Ash, Silica Fume, Slag and Natural Pozzolans in Concrete.* ACI Special Publication SP 91, (V. M. Malhotra, ed.), Madrid, Spain, 1986.
9. *Proc., 1st International Conference on the Use of Fly Ash, Silica Fume, Slag and Other Mineral By-Products in Concrete,* ACI Special Publication SP 79, (V. M. Malhotra, ed.), Canada, August 1983.
10. Hooton, R. D., and C. A. Rogers. Appendix A, CSA CAN3-A23.2-XXC. Presented at the Conference on Canadian Developments in Testing Concrete Aggregates for Alkali-Aggregate Reactivity. Report EM-92, Engineering Materials Office, Ministry of Transportation, Canada, Toronto, Ontario, March 1990, pp. 233–240.
11. Hooton, R. D., and C. A. Rogers. Evaluation of Rapid Test Methods for Detecting Alkali-Reactive Aggregates. *Proc., 8th International Conference on Alkali-Aggregate Reaction,* Kyoto, Japan, 1989.
12. Oberholster, R. E., and G. Davies. Accelerated Method for Testing the Potential Alkali Reactivity of Siliceous Aggregates. *Cement and Concrete Research,* Vol. 16, No. 2, March 1986, pp. 181–189.
13. Berube, M. A., and Fournier. *Canadian Experience with Rapid Testing Methods for Alkali-Aggregate Reactivity.* Department of Geology, Laval University, Sainte-Foy, Quebec, Canada.
14. Ineson, P. R. Siliceous Components in Aggregates. *Cement and Concrete Composites,* Vol. 12, No. 3, 1990, pp. 185–190.
15. Canadian Standards Association, Concrete Materials and Methods of Concrete Construction, Method of Test for Concrete, CAN/CSA-A23.1-M90, CAN/CSA-A23.2-M90, National Standards of Canada, Rexdale, Ontario, March 1990.
16. Swamy, R. N., and M. M. Alasali. New Test Methods for Alkali-Silica Reaction. *Proc., 7th International Conference on Concrete Alkali-Aggregate Reactions.* Ottawa, Ontario, Canada, 1986, pp. 324–329.
17. Chatterji, S., N. Thaulow, and A. D. Jensen. Studies of Alkali-Silica Reaction, Part 4: Effect of Different Alkali-Salt Solutions on Expansion. *Cement and Concrete Research,* Vol. 17, No. 5, Sept. 1987, pp. 777–783.
18. Hobbs, D. W. Alkali-Silica Reaction in Concrete. *The Structural Engineer (London),* Vol., 64A, No. 12, Dec. 1986, pp. 381–383.
19. Nixon, P. J., and M. E. Gaze. Use of Fly Ash and Granulated Blast-Furnace Slag to Reduce Expansion Due to Alkali-Aggregate Reaction. *Proc., 5th International Conference on Alkali-Aggregate Reaction in Concrete,* Cape Town, South Africa, 1981.
20. Farbriaz, J., and R. Carrasquillo. Alkali-Aggregate Reaction in Concrete Containing Fly Ash. *Proc., Katharine and Bryant Mather International Conference on Concrete Durability, ACI Special Publication* SP100, (John M. Scanlon, ed.), Vol. 2, Atlanta, Ga., 1987. pp. 1787–1808.
21. Berube, M. A., and B. Fournier. Testing Field Concrete for Further Expansion by Alkali-Aggregate Reactions. Presented at the American Concrete Institute Convention. Engineering Materials Report 92, Ministry of Transportation, Ontario, Canada, March 1990, pp. 162–180.
22. Ramakrishnan, V., and S. Kakodkar. The Influence of ASTM Class C Fly Ashes on the ASR Expansions of Mortar Bars Made with Five Different Reactive and NonReactive Sands. Report No. 92 D-VR-F, Midwest Fly Ash Company, Inc., Sioux City, Iowa, Dec. 1992 (unpublished.)

Publication of this paper sponsored by Committee on Chemical Additions and Admixtures for Concrete.

Effect of Natural Pozzolan Addition on Expansions Caused by Alkali-Silica Reaction

V. RAMAKRISHNAN, DAN JOHNSTON, AND PRASAD NUNNA

The use of natural pozzolans to prevent excessive expansion of concrete caused by an alkali-silica reaction is referred to in the published literature. However, few data have been published on the use of natural pozzolans in field concrete. Results of an extensive study to determine the influence of natural pozzolans in reducing deleterious expansion due to alkali-silica reaction are presented. Twenty-six different types of natural pozzolans were collected from various locations in the Black Hills of western South Dakota and tested to determine their mineralogical content, chemical composition, and physical properties. On the basis of the strength activity index test with cement, the 10 most promising pozzolans were selected. Those were tested to determine their effectiveness in controlling the alkali-silica reaction. That was done by blending 10, 15, and 25 percent of natural pozzolans (by weight) with Type I/II cement. The blended cements then were tested according to ASTM P214, using mortar bars. Test results indicated that all the natural pozzolans tested except one were effective in reducing expansion due to alkali-silica reaction. A comparison of the effectiveness of reducing deleterious expansion by fly ash and natural pozzolan blended cements indicated that two natural pozzolan-blended cements were more effective than the Class F fly ash-blended cement in reducing expansion.

Cracks caused by the use of sands that are prone to alkali-aggregate reaction were observed in pavements in South Dakota. South Dakota Department of Transportation (SDDOT) tested some of the sands using ASTM C289. Test results indicated the possibility of the deleterious nature of the sands used in the construction of pavements. Although fly ashes and natural pozzolans such as pumice, volcanic ash, diatomaceous earth, and siliceous shales have been used to control alkali-silica reaction (ASR) (*1–12*), problems associated with homogeneity, variability in composition, and uniformity and anomalous expansion, persist, and it is difficult to maintain quality control. By producing suitable pozzolan under controlled conditions and blending it with the cement in the plant under controlled conditions, one can eliminate many of these problems. The use of a natural pozzolan blended Type IP cement is a viable solution. Therefore, the feasibility of obtaining such a natural pozzolan was investigated. Adequate supplies of natural pozzolans exist near Rapid City, South Dakota, and the state-owned South Dakota Cement Plant in Rapid City can manufacture the Type IP cement. The possibility of controlling ASR expansions in pavements by replacing part of the cement with pozzolan was studied. It was necessary to determine the amount of pozzolan to be blended to obtain the optimum effectiveness in controlling ASR.

V. Ramakrishnan and P. Nunna, South Dakota School of Mines and Technology, 501 East St. Joseph Street, Rapid City, S.D. 57701–3995. D. Johnston, South Dakota Department of Transportation, 700 Broadway Avenue East, Pierre, S.D. 57501-2506.

OBJECTIVES

- To find a natural pozzolan that is more efficient, effective, and economical than fly ash in reducing the deleterious expansion due to ASR.
- To find the optimum quantity of natural pozzolan that can be blended with cement to produce a Type IP cement for minimizing ASR.
- To ensure the selected natural pozzolan for blending does not, in any way, adversely affect the fresh and hardened properties of cement, mortar, or concrete.

MATERIALS AND TEST SPECIMENS

Cement: The cement used was ASTM Type I/II, conforming to ASTM C150 specifications. It was manufactured at the South Dakota Cement Plant. Its chemical and physical properties are given in Table 1.

Fly Ash: The fly ash used was a low-calcium ASTM Class F obtained from a source in North Dakota. The fly ash was supplied by SDDOT. Its chemical analysis and other properties are also given in Table 1.

Pozzolans: Different types of natural pozzolans collected by R. Holm of the Geology Department, South Dakota School of Mines and Technology, were used in this investigation. The designation, deposit and description of the pozzolans are given in Table 2. Table 3 contains the chemical compositions determined by and inductively coupled plasma (ICP) spectrometer. With the ICP method, samples are subjected to high temperature, which causes the sample to dissociate into individual atoms and ions. The atoms and ions emit light at wavelengths characteristic of the elements present. The spectrometer sorts the various wavelengths and measures the intensity of the specific spectral lines. The intensities are directly proportional to elemental concentrations in the sample. Table 4 gives the chemical compositions as obtained using a scanning electron microscope.

Aggregates: A highly reactive fine aggregate provided by SDDOT was used for all mixes.

Water: The water used was tap water from the Rapid City Municipal supply system.

Test Specimen: Four mortar bar specimens were prepared from each mixture for the ASTM P214 test method. For strength activity index, three cubes of size 50 mm (2 in.) were cast for each mixture.

TEST PROCEDURES

ASTM P214 is able to detect within 16 days the potential for deleterious expansion of mortar bars caused by ASR. Mixture propor-

TABLE 1 Chemical and Physical Properties of Cement and Fly Ash

	PORTLAND CEMENT	FLY ASH
CHEMICAL ANALYSIS(%)		
SiO_2	22.74	52.66
Al_2O_3	4.75	18.69
Fe_2O_3	3.40	4.65
CaO	63.91	3.12
MgO	1.20	2.79
SO_3	2.10	-
TiO_2	-	5.29
Na_2O	0.15	0.40
K_2O	0.59	2.52
MnO	-	0.28
Moisture Content		0.02
Loss on Ignition	1.50	0.02
Physical Test Results		
Fineness Blaine(m^2/kg)	387	-
Fineness Retained on #325 sieve	-	16.72
Soundness Autoclave Expansion(%)	-0.01	0.09
Bogue Potential Compounds		
C_3S	44.57	
C_2S	31.58	
C_3A	6.83	
C_4AF	10.35	

tions were selected according to ASTM P214, 1 part cement and 2.25 parts graded aggregate. The cement was replaced by the pozzolan with 10, 15, and 25 percent by weight of cement. For the fly ash, two additional percentages, 30 and 40 percent, were included. The water cementitious ratio used was 0.44 for all mixtures. The aggregate was washed, cleaned, and graded, and appropriate quantities were weighed and mixed to obtain a uniform gradation, as specified in ASTM P214.

The specimens (mortar bars) used for the test were made according to ASTM C227. The molds were stripped after 1 day, and the bars were placed in water that was heated to 80°C. On the second day, initial measurements were taken and the bars stored in 1 N NaOH solution at 80°C. The bar expansions were measured when they were hot, within 15 sec of removal from the container. Expansions were monitored for 14 days.

Strength Activity Index with Cement

Cubes 50 mm (2 in.) were cast from the control mixture and from each of the test mixtures in accordance with ASTM C109. Mixture proportions were selected according to ASTM C311. For control mixture, 250 g of cement, 687.5 of sand and water-to-cement ratio of 0.484 were used in molding three specimens. For the test mixture, 20 percent of the cement used in the control mixture was replaced by the pozzolans and water was added to achieve adequate workability. The water-to-cement plus pozzolan ratios are given in Table 5.

Molded specimens were covered with polythene sheets and stored for 24 hr at 23°C (73°F). The cubes were removed from the molds and cured in lime-saturated water for 28 days. Compressive strength was determined for both the control and the test mixture according to ASTM C109. To study the effect of calcining, the pozzolans were calcined at different temperatures (Table 6). A strength activity index was determined for the calcined pozzolans at the age of 7 days.

Density

Density was determined according to ASTM C188.

Fineness by No. 325 Sieve

The raw pozzolan materials were crushed using different sized crushing machines and ground to fine powder in a ball mill. The fineness of each pozzolan was determined by calculating the amount of pozzolan retained when wet sieved on a No. 325 sieve in accordance with ASTM C430.

Blaine Fineness

Fineness related to the air permeability (ASTM C204) was used to determine the Blaine fineness of the pozzolans and fly ash. Because the materials are not cement, the constant *b*, necessary to the equation for determining Blaine fineness, was obtained. The procedure for calculating the constant *b* is given in ASTM C204.

TABLE 2 Designation, Deposit, and Description of Pozzolans

SAMPLE DESIGNATION	DEPOSIT	DESCRIPTION
PR1	Rockyford ash	Light gray tuff (Zeolite)
F1	Fuson shale of Dakota FM	Gray clay weathered to nodules
F2	Fuson shale of Dakota FM	Reddish (burnt color) shale yellowish coat on weathered surface
W1	Sharps FM just above Rockyford ash member	White to light gray, hard, resistant to weathering
W2	Rockyford ash member of Sharps FM	Very white Zeolitic tuff
MW1	Mowry shale	Shale, dark gray weathers medium gray
MW2	Mowry shale	Weathered sample
SM1	Upper part of Rockyford ash	Weathered, light gray volcanic tuff
SM2	Lower part of Rockyford ash	Very white, hard volcanic tuff
CB1	Rockyford ash	White ash (tuff)
CT1	Sharps FM 10-15 ft above Rockyford ash	Light gray, more like a siltstone
US1	Upper unit of Sharps FM	White to gray siltstone
ERC1	Rockyford ash	Highly weathered more like a pumice
PRC1	Probably middle of Sharps FM	Whitish gray, very hard, F.grained contained many 1 inch or smaller vugs w/chalk vugs
FE1	White river group(basal Chadron FM)	Brownish gray clay, sample is fairly weathered
FE2	Brule FM of White river group	Light brown weathered clay
FE3	Brule FM	Brown clay
VA1	Brule FM	White pure ash
BG1	Pierre shale	Yellowish, highly weathered Bentonite
AC1	Belle Fourche shale	Gray Bentonite
TH1	Tomahawk volcanic area	Yellow to light brown Rhyolitic Lithic tuff containing several Xenoliths
F3	Fuson shale	Light gray, nodular clay
F4	Fuson shale	Reddish fissile shale
MO1	Morrison FM	Greenish shale
VA2	Appears to be in Morrison FM	White volcanic ash
WW1	Clinker from coal mine	Light red in color
MOU	Late Jurassic Morrison FM	Volcanic tuff
PS1E	Upper Cretaceous	Brown shale, expanded Pierre shale by kiln heating
LK1	Early Cretaceous Lakota FM	Silicified volcanic tuff
LK2	Early Cretaceous Lakota FM	Silicified volcanic tuff

TEST RESULTS AND DISCUSSION

Density: Densities of all the pozzolans, portland cement, and Class F fly ash are given in Table 7. The densities of all pozzolans were less than that of the cement, and they varied between 2.13 gm/cm^3 and 2.84 gm/cm^3.

Fineness: The fineness obtained by wet sieving through No. 325 Sieve for all pozzolans was above 90 percent passing (Table 7). The objective of obtaining a pozzolan finer than 90 percent passing was therefore achieved. The fly ash was used as received, without further grinding. Blaine finenesses of selected pozzolans are indicated in Table 8.

Strength Activity Index with Portland Cement

The strength activity index was used as a prescreening method for selecting the pozzolans for further testing. Strength activity index results are given in Table 5. The pozzolans had a wide range of strength activity; the values varied between 19.78 and 91.72 percent. On the basis of the strength activity index test results, 10 pozzolans were selected for blending with cement and tested for their effectiveness in controlling expansion due to ASR. The pozzolans selected for further testing had a strength activity index of at least 60 percent, except for MW1. Some of the pozzolans (for example, VA1, VA2, and LK1, LK2) were from similar geological forma-

TABLE 3 Chemical Compositions of Pozzolan Samples Using Inductively Coupled Plasma

SAMPLE	SiO_2	Al_2O_3	Fe_2O_3	CaO	MgO	Na_2O	K_2O	TiO_2	SO_3	MnO	BaO	NiO	H_2O	L I*	TOTAL
SM2	61.29	9.88	1.62	4.23	0.61	0.52	5.19	0.23	0.30	0.40	0.60	BDL	5.25	7.56	96.68
CB1	65.47	10.13	1.46	3.48	0.66	0.38	5.13	0.20	0.17	0.03	0.05	BDL	4.22	8.42	99.80
CT1	58.82	10.43	2.39	5.84	1.16	0.30	3.37	0.38	0.03	0.05	0.09	BDL	5.96	7.53	96.45
MW1	57.23	14.51	4.12	0.96	1.58	0.05	2.61	0.62	0.27	0.04	0.01	BDL	5.50	6.52	94.02
PRC1	63.76	10.96	2.89	3.98	1.19	0.34	5.16	0.45	0.20	0.04	0.05	BDL	3.75	4.45	97.22
PS1E	58.98	16.59	6.29	1.57	2.11	0.02	4.53	0.70	1.01	0.05	0.05	BDL	0.15	1.10	93.15
US1	65.24	12.09	3.12	3.24	1.61	0.39	3.52	0.50	0.09	0.04	0.04	BDL	4.90	4.21	98.99
F3	75.00	7.44	1.73	0.95	0.65	0.04	0.92	0.68	0.16	BDL	BDL	BDL	6.00	4.28	97.85
LK2	79.94	7.58	1.11	0.25	0.15	0.01	1.53	0.35	0.13	BDL	BDL	BDL	0.81	4.37	96.23
F1	-	-	-	-	-	0.01	4.12	-	-	-	-	-	-	-	-
F2	-	-	-	-	-	0.03	2.84	-	-	-	-	-	-	-	-
LK1	-	-	-	-	-	0.01	1.71	-	-	-	-	-	-	-	-
MO1	-	-	-	-	-	0.04	6.54	-	-	-	-	-	-	-	-
MOU	-	-	-	-	-	BDL	1.88	-	-	-	-	-	-	-	-
PR1	-	-	-	-	-	0.62	6.19	-	-	-	-	-	-	-	-
W1	-	-	-	-	-	0.40	4.07	-	-	-	-	-	-	-	-
W2	-	-	-	-	-	0.34	4.22	-	-	-	-	-	-	-	-
SM1	-	-	-	-	-	0.32	5.58	-	-	-	-	-	-	-	-
ERC1	-	-	-	-	-	0.58	3.93	-	-	-	-	-	-	-	-
AC1	-	-	-	-	-	0.54	1.28	-	-	-	-	-	-	-	-
BG1	-	-	-	-	-	0.34	1.01	-	-	-	-	-	-	-	-
FE2	-	-	-	-	-	0.19	2.36	-	-	-	-	-	-	-	-
VA1	-	-	-	-	-	0.34	5.98	-	-	-	-	-	-	-	-
VA2	-	-	-	-	-	BDL	2.08	-	-	-	-	-	-	-	-
WW1	-	-	-	-	-	0.27	3.58	-	-	-	-	-	-	-	-
TH1	-	-	-	-	-	0.51	3.55	-	-	-	-	-	-	-	-

L I* - Loss on Ignition
BDL - Below detection level
SiO_2 and SO_3 were determined using wet chemistry technique.

tions. In such cases, one from each geological formation was selected for testing. Pozzolan ERC1, having a strength activity index of 67.01 percent was eliminated from further testing because of unsuitable mining conditions. Fly ash used in the investigation had a strength activity index of 75.06 percent.

Effect of Calcining on the Strength Activity Index

The strength activity index for some of the pozzolans was low. Therefore, the effect of calcining the pozzolans on the strength activity index was studied. For the investigation, MW1, PS1E (expanded shale), and CT1 were selected. The strength activity index for MW1 was 45.27 percent without calcining. The pozzolan was calcined at three temperatures: 350°C, 700°C, and 1050°C. The effect of calcining was very evident for this pozzolan (Table 6). Strength increased depending on the temperature at which it was calcined. For the pozzolan CT1, the strength activity index increased from 62.00 to 88.78 percent when the pozzolan was heated at 1050°C.

The strength activity index for PS1E (Table 5) was the percentage obtained when the pozzolan was calcined at about 1050°C.

TABLE 4 Chemical Compositions of Pozzolan Samples Using Scanning Electron Microscope

SAMPLE	SiO_2	Al_2O_3	Fe_2O_3	CaO	MgO	Na_2O	K_2O	TiO_2	SO_3	MnO	Cl	P_2O_5	H_2O	L I*	TOTAL
SM2	64.28	11.84	2.06	3.85	0.78	2.03	4.04	0.25	0.10	0.00	BDL	BDL	4.05	6.72	100.0
CB1	63.95	11.46	1.54	3.08	0.99	1.44	4.53	0.29	0.08	0.00	BDL	BDL	4.22	8.42	100.0
CT1	55.52	12.75	4.36	9.70	1.84	1.05	3.20	0.82	0.17	0.29	0.07	0.39	2.31	7.53	100.0
MW1	56.21	19.29	6.26	1.47	1.68	0.48	2.80	1.15	0.86	0.00	0.00	0.35	2.93	6.52	100.0
PRC1	61.99	11.97	4.58	5.17	1.13	1.12	5.10	0.75	0.11	0.27	0.00	0.43	2.75	4.45	100.0
PS1E	56.21	19.48	9.52	2.74	2.31	0.91	3.85	1.04	1.86	0.08	0.07	0.68	0.15	1.10	100.0
US1	60.22	14.58	4.80	5.08	2.53	1.12	3.11	0.60	0.10	0.25	0.13	0.46	2.81	4.21	100.0
LK2	82.77	8.67	0.97	0.38	0.67	0.35	0.47	0.38	0.16	0.00	BDL	BDL	0.81	4.37	100.0
F3	73.62	11.60	3.44	1.38	1.03	0.19	0.22	1.02	0.17	0.00	BDL	BDL	2.88	4.28	100.0

NiO and BaO were below detection level
L I* - Loss on Ignition
BDL - Below detection level

TABLE 5 Compressive Strength and Strength Activity Index of Natural Pozzolans with Portland Cement

Sample	Water* / Cement + Pozzolan	Compressive Strength, MPa at age 28 days	Strength activity index with cement in %
CEMENT	0.48	47.0	-
F1	0.47	22.8	48.64
F2	0.45	20.8	44.40
W1	0.50	23.5	50.00
W2	0.50	24.9	53.11
MW1	0.50	21.3	45.27
SM1	0.50	32.2	68.50
SM2	0.50	32.7	69.60
CB1	0.50	37.6	80.15
CT1	0.45	29.1	62.00
US1	0.45	29.9	63.60
ERC1	0.50	32.4	69.01
FE2	0.45	9.3	19.78
TH1	0.47	16.2	34.43
PR1	0.48	24.9	53.11
BG1	0.55	26.8	57.14
MO1	0.48	20.8	44.32
WW1	0.48	22.9	48.71
PRC1	0.46	33.5	71.43
VA1	0.46	34.1	72.67
VA2	0.44	40.2	85.56
AC1	0.44	25.9	55.10
F3	0.46	37.0	78.75
PS1E	0.46	43.1	91.72
LK1	0.47	40.0	85.12
LK2	0.46	39.0	82.93
MOU	0.46	25.9	55.23
Fly Ash	0.44	35.3	75.06

Note:* - Water cement ratios used for strength activity index of natural pozzolans and fly ash with portland cement

TABLE 6 Compressive Strength and Strength Activity Index with Cement for Calcined and Uncalcined Pozzolans

Sample Designation	Compressive strength, MPa age 7 days	Strength activity index with cement in percent	Calcining temperature °C
Cement	32.8	-	-
MW1A	23.5	71.48	350
MW1B	27.2	82.81	700
MW1C	30.3	92.24	1050
PS1A	27.7	84.38	115
PS1B	28.5	86.79	350
PS1C	31.2	95.17	700
CT1A	29.2	88.78	950

1 psi = 0.00689 MPa

TABLE 7 Density and Fineness of Pozzolans and Fly Ash

SAMPLE	DENSITY gm/cm^3 ASTM C188	FINENESS (%) PASSING # 325 SIEVE ASTM C430	SAMPLE	DENSITY gm/cm^3 ASTM C188	FINENESS (%) PASSING # 325 SIEVE ASTM C430
CEMENT	3.13	95.26	PR1	2.27	90.71
F1	2.62	92.25	BG1	2.54	95.36
F2	2.84	91.79	MO1	2.42	96.60
W1	2.73	95.51	WW1	2.39	96.60
W2	2.32	94.89	PRC1	2.38	93.80
MW1	2.41	92.41	VA1	2.53	95.05
SM1	2.50	94.43	VA2	2.48	97.99
SM2	2.22	93.19	AC1	2.59	93.96
CB1	2.13	93.96	F3	2.34	91.79
CT1	2.30	97.05	PS1E	2.34	98.77
US1	2.36	96.90	LK1	2.30	93.65
ERC1	2.42	93.80	LK2	2.27	98.30
FE2	2.33	92.26	MOU	2.25	92.25
TH1	2.59	91.50	FLY ASH	2.67	83.80

TABLE 8 Blaine Fineness of Selected Pozzolans

SAMPLE	BULK VOLUME cm^3	DENSITY gm/cm^2	CONSTANT "b"	FINENESS cm^2/gm
Cement	1.816	3.15	0.90	3990
Fly Ash	1.777	2.67	0.92	3530
LK2	2.130	2.27	1.26	3270
PS1E	1.935	2.34	1.07	4910
SM2	2.680	2.22	1.86	4420
MW1	2.000	2.41	1.34	3500
CT1	2.016	2.30	1.14	3570

Therefore, for PS1, the strength activity index was determined when the pozzolan was treated at lower temperatures of 115°C, 350°C, and 700°C. Results indicated that there was a decrease in the strength activity index when it was treated at 115°C and 350°C. However, there was no significant difference in the strength activity index when it was treated at 700°C, compared with the pozzolan calcined at 1050°C (Table 6).

It can be concluded that calcination of pozzolans influences the strength activity index. That may be the result of removing moisture from the pozzolans by the calcining.

Effect of Pozzolans on Expansions Using ASTM P214 Test Method

According to ASTM P214, when mean expansions of test specimens exceed 0.20 percent 16 days after casting, that is indicative of potentially deleterious expansion. When expansion is between 0.10 and 0.20 percent, the results are not conclusive. If the mean expansion of the test specimens is less than 0.10 percent, it is indicative of innocuous expansion.

Expansion of mortar bars made with a reactive sand and cements without or with 10, 15, or 25 percent replacement with pozzolans by weight (LK2, PS1E, and VA2) are compared in Figures 1 through 3. The most effective pozzolans, LK2 and PS1E, and the adversely effective pozzolan VA2, are selected for discussion and comparison. The other pozzolans' effectiveness was somewhere between these extreme cases. For comparative evaluation, the influence of a Class F fly ash on ASR expansion in the mortar bars made with the same reactive sand and fly ash-blended cements is shown in Figures 4 and 8. Bar charts comparing the total expansions at 16 days for mortar bars made with and without blended cements are given in Figures 5 to 7 for pozzolans LK2, PS1E, and VA2.

Test results indicated that 10 percent replacement of cement with LK2 and PS1E pozzolans had decreased the expansions below 0.1 percent. All other pozzolans, except VA2 and PRC1, when blended with cement at 10 percent replacement level had decreased the expansions. However, the total expansions at 16 days after casting were in between 0.1 and 0.2 percent. When the cement was replaced with pozzolans at 15 percent by weight, all the pozzolans except VA2 and PRC1 had decreased the ASR expansions to an innocuous level (below 0.1 percent). When the cements were blended with pozzolan at 25 percent replacement, all the pozzolans except VA2 had decreased the total expansions below 0.1 percent. Therefore, all pozzolans, except VA2, are suitable for blending with cement to inhibit effectively ASR expansions in concrete. In the case of pozzolan VA2, it was observed that its influence on ASR expansions was entirely different from that of the other pozzolans. When pozzolan VA2 was blended with cement at 10, 15, and 25 percent replacement levels, the mortar bar expansions actually increased compared with the expansions in mortar bars made with unblended cements. That is termed the "pessimum phenomenon." A pessimum limit has been observed by other researchers (*5,7*) when certain types of fly ash were added to cement. The limit represents a percent replacement of cement below which the addition of fly ash or

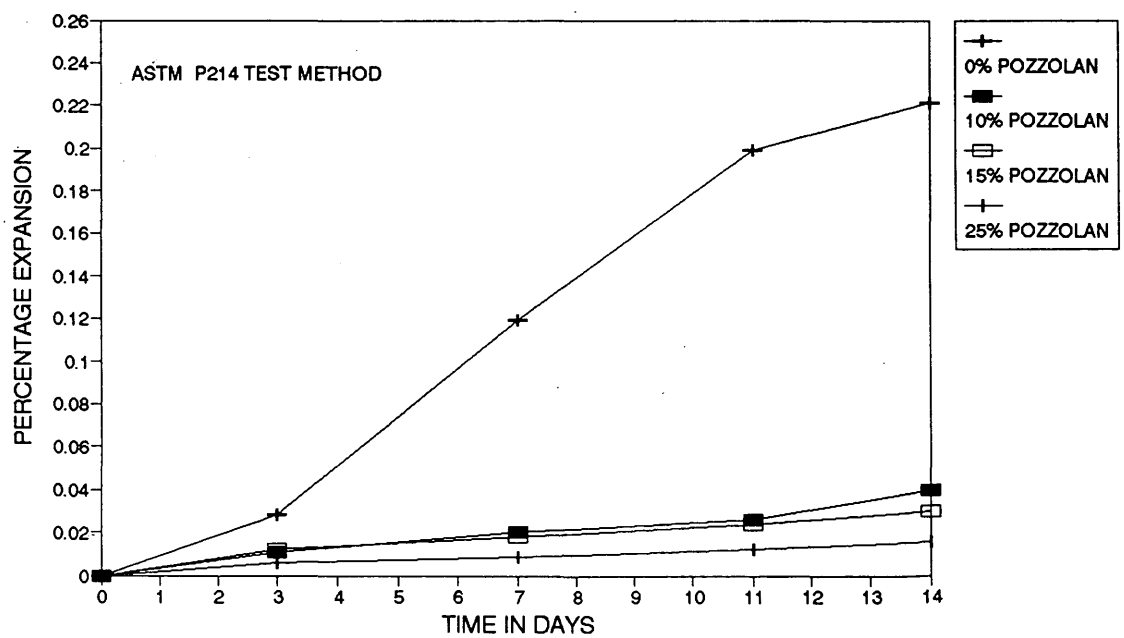

FIGURE 1 Comparison of mortar bar expansion for LK2.

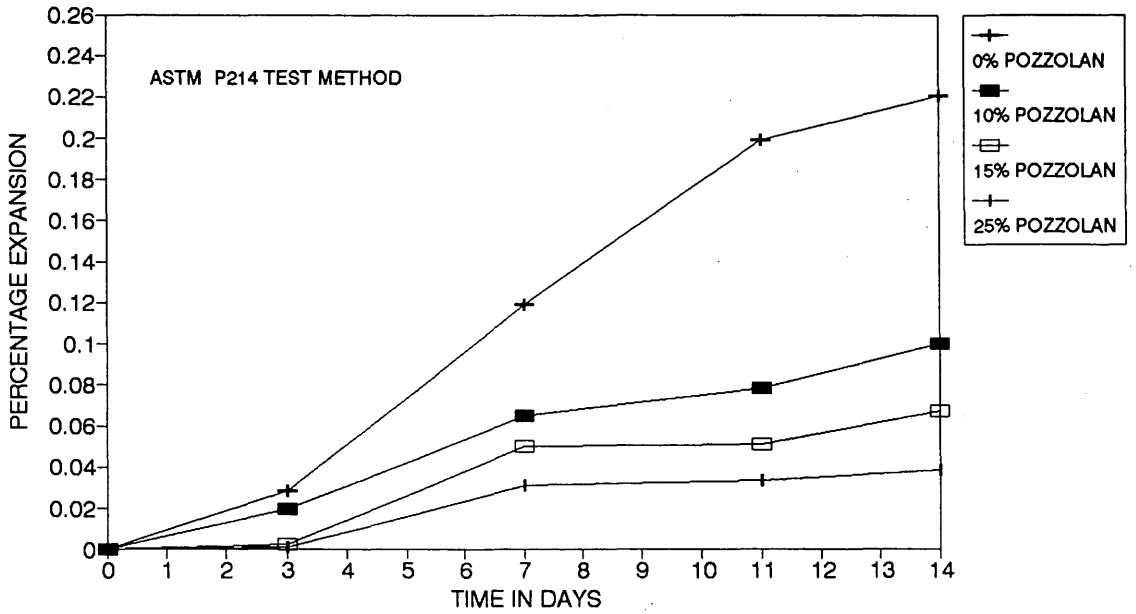

FIGURE 2 Comparison of mortar bar expansion for PS1E.

pozzolan causes equal or greater expansions in mortar bars than occurs in mortar bars without fly ash or pozzolan. When cement is blended with fly ash at a percentage above the pessimum limit, then expansions are reduced. The 10 percent replacement of cement with PRC1 pozzolan had given higher expansions than the mortar bars without pozzolan. However, at higher percentages of cement replacement with PRC1 pozzolan, the ASR expansions were reduced. Comparisons of ASR expansions in mortar bars with different types of pozzolans indicated that total expansions at 16 days after casting were below 0.1 percent in the case of mortar bars made of blended cements using all pozzolans (except VA2 and PRC1).

When a Class F fly ash was blended with cement at a replacement level of 10 to 40 percent by weight, it effectively reduced ASR expansion. However, when the quantity of fly ash blended was less than 20 percent by weight, the total expansion at 16 days was still higher than the innocuous level (0.1 percent). The expansions were reduced below the innocuous level only when the fly ash blended was higher than 25 percent by weight.

Mechanism by which Pozzolans Effectively Control Expansions Caused by ASR

Although the mechanism by which the pozzolans reduce ASR expansions is not clearly understood, it is clear that the physical and chemical properties of a pozzolan affect its effectiveness in

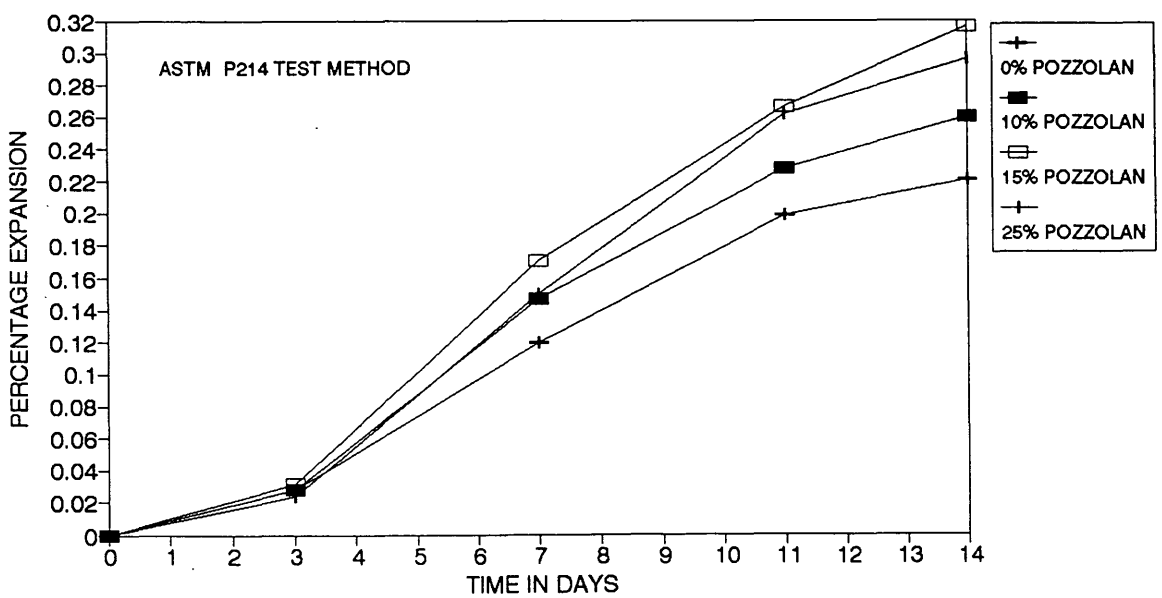

FIGURE 3 Comparison of mortar bar expansion for VA2.

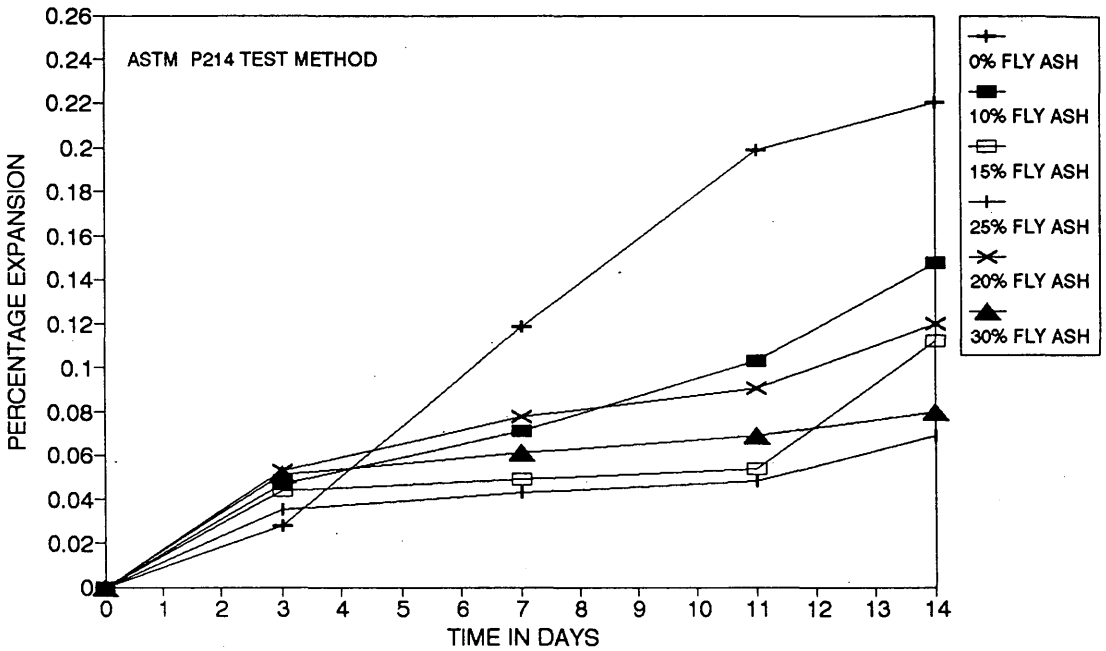

FIGURE 4 Comparison of mortar bar expansion for fly ash.

reducing ASR expansion in concrete. Because it is known that the presence of moisture increases ASR, it is possible that pozzolans are able to reduce permeability and therefore reduce ASR expansions.

In a study conducted by Larbi and Bijen (*12*) on the effect of mineral admixtures on cement paste-aggregate interface (*12*), adding fly ash or similar mineral admixtures reduced the migration of the hydroxyl ions because densification and thinning of the interfacial region prevented or reduced penetration of ions into the reactive grain and reduced ASR in concrete.

As for the chemical properties, it has been suggested that the pozzolans reduce or eliminate ASR expansion by pozzolanic reaction

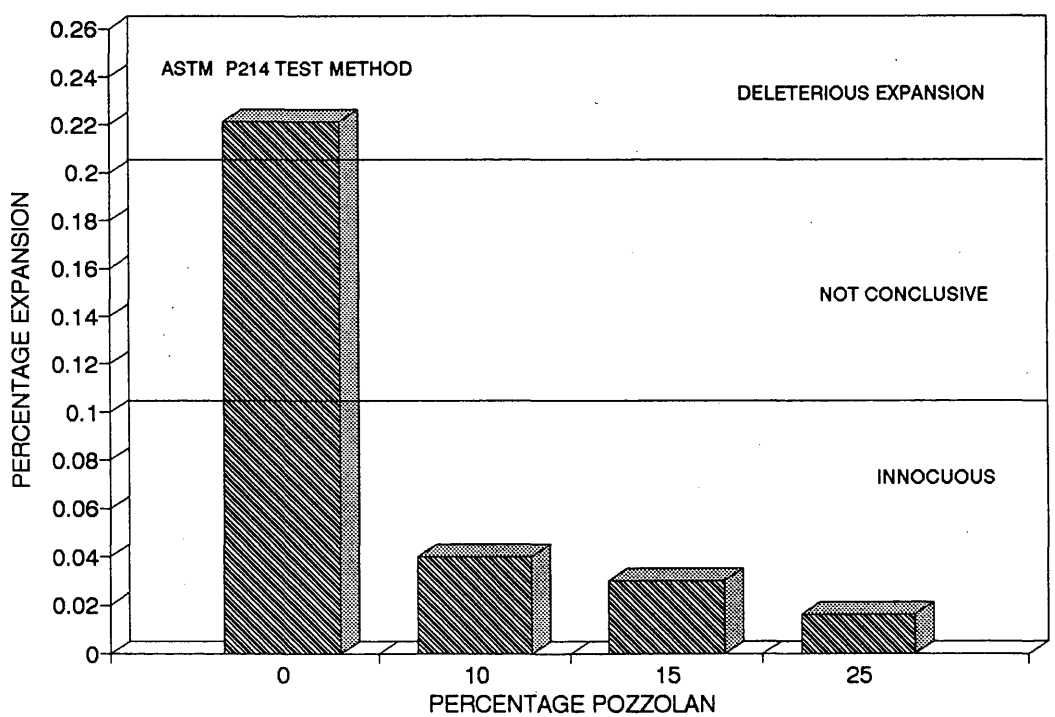

FIGURE 5 Comparison of expansions for pozzolan sample LK2.

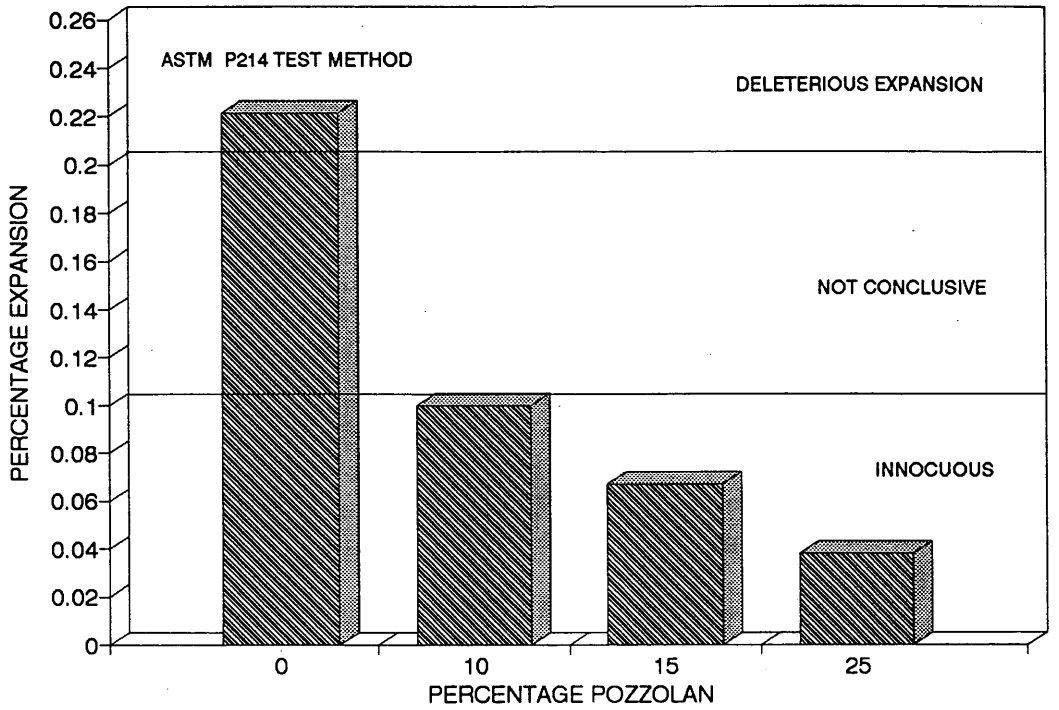

FIGURE 6 Comparison of expansions for pozzolan sample PS1E.

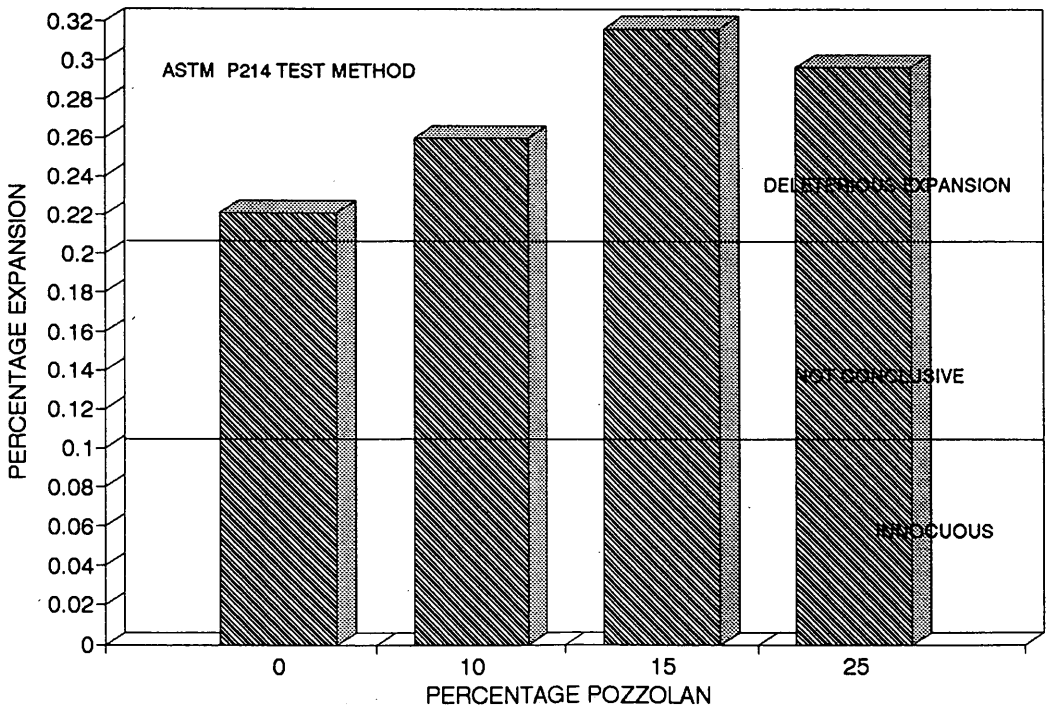

FIGURE 7 Comparison of expansions for pozzolan sample VA2.

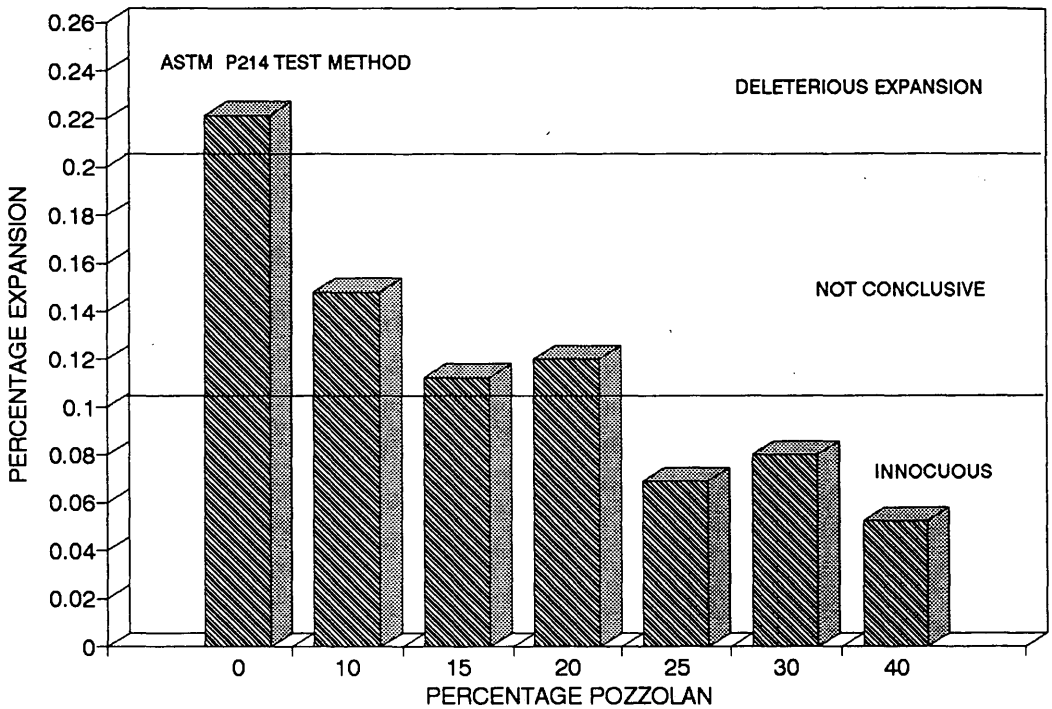

FIGURE 8 Comparison of expansions for fly ash.

and producing lower C/S mole ratio calcium silicate hydrates by reacting with the higher C/S mole ratio hydrates. The new hydrates can absorb large amounts of alkali into their structure and retain them, thereby reducing their availability for reaction with the silica in the aggregate.

CONCLUSIONS

- Two pozzolans—a gray, highly siliceous "fireclay" from the Lakota formation (LK2), and Pierre shale, which is a dark brown to black noncalcareous shale that was expanded (calcined) at about 1050°C (PS1E)—are most effective for controlling ASR. Only one pozzolan, a white volcanic ash (VA2), is unsuitable for use in controlling ASR expansion. Higher percentage replacement (15 or 25 percent) was more effective in reducing the ASR than was 10 percent replacement. Pozzolans LK2 and PS1E were more effective in controlling expansions than was the Class F fly ash investigated.
- With conventional crushing and grinding operations it is possible to produce pozzolans up to the required fineness, that is, above 90 percent passing through Sieve No. 325.
- The strength activity index of the pozzolans investigated in portland cement had a wide range of values between 19.78 and 91.72 percent. When blended with the cement, some pozzolans affected the strength of concrete adversely. Such pozzolans, even when they effectively inhibit ASR expansions, should not be used for blending with cement.
- The study on the effect of calcination of pozzolans on the strength of mortar cubes made with calcined pozzolan blended cements indicated that the strength activity index increases with an increase in the temperature of calcination.
- The Class F fly ash investigated effectively reduced ASR expansion of mortar bars made with reactive sand below the innocuous level (0.10 percent) when 25 percent of the cement was replaced with fly ash.

ACKNOWLEDGMENTS

The authors gratefully acknowledge the funding received from SSDOT and express gratitude to David Huft of SDDOT for supporting and encouraging this research.

REFERENCES

1. Blight, G. E., M. G. Alexander, T. K. Ralph, and B. A. Lewis. Effect of Alkali-Aggregate Reaction on the Performance of Reinforced Concrete Structure Over a Six-Year Period. *American Concrete Institute Journal,* Vol. 41, No. 147, June 1989, pp. 69–78.
2. Stark, D., and G. DePuy. *Alkali-Silica Reaction in Five Dams in Southwestern United States.* Concrete Durability, Katharine and Bryant Mather, International Conference, ACI, SP-100, Vol. 2, 1987, pp. 1759–1786.
3. Alasali, M. M., V. M. Malhotra, and J. A. Soles. Performance of Various Test Methods for Assessing the Potential Alkali Reactivity of Some Canadian Aggregates. Presented at International Workshop on Alkali-Aggregate Reactions in Concrete; Occurrence, Testing and Control. Halifax, Nova Scotia, Canada, May 1990.
4. Ramachandran, S., V. Ramakrishnan, and D. Johnston. The Role of High Volume Fly Ash in Controlling Alkali-Aggregate Reactivity. *Proc.,* 4th *CANMET/ACI International Conference on Fly Ash, Silica Fume, Slag, and Natural Pozzolans in Concrete,* (V. M. Malhotra, ed.), Istanbul, Turkey, May 1992, pp. 591–613.

5. Fabiarz, J., and R. Carrasquillo. *Alkali-Aggregate Reaction in Concrete Containing Fly Ash.* Concrete Durability, Katherine and Bryant Mather, International Conference, ACI, SP-100, Vol. 2, 1987, pp. 1787–1808.
6. Gaze, M. E., and P. J. Nixon. The Effect of PFA Upon Alka-Aggregate Reaction. *American Concrete Institute Journal,* Vol. 35, No. 123, June 1983, pp. 107–110.
7. Carrasquillo, R. L., and P. G. Snow. Effect of Fly Ash on Alkali-Aggregate Reaction in Concrete. *American Concrete Institute Materials Journal,* Vol. 84, No. 4, July-Aug. 1987, pp. 299–305.
8. Diamond, S., and P. K. Mukherjee. Influence of Fly Ash in Alkali-Aggregate Reaction. *Proc., 7th International Conference on Concrete Alkali-Aggregate Reaction,* (Patrick E. Grattan-Bellew, ed.), Ottawa, Ontario, Canada, 1986, pp. 44–48.
9. Soles, J. A., V. M. Malhotra and R. W. Suderman. The Role of Supplementary Cementing Materials in Reducing the Effects of Alkali-Aggregate Reactivity; CANMET Investigations. *Proc., 7th International Conference on Concrete Alkali-Aggregate Reactions,* (Patrick E. Grattan-Bellew, ed.), Ottawa, Ontario, Canada, 1986, pp. 79–82.
10. Samuel, S., and P. E. Tyson. Control of Alkali-Silica Reactivity in Recycled Concrete Using Fly Ash. *Proc., 4th CANMET/ACI International Conference on Fly Ash, Silica Fume, Slag, and Natural Pozzolans in Concrete,* Istanbul, Turkey, May 1992, pp. 15–20.
11. Grattan-Bellew, P., and J. Gillott. *Three Decades of Studying the Alkali Reactivity of Canadian Aggregates.* Concrete Durability, Katharine and Bryant Mather, International Conference, ACI, SP-100, Vol. 2, 1987, pp. 1365–1384.
12. Larbi, J. A., and J. M. Bijen. Effect of Mineral Admixtures on the Cement Paste Aggregate Interface. *Proc., 4th CANMET/ACI International Conference on Fly Ash, Silica Fume, Slag, and Natural Pozzolans in Concrete,* (V. M. Malhotra, ed.) Istanbul, Turkey, May 1992, pp. 655–669.

The views expressed in this paper are those of the authors and do not necessarily reflect official views of SSDDT.

Publication of this paper sponsored by Committee on Chemical Additions and Admixtures for Concrete.

Interpretation of Accelerated Test Method ASTM P214 Test Results

DANIEL P. JOHNSTON

In South Dakota during the last decade, alkali-silica reactivity (ASR) has changed from a localized occurrence to a statewide problem. ASTM P214 was chosen as the preferred test for determining potential reactivity of sands used for concrete in the state. The test was modified to use different NaOH concentrations to explore the feasibility of using two different base strengths to better predict reactivity. Of 30 sands tested, over 40 percent gave results that were inconclusive (expansion values in the 0.1 to 0.2 percent range), and only 10 percent of the sands were nonreactive. A modified interpretation of the test results to include a best fit for expansion at 3, 7, 11, and 14 days, using the general equation $Y = A_2 X^2 + A_1 X + A_0$ (X = Time $^{1/2}$) gave a much clearer pattern of projected reactivity when the A_1 coefficients were plotted against the A_2 coefficients for all 30 sands. The sands break out into two linear "families" of coefficients: one reactive and one nonreactive. It appears the method also can be used to determine the effectiveness of pozzolans at reducing ASR.

During the past decade in South Dakota, alkali-silica reactivity (ASR) has changed from a localized occurrence to a statewide problem, with a tremendous potential impact on the durability and expected service life of the state's PCC pavements. The first significant manifestation of ASR occurred in the late 1970s on a section of I-90 built in 1972. A local sand used in the concrete mix proved to be highly reactive. Mineralogical analysis of the sand confirmed it contained 44 percent chert. To address this problem, the cement specification for concrete paving mixes was changed to a low alkali cement (Na_2O equivalent $\leq$ 0.6 percent) in 1983.

Since 1980, several other concrete pavements have exhibited varying degrees of ASR-related distress involving concrete sands. In addition, the premiere coarse aggregate for concrete in the eastern part of the state, a quartzite, was found to be slow, late-expanding alkali-silica reactive (*1*). Exhaustion of existing sand pits during the past 20 years, coupled with the unknown reactivity of potential new sand sources and concern about the long-term effectiveness of low alkali cement in reducing ASR, prompted an evaluation of all concrete sands being used in South Dakota.

ASTM P214

The primary test chosen for determining the ASR potential of various sands was ASTM P214 Accelerated Detection of Potentially Deleterious Expansion of Mortar Bars Due to Alkali-Silica Reaction (*2,3*). The test is rapid and reproducible, but interpretation of the test results can be difficult without additional testing. Table 1 lists the test results for 30 sands, and Figure 1 indicates the 95 percent confidence limits (dashed lines). Of the 30 sands, only three can be classified as nonreactive using the 0.1 percent expansion criterion (*4*). Fourteen sands have expansion values that lie in the inconclusive range and thirteen sands are definitely alkali-silica reactive. Using upper values for 95 percent confidence limits adds two more sands (Sands 92 and 120) to the reactive list. Field performance confirms that these sands are indeed reactive; 40 percent of the sands remain in the inconclusive category. ASTM C289 Potential Reactivity of Aggregates (Chemical Method) was also used as a screening method for some of these sands but, unfortunately, a comparison of the two test results with actual field performance complicates interpretation.

In an attempt to determine the effect of base strength on the P214 test, a series of different concentrations of sodium hydroxide (NaOH) was substituted for 1N NaOH. Sand 57, one of the most reactive of the 30 sands, was used in these tests. A control series of mortar bars made with Ottawa sand was run in parallel to determine whether any other factor was involved. Results are listed in Table 2 and presented graphically in Figure 2. Readings were taken up to 30 days after fabrication of the bars to indicate possible long-term trends. Control samples did not undergo expansion at any time regardless of concentration.

The major effect of OH^- concentration is on the rate of expansion. With 0.25N NaOH, the final expansion at 28 days was only 0.008 percent as compared with 0.449 percent for 1N solutions. The 0.5N solution achieved an expansion of 0.228 percent at 28 days, roughly half that of the 1N solution. Both stronger NaOH concentrations had expansion curves that fit the general equation:

$$\text{Expansion (\%)} = A_2 \text{ Time} + A_1 \text{ Time}^{1/2} + A_0 \quad (1)$$

where R^2 values are 0.9992 (1N) and 0.9912(0.5N), even though the 1N curve is convex and the 0.5 curve is concave. The data for the 0.25N curve also fit the equation, but only for expansion values beyond 17 days (R^2 = 0.9460). In all cases, the zero value was excluded from the curve-fitting data.

A comparison of response to concentration at 14 and 28 days (Figure 3) shows an almost linear relationship at 14 days but a definite curvilinear one at 28 days. The expansion reaction is subject to a diffusion-controlled delay during the first 2 days and to a significant reduction in reaction rate at later ages owing, no doubt, to get formation and reaction rims interfering with the alkali-silica reactions. A modification of P214 to include expansion testing at more than 1N NaOH concentration, somewhere between 0.5 and 1N, would probably improve the reliability of the test in predicting potential ASR.

The same equation type can be used to analyze the expansion of the 30 sands using the standard 1N concentration. Figures 4, 5, and 6 illustrate three typical curve types obtained from the analyses. Sand 57 is highly reactive and gives a convex curve. The other line in the figure is a regression fit using the same type of equation but

South Dakota Department of Transportation, 700 East Broadway Ave., Pierre, S.D. 57501–2586.

TABLE 1 ASTM P214 Test Results

SAND	% EXPANSION	s	95% CONFIDENCE +	95% CONFIDENCE -	ASTM C289	FIELD PERFORMANCE
22	0.152	0.007	0.164	0.139	Innocuous	Nonreactive
29	0.202	0.008	0.211	0.193	Innocuous	Reactive
36	0.300	0.013	0.315	0.285	Innocuous	Reactive
43	0.125	0.016	0.144	0.106	Deleterious	Reactive ??
50	0.274	0.018	0.295	0.253	Pot. Delet.	Reactive
57	0.315	0.009	0.326	0.304	Deleterious	N/A
64	0.329	0.004	0.335	0.322	Deleterious	Reactive
71	0.261	0.013	0.276	0.246	Deleterious	Reactive
78	0.261	0.026	0.291	0.231	Pot. Delet.	Reactive
85	0.207	0.005	0.216	0.198	Deleterious	Reactive
92	0.186	0.024	0.214	0.159	Deleterious	Reactive
99	0.161	0.010	0.172	0.149	Innocuous	Nonreactive
106	0.128	0.015	0.146	0.110	Innocuous	Nonreactive
113	0.113	0.004	0.117	0.109	Innocuous	Nonreactive
120	0.192	0.020	0.215	0.169	Deleterious	Reactive
127	0.076	0.005	0.082	0.071	Pot. Delet.	Nonreactive
134	0.128	0.008	0.137	0.118	N/A	N/A
141	0.106	0.002	0.108	0.103	N/A	N/A
148	0.213	0.023	0.240	0.186	Innocuous	Reactive
155	0.044	0.001	0.045	0.043	Innocuous	Nonreactive
162	0.211	0.007	0.220	0.203	Innocuous	Reactive
169	0.164	0.003	0.168	0.160	Pot. Delet.	Nonreactive
176	0.208	0.023	0.235	0.180	Deleterious	Reactive
183	0.124	0.007	0.132	0.115	Innocuous	Reactive
190	0.062	0.005	0.068	0.057	Innocuous	N/A
197	0.140	0.017	0.160	0.120	N/A	N/A
204	0.113	0.028	0.145	0.080	N/A	N/A
211	0.280	0.004	0.284	0.275	N/A	N/A
218	0.367	0.019	0.389	0.345	N/A	N/A
225	0.181	0.008	0.190	0.171	N/A	N/A
Average	0.1874	0.012				

including zero. Sand 169 is inconclusive and fits a concave curve. Sand 183 is *Slear* quartzite and does not correspond in its behavior to any other sand tested. All of the sands fit the general equation well except for the three sands with expansion values below 0.10 percent Table 3 lists second degree polynomial coefficients for the various sands.

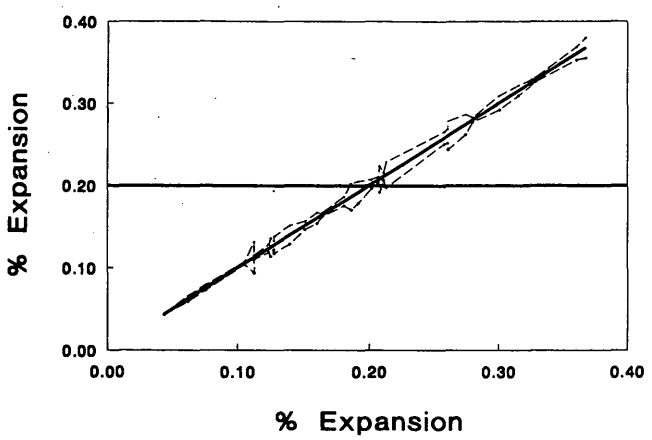

FIGURE 1 95 percent confidence intervals for 30 sands.

The major problem with using the 14-day expansion value as a primary indicator of reactivity is that it is an isolated point and does not reflect the way a certain sand or coarse aggregate expands during the test. ASTM P214 is a very severe test and causes expansion to occur even when the aggregate tested is nonreactive in its field performance. By examining the coefficients for the general expansion curve and combining these with the 14-day test results, it may be possible to clarify the "inconclusive" range. The manner in which a sand expands can be considered an index of the sand's reactivity, regardless of the final expansion value achieved. Coefficients for each sand represent how the expansion develops, as they

TABLE 2 Percentage Expansion at Different NaOH Concentrations

DAY	% EXPANSION		
	0.25 N	0.5 N	1.0 N
3	0.004	0.002	0.02
7	0.002	0.008	0.168
11	0.003	0.038	0.267
14	0.004	0.072	0.312
17	0.002	0.117	0.347
21	0.004	0.163	0.387
25	0.005	0.206	0.424
28	0.008	0.228	0.449

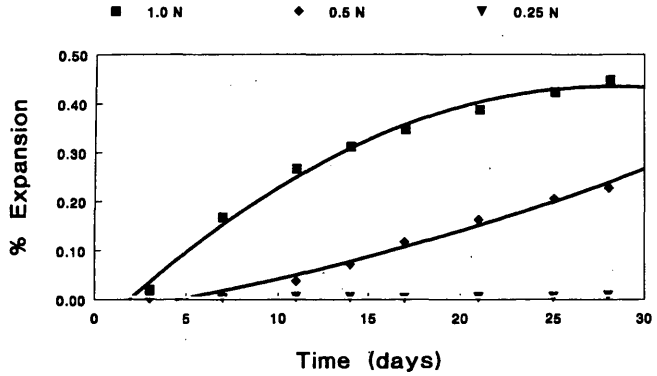

FIGURE 2 Percentage expansion versus time for Sand 57.

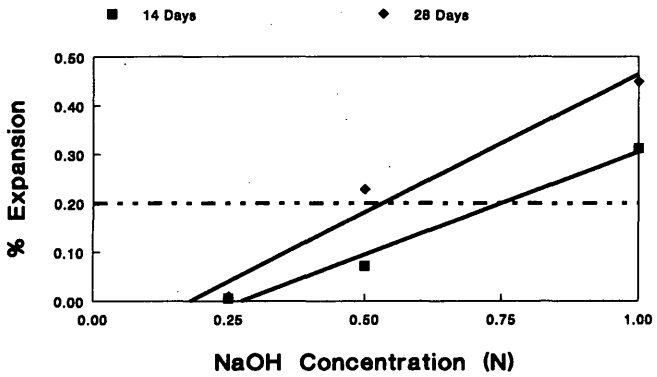

FIGURE 3 Percentage expansion versus NaOH concentration.

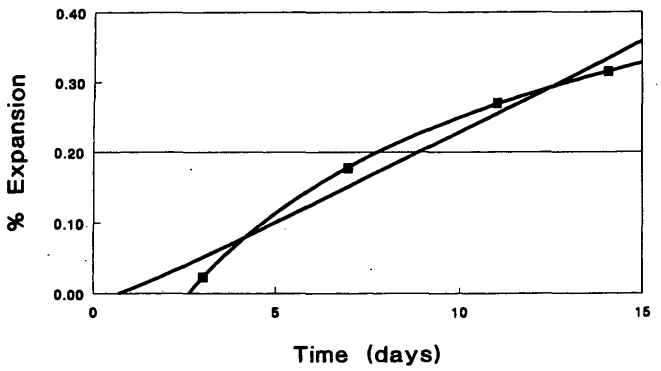

FIGURE 4 Typical ASTM P214 test result (Sand 57).

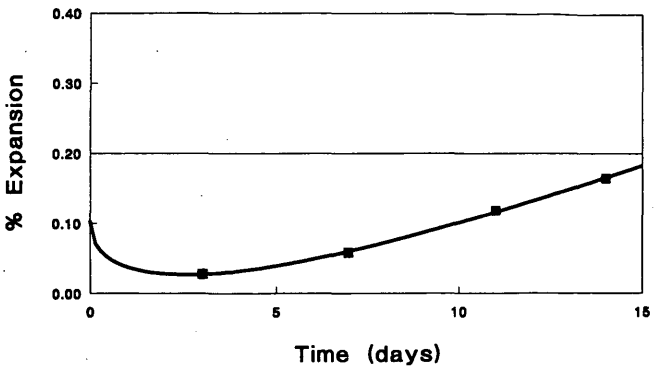

FIGURE 5 Typical ASTM P214 test result (Sand 169).

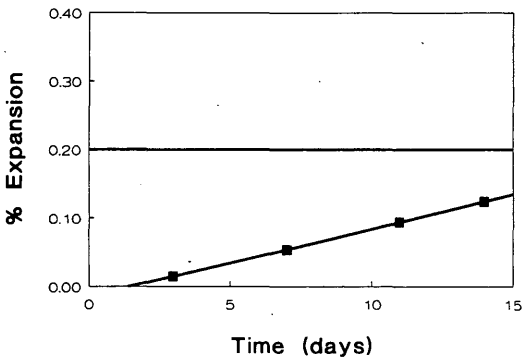

FIGURE 6 ASTM P214 test results (Sand 183, quartzite).

are proportional to the intrinsic properties of each individual curve, such as curvature and displacement from the vertical and horizontal axes.

At first glance, these coefficients do not appear to contain any more information than the 14-day expansion values. When the coefficients are plotted against each other, however, they separate into two distinct groups, one reactive and the other nonreactive. Figure 7 is a plot of A_1 (the first order coefficient) versus A_2 (the second order coefficient) for the general equation for all 30 sands. Both groups form a linear relationship with respect to the coefficients to a high degree of significance. A comparison of the 14-day expansion criteria with the linear classes of sands indicates an upward trend along the bottom unreactive line until Sand 169 is reached at a 0.164 percent expansion. All sands more expansive than this lie on the reactive line with the degree of expansion generally trending upward from right to left. Figure 8 is an expansion of Figure 7 in the region where most sands are plotted. It shows a clear differentiation between reactive and unreactive sands. Only three sands are somewhat "inconclusive" (Sands 99, 183, and 225). Sand 183 is quartzite and lies between the reactive and unreactive zones, presumably in a region where a slow, late expanding ASR aggregate belongs. Sand 99 is not quite on the nonreactive line but is considerably closer to the nonreactive sands than to the reactive ones. Sand 225 is much closer to the reactive sands and probably could be classified as reactive.

A comparison of projected reactivity with known field performance indicates striking accuracy of the coefficient plots at predicting potential reactivity. Of the sands with 20 or more years of use in South Dakota concrete pavements, the projected reactivity matched the known field performance in all but two cases. Sand 43 was used in a pavement that showed signs of severe ASR approximately 15 years after construction. Unfortunately, the coarse aggregate use in the pavement came from the same supplier and may be the actual source of the deterioration reaction. The mineralogical composition of Sand 43 is primarily dolomitic, and the estimated chert content by polarized light microscopy is under 5 percent; both facts argue in favor of its not being alkali-silica reactive. Sand 99 is also a dolomitic sand and comes from the same region of the state as Sand 43. There is a possibility that both aggregate are alkali-carbonate reactive, as discussed by Mather et al. (5).

TABLE 3 Coefficients for Equation 1

SAND	% EXPANSION	A2	A1	A0	PROJECTED REACTIVITY
22	0.152	0.0306	-0.0979	0.0914	Nonreactive
29	0.202	0.0370	-0.1069	0.0874	Reactive
36	0.300	-0.0158	0.2228	-0.3108	Reactive
43	0.125	0.0271	-0.0910	0.0867	Nonreactive
50	0.274	0.0173	0.0351	-0.0952	Reactive
57	0.315	-0.0222	0.2673	-0.3731	Reactive
64	0.328	-0.0301	0.3136	-0.4246	Reactive
71	0.261	0.0208	0.0077	-0.0577	Reactive
78	0.261	0.0113	0.0618	-0.1252	Reactive
85	0.207	0.0244	-0.0341	-0.0020	Reactive
92	0.186	0.0336	-0.0952	0.0754	Reactive
99	0.161	0.0299	-0.0875	0.0723	Nonreactive
106	0.128	0.0284	-0.0953	0.0901	Nonreactive
113	0.113	0.0232	-0.0759	0.0729	Nonreactive
120	0.192	0.0279	-0.0651	0.0479	Reactive
127	0.076	0.0124	-0.0345	0.0316	Nonreactive
134	0.128	0.0268	-0.0930	0.1014	Nonreactive
141	0.106	0.0176	-0.0548	0.0645	Nonreactive
148	0.213	0.0321	-0.0815	0.0710	Reactive
155	0.044	0.0056	-0.0172	0.0297	Nonreactive
162	0.211	0.0270	-0.0567	0.0481	Reactive
169	0.164	0.0301	-0.0961	0.1038	Nonreactive
176	0.208	0.0329	-0.0898	0.0861	Reactive
183	0.124	0.0107	-0.0043	-0.0099	Reactive
190	0.062	0.0067	-0.0111	0.0097	Nonreactive
197	0.140	0.0268	-0.0860	0.0884	Nonreactive
204	0.113	0.0211	-0.0705	0.0810	Nonreactive
211	0.280	-0.0030	0.1413	-0.2049	Reactive
218	0.367	-0.0382	0.3663	-0.4693	Reactive
225	0.181	0.0312	-0.0847	0.0633	Reactive
Gabbro	0.015	-0.0029	0.0194	-0.0175	Nonreactive
G+4.5% Opal	0.271	-0.0323	0.3119	-0.4163	Reactive
Harzburgite	0.051	0.0049	-0.0047	0.0087	Nonreactive
H+4.5% Opal	0.276	-0.0378	0.3399	-0.4438	Reactive

Further confirmation of the status of an aggregate can be obtained by plotting the zero order coefficient, A_0, against A_2, as shown in Figure 9. Again, two straight lines are obtained with the points on one representing reactive sands and those on the other nonreactive. The relationship is not quite as clear as the previous one, but using the combination of the two plots allows some refinement of the projected reactivity. For instance, if A_0 is negative, then the sand is reactive. The quartzite sample is off by itself, but it does have a negative A_0. Sand 225 is reactive, and whether Sand 99 is remains inconclusive.

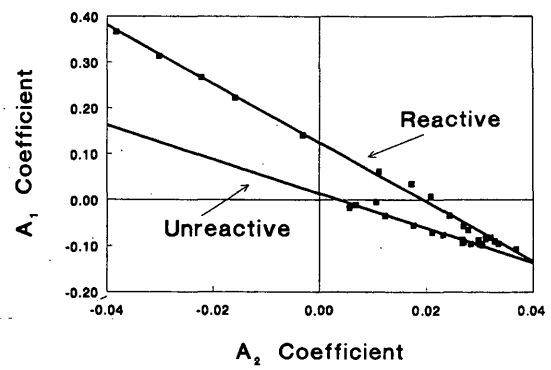

FIGURE 7 Plot of A_1 versus A_2 for 30 sands.

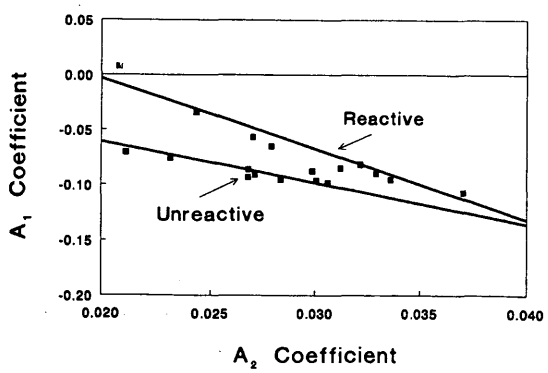

FIGURE 8 Plot of A_1 versus A_2 for 30 sands.

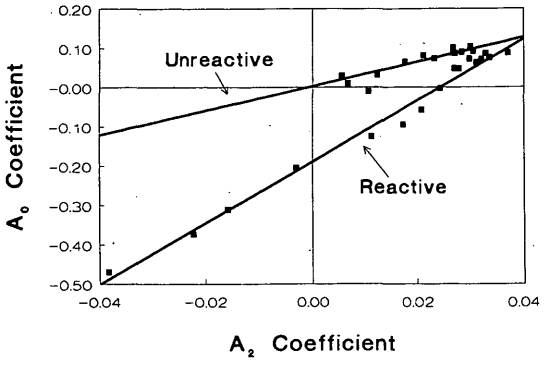

FIGURE 9 Plot of A_0 versus A_2 for 30 sands.

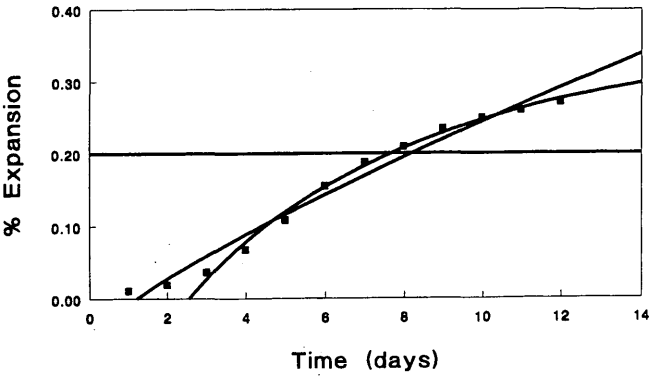

FIGURE 10 Expansion results for gabbro and 4.5 percent opal (6).

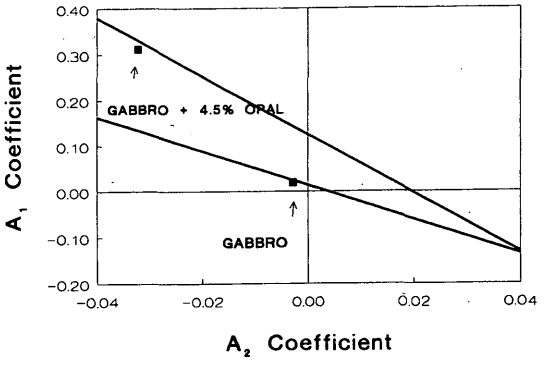

FIGURE 11 Plot of A_1 versus A_2 for gabbro and 4.5 percent opal (6).

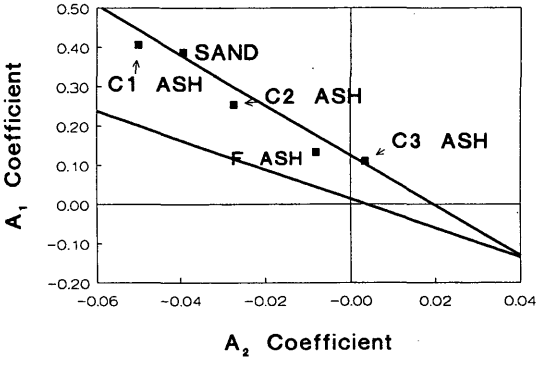

FIGURE 12 Plot of A_1 versus A_2 for Sand 57 with four fly ashes (10 percent).

The use of coefficients to clarify potential ASR is possibly of great benefit. The unusual linearity in the coefficient plots can be attributed to the existence of two separate mechanisms for expansion. Coefficient A_2 is directly proportional to the curvature of the expansion curve. A_1 is directly proportional to the horizontal displacement of the curve from zero, and A_0 is related to the vertical displacement. The existence of "families" of curves indicates systematic reactions. The preliminary least square fits for reactive sands are

$$A_1 = -6.409\,A_2 + 0.125$$

$$A_0 = 7.802\,A_2 - 0.190$$

and for the nonreactive sands are

$$A_1 = 3.733\,A_2 + 0.014$$

$$A_0 = 3.119\,A_2 + 0.002$$

The true applicability of the method for determining potential reactivity cannot be determined without using data on other aggregates obtained by other laboratories. An initial attempt to do so involved data on two coarse aggregates, a gabbro and an harzburgite, tested by Daoud (*6*). Both aggregates are nonreactive, so Daoud added the pessimum amount of opal to each and retested them. He also took daily readings of expansion up to 12 days after the zero reading. Figure 10 presents a plot of his data for the gabbro + 4.5 percent opal. The general equation was fitted to his Daoud's data in two ways. The first relatively poor fit included the zero reading and readings at days 1 and 2, whereas the much more exact fit used only data from days 3 to 12. Figure 11 is a plot of A_1 versus A_2 for the gabbro, and for the gabbro + 4.5 percent opal. Results support the wide application of the method.

Determining Pozzolans Effectiveness for Reducing ASR

A promising application of the proposed method of interpreting ASTM P214 test results would be as an accelerated replacement for ASTM C441 Effectiveness of Mineral Admixtures or Ground Blast-Furnace Slag in Preventing Excessive Expansion of Concrete Due to the Alkali-Silica Reaction. Figure 12 illustrates the effect of 10 percent addition of three Class C fly ashes and one Class F fly ash on the expansion behavior of Sand 57. Figure 13 is based on data from Ramakrishnan and Ramachandran (*7*) and demonstrates the effect of increasing addition of a Class F fly ash on the reactivity of Sand 57. Several items of note from the graphs follow:

- At a 10 percent addition rate, the fly ashes do not mitigate the potential reactivity of Sand 57, although they decrease the rate of reactivity.

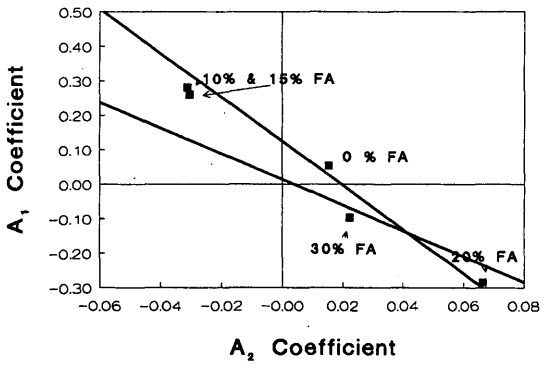

FIGURE 13 Plot of A_1 versus A_2 for Sand 57 with various percentages of Class F fly ash (FA).

• Ramakrishnan (*7*) and Ramachandran obtained a somewhat lower 14-day expansion for Sand 57 (0.2755 percent versus 0.315 percent), but the coefficient plot still indicates reactivity.

• A 20 percent addition of the fly ash reduces the 14-day expansion below 0.20 percent, but the coefficient plot still indicates reactivity.

• A 30 percent addition eliminates potential ASR, and the coefficient plot confirms this.

CONCLUSIONS

• ASTM P214 is a good test for determining potential ASR.

• Using two different NaOH concentrations for the test, one at 1N and the other somewhere between 0.5 and 1N, may help minimize inconclusive results.

• Using a curve-fitting equation of the form $Y = A_2 X^2 + A_1 X + A_0$ (X = Time$^{1/2}$) and plotting the polynomial coefficients against each other appears to increase the predictive value of test results in the 0.1 to 0.2 percent expansion range.

• ASTM P214 can also be used to determine the effectiveness of various pozzolans at reducing potential ASR.

• Further work in analyzing data for different aggregates subjected to ASTM P214 by various laboratories is needed before the validity and limitations of the proposed method of interpreting ASTM P214 can be properly evaluated. It may be necessary for each laboratory to develop its own correlations to ensure proper interpretation.

REFERENCES

1. Buck, A. D. Alkali Reactivity of Strained Quartz as a Constituent of Concrete Aggregate. *Cement, Concrete and Aggregates,* CCAGDP, Vol. 5. No. 2, Winter 1983, pp. 131–113.
2. Oberholster, R. E., and G. Davies. An Accelerated Method for Testing the Potential Alkali Reactivity of Siliceous Aggregates. *Cement and Concrete Research,* Vol. 16, 1986, pp. 181–189.
3. Davies, G., and R. E. Oberholster. Use of the NBRI Accelerated Test to Evaluate the Effectiveness of Mineral Admixtures in Preventing the Alkali-silica Reaction. *Cement and Concrete Research,* Vol. 17, 1987, pp. 97–107.
4. Hooton, R. D., and C. A. Rogers. Evaluation of Rapid Test Methods for Detecting Alkali-Reactive Aggregates. *Proc., 8th International Conference on Alkali-Aggregate Reaction,* Kyoto, Japan, 1989, pp. 439–444.
5. Mather, K., A. D. Buck, and W. I. Luke. Alkali-Silica and Alkali-Carbonate Reactivity of Some Aggregates from South Dakota, Kansas, and Missouri. In *Highway Research Record 45,* HRB, National Research Council, Washington, D.C., 1964, pp. 72–109.
6. Daoud, O. E. K. Properties and Reactivity of Gabbro and Harzburgite Gravels Used in Concrete Work in Kuwait. *ACI Materials Journal,* Vol. 87, No. 5, Sept.-Oct., 1990, pp. 446–456.
7. Ramakrishnan, V., and S. Ramachandran. Alkali Reactivity of Concrete Aggregates. *SDDOT Report,* SD90–01-F, Pierre, June 1991.

Publication of this paper sponsored by Committee on Chemical Additions and Admixtures for Concrete.